frontiers | Research Topics

Inhibitors of CDK family: New perspective and rationale for drug combination in preclinical model of solid tumors

Edited by
Andrea Cavazzoni and Arianna Palladini

Published in
Frontiers in Oncology
Frontiers in Pharmacology

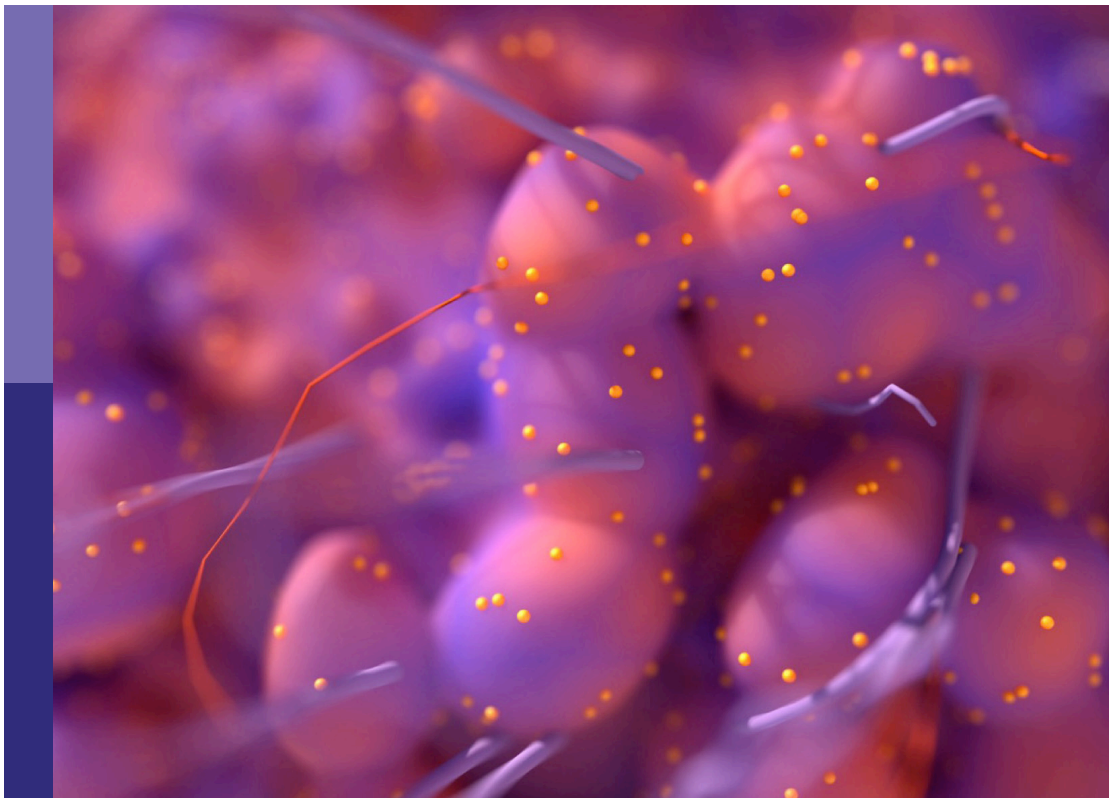

ISSN 1664-8714
ISBN 978-2-83252-149-6
DOI 10.3389/978-2-83252-149-6

About Frontiers

Frontiers is more than just an open access publisher of scholarly articles: it is a pioneering approach to the world of academia, radically improving the way scholarly research is managed. The grand vision of Frontiers is a world where all people have an equal opportunity to seek, share and generate knowledge. Frontiers provides immediate and permanent online open access to all its publications, but this alone is not enough to realize our grand goals.

Frontiers journal series

The Frontiers journal series is a multi-tier and interdisciplinary set of open-access, online journals, promising a paradigm shift from the current review, selection and dissemination processes in academic publishing. All Frontiers journals are driven by researchers for researchers; therefore, they constitute a service to the scholarly community. At the same time, the *Frontiers journal series* operates on a revolutionary invention, the tiered publishing system, initially addressing specific communities of scholars, and gradually climbing up to broader public understanding, thus serving the interests of the lay society, too.

Dedication to quality

Each Frontiers article is a landmark of the highest quality, thanks to genuinely collaborative interactions between authors and review editors, who include some of the world's best academicians. Research must be certified by peers before entering a stream of knowledge that may eventually reach the public - and shape society; therefore, Frontiers only applies the most rigorous and unbiased reviews. Frontiers revolutionizes research publishing by freely delivering the most outstanding research, evaluated with no bias from both the academic and social point of view. By applying the most advanced information technologies, Frontiers is catapulting scholarly publishing into a new generation.

What are Frontiers Research Topics?

Frontiers Research Topics are very popular trademarks of the *Frontiers journals series*: they are collections of at least ten articles, all centered on a particular subject. With their unique mix of varied contributions from Original Research to Review Articles, Frontiers Research Topics unify the most influential researchers, the latest key findings and historical advances in a hot research area.

Find out more on how to host your own Frontiers Research Topic or contribute to one as an author by contacting the Frontiers editorial office: frontiersin.org/about/contact

Inhibitors of CDK family: New perspective and rationale for drug combination in preclinical model of solid tumors

Topic editors

Andrea Cavazzoni — University of Parma, Italy

Arianna Palladini — University of Pavia, Italy

Citation

Cavazzoni, A., Palladini, A., eds. (2023). *Inhibitors of CDK family: New perspective and rationale for drug combination in preclinical model of solid tumors*. Lausanne: Frontiers Media SA. doi: 10.3389/978-2-83252-149-6

Table of contents

frontiers | Frontiers in Oncology

TYPE Editorial
PUBLISHED 28 March 2023
DOI 10.3389/fonc.2023.1180650

OPEN ACCESS

EDITED AND REVIEWED BY
Olivier Feron,
Université catholique de Louvain, Belgium

*CORRESPONDENCE
Andrea Cavazzoni
andrea.cavazzoni@unipr.it

SPECIALTY SECTION
This article was submitted to Pharmacology of Anti-Cancer Drugs, a section of the journal Frontiers in Oncology

RECEIVED 06 March 2023
ACCEPTED 13 March 2023
PUBLISHED 28 March 2023

CITATION
Cavazzoni A and Palladini A (2023) Editorial: Inhibitors of CDK family: New perspective and rationale for drug combination in preclinical models of solid tumors.
Front. Oncol. 13:1180650.
doi: 10.3389/fonc.2023.1180650

Editorial: Inhibitors of CDK family: New perspective and rationale for drug combination in preclinical models of solid tumors

Andrea Cavazzoni[1]* and Arianna Palladini[2]

[1]Department of Medicine and Surgery, University of Parma, Parma, Italy, [2]Department of Molecular Medicine, University of Pavia, Pavia, Italy

KEYWORDS

CDK, solid tumors, pre-clinical, combination, Rb

Editorial on the Research Topic
Inhibitors of CDK family: New perspective and rationale for drug combination in preclinical model of solid tumors

The CDK family includes enzymes involved in cell cycle progression and transcriptional regulation. CDK catalytic activity is strictly dependent on cyclin binding. Although various CDKs and cyclins have been identified, specific CDK-cyclin complexes are mandatory to control cell cycle progression, i.e., through the G_1, S, G_2, and M phases. Thus, CDK family activity can be modulated by cyclin partners and cyclin-dependent kinase inhibitors (CKIs).

The activity of CDK4/6 is mainly addressed to the tumor suppressor protein retinoblastoma (Rb) that causes the inactivation of Rb activity through hyperphosphorylation and the subsequent progression of the cell cycle from the G_1 to the S phase. In detail, the cyclin D-CDK4/6 kinase complex phosphorylates Rb, thus removing the control on the E2F transcription factor, allowing the transcription of genes critical for DNA replication and cell cycle progression from the G_1 to the S-phase. On the contrary, in its non-phosphorylated state, Rb binds the E2F transcription factor, actively suppressing the G_1-S progression.

A high level of Rb protein phosphorylation has been detected in several tumors and associated to the high expression of the cyclinD-CDK4/6 complexes. Thus, targeting these complexes is an attractive strategy to fight cancers. This strategy is currently approved for the treatment of estrogen receptor (ER)-positive, human epidermal growth factor receptor (Her) 2-negative breast cancer in combination with the aromatase inhibitor letrozole. Furthermore, several experimental data suggest the opportunity to extend the therapeutic strategy to other solid tumors. Moreover, encouraging results have shown that other members of the CDK family could be an attractive target to fight different tumors.

The Research Topic titled "*Inhibitors of CDK family: New Perspective and Rationale for Drug Combination in Preclinical Models of Solid Tumors*" focuses on the recent progress made with the aim of improving the efficacy of cyclin–CDK complex inhibitors. The Special Issue published nine articles, consisting of seven original articles and two review articles.

The paper by Digiacomo et al. described the efficacy of combining the CDK4/6 inhibitors abemaciclib or palbociclib with the antiangiogenic factor lenvatinib in a panel of human HCC cell lines. The simultaneous combination presented a significant antiproliferative effect compared to single therapy and different schedules of treatment. Growth inhibition was associated with a marked c-myc downregulation and a shutdown of the main intracellular signaling pathways. Moreover, the planned combo therapy was responsible for the irreversible inhibition of tumor growth due to the acquisition of a senescent phenotype.

Chilà et al. analyzed the role of CDK12, a member of the CDK family, involved in the phosphorylation and activation of the RNA polymerase II, the most important enzyme regulating the transcriptional process in eukaryotic cells. CDK12 is mainly inactivated in ovarian cancer, but, to date, the precise contribution of CDK12 to tumor progression still needs to be clarified. By generating stable CDK12 KO ovarian cancer cells, the authors observed a significant shutdown of cell growth in both *in vitro* and *in vivo* models, suggesting an oncogenic driver role of CDK12. Moreover, DNA content and chromosome doubling was observed in the absence of CDK12 over parental cells, suggesting an involvement of CDK12 in the maintenance of genome integrity.

As the CDK family is composed of numerous protein kinases involved in cell cycle regulation, the discovery and evaluation of new agents targeting specific CDK family members is encouraged.

In this context, the paper proposed by (1) described the activity of a new compound against the CDK1 inhibitor. This molecule is an active metabolite of the antiparasitic drug nitazoxanide (NTZ) and exhibited antiproliferative properties, with G_2/M cell cycle arrest and apoptosis induction, on a panel of glioma cells.

Sun et al. proposed an attractive manuscript proving that high CDK6 mRNA and protein levels predict poor prognosis in patients with advanced bladder carcinoma (BLCA). Moreover, they proposed that bladder cancer cells with high CDK6 protein levels display high sensitivity to CDK4/6 inhibitors such as palbociclib and ribociclib. Despite the interesting results, the authors suggested that it is still arbitrary to use CDK6 mRNA as markers for patient selection. They underlined the critical role of the tumor microenvironment and the need to develop 3D cultures from tumor patients for precise prediction of the sensitivity to CDK4/6 inhibitors.

Recently, the third-generation retinoid adapalene (ADA) has been emerging as a potent anticancer agent, and using ADA in combination with existing therapeutic regimens may improve its effectiveness and minimize toxicities and drug resistance.

Two research articles focused on the role of ADA in prostate and triple negative breast cancer (TNBC).

Nong et al. (2) observed that ADA suppressed the proliferation of prostate cancer cells both *in vitro* and *in vivo*, with a reduction of metastatic lesions at the bone marrow level.

Moreover, ADA triggered S-phase arrest in prostate cancer cells by inhibiting CDK2, Cyclin A2, and Cyclin E1 and promoted apoptotic cell death because of BAX upregulation.

The second research article assessed the anticancer efficacy of ADA as a combination strategy with the PI3K inhibitor (GDC-0941) in *in vitro* TNBC models. This combination exerted a synergistic effect in term of inhibition of cell proliferation, inducing apoptosis, suggesting that this therapeutic option could be valuable for patients with TNBC.

Interestingly, the authors observed that CDK2 is the main target of ADA. CDK2 is often overexpressed in breast tumors and plays a key role in controlling cell cycle regulation, in particular the S-phase, making CDK2 an attractive therapeutic target. Molecular docking studies revealed that ADA binds with CDK2, inducing a significant reduction of CDK2 protein levels, confirming that S-phase arrest is a direct consequence of CDK2 abrogation by ADA treatment (3).

Recently, different immunomodulatory effects of CDK4/6 inhibition have been proposed, such as the increase of immune cells in the tumor microenvironment, which strengthens the antitumor immune response; these studies enforce the modulatory role of CDK inhibitors toward immune cells.

As reported by (4), palbociclib resulted in reversibly inhibiting the cell growth of human $CD3^+$ T cells, with a consequent decrease of the pro-inflammatory cytokines IFN-γ and TNF-α, suggesting a shut-down of T-cell killing activity. These results may have consequences for the planning of treatment based on the simultaneous combination of CDK4/6 inhibitors and T-cell-based cancer immunotherapeutic strategies, and they suggest a palbociclib-free period for an effective immunotherapy approach.

The employment of CDK inhibitors could be also expanded to sarcoma patients. As reported in the review by Higuchi et al., palbocilcib addiction significantly reduced PDX growth in patients with sarcomas from different origins. The regression of PDX is achieved by addiction to different drugs, such as the multikinase inhibitor sorafenib and the recombinant methioninase, suggesting that the combination with palbociclib could be a promising therapeutic option to improve sarcoma therapy in the clinic.

The study of cell cycle control in the sarcoma histotype will be critical for the progress of combination treatment of CDK inhibitors with targeted therapies or immunotherapeutic strategies. Emerging data have confirmed the CDKN2A gene as the most altered gene in bone sarcoma and soft tissue sarcoma patients, confirming the biological value of p16INK4a-CDK4/6-pRb signaling in sarcomas.

At present, few phase I and II clinical trials are focusing on the addiction to CDK inhibitors in sarcoma patients, and the majority address CDK drugs in monotherapy.

Only three phase II clinical trials were based on the combination of CDK compounds with other anticancer drugs (chemotherapy) or with immune checkpoint inhibitors, the last one being the most promising strategy, based on results from breast cancer patients treated with letrozole, palbociclib, and pembrolizumab (Merlini et al.).

Author contributions

All authors listed have made a substantial, direct, and intellectual contribution to the work and approved it for publication.

Conflict of interest

The authors declare that the research was conducted in the absence of any commercial or financial relationships that could be construed as a potential conflict of interest.

Publisher's note

References

1. Huang S, Xiao J, Wu J, Liu J, Feng X, Yang C, et al. Tizoxanide promotes apoptosis in glioblastoma by inhibiting Cdk1 Activity. *Front Pharmacol* (2022) 13:895573. doi: 10.3389/fphar.2022.895573

2. Nong HB, Zhang YN, Bai YG, Zhang Q, Liu MF, Zhou Q, et al. Adapalene inhibits prostate cancer cell proliferation *in vitro* and *in vivo* by inducing DNA damage, S-Phase cell cycle arrest, and apoptosis. *Front Pharmacol* (2022) 13:801624. doi: 10.3389/fphar.2022.801624

3. Mehraj U, Wani NA, Hamid A, Alkhanani M, Almilaibary A, Mir MA. Adapalene inhibits the growth of triple-negative breast cancer cells by S-Phase arrest and potentiates the antitumor efficacy of Gdc-0941. *Front Pharmacol* (2022) 13:958443. doi: 10.3389/fphar.2022.958443

4. Arndt C, Tunger A, Wehner R, Rothe R, Kourtellari E, Luttosch S, et al. Palbociclib impairs the proliferative Capacity of activated T cells while retaining their cytotoxic efficacy. *Front Pharmacol* (2023) 14:970457. doi: 970457

frontiers in Pharmacology

ORIGINAL RESEARCH
published: 22 February 2022
doi: 10.3389/fphar.2022.801624

Adapalene Inhibits Prostate Cancer Cell Proliferation *In Vitro* and *In Vivo* by Inducing DNA Damage, S-phase Cell Cycle Arrest, and Apoptosis

Hai-bin Nong[1†], Ya-nan Zhang[2†], Yi-guang Bai[1,3], Qiong Zhang[4], Ming-fu Liu[1], Quan Zhou[2], Zhuo-hua Shi[1], Gao-feng Zeng[4] and Shao-Hui Zong[1,5*]*

[1]Department of Spine Osteopathia, The First Affiliated Hospital of Guangxi Medical University, Guangxi Medical University, Nanning, China, [2]Collaborative Innovation Center of Guangxi Biological Medicine, Guangxi Medical University, Nanning, China, [3]Department of Orthopaedics, Nanchong Central Hospital, The Second Clinical Institute of North Sichuan Medical College, Nanchong, China, [4]Department of Nutrition and Food Hygiene, College of Public Hygiene of Guangxi Medical University, Nanning, China, [5]Research Centre for Regenerative Medicine and Guangxi Key Laboratory of Regenerative Medicine, Guangxi Medical University, Nanning, China

OPEN ACCESS

Edited by:
Arianna Palladini,
University of Bologna, Italy

Reviewed by:
Graziana Digiacomo,
University of Parma, Italy
Stefania Croci,
IRCCS Local Health Authority of Reggio Emilia, Italy

***Correspondence:**
Shao-Hui Zong
xiaohui3008@126.com
Gao-feng Zeng
1685858372@qq.com

[†]These authors have contributed equally to this work

Specialty section:
This article was submitted to Pharmacology of Anti-Cancer Drugs, a section of the journal Frontiers in Pharmacology

Received: *25 October 2021*
Accepted: *07 February 2022*
Published: *22 February 2022*

Citation:
Nong H-b, Zhang Y-n, Bai Y-g, Zhang Q, Liu M-f, Zhou Q, Shi Z-h, Zeng G-f and Zong S-H (2022) Adapalene Inhibits Prostate Cancer Cell Proliferation In Vitro and In Vivo by Inducing DNA Damage, S-phase Cell Cycle Arrest, and Apoptosis. Front. Pharmacol. 13:801624. doi: 10.3389/fphar.2022.801624

Aims: Prostate cancer is a well-known aggressive malignant tumor in men with a high metastasis rate and poor prognosis. Adapalene (ADA) is a third-generation synthetic retinoid with anticancer properties. We investigated the anti-tumor activity and molecular mechanisms of ADA in the RM-1 prostate cancer cell line *in vivo* and *in vitro*.

Methods: The effects of ADA on cell proliferation were estimated using the CCK-8 and colony formation assays. The wound-healing assay and the Transwell assay were employed to examine the migratory capacity and invasiveness of the cells. Flow cytometry was utilized to evaluate the cell cycle and apoptosis, and Western blotting analysis was used to assess the expression of the associated proteins. Micro-CT, histomorphological, and immunohistochemical staining were used to assess the effects of ADA on bone tissue structure and tumor growth in a mouse model of prostate cancer bone metastasis.

Result: ADA dramatically inhibited cell proliferation, migration, invasiveness, and induced S-phase arrest and apoptosis. ADA also regulated the expression of S-phase associated proteins and elevated the levels of DNA damage markers, p53, and p21 after ADA treatment, suggesting that the anti-tumor effect of ADA manifests through the DNA damage/p53 pathway. Furthermore, we observed that ADA could effectively inhibited tumor growth and bone destruction in mice.

Conclusion: ADA inhibited prostate cancer cell proliferation, elicited apoptosis, and arrested the cell cycle in the S-phase. ADA also slowed the rate of tumor growth and bone destruction *in vitro*. Overall, our results suggest that ADA may be a potential treatment against prostate cancer.

Keywords: adapalene, prostate cancer, DNA damage, cell cycle, apoptosis

INTRODUCTION

Approximately 1.41 million new cases and 37.5 million deaths worldwide are estimated to be caused by prostate cancer, which was the second most frequent cancer in 2020 and the fifth leading cause of cancer-related deaths (Sung et al., 2021). Furthermore, 85–100% of patients who died from prostate cancer presented bone metastasis (Carlin and Andriole, 2000). Prostate cancer is often androgen-dependent and initially responds to hormone therapy (Tang and Porter, 1997). Currently, the standard treatments for prostate cancer include hormone therapy, chemotherapy and radiotherapy (Cornford et al., 2017). Unfortunately, these treatments are eventually difficult to avoid androgen resistance and tumor metastasis (Gao et al., 2015). Moreover, these forms of treatment not only cannot inhibit tumor development and metastasis, but also are highly toxic and drug resistance in normal tissues (Li et al., 2015). Therefore, the search for safe, effective, and reliable treatments, especially those targeting androgens remains a hot topic in the field of prostate cancer research.

Adapalene, a synthetic derivative of retinoic acid, is a topical retinoid that is often used clinically to treat various skin diseases (Rusu et al., 2020). The pharmacological effects of ADA including comedolytic activity, anti-inflammatory activity, and anticancer activity have been studied widely (Millikan, 2010). In the field of anticancer research, one study found that ADA exhibited greater anticancer effects through inhibit CDK2 in colorectal cell lines (Shi et al., 2015). Retinoic acid as an anticancer drug exerts differentiation-promoting activity, which may be associated with intrinsic cytotoxic and pro-apoptotic effects (Simoni and Tolomeo, 2001). As recently reported, ADA inhibited the growth of ovarian cancer ES-2 cells by targeting glutamicoxaloacetic transaminase 1 (GOT1) and induced apoptosis by regulating the Bax/Bcl-2 ratio in hepatoma cells (Ocker et al., 2004; Wang et al., 2019). ADA triggered cell cycle arrest in the G1 phase of colorectal cancer cells and inhibited the proliferation of melanoma cells through the arrest of the cell cycle in the S phase, and then inhibited apoptosis by inducing DNA damage (Ocker et al., 2003; Li et al., 2019). However, to date, there are no reports on the use of ADA in the treatment of prostate cancer. Hence, we aimed to investigate the anticancer effect of ADA in the prostate cancer cell and provide a novel strategy for prostate cancer treatment.

MATERIALS AND METHODS

Chemicals and Antibodies

Adpalene (ADA, 106685-40-9) was purchased from AbMole Bioscience (Shanghai, China), Antibodies Cyclin-B1, CyclinD2, CDK2, Rb, ATM, phosphorylated histone variant H2A.X at serine139 (γ-H2A.X), p-CDK2 (Thr-160), and β-actin were procured from CST (Cell Signaling Technology, Beverly, MA, United States). Bax, Bcl-2, p53, p21 Waf1/Cip1(p21), Cyclin-A2, Cyclin-E1, phosphorylated (p)-CDK2, p-Rb(Ser-795), and the secondary antibody(goat anti-rabbit horseradish peroxidase-conjugated IgG) were acquired from Beyotime Biotechnology (Beijing, China).

Cell Lines and Cell Culture

The RM-1 cell line was purchased from the Shanghai Biochemical Cell Institute of the Chinese Academy of Sciences. RM-1 cells were cultured in DMEM (Gibco, United States) containing 10% FBS (VWR, Australia), 100 U/ml penicillin, and 100 pg/ml streptomycin (Gibco) at a temperature of 37°C, 5% CO_2 concentration, and 95% humidified air. Cells were passaged every 48–72 h using 0.25% trypsin containing 0.02% EDTA (Solarbio, Beijing, China).

Proliferation-Cytotoxicity Assay

RM-1 cells were collected and suspended in DMEM at a concentration of 2×10^4 cells/ml. The suspended cells were subsequently seeded overnight in 96-well plates with each well containing 100 µl medium and treated with increasing ADA dosages (0–40 µM) and then incubated for 24 h or 48 h in a humidified incubator at 37°C and 5% CO_2. Next, 100 µl fresh DMEM containing 10% CCK-8 reagent (Dojindo, Japan) was added to each well and the cells were incubated at37 °C in the dark for 30 min. The absorbance of each well was measured using a microplate reader (Gen5; BioTek, United States) at a wavelength of 450 nm.

Colony Formation Assay

RM-1 cells were collected and suspended at a concentration of 100 cells/ml. Then, the suspended cells were seeded in 6-well culture plates at a volume of 2 ml per well overnight and treated with (0, 1.25, 2.5, and 5 µM) ADA for 24 h. The cells were cultured for an additional week after the replacement of fresh DMEM. Next, the cells were fixed using 4% paraformaldehyde for 20 min and stained using 0.5% crystal violet solution at room temperature for 10 min. Colonies containing more than 50 cells were pictured and then quantified using the Image-J software.

Wound-Healing Assay

RM-1 cells were collected and suspended in DMEM at a concentration of 3×10^5 cells/ml. Subsequently, the suspended cells were plated in 6-well culture plates in a volume of 2 ml per well and placed in an incubator until the cell density was 90% or more. A sterile 100-µl plastic pipette tip was used to create a wound. The cell debris was cleaned by washing with PBS and the wounds were imaged using an inverted light microscope (Olympus Corporation) with a digital camera (magnification 40X) at 0 h. Each well was added serum-free DMEM containing different concentrations of ADA and were incubated for 12 or 24 h. After washing the cells with PBS, 10 fields were randomly photographed using an inverted light microscope. The areas of wound healing were analyzed using the Image-J software.

Cell Invasion Experiments

Cell invasiveness was detected using an 8-µm Transwell assay. Following treatment with different concentrations of ADA for 24 h, the cells were collected and then resuspended with serum-

free DMEM, and adjusted to a concentration of 5×10^5 cells/ml. The upper chamber was covered with the BD MatrigelTM matrix as per the protocols instructions. The Transwell inserts were plated in a 24-well plate, and 600 µl of DMEM containing 20% FBS was added to the lower chamber, a volume of 100 µl of the cell suspension was introduced into the upper chamber. The Transwell plate was placed in an incubator for 24 h, after which, the medium was aspirated and a cotton swab was used to gently wipe the cells on the upper surface of the chamber. The cells in lower chamber were subsequently fixed with 4% paraformaldehyde for 20 min at ambient temperature, and then stained using 0.5% crystal violet solution for 10 min. The cells were then washed thrice using PBS to remove the unbound crystal violet. After drying, six visual fields were randomly selected, imaged, and the cells were quantified using an inverted light microscope.

Apoptosis Assay

Trypsin without EDTA was used to digest RM-1 cells, which were then suspended at a concentration of 2×10^5 cells/ml. The suspended cells were plated overnight into 6-well culture plates (2 ml per well) and treated with the indicated doses of ADA for 24 or 48 h, and cell morphology was observed. Next, apoptosis was assessed using an Annexin V-APC Apoptosis Detection Kit (Invitrogen, CA, United States); the cells were collected, washed once in pre-cooled PBS, then once in 1X binding buffer, resuspended, and incubated with Annexin V-APC working solution for 15 min at ambient temperature. The cells were then washed once in 1X binding buffer, resuspended, and incubated with propidium iodide (PI) working solution at ambient temperature for 10 min. After incubation, the cells were stored at 2–8°C in the dark and subjected to flow cytometry (Beckman Coulter, United States) within 4 h.

Cell Cycle Analysis

The cell cycle was analyzed using a Cell Cycle Analysis Kit (Beyotime Biotechnology, Beijing, China). Trypsin without EDTA was used to digest the cells and suspend cells at the concentration of 2×10^5 cells/ml. The suspended cells were plated into 6-well culture plates at a volume of 2 ml per well overnight and then treated using the specified doses of ADA for 12 or 24 h. The cells were then harvested and fixed in 70% ice-cold ethanol at a temperature of 4°C overnight. The cells were then washed using PBS and incubated with PI staining solution for 30 min at ambient temperature. Subsequently, the cells were subjected to flow cytometry. The data obtained were evaluated using the FlowJo V10 software to determine the cell cycle progression.

Western Blotting

After treatment with ADA for 24 h, RM-1 cells were collected and washed thrice with ice-cold PBS, and subsequently lysed using RIPA lysis buffer on ice for 30 min. The total protein concentration was then determined using the BCA assay kit (Beyotime, China). Subsequently, 60 µg of protein was separated on an 8–16% SDS-PAGE separation system at 100V. Proteins were then transferred to a 0.22 µm PVDF membrane (Millipore, Billerica, MA, United States). The PVDF membranes were blocked using TBST comprising 5% BSA at ambient temperature for 1 h and incubated with primary antibodies at 4°C overnight. Each antibody was diluted as per manufacturer instructions. The PVDF membranes were washed three times using TBST, 5 min each, and incubated with secondary antibodies for 1 h at ambient temperature. Finally, the intensity of the immunoreactive bands was detected using the GE Amersham Imager 600 (General Electric, Boston, MA, United States). The data were analyzed using the Image J and SPSS software.

Animals and Experimental Groups

All mice (C57BL/6; Female; weighing 20–25 g; 8 weeks old) were procured and maintained at the Laboratory Animal Center of Guangxi Medical University. The mice were reared in specified pathogen-free environments and subjected to light/dark cycles of 12 h at 50–60% humidity at 22–26°C. The environment was disinfected and nursed as per the standards of the Experimental Animal Ethics Committee of Guangxi Medical University (China). To construct the bone metastasis model, RM-1 cells were collected, and resuspended in serum and adjusted to a concentration of 2×10^7 cells/mL. The mice were weighed and anesthetized intraperitoneally using 5% chloral hydrate at a dose of 400 mg/kg. Subsequently, the skin of the left knee was prepared and disinfected, at the anterior slope of the tibial plateau. A 1 ml syringe needle was used to rotate into the medullary cavity along the long axis of the tibia and long axis of the tibia and withdrawn. A 10 µl volume of RM-1 cells was injected slowly into the medullary cavity formed using a 100 µl microsyringe. After one week, if the volume of the tumor increased to about 80–100 mm^3, the mice were randomly divided into groups (5 mice/group). Subsequently, the mice received daily treatment with 0.5% carboxymethylcellulose (CMC)-NaCl (Yuanye Biotechnology, China) containing varying doses of ADA (15, 30, and 60 mg/kg) for 14 days Shi et al., 2015. The tumor growth was monitored every 3 days. Subsequently, the mice were anesthetized and sacrificed by cervical dislocation; the left leg tumors were removed, weighed, measured, and scanned using a micro-CT scanner, and subjected to histomorphological and immunohistochemical staining, and images were captured and analyzed using the Image J software. The tumor volume was computed using the equation $V = ab^2/2$ (a = longest axis; b = shortest axis).

Osteolytic Lesions and Architecture Assay

Osteolytic lesions and architecture were determined using the µCT system (SkyScan1072; Skyscan, Aartselaar, Belgium). Three-dimensional reconstructions were constructed and evaluated using the Skyscan NRecon and CTAn software (Bruker). For tibial specimens, a square region of interest was delineated near the bone growth plate for quantitative and qualitative analysis. For each tibia specimen, the morphometric bone parameters of trabecular spacing (Tb.Sp, mm), trabecular number (Tb.N, 1/

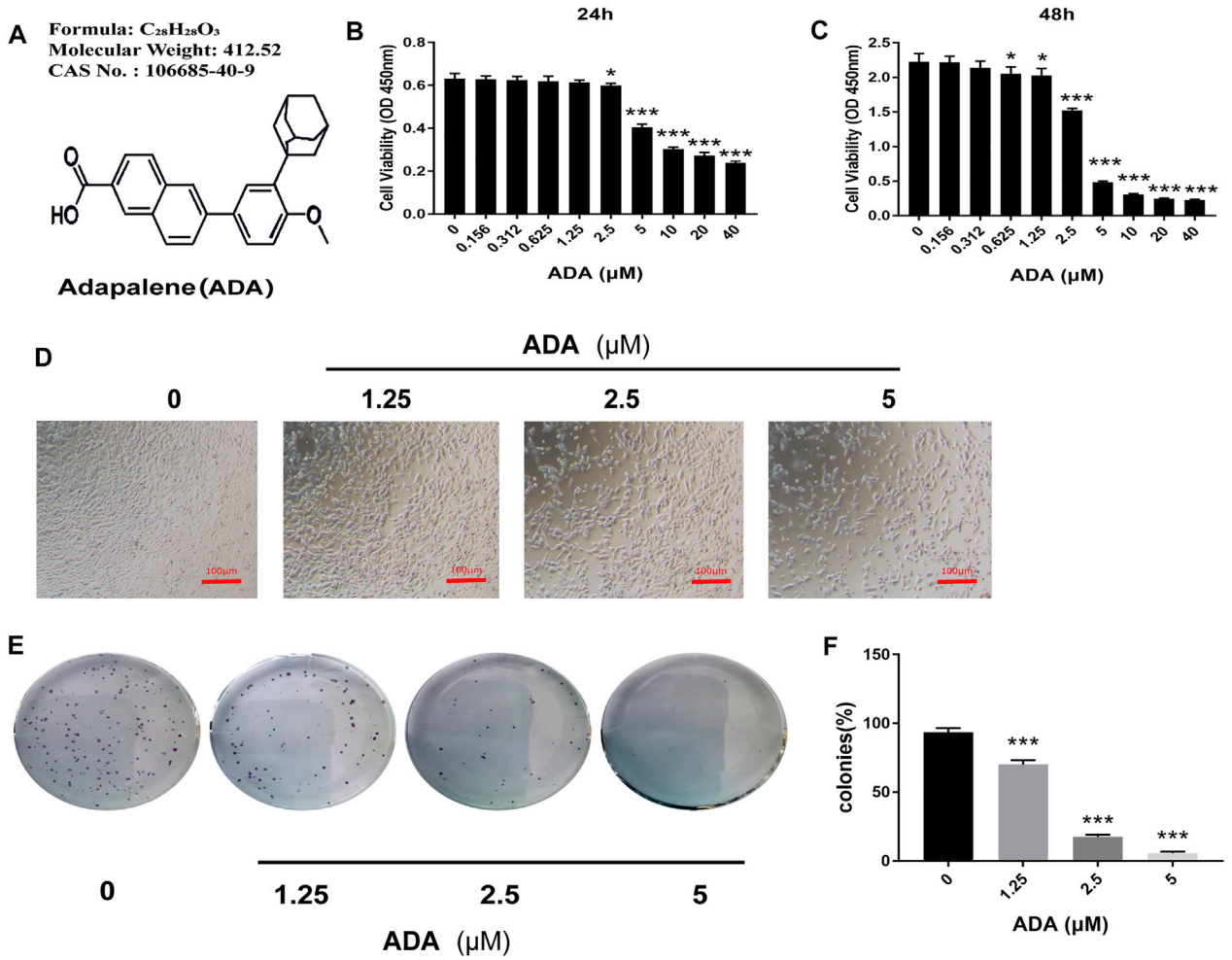

FIGURE 1 | ADA significantly suppressed the proliferation of RM-1 cells. **(A)** Molecular structure of ADA. **(B,C)** CCK8 assays were used to detect the effects of varying ADA concentrations (0–40 μM) on the proliferation of RM-1 cells and evaluated by CCK8 assays. **(D)** Following treatment of ADA for 24 h, the morphology of RM-1 cells was visualized and captured utilizing an inverted microscope (100×). **(E)** The long-term effects of ADA in RM-1 cells were detected by colony formation assays and the colonies were stained by 0.5% crystal violet solution and manually counted. **(F)** ADA significantly inhibited colony formation in a dosage-dependent way. Data are shown as mean ± standard deviation. (*$p < 0.05$; **$p < 0.01$; ***$p < 0.001$ vs. control)

mm), trabecular thickness (Tb.Th, mm), and bone volume to tissue volume (BV/TV, %) were measured.

Histomorphology and Immunohistochemical Analysis

The excised tumors were fixed in 4% paraformaldehyde, neutral polyformaldehyde, paraffin-embedded, dewaxed, sliced and subsequently stained using hematoxylin and eosin (H&E). The Ki-67 Immunohistochemistry Detection System Kit (Yaji Biological, Shanghai, China) was used to determine tumor cell proliferation in tissues. Tumor segments were subjected to incubation using primary antibody against Ki-67 at 4°C overnight. Subsequently, the tumor segments were incubated in the presence of horseradish peroxidase-conjugated secondary antibody for 30 min at ambient temperature and visualized using DAB Horseradish Peroxidase Chromogenic kit. Images were captured using a Zeiss microscope.

Tumor Tissue Apoptosis Analysis

To detect whether ADA induced tumor apoptosis, TUNEL staining was employed. The tumor segments were stained and incubated to allow the TUNEL reaction as per the instructions provided for the FITC-TUNEL cell apoptosis detection kit (Wuhan Servicebio Technology, Hubei, China). With the aid of an upright fluorescent microscope (Olympus BX53, Tokyo, Japan), the TUNEL-stained segments were examined and photographed. TUNEL-positive cells were quantified as a percentage of all cells in tumor tissue specimens from different cohorts.

Statistical Analysis

All data were analyzed the SPSS software (v22.0; IBM Corp) and are expressed as the mean ± SD of three replicates experiments. One-way analysis of variance was used to demonstrate the differences among the groups. Histograms were drawn and analyzed using the GraphPadPrism 7.0 software. p-value < 0.05 was considered statistically significant.

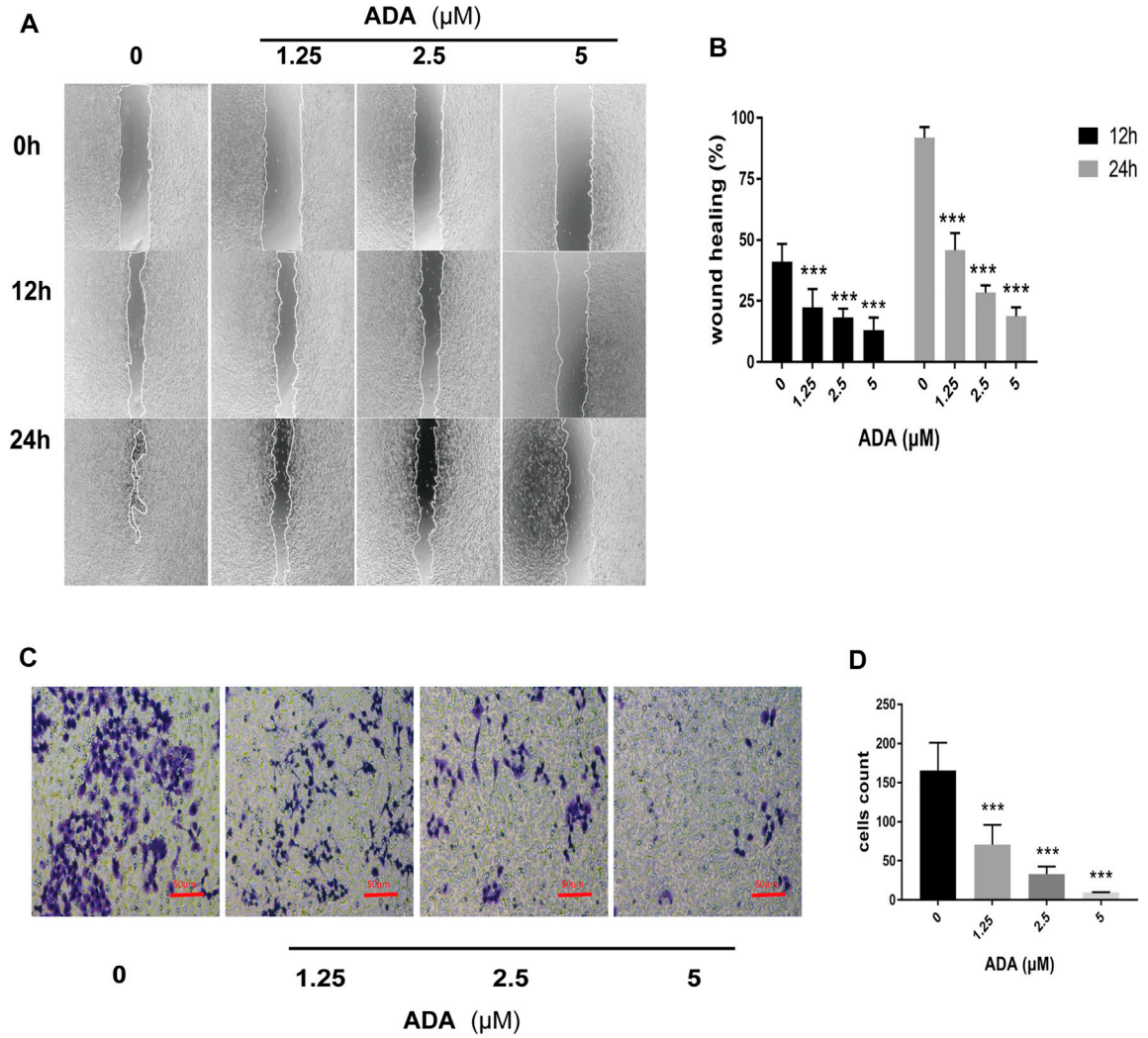

FIGURE 2 | ADA suppressed the migration and invasion of RM-1 cells. **(A,B)** The healing effect and migration of RM-1 cells was determined using the scratch test. After treatment with varying concentrations of ADA for 12 or 24 h, the degree of wound healing of the cells was measured (40×). **(C,D)** The ratio of invasion of RM-1 cells was further determined using Transwell assay. After treating cells with varying ADA concentrations for 24 h, the proportion of invaded cells was stained and calculated (200×), Data are articulated as mean ± standard deviation. (*$p < 0.05$, **$p < 0.01$,***$p < 0.001$ vs. control).

RESULT

Adapalene Inhibited the Proliferation of RM-1cells

To evaluate the anticancer properties of ADA in prostate cancer, RM-1 cells were treated with(0, 0.156, 0.312, 0.625, 1.25, 2.5, 5, 10, 20, and 40 μM) ADA for 24 and 48 h. CCK-8 assay of the treated cells revealed that ADA suppressed the proliferation and viability of RM-1 cells and that the inhibitory effect was proportional to the treatment time and dose (**Figures 1A–C**). The half-maximal inhibitory concentration (IC50) of ADA was approximately 8.23 μM for RM-1 cells at 24 h whereas 3.08 μM at 48 h. Furthermore, RM-1 cells showed dramatic morphological changes after treatment with ADA after 24 h—cell proliferation was inhibited and the number of dead cells was increased in a dose-dependent manner (**Figure 1D**). Colony formation assays were performed to further assess if ADA showed anti-proliferative effects on RM-1 cells in the long term. We found that ADA significantly inhibited the colony-forming ability of RM-1 cells in a dose-dependent manner (**Figures 1E,F**). These findings indicate that ADA has an anti-proliferation effect on RM-1 cells.

Adapalene Suppressed the Migration and Invasion of RM-1 Cells

The wound healing assay was used to determine the migration of RM-1 cells. We found that ADA significantly suppressed the migration ability of RM-1 cells and delayed wound healing time and ratio of acreage in a dose-dependent manner (**Figures 2A,B**). Furthermore, a Transwell assay was performed to determine the invasiveness of RM-1 cells. We found that ADA at high doses decreased the invasiveness of RM-1 cells (**Figures 2C,D**). Taken

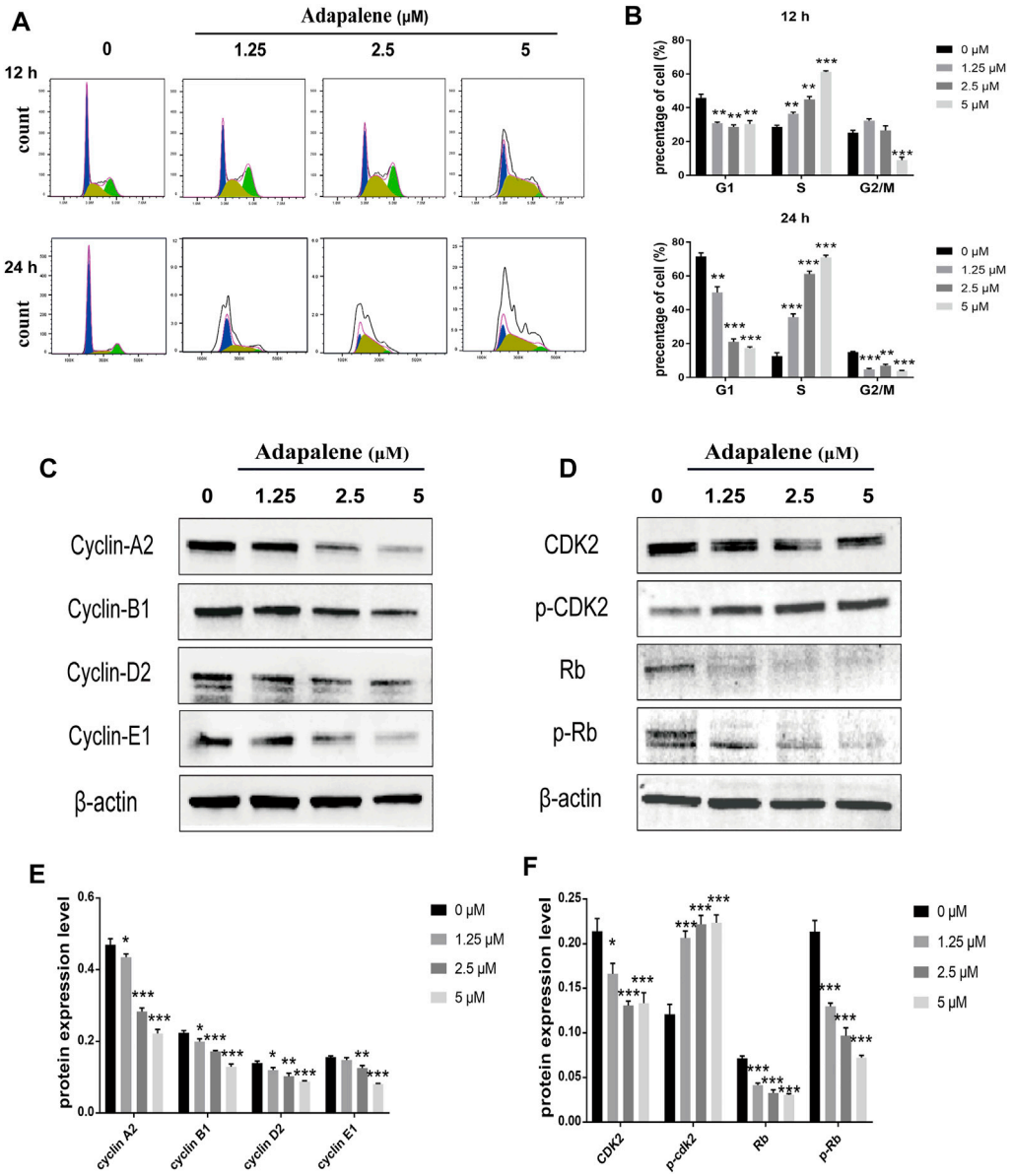

FIGURE 3 | Impacts of ADA on cell cycle distribution and expression of related proteins in RM-1 cells. RM-1 cells were treated using 1.25, 2.5, or 5 μM ADA for 12 or 24 h. **(A)** The proportion of cells in each cell cycle phase was evaluated utilizing flow cytometry. **(B)** Histograms showed quantitative data on the cell cycle distribution. **(C,D)** The protein expression of CDK2, P-CDK2, Cyclin A2, Cyclin B1, Cyclin D2, Cyclin E1, Rb, and P-Rb were detected by western blotting and **(E,F)** Histograms illustrated the expression of each protein, and β-actin acted as the loading control. The samples derive from the same experiment and that blots were processed in parallel. Data are articulated as mean ± standard deviation. (*$p < 0.05$; **$p < 0.01$; ***$p < 0.001$ vs. control).

together, these results indicated that ADA prevented further RM-1 cells migration and invasion.

Adapalene Induced Dramatic S Phase Arrest and Affected the S Phase-Related Proteins in RM-1 Cells

After treatment with ADA (0, 1.25, 2.5, and 5 μM) for 12 or 24 h, the percentage of cells in the S phase increased from 28.7% to 36.7%, 44.9%, and 61.2% in RM-1 cells after 12 h, respectively, and the percentage of cells in S phase increased from 12.6% to 35.5%, 61.1%, and 70.9% after 24 h, respectively (**Figures 3A,B**). associated proteins perform crucial functions in cell cycle progression in many tumors. Thus, to further explore the effects of ADA on the cell cycle, we assessed the expressions of cell cycle-related proteins in RM-1 cells by Western blotting. The results illustrated that ADA treatment considerably suppressed the expression of CDK2, Cyclin A2, Cyclin B1, Cyclin D2, Cyclin E1, Rb, and p-Rb in RM-1 cells at 24 h (**Figures 3C–F**), leading to S phase arrest in RM-1 cells.

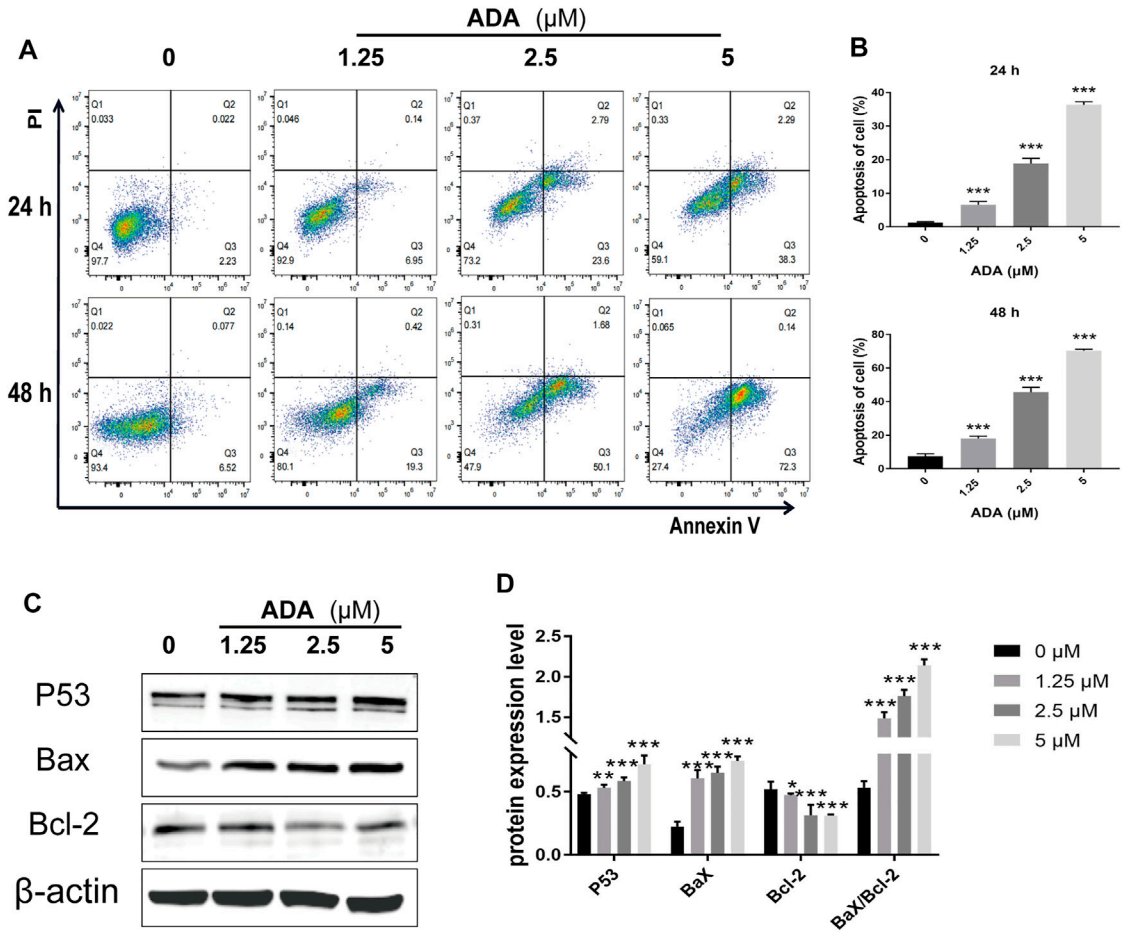

FIGURE 4 | ADA significantly induced apoptosis and regulated the expression of related proteins in RM-1 cells. RM-1 cells were treated with ADA (0, 1.25, 2.5, and 5 μM) for 24 or 48 h respectively. **(A)** Cell apoptosis was detected by Annexin V-APC/PI double staining. **(B)** Histograms showed the proportion of apoptosis cells by flow cytometry. **(C)** Bax, Bcl-2, and P53 protein expression was evaluated utilizing western blotting after 24 h, and **(D)** histograms showed quantitative protein analyzes and the Bax/Bcl-2 ratio β-actin acted as the loading control. The samples derive from the same experiment and that gels/blots were processed in parallel. Data are articulated as mean ± standard deviation. (*$p < 0.05$; **$p < 0.01$; ***$p < 0.001$ vs. control).

Adapalene Induces Apoptosis in RM-1 Cells

After treatment with ADA (0, 1.25, 2.5, and 5 μM) for 24 or 48 h, respectively, compared with the controls, the percentage of apoptotic cells increased from 2.23% to 6.95%, 23.6%, and 38.3% in RM-1 cells after 24 h, 6.52% to 19.3%, 50.1%, and 72.3% after 48 h (**Figures 4A,B**). Furthermore, we detected Bax and Bcl-2 activation by Western blotting analysis and found that ADA treatment elevated Bax and suppressed Bcl-2 expression, and upregulated the Bax/Bcl-2 ratio in RM-1 cells in a dose-dependent manner (**Figures 4C,D**). Therefore, ADA promoted apoptosis, which may be responsible for the antiproliferative effect induced in RM-1 cells.

Adapalene Induced Cell Cycle Arrest by Activating the DNA Damage/p53/p21 Pathway in RM-1 Cells

To assess the affect of ADA on cell DNA damage and repair, we assessed the expression of DNA damage, DNA repair, and cell cycle-related proteins by Western blotting in RM-1 cells following ADA treatment. The expression of γ-H2A.X, P-ATM, p53, and p21 in ADA-treated RM-1 cells was dramatically elevated in a dosage-dependent manner, and the expression of ATM, Cyclin A2, Cyclin E1, and CDK2 was lowered in a dose-dependent manner (**Figures 5A–D**). Above all, the findings illustrated that ADA mediated its anticancer effects through the activation of the DNA damage/p53/p21 pathway and inhibition of DNA repair may be due to the arrest of the cell cycle in RM-1 cells.

Adapalene Inhibited Tumor Growth and Inhibited Osteolytic Lesions *in vivo*

To confirm the anticancer effects of ADA *in vivo*, we used a bone metastasis mouse model for further studies. The mice were treated with varying doses of ADA (10, 30, and 60 mg/kg in 0.5% CMC-NaCl) by oral gavage each day for 14 days; all the mice survived till the end of the experiment. We found that tumor volume and weight reduced in mice treated with 30

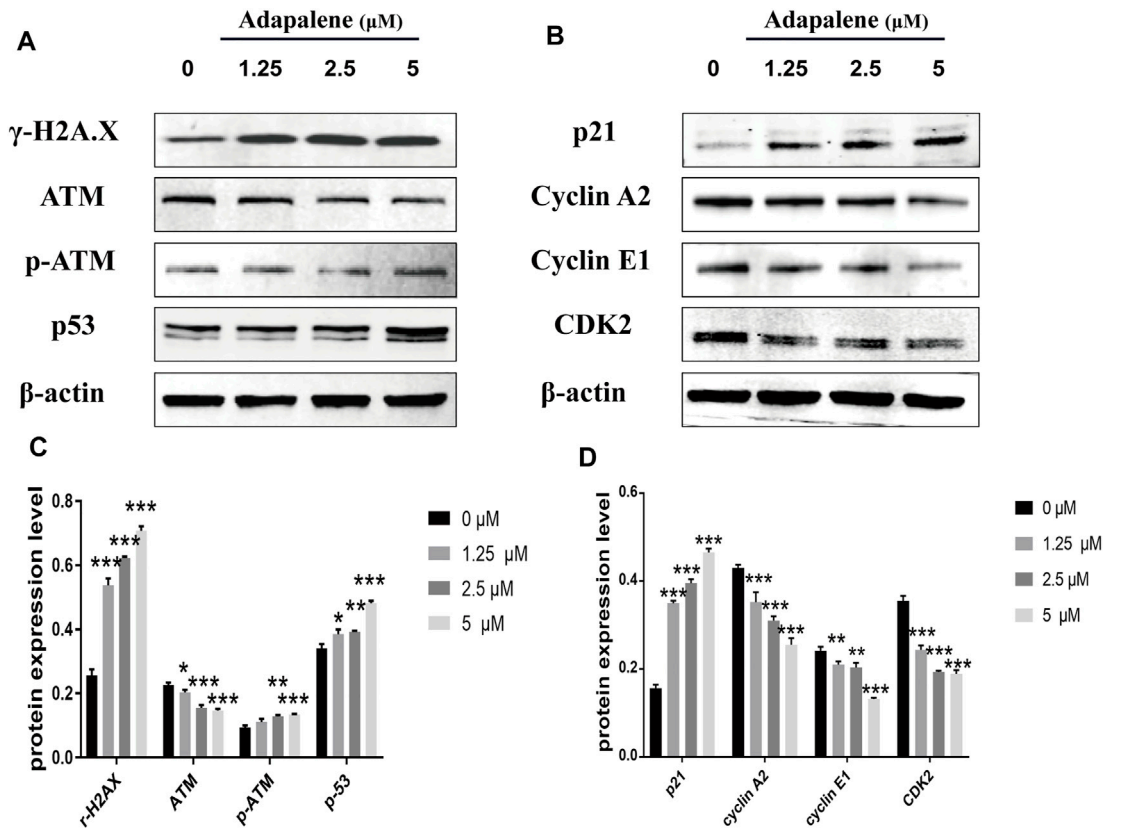

FIGURE 5 | ADA triggered a significant DNA damage pathway/p53/p21 in RM-1 cells. RM-1 cells were treated with the specified dosages of ADA for 24 h. **(A,B)** The protein expressions of γ-H2A.X, ATM, p-ATM, p53, p21, Cyclin A2, Cyclin E1, and CDK2 were analyzed by western blotting, and **(C,D)** histograms showed the protein quantitative analyses, and β-actin acted as the loading control. The samples derive from the same experiment and that gels/blots were processed in parallel. Data are articulated as mean ± standard deviation. (*$p < 0.05$; **$p < 0.01$; ***$p < 0.001$ vs. control).

and 60 mg/kg than in control mice, while mice treated with 10 mg/kg ADA showed no considerable difference from the control mice (**Figures 6A,B**). Areas of osteolytic lesions and architecture were determined using a high-resolution micro-CT scanner (**Figure 6C**). Morphometric parameters of the osteolytic lesions, including trabecular separation (Tb.Sp, mm), connectivity density (1/mm^3), trabecular thickness (Tb.Th, mm), trabecular number (Tb.N, 1/mm), and bone volume/tissue volume (BV/TV,%), were measured. We found that the microarchitectural bone parameters, namely, Tb.Th, Tb.N, and BV/TV,% was greater in mice treated with high doses of ADA(30 and 60 mg/kg) than in control mice, and the associated reduction in Tb.Sp was also detected in mice treated with high doses of ADA while no significant difference from control mice was found in mice receiving lower doses of ADA (**Figure 6D**). Furthermore, the tissue of bone tumor metastases was stained with H&E (**Figure 6E**). We found that in control mice, all trabecular bones were destroyed and the growth plate and bone marrow cavity were completely replaced by metastatic RM-1 cells. In contrast, ADA-treated mice showed reduced colonization of metastatic RM-1 prostate cancer cells and part of the trabecular bones remained intact.

Adapalene Inhibited the Expression of Ki-67 and Promoted Apoptosis in Mice Bone Metastasized With RM-1 Cells

The Ki-67 expression in tumor tissues was analyzed by immunohistochemical staining (**Figures 7A,B**). The expression of Ki-67 was greatly reduced in the tumor tissues of ADA-treated mice than in control mice. Further, the tumor tissues were stained by TUNEL staining (**Figure 7C**). The proportion of TUNEL-positive cells was substantially elevated in ADA-treated mice than in control mice (**Figure 7D**). Taken together, these findings indicate that ADA significantly inhibited the growth of RM-1 xenografts in mice and induced apoptosis in a dose-dependent manner in RM-1 prostate cancer cells.

DISCUSSION

Prostate cancer is the most malignant cancer of the male urinary tract and often presents with bone invasion and metastasis. ADA is a third-generation synthetic retinoid with anti-inflammatory and anti-cancer activity. In this study, we assessed the impact of ADA on the proliferation of the prostate cancer cell line RM-1.

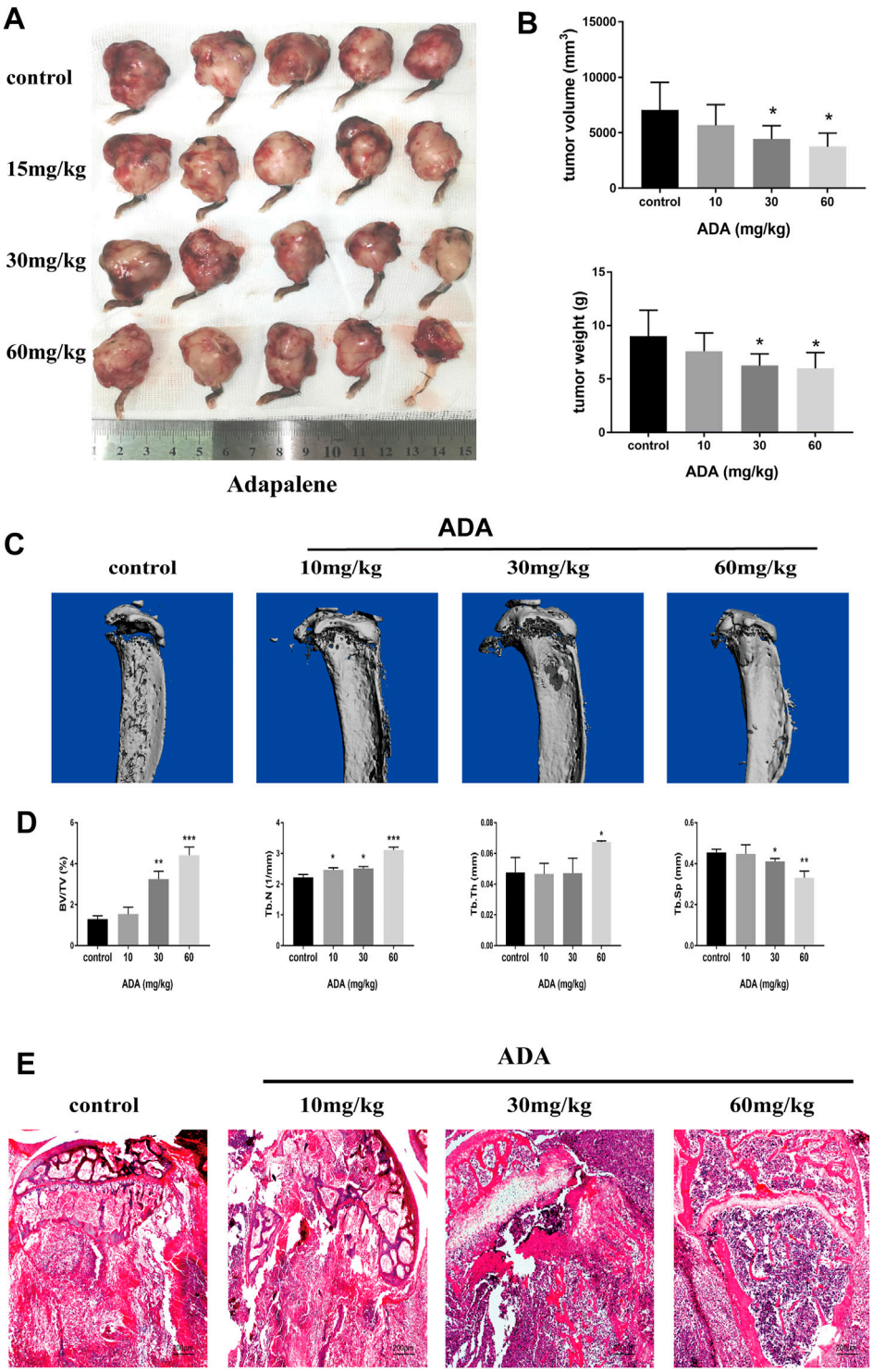

FIGURE 6 | ADA significantly suppressed tumor growth and osteolytic lesions in mice bone metastased with RM-1 cells. Bone metastasis mice were sacrificed after treatment following treatment with increasing doses of ADA (15, 30, and 60 mg/kg) for 14 days. **(A)** Tumors were measured and photographed at the end of treatment. **(B)** Analysis of tumor volume and weight. **(C)** The evaluation of osteolytic lesions and architecture were determined using a micro-CT scanner. **(D)** Statistical analysis of bone parameters in osteolytic lesions, including trabecular separation (Tb.Sp, mm), connectivity density ($1/mm^3$), trabecular thickness (Tb.Th, mm), trabecular number (Tb.N, 1/mm), and bone volume/tissue volume (BV/TV,%). **(E)** Bone tumor tissues were detected using Hematoxylin and eosin staining (100×). Data are articulated as mean ± standard deviation. (*$p < 0.05$; **$p < 0.01$; ***$p < 0.001$ vs. control).

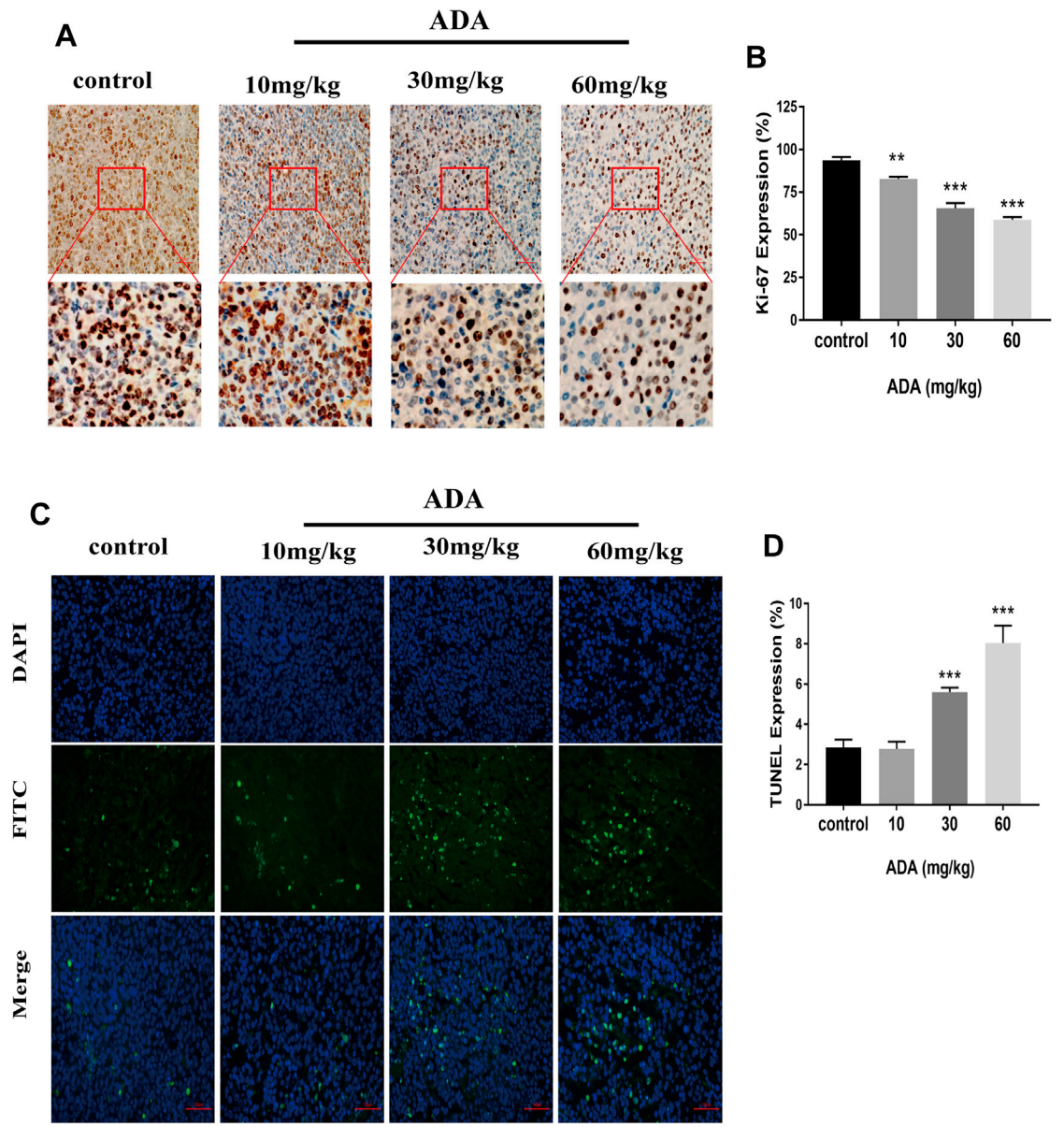

FIGURE 7 | ADA inhibited the Ki-67 expression and promotes the apoptosis of RM-1 prostate cancer cells in tumor tissues. **(A)** The expression of Ki-67 was analyzed by immunohistochemistry (IHC) staining (200×). **(B)** Histograms showing quantitative Ki-67 expression analyses. **(C)** The RM-1 cells were stained by TUNEL staining (400×). **(D)** Histograms showing the quantitative percentage of TUNEL-positive cells. Data are presented as mean ± standard deviation. (*$p < 0.05$; **$p < 0.01$; ***$p < 0.001$ vs. control).

Almost all tumors present the same characteristic of uncontrolled cell proliferation (Dick, 2008), and the objective of anti-tumor therapy is to suppress tumor cell proliferation and invasion and to promote tumor cell apoptosis. To confirm the anti-proliferative effects of ADA on RM-1 cells, CCK-8 analysis, colony formation, migration, and invasion assays were performed *in vitro*. As expected, the results of the CCK-8 analysis revealed that ADA suppressed the growth of RM-1 cells in a dose- as well as time-dependent manner. With time, ADA significantly inhibited the colony-forming ability of RM-1 cells. In addition, ADA also decreased the migration ability and invasiveness of RM-1 cells in a dose- and time-dependent manner. *In vivo* experiments in an RM-1 cell bone metastasis mouse model revealed that ADA effectively inhibited tumor size and weight. Furthermore, we found that ADA inhibited Ki-67 expression in tumor tissue in a dose-dependent manner. The morphometric analysis of microarchitectural bone parameters and tumor tissue by H&E staining revealed that ADA effectively inhibited bone destruction in mice. Taken together, the *in vivo* and *in vitro* studies indicated that ADA effectively inhibited the proliferation of RM-1 cells.

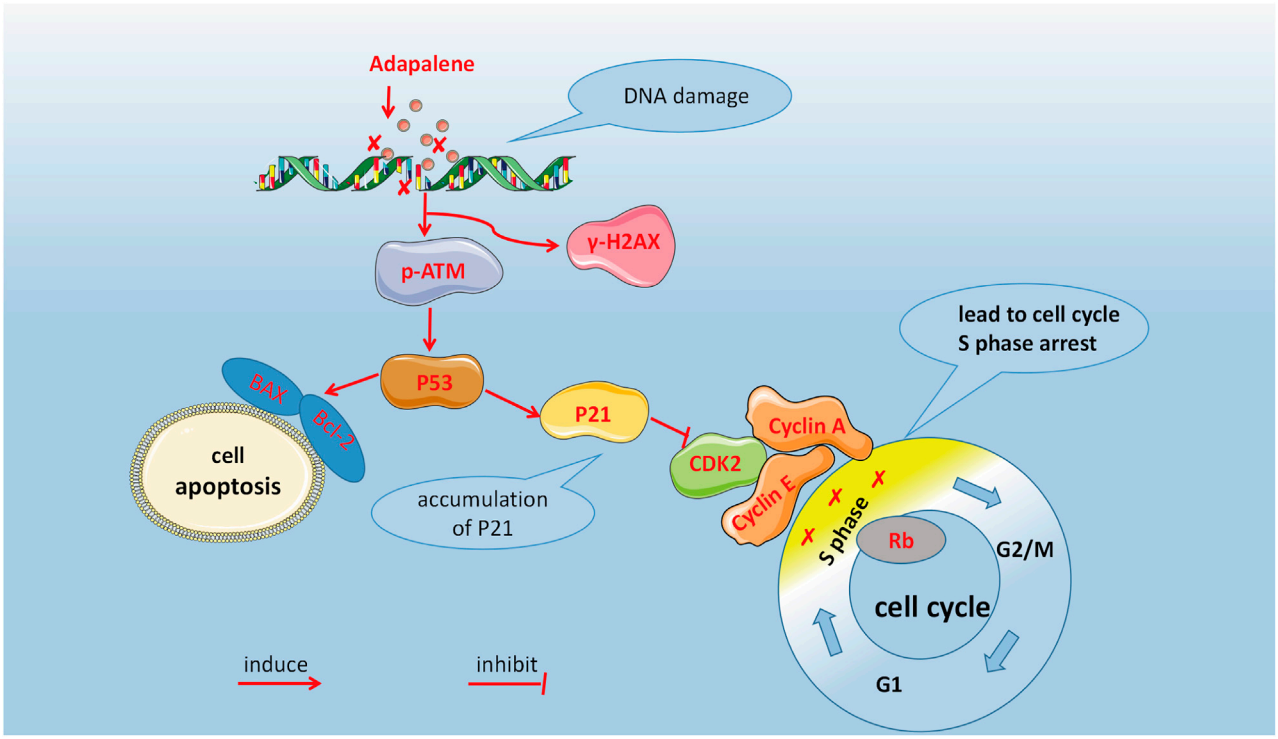

FIGURE 8 | Anticancer mechanism of ADA in RM-1 cells.

According to several studies, ADA was involved in cell cycle arrest by regulating cell cycle independent kinase (CDK). For instance, ADA inhibits the melanoma cells proliferation by arresting the S phase and subsequently inducing apoptosis caused by DNA damage (Li et al., 2019). ADA has also been shown to suppress the growth of colorectal cancer cells by inhibiting the activity of CDK2 (Ocker et al., 2004; Shi et al., 2015). CDK2 is a significant target for cancer therapy (Roskoski, 2019). CDK2 with its binding partners performs a critical function throughout the cell cycle progression (Bertoli et al., 2013). The CDK2 complexes with cyclin E or cyclin A and is necessary for the initiation and progression of the S phase, and the CDK1 complexes with cyclin A or cyclin B are essential for cell mitosis (Malumbres and Barbacid, 2009). CDK2 can drive the cell cycle into the S phase and initiate replication; CDK2 activity increases with cell entry into the G2 phase and the S phase (Spencer et al., 2013). During phase transition from G1- to S-phase, the cyclin partners switch from cyclin E to CyclinA, and the CyclinE-CDK2 and CyclinD1-CDK4 complexes are activated sequentially and Rb is hyper-phosphorylated (Cobrinik, 2005; Ditano et al., 2021). In this study, we investigated cell cycle distribution by flow cytometry and found that ADA induced S phase arrest in RM-1 cells after ADA treatment. We also assessed the expression of cell cycle-related proteins in RM-1 cells and found that ADA triggered S-phase arrest in RM-1 cells by inhibiting CDK2, Cyclin A2, Cyclin E1, Rb, and P-Rb at 24 h. During the transition from the G1- to S-phase, CDK2, Cyclin A2, Cyclin E1, Rb, and P-Rb play a significant role. Therefore, the reduced activity of CDK2/Cyclin A2 that drives entry into the G2 phase from the S-phase, and CDK2/Cyclin E1 and Cyclin A2 downregulation eventually caused the cell cycle arrest in the S-phase.

In addition, we found that ADA induced S phase arrest while promoting apoptosis in RM-1 cells. The percentage of cells arrested in the S-phase increased 44.9% (12 h) and 70.9%(24 h) after treatment with ADA (5 μM), the percentage of apoptotic cells only increased to 38.3% at 24 h but 72.3% at 48 h. The percentage of cell arrest increased at first, subsequently, the percentage of apoptosis increased. Therefore, we postulated that S-phase cell cycle arrest might be a reason for inducing apoptosis after prolonged ADA treatment. ADA also induced up-regulation of the expression of Bax/Bcl-2 as p53 expression increased. Apoptosis is a process of cellular suicide, which usually responds to growth hormone or cytokine exposure, factor deprivation, and DNA damage (Sharma et al., 2012). Some Bcl-2 family members including Bak and Bax are activated by p53, while Bcl-2 is inhibited by p53 (Tang et al., 2021). Previous studies have shown that ADA possesses anti-proliferative and pro-apoptotic function in colon carcinoma and hepatoma cell lines by increasing caspase-3 activity by increasing Bax and reducing Bcl2 expression (Ocker et al., 2003; Ocker et al., 2004). In addition, the p53/p21 complex modulates the invasion as well as apoptosis of cancer cells by targeting Bcl-2 family proteins (Kim et al., 2017). Herein, ADA significantly promoted the expression of p53, and thereby promoted the Bax expression and suppressed the Bcl-2 expression, positively regulating the

alteration in the Bax/Bcl-2 ratio, leading to the induction of RM-1 cell apoptosis. Furthermore, TUNEL staining illustrated that the proportion of TUNEL-positive cells was considerably elevated after ADA treatment. Therefore, our study suggests that ADA effectively inhibited proliferation and triggered apoptosis in RM-1 cells.

The fate of cells is determined by the dynamic equilibrium between DNA damage and repair. DNA is vulnerable to environmental and dietary carcinogens, endogenous metabolites, anti-inflammatory drugs, and genotoxic cancer drugs (Roos et al., 2016). The induction of DNA damage activates either interim checkpoints that facilitate the genetic repair or nonreversible growth arrest that leads to cell necrosis and apoptosis (Krüger et al., 2018). Thus, activation of checkpoints encompasses a comprehensive response involving sensors (ATM, CHK, BRCA, and RAD) and effectors (p53, p21, CDK) (Pawlik and Keyomarsi, 2004; He et al., 2005; Wang, 2019). As reports showed that the rapid phosphorylation of H2AX at ser139 (a biomarker of DNA damage) was triggered by ATM in the presence of DNA damage, which is necessary for recruiting DNA-damage response proteins (Tanaka et al., 2006; Yuan et al., 2010). We observed that the expression of P-ATM and γ-H2AX increased significantly in RM-1 cells after ADA treatment, indicating that DNA damage was induced. Consequently, the continuous increase in DNA damage may have induced S-phase arrest of the cell cycle and subsequent cell apoptosis.

P21 is encoded by the CDKN1A gene and has been identified as a CDK regulator that participates in a variety of cell functions, such as cell cycle progression, DNA damage, and cell growth (Lee et al., 1998). As the main inhibitor of CDK2, p21 can arrest the G1/S phase of the cell cycle and inhibit the phosphorylation of retinoblastoma protein (Rb) (Cheng and Scadden, 2002). Thus, p21 is also called CDK-interaction protein (CIP1) or CDKN1A (p21) (Gartel and Radhakrishnan, 2005). p53 tumor suppressor/transcription factor regulates multiple cellular functions, including cell growth, migration, invasion, apoptosis, and aging (Muller et al., 2011). p21 inhibits the growth of tumors by targeting p53, and interaction between p21 and proliferating cell nuclear antigen maintains cell cycle arrest after DNA damage (Xiao et al., 2020). In addition, elevated levels of p21 result in a delay of S phase progression and cell mitosis (Moniaux et al., 2020). We found that the levels of p53 and p21 gradually increased in ADA-treated cells in a dose- and time-dependent manner. In contrast, the expression of CDK2, Rb, and p-Rb, the downstream molecules of p21, decreased gradually with the increase in p21 expression, suggesting that ADA promoted the expression of p21 through a p53-dependent pathway, which may represent the mechanism of action of ADA in prostate cancer treatment.

There are some deficiencies in our research. Although many biological functions and behavior of RM-1 cells with prostate cancer model are close to human cells (Li et al., 2021), our results can not completely represent the effects of ADA in human prostate cancer cells, and further research should be combined with human prostate cancer cell experiments in the future.

In summary, our study showed that ADA inhibits prostate cancer cell proliferation *in vivo* and *in vitro*. As shown in **Figure 8**, DNA damage activated the ATM/p53/p21 signaling and arrested cell cycle in the S-phase by suppressing CDK2 levels, as well as induced apoptosis by regulating the Bax/Bcl-2 ratio. In conclusion, ADA controls the growth and proliferation of prostate cancer cells likely by inducing DNA damage. Therefore, ADA may be a prospective therapeutic agent for treating prostate cancer.

DATA AVAILABILITY STATEMENT

The original contributions presented in the study are included in the article/**Supplementary Material**, further inquiries can be directed to the corresponding authors

ETHICS STATEMENT

The animal study was reviewed and approved by The Animal Care and Welfare Committee of Guangxi Medical University.

AUTHOR CONTRIBUTIONS

Study concept and design: S-HZ and G-fZ; Data analysis and drafting of the original manuscript: H-bN, Y-nZ, Y-gB; Data collection, analysis, and the manuscript reviewing: QiZ, M-fL, Z-hS, QuZ. All authors reviewed and approved the final manuscript.

FUNDING

These studies were funded by the National Natural Science Foundation of China, No. 81860391 (to G-fZ), Guangxi Medical High-level Key Talents Training "139" Program Training Project and Guangxi Special Foundation "Ten, Hundred, Thousand" Talents Project.

ACKNOWLEDGMENTS

The authors would like to greatly thank the basic laboratory of Guangxi Medical University and the High-Level Innovation Team and the Excellence Scholars Program of Guangxi High Education Institutions, for their support, which was fundamental to the realization of this work.

SUPPLEMENTARY MATERIAL

The Supplementary Material for this article can be found online at: https://www.frontiersin.org/articles/10.3389/fphar.2022.801624/full#supplementary-material

REFERENCES

Bertoli, C., Skotheim, J. M., and de Bruin, R. A. (2013). Control of Cell Cycle Transcription during G1 and S Phases. *Nat. Rev. Mol. Cel Biol* 14 (8), 518–528. doi:10.1038/nrm3629

Carlin, B. I., and Andriole, G. L. (2000). The Natural History, Skeletal Complications, and Management of Bone Metastases in Patients with Prostate Carcinoma. *Cancer* 88 (12 Suppl. l), 2989–2994. doi:10.1002/1097-0142(20000615)88:12+<2989::aid-cncr14>3.3.co;2-h

Cheng, T., and Scadden, D. T. (2002). Cell Cycle Entry of Hematopoietic Stem and Progenitor Cells Controlled by Distinct Cyclin-dependent Kinase Inhibitors. *Int. J. Hematol.* 75 (5), 460–465. doi:10.1007/bf02982107

Cobrinik, D. (2005). Pocket Proteins and Cell Cycle Control. *Oncogene* 24 (17), 2796–2809. doi:10.1038/sj.onc.1208619

Cornford, P., Bellmunt, J., Bolla, M., Briers, E., De Santis, M., Gross, T., et al. (2017). EAU-ESTRO-SIOG Guidelines on Prostate Cancer. Part II: Treatment of Relapsing, Metastatic, and Castration-Resistant Prostate Cancer. *Eur. Urol.* 71 (4), 630–642. doi:10.1016/j.eururo.2016.08.002

Dick, J. E. (2008). Stem Cell Concepts Renew Cancer Research. *Blood* 112 (13), 4793–4807. doi:10.1182/blood-2008-08-077941

Ditano, J. P., Sakurikar, N., and Eastman, A. (2021). Activation of CDC25A Phosphatase Is Limited by CDK2/cyclin A-Mediated Feedback Inhibition. *Cell Cycle* 20 (13), 1308–1319. doi:10.1080/15384101.2021.1938813

Gao, W., Su, X., Dong, X., Chen, Y., Zhou, C., Xin, P., et al. (2015). Cycloartan-24-ene-1α,2α,3β-triol, a Cycloartane-type Triterpenoid from the Resinous Exudates of Commiphora Myrrha, Induces Apoptosis in Human Prostatic Cancer PC-3 Cells. *Oncol. Rep.* 33 (3), 1107–1114. doi:10.3892/or.2015.3725

Gartel, A. L., and Radhakrishnan, S. K. (2005). Lost in Transcription: P21 Repression, Mechanisms, and Consequences. *Cancer Res.* 65 (10), 3980–3985. doi:10.1158/0008-5472.Can-04-3995

He, G., Siddik, Z. H., Huang, Z., Wang, R., Koomen, J., Kobayashi, R., et al. (2005). Induction of P21 by P53 Following DNA Damage Inhibits Both Cdk4 and Cdk2 Activities. *Oncogene* 24 (18), 2929–2943. doi:10.1038/sj.onc.1208474

Kim, E. M., Jung, C. H., Kim, J., Hwang, S. G., Park, J. K., and Um, H. D. (2017). The P53/p21 Complex Regulates Cancer Cell Invasion and Apoptosis by Targeting Bcl-2 Family Proteins. *Cancer Res.* 77 (11), 3092–3100. doi:10.1158/0008-5472.CAN-16-2098

Krüger, K., Geist, K., Stuhldreier, F., Schumacher, L., Blümel, L., Remke, M., et al. (2018). Multiple DNA Damage-dependent and DNA Damage-independent Stress Responses Define the Outcome of ATR/Chk1 Targeting in Medulloblastoma Cells. *Cancer Lett.* 430, 34–46. doi:10.1016/j.canlet.2018.05.011

Lee, C. W., Sørensen, T. S., Shikama, N., and La Thangue, N. B. (1998). Functional Interplay between P53 and E2F through Co-activator P300. *Oncogene* 16 (21), 2695–2710. doi:10.1038/sj.onc.1201818

Li, C. Y., Chen, C. Y., An, J. H., Wu, J. B., and Shen, H. (2021). Normal Basal Epithelial Cells Stimulate the Migration and Invasion of Prostate Cancer Cell RM-1 by TGF-B1/stat3 Axis *In Vitro*. *Cancer Manag. Res.* 13, 3685–3697. doi:10.2147/cmar.S303122

Li, H., Wang, C., Li, L., Bu, W., Zhang, M., Wei, J., et al. (2019). Adapalene Suppressed the Proliferation of Melanoma Cells by S-phase Arrest and Subsequent Apoptosis via Induction of DNA Damage. *Eur. J. Pharmacol.* 851, 174–185. doi:10.1016/j.ejphar.2019.03.004

Li, Y., He, N., and Zhai, C. (2015). Peperotetraphin Inhibits the Proliferation of Human Prostate Cancer Cells via Induction of Cell Cycle Arrest and Apoptosis. *Med. Oncol.* 32 (2), 468. doi:10.1007/s12032-014-0468-8

Malumbres, M., and Barbacid, M. (2009). Cell Cycle, CDKs and Cancer: a Changing Paradigm. *Nat. Rev. Cancer* 9 (3), 153–166. doi:10.1038/nrc2602

Millikan, L. E. (2010). Adapalene: an Update on Newer Comparative Studies between the Various Retinoids. *Int. J. Dermatol.* 39 (10), 784–788. doi:10.1046/j.1365-4362.2000.00050.x

Moniaux, N., Lacaze, L., Gothland, A., Deshayes, A., Samuel, D., and Faivre, J. (2020). Cyclin-dependent Kinase Inhibitors P21 and P27 Function as Critical Regulators of Liver Regeneration Following 90% Hepatectomy in the Rat. *World J. Hepatol.* 12 (12), 1198–1210. doi:10.4254/wjh.v12.i12.1198

Muller, P. A., Vousden, K. H., and Norman, J. C. (2011). p53 and its Mutants in Tumor Cell Migration and Invasion. *J. Cel Biol* 192 (2), 209–218. doi:10.1083/jcb.201009059

Ocker, M., Herold, C., Ganslmayer, M., Hahn, E. G., and Schuppan, D. (2003). The Synthetic Retinoid Adapalene Inhibits Proliferation and Induces Apoptosis in Colorectal Cancer Cells *In Vitro*. *Int. J. Cancer* 107 (3), 453–459. doi:10.1002/ijc.11410

Ocker, M., Herold, C., Ganslmayer, M., Zopf, S., Hahn, E. G., and Schuppan, D. (2004). Potentiated Anticancer Effects on Hepatoma Cells by the Retinoid Adapalene. *Cancer Lett.* 208 (1), 51–58. doi:10.1016/j.canlet.2003.12.026

Pawlik, T. M., and Keyomarsi, K. (2004). Role of Cell Cycle in Mediating Sensitivity to Radiotherapy. *Int. J. Radiat. Oncol. Biol. Phys.* 59 (4), 928–942. doi:10.1016/j.ijrobp.2004.03.005

Roos, W. P., Thomas, A. D., and Kaina, B. (2016). DNA Damage and the Balance between Survival and Death in Cancer Biology. *Nat. Rev. Cancer* 16 (1), 20–33. doi:10.1038/nrc.2015.2

Roskoski, R., Jr. (2019). Cyclin-dependent Protein Serine/threonine Kinase Inhibitors as Anticancer Drugs. *Pharmacol. Res.* 139, 471–488. doi:10.1016/j.phrs.2018.11.035

Rusu, A., Tanase, C., and Pascu, G. A. (2020). Recent Advances Regarding the Therapeutic Potential of Adapalene. *Pharmaceuticals (Basel)* 13 (9). doi:10.3390/ph13090217

Sharma, A., Singh, K., and Almasan, A. (2012). Histone H2AX Phosphorylation: a Marker for DNA Damage. *Methods Mol. Biol.* 920, 613–626. doi:10.1007/978-1-61779-998-3_40

Shi, X. N., Li, H., Yao, H., Liu, X., Li, L., Leung, K. S., et al. (2015). Adapalene Inhibits the Activity of Cyclin-dependent Kinase 2 in Colorectal Carcinoma. *Mol. Med. Rep.* 12 (5), 6501–6508. doi:10.3892/mmr.2015.4310

Simoni, D., and Tolomeo, M. (2001). Retinoids, Apoptosis and Cancer. *Curr. Pharm. Des.* 7 (17), 1823–1837. doi:10.2174/1381612013397168

Spencer, S. L., Cappell, S. D., Tsai, F. C., Overton, K. W., Wang, C. L., and Meyer, T. (2013). The Proliferation-Quiescence Decision Is Controlled by a Bifurcation in CDK2 Activity at Mitotic Exit. *Cell* 155 (2), 369–383. doi:10.1016/j.cell.2013.08.062

Sung, H., Ferlay, J., Siegel, R. L., Laversanne, M., Soerjomataram, I., Jemal, A., et al. (2021). Global Cancer Statistics 2020: GLOBOCAN Estimates of Incidence and Mortality Worldwide for 36 Cancers in 185 Countries. *CA Cancer J. Clin.* 71 (3), 209–249. doi:10.3322/caac.21660

Tanaka, T., Halicka, H. D., Traganos, F., and Darzynkiewicz, Z. (2006). Phosphorylation of Histone H2AX on Ser 139 and Activation of ATM during Oxidative Burst in Phorbol Ester-Treated Human Leukocytes. *Cell Cycle* 5 (22), 2671–2675. doi:10.4161/cc.5.22.3472

Tang, D. G., and Porter, A. T. (1997). Target to Apoptosis: a Hopeful Weapon for Prostate Cancer. *Prostate* 32 (4), 284–293. doi:10.1002/(sici)1097-0045(19970901)32:4<284::aid-pros9>3.0.co;2-j

Tang, J. F., Li, G. L., Zhang, T., Du, Y. M., Huang, S. Y., Ran, J. H., et al. (2021). Homoharringtonine Inhibits Melanoma Cells Proliferation *In Vitro* and Vivo by Inducing DNA Damage, Apoptosis, and G2/M Cell Cycle Arrest. *Arch. Biochem. Biophys.* 700, 108774. doi:10.1016/j.abb.2021.108774

Wang, J. Y. J. (2019). Cell Death Response to DNA Damage. *Yale J. Biol. Med.* 92 (4), 771–779.

Wang, Q., Zhang, Q., Luan, S., Yang, K., Zheng, M., Li, K., et al. (2019). Adapalene Inhibits Ovarian Cancer ES-2 Cells Growth by Targeting Glutamic-Oxaloacetic Transaminase 1. *Bioorg. Chem.* 93, 103315. doi:10.1016/j.bioorg.2019.103315

Xiao, B. D., Zhao, Y. J., Jia, X. Y., Wu, J., Wang, Y. G., and Huang, F. (2020). Multifaceted P21 in Carcinogenesis, Stemness of Tumor and Tumor Therapy. *World J. Stem Cell* 12 (6), 481–487. doi:10.4252/wjsc.v12.i6.481

Yuan, J., Adamski, R., and Chen, J. (2010). Focus on Histone Variant H2AX: to Be or Not to Be. *FEBS Lett.* 584 (17), 3717–3724. doi:10.1016/j.febslet.2010.05.021

Conflict of Interest: The authors declare that the research was conducted in the absence of any commercial or financial relationships that could be construed as a potential conflict of interest.

frontiers | Frontiers in Oncology

ORIGINAL RESEARCH
published: 08 April 2022
doi: 10.3389/fonc.2022.819003

CDK6 Immunophenotype Implicates Potential Therapeutic Application of CDK4/6 Inhibitors in Urothelial Carcinoma

Ran Sun[1†], Xuemei Wang[2†], Leichao Zhang[2], Yu Gu[2], Shaojuan Yang[2], Liping Wang[2] and Xueju Wang[2]*

[1] Center for Reproductive Medicine, China-Japan Union Hospital, Jilin University, Changchun, China, [2] Department of Pathology, China-Japan Union Hospital, Jilin University, Changchun, China

OPEN ACCESS

Edited by:
Andrea Cavazzoni, University of Parma, Italy

Reviewed by:
Rosalyn Adam, Boston Children's Hospital and Harvard Medical School, United States
Albert Font, Institut Català d'Oncologia (ICO), Spain

***Correspondence:**
Xueju Wang
xueju@jlu.edu.cn

[†]These authors share first authorship

Specialty section:
This article was submitted to Pharmacology of Anti-Cancer Drugs, a section of the journal Frontiers in Oncology

Received: *20 November 2021*
Accepted: *26 January 2022*
Published: *08 April 2022*

Citation:
Sun R, Wang X, Zhang L, Gu Y, Yang S, Wang L and Wang X (2022) CDK6 Immunophenotype Implicates Potential Therapeutic Application of CDK4/6 Inhibitors in Urothelial Carcinoma. Front. Oncol. 12:819003. doi: 10.3389/fonc.2022.819003

Background: Infiltrating bladder urothelial carcinoma is the most common bladder malignancy with limited therapeutic options and poor prognosis. Identifying new therapeutic targets or strategies has important clinical significance. The data from public sources indicate poor prognosis in urothelial carcinoma cases with high CDK6 mRNA levels. Furthermore, studies have shown that CDK6 expression is elevated in urothelial carcinoma tissue compared to the surrounding urothelium, thus presenting a case for performing CDK4/6 inhibitor targeted research in urothelial carcinoma. However, a phase II trial showed that CDK4/6 inhibitors are not effective for advanced urothelial carcinoma, suggesting that case screening is important for targeted therapy.

Objective: Immunohistochemistry (IHC) is simple and easy to perform and can be used to screen urothelial carcinoma cases with high CDK6 expression in clinical practice. The aim of this study was to determine the CDK6 expression threshold for positive cases.

Methods: We evaluated the correlation between the H-score of CDK6 protein expression and survival or CDK6 mRNA level using RNA sequencing. The effects of different CDK4/6 inhibitors were tested on bladder carcinoma cell lines with different CDK6 expression levels.

Results: The H-score, which predicts poor prognosis and reflects a high CDK6 mRNA level, was determined as the selection criterion for positive cases. Furthermore, we found that urothelial carcinoma cell lines with higher CDK6 expression levels displayed greater sensitivity to CDK4/6 inhibitors than cells with lower expression levels.

Conclusions: IHC staining for CDK6 protein in urothelial carcinoma is proposed as a promising screening platform for CDK4/6 inhibitor targeted therapy.

Keywords: CDK6, urothelial carcinoma, CDK4/6 inhibitor, precision medicine, immunohistochemistry staining

INTRODUCTION

Infiltrating urothelial carcinoma is the most common bladder carcinoma (BLCA), with limited therapeutic options and poor prognosis (1). Conventional BLCA is typically divided into low- and high-grade lesions, depending on the architecture disorder, nuclear pleomorphism, and pathological mitoses. High-grade invasive BLCA presents remarkable diversity in morphological features, such as a wide range of architectural patterns, variegated cytological changes, and more aggressive behavior than low-grade counterparts. Approximately one-fourth of high-grade BLCA cases are accompanied by histological variants, such as squamous, nested, or plasmacytoid differentiation (2). Although several histological variants of BLCA are listed in the 2016 World Health Organization classification of urothelial tract tumors (3, 4), there remains controversial evidence on the influence of these histological variants on the prognosis and response to BLCA treatment because of the limited number of cases involved (2, 4). Furthermore, an increasing number of molecular subtypes have been defined in BLCA; basal and luminal subtypes are the most stably accepted subtypes and display the upregulation of KRT5, KRT6, or GATA3 genes, and it is well known that BLCA with basal subtypes predicts worse prognosis (5).

Cell cycle progression is promoted by CDK6 through interaction with D-type cyclins to phosphorylate the retinoblastoma tumor suppressor and displays oncogenic potency by kinase activity in several types of malignant tumors (6–8). A study involving 31 urothelial carcinoma cases showed higher CDK6 expression levels in the BLCA tissues than in adjacent non-neoplastic tissues (9), suggesting that CDK6 could be a potential therapeutic target for urothelial carcinoma. CDK4/6 inhibitors have been approved by the US Food and Drug Administration for the treatment of postmenopausal women with advanced breast cancer (10) and have been involved in the clinical trial of several solid tumors and lymphomas (11). Research has shown that CDK4/6 inhibitors are active as a novel therapeutic approach *in vitro* and *in vivo* in bladder cancer cells (12). However, a phase II clinical trial showed that the CDK4/6 inhibitor palbociclib does not demonstrate meaningful activity in 12 selected patients with platinum-refractory metastatic urothelial carcinoma (13). In this study, cases with p16 loss and Rb intact immunophenotype were included, CDK6 expression levels were ignored (13). Actually, independent of kinase activity, CDK6 also demonstrate transcriptional regulation activity in malignant tumor (14). Thus, it is imperative to explore the relationship between CDK6 expression and therapeutic options in BLCA.

We investigated the Cancer Genome Atlas (TCGA) and GEO databases and found that high CDK6 transcriptional levels were correlated with poor prognosis, and more frequently accumulated in muscle-invasive bladder cancer (MIBC) than in non-muscle-invasive bladder cancer (NMIBC) cases. Thus, it is worthwhile to evaluate CDK6 gene expression in BLCA cases for the potential application of CDK4/6 inhibitor target therapy. The evaluation of mRNA levels is relatively more expensive and time-consuming than immunohistochemistry (IHC) staining in clinical practice (15, 16). Both increased cytoplasmic and nuclear distributions of CDK6 protein are observed in several solid tumors by IHC method. In these studies, nuclear distribution of CDK6 protein is more objectively evaluated than cytoplasmic distribution to associate with unfavorable prognosis (7, 9, 17). The goal of this study was to establish a screening platform by IHC staining of CDK6 protein to predict prognosis and potential opportunities for CDK4/6 inhibitor treatment in BLCA.

MATERIALS AND METHODS

Study Design

Eighty-five patients diagnosed as primary BLCA by transurethral resection or radical cystectomy or cystoprostatectomy from June 2010 to June 2014 at the China-Japan Union Hospital of Jilin University (Changchun City, Jilin Province, People's Republic of China), were retrospectively selected for the study. Related clinicopathological information was obtained by an investigator blinded to the other results. Histological grading was briefly classified as low-grade or high-grade. *In situ* cancer should display a high-grade morphology. Cancer staging was performed according to the American Joint Committee on Cancer 8th Edition manual. Detailed clinicopathological descriptions of all cases are presented in **Table 1**. Formalin-fixed and paraffin-embedded (FFPE) specimens of 85 patients were used for IHC studies, of which 22 fresh frozen tissue samples stored immediately at −80°C in a tissue bank were used for RNA sequencing experiments. This study was approved by the Institutional Medical Ethics Review Board of the China-Japan Union Hospital of Jilin University in compliance with the Declaration of Helsinki. The reference number was 2021-KYLL-030003. All patients gave informed written consent for the provision of a tumor sample.

Analysis of GEO and TCGA Databases

The gene expression profile of GSE13507 was downloaded from the GEO database (https://www.ncbi.nlm.nih.gov/). GSE13507 included 165 primary bladder cancer samples, of which 62 were MIBC cases and 103 NMIBC cases. Another expression profile of BLCA samples from the TCGA database was analyzed using UALCAN-UAB (http://ualcan.path.uab.edu) (18). TCGA data consisted of 406 cases, with most cases in the advanced stage (n = 403). Both GSE13507 and TCGA data had complete corresponding clinical information. Comparison of CDK6 expression between MIBC and NMIBC was evaluated using GSE13507. Comparison of CDK6 expression among advanced stages and cancer-specific survival analysis was performed in both GSE13507 and TCGA.

IHC Staining

The IHC assay was performed as previously described (19). The monoclonal mouse anti-CDK6 antibody (1:200 dilution; ab124821, Abcam, Cambridge, MA, USA) was used for primary antibody incubation at 4°C overnight. A slide incubated without the primary antibody was used as a negative

TABLE 1 | Clinical-pathological information of 85 bladder carcinoma (BLCA) patients in this study.

Case No.	Age	Gender	Surgery	AJCC staging*
1	70	M	RC	II
2	48	M	RC	III
3	71	M	TUR	II
4	69	M	RC	IV
5	47	M	RC	IV
6	56	M	RC	IV
7	49	F	TUR	0is
8	73	M	TUR	I
9	69	M	TUR	I
10	65	F	TUR	I
11	69	M	RC	III
12	64	F	TUR	IV
13	37	M	TUR	0a
14	42	M	TUR	I
15	73	M	TUR	I
16	75	F	TUR	I
17	66	M	RC	II
18	56	F	TUR	0is
19	62	M	RC	III
20	65	M	TUR	I
21	77	M	TUR	IV
22	86	F	TUR	II
23	60	M	TUR	I
24	78	M	TUR	IV
25	55	M	TUR	0is
26	86	M	TUR	I
27	58	M	TUR	0a
28	63	M	TUR	0
29	76	M	TUR	0
30	54	M	TUR	I
31	60	M	TUR	0
32	53	M	RC	II
33	66	M	TUR	I
34	64	M	TUR	IV
35	70	M	RC	II
36	57	M	TUR	II
37	87	M	TUR	0
38	54	M	RC	I
39	61	M	RC	III
40	54	F	TUR	0
41	74	M	RC	III
42	69	M	RC	I
43	53	M	TUR	0a
44	73	M	RC	I
45	53	M	RC	III
46	53	M	TUR	I
47	43	M	TUR	I
48	60	F	TUR	0is
49	49	M	TUR	0a
50	41	M	TUR	II
51	72	M	TUR	0a
52	68	M	TUR	0a
53	77	F	TUR	0is
54	52	M	RC	III
55	70	F	TUR	I
56	70	M	RC	II
57	56	F	TUR	0a
58	67	M	RC	III
59	65	M	TUR	II
60	84	M	RC	IV
61	63	M	TUR	I
62	59	M	TUR	I
63	71	F	TUR	0is
64	38	M	TUR	IV
65	64	M	RC	I
66	60	M	TUR	0is
67	63	M	TUR	I
68	68	M	RC	IV
69	73	M	TUR	I
70	61	M	TUR	0a
71	74	F	TUR	IV
72	57	M	TUR	I
73	85	M	TUR	I
74	72	M	TUR	I
75	48	M	RC	IV
76	67	M	RC	III
77	65	M	RC	III
78	51	M	RC	II
79	73	M	RC	IV
80	46	M	RC	IV
81	67	M	RC	II
82	55	M	RC	III
83	76	F	RC	IV
84	64	M	RC	I
85	64	M	RC	I

*RC, radical cystectomy or cystoprostatectomy; TUR, transurethral resection; *American Joint Committee on Cancer (AJCC) 8th Edition.*

control. A secondary antibody was applied using the Elivision Plus Kit (Dako, Glostrup, Denmark) according to the manufacturer's instructions.

IHC Evaluation

All staining slides were blindly and independently reviewed by three pathologists for scoring CDK6 nuclear staining. The staining intensity was scored as 0, 1 (weakly positive), 2 (moderately positive), and 3 (strongly positive). The percentage of positive cells was scored as 0, 1 (< 5% positive), 2 (5%–50%), and 3 (> 50%). The H-score was calculated as the product of the multiplication of the percentage of area stained at each intensity level multiplied by the weighted intensity (20). The H-scores ranged from 0 to 300. The median H-score was 210.

RNA Sequencing

RNA sequencing was performed on total RNA extracted from fresh frozen tissue samples of 22 BLCA cases. The RNA Nano 6000 Assay Kit of the Bioanalyzer 2100 system (Agilent Technologies, Santa Clara, CA, USA) was used to assess RNA integrity. A total of 1 μg RNA per sample was used as the input material for the RNA sample preparations. Clustering of the index-coded samples was performed on a cBot Cluster Generation System using TruSeq PE Cluster Kit v3-cBot-HS (Illumina) according to the manufacturer's instructions. After cluster generation, the library preparations were sequenced on an Illumina Novaseq platform and 150 bp paired-end reads were generated. Normalized read count data and fragments per kilobase of exon per million reads (FPKM) were used to evaluate gene expression.

Cell Lines and Cell Culture

The T24 and 5637 cells (human bladder cancer cell lines) were obtained from the American Type Culture Collection and grown in RPMI 1640-medium supplemented with 10% fetal bovine serum (Hyclone), 2 mM glutamine, and antibiotics (100 U/mL penicillin and 100 μg/mL streptomycin) at 37°C in a humidified 5% CO2 atmosphere.

CDK4/6 Inhibitors and Proliferation Inhibition Assay

To investigate the potential inhibitory effects of CDK4/6 inhibitor on T24 and 5637 cells, we tested the inhibitory effect of two CDK4/6 inhibitors, ribociclib (Cat No: HY15777, MCE) and palbociclib (Cat No: HY50767, MCE) on human bladder carcinoma cells. The T24 or 5637 cells (1.5×10^4 cells per well) were plated in a 96-well plate, and the cells were treated with ribociclib or palbociclib alone at concentrations from 0 to 50 μM for 72 h at 37°C. Cell proliferation was determined by an assay using the Cell Counting Kit-8 (DojinDo, cat#:CK04) and expressed as mean A450 value (absorbance value) ± standard deviation (SD) of triplicate wells. GraphPad Prism software version 8.3.0 (GraphPad, Inc., San Diego, CA, USA) was used to calculate IC50 values and create a relative inhibition curve. The experiments were independently repeated three times. The mean IC50 value ± standard error of the mean (SEM) of three independent experiments was used for statistical analysis.

Western Blotting

Cells were collected using radioimmunoprecipitation assay buffer (Thermo Scientific, cat# 89901) supplemented with protease inhibitors, phosphatase inhibitors, and PMSF, all of which were purchased from Boster Biotech, China. Protein concentrations were determined using the Pierce BCA Protein Assay Kit (Thermo Scientific, cat# RD231228). The total proteins were separated on a 10% sodium dodecyl sulphate-polyacrylamide gel and then transferred to a nitrocellulose membrane (AR0135-02, Boster, China). After blocking the membrane in 5% (w/v) Difco Skimmed Milk (Biotopped, China) for 2 h at 15–25°C, the membranes were incubated with antibodies against CDK6 (ab124821, Abcam, Cambridge, MA, USA) and tubulin (#2148, CST, USA) at a concentration of 1:5000 at 4°C overnight. The membranes were washed three times with PBS/T and visualized using the LI-COR Odyssey Detection Kit.

Follow-Up

The follow-up period of the patients was at least 6 years after the initial pathological diagnosis of BLCA. Recurrence and BLCA-specific survival were recorded for statistical analyses in this study. Patients who died owing to causes other than BLCA were excluded.

Statistical Analysis

A non-parametric test was performed to compare the distribution of CDK6 expression between the NMIBC and MIBC groups. The correlation between CDK6 expression and clinical-pathological features was determined by the Fisher's exact test. The R project (using "survminer" packages) was used to determine the optimal cutoff value of CDK6 levels for prognostic and cancer-specific survival analysis (21, 22). Log-rank (Mantel–Cox) and Gehan–Breslow–Wilcoxon tests were applied to verify the survival analysis results. Correlation analysis between the H-score and gene expression designated either by gene counts or FPKM was performed using Pearson correlation analysis. Statistical analysis of cell proliferation was performed using the Student's *t*-test. Values of $p < 0.05$ were considered significant.

RESULTS

High CDK6 Transcriptional Level Is Associated With Advanced Stage and Poor Prognosis in BLCA Cases Obtained From a Public Database

To observe the relationship between CDK6 expression and cancer progression, we compared the transcriptional level of CDK6 between MIBC (n = 62) and NMIBC (n = 103) in the GSE13507 cohort (including 165 BLCA cases). As shown in **Figure 1A**, there were significantly higher CDK6 levels in MIBC than in NMIBC ($p < 0.001$). There were also no differences in the CDK6 transcriptional level of the TCGA and GSE13507 cohorts from stages II to IV (**Figures 1B, C**). Furthermore, the high-CDK6 transcriptional cases in 93 (23%) out of 406 cases from the TCGA database displayed worse prognosis than those in the low-level group (n = 313) ($p < 0.001$, **Figure 1D**). Similarly, CDK6 transcriptional cases in 48 (29%) out of 165 cases also showed worse prognosis than those in the low-level group (n = 117) in the GSE13507 cohort ($p < 0.05$, **Figure 1E**). Based on these results, we hypothesized that CDK6 was associated with cancer progression from the NMIBC to MIBC stage and approximately one-fourth of BLCA cases (23% in TCGA database and 29% in GSE13507 cohort), displayed high CDK6 transcriptional levels correlated with reduced survival. Thus, it is worthwhile to detect transcriptional CDK6 levels to predict prognosis and evaluate target therapy potential in BLCA cases. However, mRNA detection is relatively expensive and complicated for clinical practice; thus, it is important to develop a simplified screening platform.

Correlation of CDK6 Expression and Clinical-Pathological Features in BLCA Cases

To simplify the validation of CDK6 expression in routine clinical practice, FFPE tissues from 85 BLCA cases in the pathology department of the China-Japan Union Hospital were used in this study for IHC staining of CDK6 protein. Representative images of negative and diffusely strong positive staining for CDK6 are shown in **Figure 2A**. Although there were no significant differences in the distribution of age, sex, histological grade, and recurrence rate between groups with either high or low CDK6 H-scores ($p > 0.05$, **Table 2**). The best cutoff value of

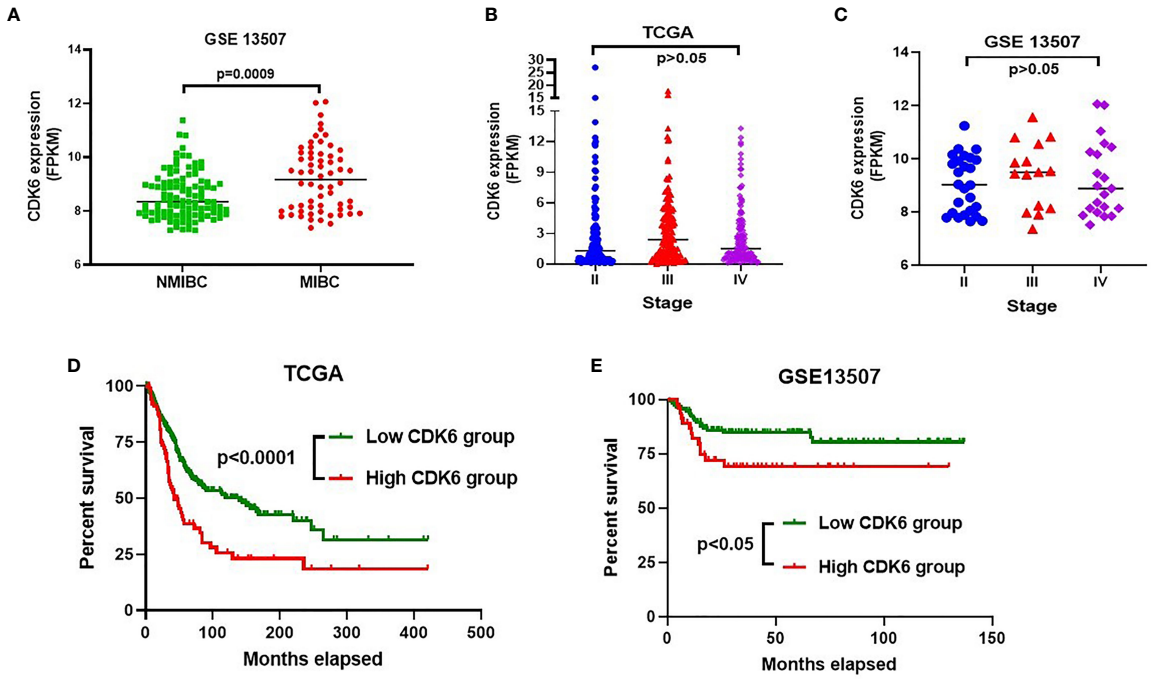

FIGURE 1 | CDK6 transcriptional level analysis in bladder carcinoma (BLCA) from GEO and TCGA database. Muscle-invasive bladder cancer (MIBC) group displayed significantly higher CDK6 level than that in non-muscle-invasive bladder cancer (NMIBC) group (p<0.001) **(A)**. There was no difference on the CDK6 transcriptional level through stage II to IV by analyzing both GSE13507 **(B)** and TCGA **(C)** cohorts (p>0.05). High CDK6 transcriptional cases in 93 (23%) out of 406 cases from TCGA database displayed worse prognosis than that in low level group (n=313) (p<0.001) **(D)**. Similarly, CDK6 transcriptional cases in 48 (29%) out of 165 cases also showed worse prognosis than that in low level group (n=117) in GSE13507 cohort (p<0.05) **(E)**.

H-score was calculated by R project (21, 22). The BLCA cases with H-scores higher than 240 (n = 24) accounted for 28% (24/85), which displayed increased metastasis potential (p < 0.0001, **Table 2**) and worse prognosis (p < 0.0001, by both the log-rank (Mantel–Cox) test and the Gehan–Breslow–Wilcoxon test; **Figure 2B**) than those with H-scores less than or equal to 240 (n = 61). Cases with high CDK6 H-scores were accumulated more in MIBC group (n = 38, including stage II to IV) than the NMIBC group (n = 47, including stage 0 to I) (p < 0.0001, **Figure 2C**). Furthermore, there was no difference in MIBC group among the advanced stages (n=38, from stage II to IV, p > 0.05, **Figure 2D**). These data suggest that CDK6 is involved in the advance stages (from stage II to IV) of BLCA and meaningful to be detected by IHC for evaluating prognosis and therapeutical potential of CDK4/6 inhibitors in these populations.

Correlation Between Protein and mRNA Levels of CDK6 Expression in BLCA Cases

To observe the consistency between protein and mRNA levels of CDK6 in BLCA cases, we further conducted RNA sequencing on 22 cases and compared either gene counts or FPKM values to the CDK6 H-score. As shown in **Figures 3A, C**, a moderate correlation was observed (R = 0.46, p = 0.03 by H-score vs. gene counts; R = 0.45, p = 0.03 by H-score vs. FPKM value). Narrowing to cases with CDK6 scores higher than 240, there was a strong correlation between IHC and RNA-sequencing methods (R = 0.94, p = 0.01 by IHC scores vs. gene counts; R = 0.9, p = 0.01 by IHC scores vs. FPKM value; **Figures 3B, D**), suggesting that high CDK6 H-score level is consistent with high CDK6 mRNA levels in BLCA cases.

CDK6 Protein Level Was Correlated to CDK4/6 Inhibitor Effect in BLCA Cell Lines

We selected two urothelial carcinoma cell lines, T24 and 5637, with different CDK6 protein expression levels (**Figure 4A**), to observe the inhibitory effect of CDK4/6 inhibitors. The T24 or 5637 cells were incubated for 72 h with the CDK4/6 inhibitors ribociclib or palbociclib at a series of concentrations and the IC50 value of each drug on each cell line was calculated. Both ribociclib and palbociclib significantly inhibited the proliferation of 5637 and T24 cells in a dose-dependent manner. As shown in **Figures 4B, C**, mean IC50 value of ribociclib was 21.12 ± 0.36 μM for the 5637 cells and 5.88 ± 0.86 μM for the T24 cells (p <0.001), and mean IC50 value of palbociclib was 28.44 ± 4.4 μM for the 5637 cells and 1.16± 0.89 μM for the T24 cells (p = 0.001). The IC50 of ribociclib in the 5637 cells was almost four times higher than that in the T24 cells, and the IC50 of palbociclib in the 5637 cells was approximately 28 times higher than that in the T24 cells. The T24 cells displayed higher CDK6 protein expression levels and more sensitivity to CDK4/6 inhibitors than those of the 5637 cells, suggesting that sensitivity to CDK4/6 inhibitors is accompanied by CDK6 protein expression levels in BLCA.

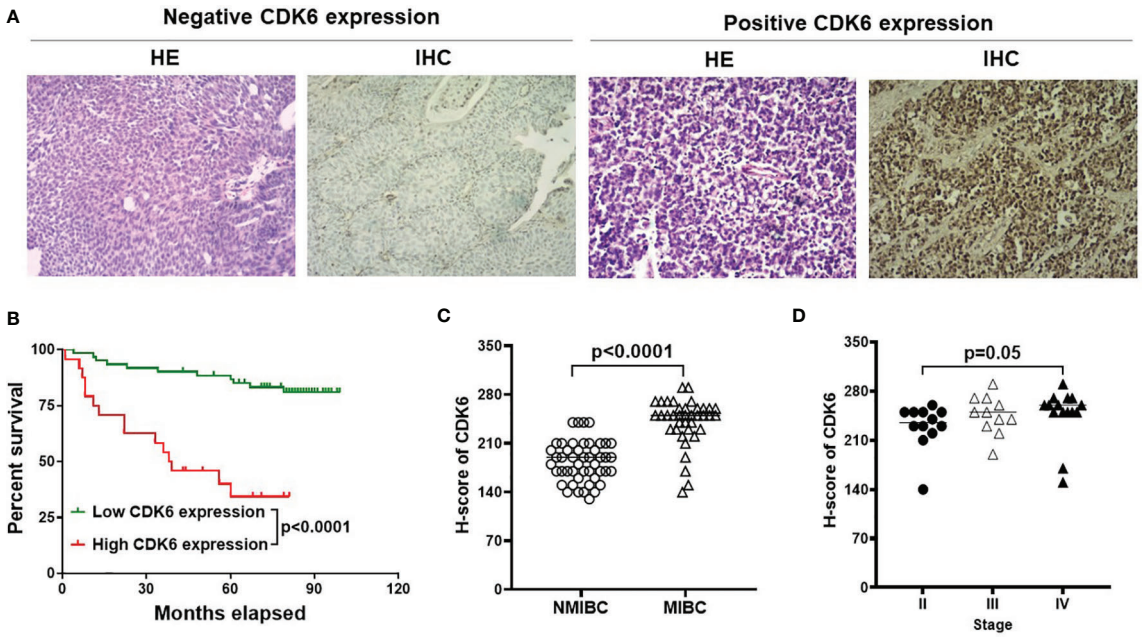

FIGURE 2 | IHC for CDK6 expression in BLCA. Representative images of H&E and IHC staining from negative and diffusely strong positive cases [**(A)**, Magnification, X40]. Cases with high H-score was correlated with worse prognosis compared with low or no expression group [$p < 0.0001$, **(B)**]. Furthermore, MIBC group (n=38) displayed higher CDK6 expression compared to NMIBC group (n=47) [$p < 0.0001$, **(C)**], but there was no difference among advanced stages [from stage II to IV, $p = 0.05$, **(D)**].

DISCUSSION

The IHC of CDK6 protein may be used for predicting prognosis in BLCA cases, especially those with high-grade morphology. In this study, we found that both high mRNA level and high H-score of CDK6 protein correlated with poor prognosis in BLCA. However, only 85 cases were evaluated for CDK6 protein IHC staining. We should increase the number of cases, especially cases in advanced stages to further validate the prediction effect of IHC staining in the future. Furthermore, the basal phenotype displayed worse prognosis than the luminal phenotype in BLCA and Guo et al. developed a routine IHC staining of GATA3 and KRT5/6 to designate basal and luminal molecular subtypes, respectively, for routine clinical practice (5). This provides us with a further research direction for identifying the relationship between the CDK6 protein and molecular phenotype. As a next step, we may observe the relationship between the expression of CDK6 and GATA3 or KRT5/6 by IHC staining to determine whether CDK6 gene expression is the signature of the basal phenotype.

CDK4 and CDK6 are known as homologous enzyme in cell cycle regulation. In this study, we observed the activity of CDK6 in urothelial carcinoma cases and defined about 28% (24/85) CDK6 high expression cases with unknown CDK4 state. It will be meaningful to explore CDK4 level in cases with either CDK6 high level or low level and evaluate the influence of CDK4 expression on the sensitivity to CDK4/6 inhibitors in BLCA in the next step. Furthermore, since CDK6 display both kinase activity in cell cycle regulation and transcriptional regulation activity (14), it will be useful to investigate the oncogenic mechanism of CDK6 in urothelial carcinoma by either knockdown or overexpression of CDK6 *in vitro* experiment in the future.

As CDK6 participates in cell cycle dysregulation in many solid tumors and lymphoma (6, 8), there is a potential benefit of CDK4/6 inhibitors for the treatment of these tumors (23); however, *de novo* or acquired treatment resistance has also been reported in several tumor models. Acquired CDK6 amplification has been found to promote breast cancer resistance to CDK4/6 inhibitors (24). In a pancreatic ductal adenocarcinoma cell model, CDK4/6 inhibition was associated with increased mTORC1 activity, which produces ATP accumulation at the mitochondrial level and induces drug resistance (25). In addition to kinase activity, CDK6 can participate in the transcriptional regulation of malignancy. For example, native CDK6 levels promote cell proliferation in T-cell lymphoma, yet forced overexpression of CDK6 protein inhibits cell proliferation by participating in positive transcriptional regulation of the tumor suppressor p16INK4a (26). In a chronic myeloid leukemia stem cell model, persistent application of CDK4/6 inhibitor resulted in CDK6-induced p53 mutation *via* a transcriptional regulation mechanism (27). These results suggest that CDK6 overexpression may be a double-edged sword for potential therapeutic targets in malignant tumors. Thus, ongoing research is currently focused either on the combination of CDK4/6 inhibitors and resistance-

TABLE 2 | Correlation of CDK6 expression and clinical-pathological features in Bladder carcinoma (BLCA).

BLCA Patients	Numbers	CDK6 expression		*p* values
		Low	High	
Age (years)				
Median	64	64	64	>0.05
Range	37-87	37-87	41-86	
Sex				
Male	71	51	20	>0.05
Female	14	10	4	
Histological grading				
Low grade	8	8	0	>0.05
High grade	77	53	24	
Recurrence				
No	40	32	8	>0.05
Yes	45	29	16	
Metastasis				
No	68	58	10	<0.0001*
Yes	17	3	14	

**Means that Values of p were considered significant.*

relevant antagonists (25, 28) or on precise medicine to avoid the occurrence of resistance (25, 29, 30). For example, research using the CRISPR-dCas9 screening approach in bladder cancer has indicated the beneficial effects of a combination of CDK4/6 inhibitors with some inhibitors against PI3K-Akt, Ras/MAPK, JAK/STAT, or Wnt signaling pathways in bladder cancer therapy (31).

Ex vivo tumor culture systems for drug sensitivity and resistance tests are an option for precision therapy for malignancy (32, 33). In this study, we identified that both high mRNA and protein levels of CDK6 predicted poor prognosis in BLCA cases through public database analysis and IHC staining of FFPE samples. We identified that the BLCA cell line with higher expression of CDK6 protein displayed greater sensitivity to CDK4/6 inhibitors. However, it is still arbitrary to judge whether patients with BLCA will be sensitive to CDK4/6 inhibitors using only mRNA evaluation or scoring the expression of CDK6 protein in FFPE specimens. Furthermore, passaging of BLCA cell lines cannot completely restore the tumor microenvironment. As fresh specimens of BLCA can be acquired after satisfying the need for diagnosis, we can attempt to develop an optimized and simplified procedure for tumor slices and various 3D culture systems to mimic the *in vivo* tumor microenvironment for precise prediction of the sensitivity and potential resistance to CDK4/6 inhibitors in the future.

In addition to BLCA, high transcriptional CDK6 mRNA also predicts poor prognosis in pancreatic adenocarcinoma, adrenocortical adenocarcinoma, uterine corpus endometrial carcinoma, lung adenocarcinoma, low-grade glioma, mesothelioma, and sarcoma from TCGA database analyzed

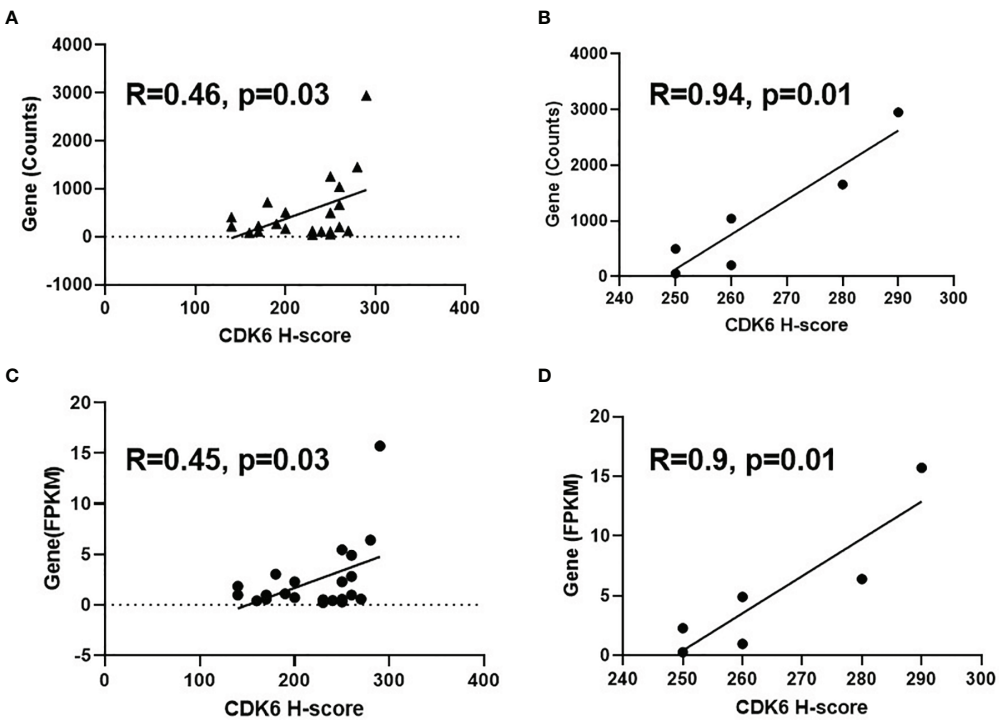

FIGURE 3 | Correlation between IHC score and mRNA level of CDK6 expression. Moderate correlation was observed [R=0.46, *p*=0.03 by H-score vs gene counts, **(A)**; R=0.45, *p*=0.03 by H-score vs FPKM value, **(C)**] for the comparison of H-score and mRNA level of 22 cases. Strong correlation was shown between IHC and RNA-sequencing methods [R=0.94, *p*=0.01 by IHC scores vs gene counts, **(B)**; R=0.9, *p*=0.01 by IHC scores vs FPKM value, **(D)**] after narrowing to the cases with CDK6 scores higher than 240.

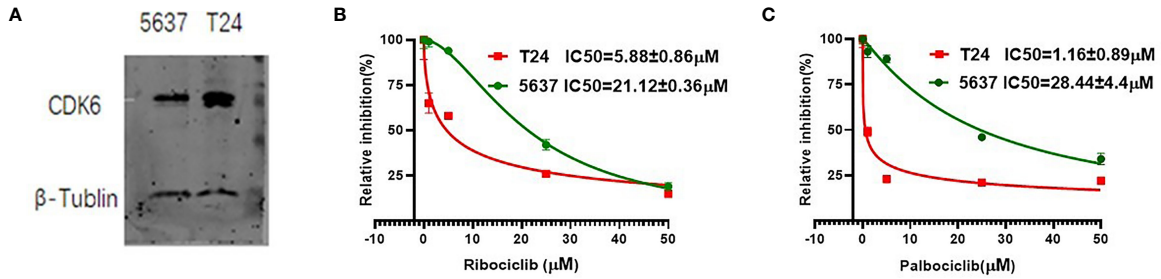

FIGURE 4 | The CDK6 protein expression and IC50 value of CDK4/6 inhibitors in urothelial carcinoma cell lines. Western blot analysis showed higher CDK6 protein expression in T24 cell lines compared to 5637 cell lines **(A)**. Relative growth inhibition curves of ribociclib **(B)** and palbociclib **(C)** in 5637 or T24 cell lines were from three independent experiments. Mean IC50 value of ribociclib was 21.12 ± 0.36 μM for the 5637 cells and 5.88 ± 0.86 μM for the T24 cells ($p < 0.001$), and mean IC50 value of palbociclib was 28.44 ± 4.4 μM for the 5637 cells and 1.16± 0.89 μM for the T24 cells ($p = 0.001$).

using the UALCAN website (18). More interestingly, uterine corpus endometrial carcinoma displayed lower median transcriptional levels of CDK6 than normal tissues ($p < 0.001$) (data not shown), suggesting that malignancy displays high heterogeneity, and it is practical to evaluate IHC staining of CDK6 in these entities for precision therapy.

DATA AVAILABILITY STATEMENT

The raw RNA-sequencing data has been deposited in SRA database, BioProject number: PRJNA805290.

ETHICS STATEMENT

The studies involving human participants were reviewed and approved by the Institutional Medical Ethics Review Board of the China-Japan Union Hospital of Jilin University in compliance with the Declaration of Helsinki. The reference number was 2021-KYLL-030003. The patients/participants provided their written informed consent to participate in this study. Written informed consent was obtained from the individual(s) for the publication of any potentially identifiable images or data included in this article.

AUTHOR CONTRIBUTIONS

XJW developed the concept, analyzed the data and wrote the manuscript. XJW and RS designed the study. RS fulfilled cell proliferation experiments and western blot assay. XMW revised the manuscript. LCZ and YG were responsible for reviewing HE slides and scoring the IHC slides. SJY performed optimization of CDK6 antibody in IHC staining assay. LPW kindly provided technological supports and partial funding supports. All authors contributed to the article and approved the submitted version.

FUNDING

This work is supported by the National Science and Technology Major Project of the Ministry of Science and Technology of China (subject grant No. 2017YFC0110105), the Young Scientists Fund of the National Natural Science Foundation of China (grant No. 81700198), the Science and Technology Development Project of Jilin Province (grant No. 20190701064GH), the Open Project of Key Laboratory of Tumor Immunology and Pathology (Army Medical University), Ministry of Education (2018jsz101), and Natural Science Foundation of Jilin province (20210101252JC).

ACKNOWLEDGMENTS

We thank department of tissue bank in China-Japan Union Hospital of Jilin University for providing fresh frozen tissue samples. We thank Novogene Ltd. Co. (Beijing) for assistance in RNA sequencing data processing. We thank Yan Ning in department of breast surgery and Songqi, Bi in Norman Bethune Health Science Center of Jilin University for assistance in statistical data analysis.

REFERENCES

1. Minoli M, Kiener M, Thalmann GN, Kruithof-de Julio M, Seiler R. Evolution of Urothelial Bladder Cancer in the Context of Molecular Classifications. *Int J Mol Sci* (2020) 21(16):5670. doi: 10.3390/ijms21165670
2. Naspro R, Finati M, Roscigno M, Pellucchi F, La Croce G, Sodano M, et al. The Impact of Histological Variants on Outcomes After Open Radical Cystectomy for Muscle-Invasive Urothelial Bladder Cancer: Results From a Single Tertiary Referral Centre. *World J Urol* (2020) 39(6):1917–26. doi: 10.1007/s00345-020-03364-z
3. Compérat EM, Burger M, Gontero P, Mostafid AH, Palou J, Rouprêt M, et al. Grading of Urothelial Carcinoma and The New "World Health Organisation Classification of Tumours of the Urinary System and Male Genital Organs 2016". *Eur Urol Focus* (2019) 5(3):457–66. doi: 10.1016/j.euf.2018.01.003

4. Lobo N, Shariat SF, Guo CC, Fernandez MI, Kassouf W, Choudhury A, et al. What Is the Significance of Variant Histology in Urothelial Carcinoma? *Eur Urol Focus* (2020) 6(4):653–63. doi: 10.1016/j.euf.2019.09.003
5. Guo CC, Bondaruk J, Yao H, Wang Z, Zhang L, Lee S, et al. Assessment of Luminal and Basal Phenotypes in Bladder Cancer. *Sci Rep* (2020) 10:9743. doi: 10.1038/s41598-020-66747-7
6. Tadesse S, Yu M, Kumarasiri M, Le BT, Wang SD. Targeting CDK6 in Cancer: State of the Art and New Insights. *Cell Cycle* (2015) 14(20):3220–30. doi: 10.1080/15384101.2015.1084445
7. Li H, Zhang J, Xie Y. Elevated Nuclear CDK6 Is Associated With an Unfavorable Prognosis in Lung Adenocarcinoma Patients. *Int J Clin Exp Pathol* (2017) 10(9):9614–20.
8. Wang XJ, Dasari S, Nowakowski GS, Lazaridis KN, Wieben ED, Kadin ME, et al. Retinoic Acid Receptor Alpha Drives Cell Cycle Progression and Is Associated With Increased Sensitivity to Retinoids in T-Cell Lymphoma. *Oncotarget* (2017) 8(16):26245–55. doi: 10.18632/oncotarget.15441
9. Wang G, Zheng L, Yu Z, Liao G, Lu L, Xu R, et al. Increased Cyclin-Dependent Kinase 6 Expression in Bladder Cancer. *Oncol Lett* (2012) 4.1:43–6. doi: 10.3892/ol.2012.695
10. Pernas S, Tolaney SM, Winer EP, Goel S. CDK4/6 Inhibition in Breast Cancer: Current Practice and Future Directions. *Ther Adv Med Oncol* (2018) 10:1758835918786451. doi: 10.1177/1758835918786451
11. Hamilton E, Infante JR. Targeting CDK4/6 in Patients With Cancer. *Cancer Treat Rev* (2016) 45:129–38. doi: 10.1016/j.ctrv.2016.03.002
12. Rubio C, Martínez-Fernández M, Segovia C, Lodewijk I, Suarez-Cabrera C, Segrelles C, et al. CDK4/6 Inhibitor as a Novel Therapeutic Approach for Advanced Bladder 9- Cancer Independently of RB1Status. *Clin Cancer Res* (2019) 25(1):390–402. doi: 10.1158/1078-0432.CCR-18-0685
13. Rose TL, Chism DD, Alva AS, Deal AM, Maygarden SJ, Whang YE, et al. Phase II Trial of Palbociclib in Patients With Metastatic Urothelial Cancer After Failure of First-Line Chemotherapy. Phase II Trial of Palbociclib in Patients With Metastatic Urothelial Cancer After Failure of First-Line Chemotherapy. *Br J Cancer* (2018) 119:801–7. doi: 10.1038/s41416-018-0229-0
14. Tigan AS, Bellutti F, Kollmann K, Tebb G, Sexl V. CDK6—A Review of the Past and a Glimpse Into the Future: From Cell-Cycle Control to Transcriptional Regulation. *Oncogene* (2016) 35:3083–91. doi: 10.1038/onc.2015.407
15. Wang XJ, Boddicker RL, Dasari S, Sidhu JS, Kadin ME, Macon WR, et al. Expression of P63 Protein in Anaplastic Large Cell Lymphoma: Implications for Genetic Subtyping. *Hum Pathol* (2017) 64:19–27. doi: 10.1016/j.humpath.2017.01.003
16. Rizzardi AE R, Johnson AT, Vogel RI, Pambuccian SE, Henriksen J, Skubitz AP, et al. Quantitative Comparison of Immunohistochemical Staining Measured by Digital Image Analysis Versus Pathologist Visual Scoring. *Diagn Pathol* (2012) 7:42. doi: 10.1186/1746-1596-7-42
17. Poomsawat S, Sanguansin S, Punyasingh J, Vejchapipat P, Punyarit P. Expression of Cdk6 in Head and Neck Squamous Cell Carcinoma. *Clin Oral Investig* (2016) 20(1):57–63. doi: 10.1007/s00784-015-1482-8
18. Chandrashekar DS, Bashel B, Balasubramanya SAH, Creighton CJ, Ponce-Rodriguez I, Chakravarthi BVSK, et al. UALCAN: A Portal for Facilitating Tumor Subgroup Gene Expression and Survival Analyses. *Neoplasia* (2017) 19 (8):649–58. doi: 10.1016/j.neo.2017.05.002
19. Sorokin M, Ignatev K, Poddubskaya E, Vladimirova U, Gaifullin N, Lantsov D, et al. RNA Sequencing in Comparison to Immunohistochemistry for Measuring Cancer Biomarkers in Breast Cancer and Lung Cancer Specimens. *Biomedicines* (2020) 8(5):114. doi: 10.3390/biomedicines8050114
20. Mazières J, Brugger W, Cappuzzo F, Middel P, Frosch A, Bara I, et al. Evaluation of EGFR Protein Expression by Immunohistochemistry Using H-Score and the Magnification Rule: Re-Analysis of the SATURN Study. *Lung Cancer* (2013) 82(2):231–7. doi: 10.1016/j.lungcan.2013.07.016
21. Kassambara A, Kosinski M, Biecek P, Fabian S. Available at: https://cran.r-project.org/web/packages/survminer/index.html.
22. López-Ratón Mónica, Rodríguez-Álvarez María, Cadarso-Suárez C, Gude F. OptimalCutpoints: An R Package for Selecting Optimal Cutpoints in Diagnostic Tests. *J Stat Software* (2014) 61:1–36. doi: 10.18637/jss.v061.i08
23. Du Q, Guo X, Wang M, Li Y, Sun X, Li Q. The Application and Prospect of CDK4/6 Inhibitors in Malignant Solid Tumors. *J Hematol Oncol* (2020) 13:41. doi: 10.1186/s13045-020-00880-8
24. Yang C, Li Z, Bhatt T, Dickler M, Giri D, Scaltriti M, et al. Acquired CDK6 Amplification Promotes Breast Cancer Resistance to CDK4/6 Inhibitors and Loss of ER Signaling and Dependence. *Oncogene* (2017) 36(16):2255–64. doi: 10.1038/onc.2016.379
25. Franco J, Balaji U, Freinkman E, Witkiewicz AK, Knudsen ES. Metabolic Reprogramming of Pancreatic Cancer Mediated by CDK4/6 Inhibition Elicits Unique Vulnerabilities. *Cell Rep* (2016) 14(5):979–90. doi: 10.1016/j.celrep.2015.12.094
26. Kollmann K, Heller G, Schneckenleithner C, Warsch W, Scheicher R, Ott RG, et al. A Kinase-Independent Function of CDK6 Links the Cell Cycle to Tumor Angiogenesis [Published Correction Appears in Cancer Cell. *Cancer Cell]* (2013) 24(2):167–81. doi: 10.1016/j.ccr.2013.07.012
27. Bellutti F, Tigan AS, Nebenfuehr S, Dolezal M, Zojer M, Grausenburger R, et al. CDK6 Antagonizes P53-Induced Responses During Tumorigenesis. *Cancer Discov* (2018) 8(7):884–97. doi: 10.1158/2159-8290.CD-17-0912
28. Teh JLF, Aplin AE. Arrested Developments: CDK4/6 Inhibitor Resistance and Alterations in the Tumor Immune Microenvironment. *Clin Cancer Res* (2019) 25(3):921–7. doi: 10.1158/1078-0432.CCR-18-1967
29. Mo Q, Li R, Adeegbe DO, Peng G, Chan KS. Integrative Multi-Omics Analysis of Muscle-Invasive Bladder Cancer Identifies Prognostic Biomarkers for Frontline Chemotherapy and Immunotherapy. *Commun Biol* (2020) 3:784. doi: 10.1038/s42003-020-01491-2
30. Rinaldetti S, Rempel E, Worst TS, Eckstein M, Steidler A, Weiss CA, et al. Subclassification, Survival Prediction and Drug Target Analyses of Chemotherapy-Naïve Muscle-Invasive Bladder Cancer With a Molecular Screening. *Oncotarget* (2018) 9(40):25935–45. doi: 10.18632/oncotarget.25407
31. Tong Z, Sathe A, Ebner B, Qi P, Veltkamp C, Gschwend JE, et al. Functional Genomics Identifies Predictive Markers and Clinically Actionable Resistance Mechanisms to CDK4/6 Inhibition in Bladder Cancer. *J Exp Clin Cancer Res* (2019) 38(1):322. doi: 10.1186/s13046-019-1322-9
32. Martin SZ, Wagner DC, Hörner N, Horst D, Lang H, Tagscherer KE, et al. *Ex Vivo* Tissue Slice Culture System to Measure Drug-Response Rates of Hepatic Metastatic Colorectal Cancer. *BMC Cancer* (2019) 19:1030. doi: 10.1186/s12885-019-6270-4
33. Popova Anna A, Levkin Pavel A. Precision Medicine in Oncology: *In Vitro* Drug Sensitivity and Resistance Test (DSRT) for Selection of Personalized Anticancer Therapy. *Advanced Therapeutics* (2020) 3(2). doi: 10.1002/adtp.201900100

Conflict of Interest: The authors declare that the research was conducted in the absence of any commercial or financial relationships that could be construed as a potential conflict of interest.

frontiers | Frontiers in Pharmacology

ORIGINAL RESEARCH
published: 25 May 2022
doi: 10.3389/fphar.2022.895573

Tizoxanide Promotes Apoptosis in Glioblastoma by Inhibiting CDK1 Activity

*Si Huang[1,2], Jingxian Xiao[3], Junyong Wu[1,2], Jiayi Liu[4], Xueping Feng[5], Chengdong Yang[6], Daxiong Xiang[1,2] and Shilin Luo[1,2]**

[1]Department of Pharmacy, The Second Xiangya Hospital, Central South University, Changsha, China, [2]Hunan Provincial Engineering Research Centre of Translational Medicine and Innovative Drug, Changsha, China, [3]School of Medical Science, Hunan University of Medicine, Huaihua, China, [4]Department of Radiology, The Second Xiangya Hospital, Central South University, Changsha, China, [5]Institute of Medical Sciences, Xiangya Hospital, Central South University, Changsha, China, [6]Department of Psychiatry, The Second Xiangya Hospital, Central South University, Changsha, China

The antiparasitic drug nitazoxanide (NTZ) has received considerable attention for its potential in cancer therapy. In this study, we demonstrate that tizoxanide (TIZ), an active metabolite of NTZ, exhibits antiglioma activity *in vitro* and *in vivo* by inducing G2/M cell cycle arrest and apoptosis. *In vitro*, TIZ dose-dependently inhibited the proliferation of U87, U118, and A172 human glioblastoma (GBM) cells at 48 h with IC_{50} values of 1.10, 2.31, and 0.73 μM, respectively. Treatment with TIZ (1 and 10 μM) also dose-dependently inhibited the colony formation of these GBM cells and accumulated ROS damage in the nucleus. In silico target fishing combined with network pharmacological disease spectrum analyses of GBM revealed that cycle-dependent kinase 1 (CDK1) is the most compatible target for TIZ and molecular docking by Molecule Operating Environment (MOE) software confirmed it. Mechanistically, TIZ inhibited the phosphorylation of CDK1 at Thr161 and decreased the activity of the CDK1/cyclin B1 complex, arresting the cell cycle at the G2/M phase. TIZ may induce apoptosis *via* the ROS-mediated apoptotic pathway. *In vivo*, TIZ suppressed the growth of established subcutaneous and intracranial orthotopic xenograft models of GBM without causing obvious side effects and prolonged the survival of nude mice bearing glioma. Taken together, our results demonstrated that TIZ might be a promising chemotherapy drug in the treatment of GBM.

Keywords: tizoxanide, glioblastoma, Cdk1, cell cycle, apoptosis

OPEN ACCESS

Edited by:
Arianna Palladini, University of Pavia, Italy

Reviewed by:
Giorgia Gri, University of Bologna, Italy
Carmen Blanco Aparicio, Spanish National Cancer Research Center (CNIO), Spain

****Correspondence:***
Shilin Luo
Shilin_luo@csu.edu.cn

Specialty section:
This article was submitted to Pharmacology of Anti-Cancer Drugs, a section of the journal Frontiers in Pharmacology

Received: *14 March 2022*
Accepted: *05 May 2022*
Published: *25 May 2022*

Citation:
Huang S, Xiao J, Wu J, Liu J, Feng X, Yang C, Xiang D and Luo S (2022) Tizoxanide Promotes Apoptosis in Glioblastoma by Inhibiting CDK1 Activity. Front. Pharmacol. 13:895573. doi: 10.3389/fphar.2022.895573

INTRODUCTION

Glioblastoma multiforme (GBM) is one of the most aggressive and malignant human brain tumors. Although progress has been made concerning its standard therapeutic regimen, which includes radiation therapy and temozolomide chemotherapy following surgical resection over the years, the current patient's overall median survival is approximately 15 months, and the 5-year survival rate is 4%–5% (Batash et al., 2017). Temozolomide (TMZ) is the oral first-line drug for the treatment of GBM in the clinic, and it increases the survival term by approximately 3 months after combination with radiation (Johnson et al., 2014). However, at least 50% of TMZ-treated patients do not respond to TMZ, and side effects and acquired resistance limit the effective application of TMZ (Lee, 2016). Therefore, more research focusing on discovering new therapeutic drugs for GBM is urgently needed.

Tizoxanide (TIZ), a nitrothiazolamide compound, is a rapid *in vivo* active metabolite of nitazoxanide (NTZ) that was approved by the US Food and Drug Administration (FDA) as an antiparasitic drug. TIZ has shown a broad spectrum of pharmacological functions in extracellular and intracellular protozoans, anaerobic and microaerophilic bacteria, helminths, and viruses (Anderson and Curran, 2007; Muller and Hemphill, 2011; Rossignol, 2014). As in-depth studies are developed, NTZ has been reported to express inhibitory effects by intervening in the crucial metabolic and pro-death signalings in tumor cells, such as autophagy, detoxifying enzyme overexpression, anti-cytokine activity, and c-Myc inhibition (Di Santo and Ehrisman, 2014; Shakya et al., 2018). A study has shown that NTZ can inhibit late-stage autophagy and promote the ING1-induced cell cycle arrest in GBM (Wang et al., 2018). However, the direct binding targets and the underlying mechanisms of the metabolite TIZ in anti-glioblastoma are still unclear.

As part of a research project on drug repurposing, in the present study, we found that treating U87, U118, and A172 glioblastoma cells with TIZ inhibited cell proliferation and colony formation. Using a strategy based on network pharmacological disease target analysis and computerized compound-target seeking, we focused on the cyclin-dependent kinase (CDK) family, especially CDK1, as a target of TIZ for its anti-GBM function. The molecular docking of TIZ with CDK1 revealed that TIZ blocked the active sites with high affinity. Furthermore, flow cytometry and immunoblotting analysis results indicated that TIZ induced apoptosis in U87MG cells by arresting the cell cycle at G2/M phases through the suppression of the CDK1/Cyclin B1 complex. TIZ also blocked the propagation of GBM and prolonged the survival rate in mice bearing orthotopic tumors. Taken together, our findings demonstrate the potential inhibitory efficacy of TIZ for GBM *in vitro* and *in vivo*, and CDK1 activity inhibition-induced TIZ-associated G2/M cell cycle arrest is the underlying molecular mechanism.

MATERIALS AND METHODS

Antibodies and Reagents

Antibodies to the following targets were used: anti-p-CDK1 Thr161 (BBI Sci, #D155339), anti-CDK1 (BBI Sci, #D260158), catalog number #8516S for anti-p-Rb Ser807/811 (Cell Signaling Technology, #), anti-Rb (Santa Cruz Biotechnology, #sc-74563), anti-CCNA1 (BBI Sci, #D220507), anti-CCNB1 (BBI Sci, #D160234), anti-GAPDH (Santa Cruz Biotechnology, #sc-47724), Annexin V-PE/7AAD Kit (Solarbio Science & Technology, #CA1030), Reactive Oxygen Species assay Kit (US Everbright INC, #R6033), and Cremophor EL (Sigma, #C5135). Tizoxanide (#S83937), N-acetyl-L-cysteine (#S20137), and D-luciferin sodium salt (#S19261) were purchased from Yuanye Bio-Technology Co. (Shanghai, China). Tizoxanide was dissolved in dimethyl sulfoxide (DMSO) at a stock concentration of 10 mM and diluted with the relevant medium for the *in vitro* experiments. The final concentration of DMSO was less than 0.1%. For *in vivo* studies, tizoxanide was dissolved in Cremophor EL/ethanol (50:50) to ensure solubility and then diluted in ultrapure water.

Cell Culture

The human glioblastoma cell line U87MG was purchased from the Cell Resource Center at the Institute of Basic Medical Sciences, Chinese Academy of Medical Sciences (Beijing, China); U87MG-luc was obtained from Shanghai Model Organisms Center, Inc., (Shanghai, China); U118 MG was acquired from Procell Life Science & Technology Co., Ltd. (Wuhan, China); and A172 was purchased from the National Collection of Authenticated Cell Cultures (Shanghai, China), where it was characterized through mycoplasma detection. The genomic aberrations of these glioma cell lines were comprehensively analyzed (Melendez et al., 2011). The cells were cultured in high-glucose DMEM supplemented with 10% fetal bovine serum (FBS) and 1% penicillin/streptomycin at 37°C, and 5% CO_2.

Cell Viability Assay

The cell viability assay was evaluated in triplicate by using Cell Counting Kit-8 (CCK-8, #C6005, NCM Biotech) according to the manufacturer's protocol. In brief, glioma cells (1×10^4 cells/well) were cultured in 96-well plates for 24 h and then treated with TIZ at 0, 0.05, 0.1, 1, and 10 μM in various wells. After incubation for 24, 48, or 72 h, 10 μl CCK-8 was added to each well and incubated for 1 h at 37°C. The OD_{450} was measured using a microplate reader (Infinite F50, TECAN). Each assay was repeated three times.

Colony Formation Assay

Glioma cells (500 cells/well) were seeded in a 6-well plate and treated with various concentrations of TIZ for 2 weeks. Next, the cells were stained with a 0.5% crystal violet solution for 15 min after washing with PBS and fixing with methanol. After washing with PBS thrice, the cells were dried in the air. The colonies with more than 50 cells were counted under a microscope. The colony-forming efficiency was calculated based on the following formula: colony-forming efficiency = (the number of colonies forming units/the number of inoculated cells) × 100%.

ROS Staining Assay and Flow Cytometric Analysis

U87MG cells were treated with TIZ at the indicated concentrations, negative control included pretreatment with N-acetyl-L-cysteine (NAC, 5 mM) for 2 h before 10 μM TIZ treatment for 24 h, and then fixed with 4% paraformaldehyde for 10 min after washing with PBS. Cells were firstly washed with carrier buffer (1% BSA, 0.3% Triton X-100, and 1% goat serum in PBS) and then treated with 10 μM DCFH-DA that was diluted in PBS for 20 min at 37°C. Finally, a carrier buffer was used to wash the cells three times, and a confocal microscope was employed to obtain the images. For flow cytometric analysis, U87MG cells were resuspended in 10 μM DCFH-DA for 20 min at 37°C after treatment with TIZ for 24 h and then subjected to the flow cytometry to analyze the degree of fluorescence.

Transfection of siRNA

The target sequence (5′-3′) of human siRNA-CDK1 (NM_001786) is ACTTCGTCATCCAAATATA; sense: 5′-ACUUCGUCAUCCAAAUAUA dTdT-3′; antisense, 3′-dTdT UGAAGCAGUAGGUUUAUAU-5′. The negative control siRNA (F: 5′-UUCUCCGAACGUGUCACGUTT-3′; R: 5′-ACGUGACACGUUCGGAGAATT-3) (Xiao et al., 2009). These siRNAs were chemically synthesized by GenePharma Co. Ltd. (Shanghai, China). U87MG cells were transfected with 20 nM siRNA using the Lipofectamine 3000 (#L3000075, Invitrogen) according to the manufacturer's protocol with Opti-MEM (#31985070, Gibco) as a transaction solution. The treated cells were incubated for 48 h and then harvested for further experiments.

Western Blotting

Cells or brain tissues were sonicated and lysed with a RIPA buffer and insoluble pellets were removed by centrifugation at 15,000 × *g* for 15 min at 4°C. Protein concentration was measured with a BCA kit. Equal amounts of protein (20–40 μg) were loaded for blotting with the corresponding antibodies. The quantitation of the western blot results was based on three independent experiments using ImageJ with the vehicle group as a baseline for comparison.

Apoptosis Assay

U87MG cells were treated with different doses of TIZ for 48 h, negative control included pretreatment with NAC (5 mM) for 2 h before 10 μM TIZ treatment, and then harvested, and washed with PBS. Cells were stained with an Annexin V-PE/7-AAD Apoptosis Detection Kit (Solarbio, Beijing, China) for 20 min at room temperature followed by flow cytometry. The data were analyzed with Flow Jo software (Tristar, CA, USA).

Cell Cycle Analysis

U87MG cells at a density of 4×10^5 cells/well were exposed to TIZ for 24 h, fixed in 75% ethanol at 4°C for 24 h, and stained with a PI/RNase staining buffer for 30 min for flow cytometric analysis.

Xenograft Animal Model Experiments

Female 6-week-old BALB/C nude mice were provided by Hunan SJA Laboratory Animal Co. Ltd. Mice were housed, maintained, and treated at the Central Laboratory of the Second Xiangya Hospital with SPF feeding conditions. For the subcutaneous tumor model, 100 μl PBS containing 1×10^7 U87MG cells was inoculated subcutaneously into the right side of the axilla of each mouse. Tumor growth was calculated every 2 days according to the formula of TV (mm^3) = $(\text{width})^2 \times (\text{length})/2$. When the tumor volume reached approximately 100 mm^3, the mice were randomly divided into three groups (n = 6). For the orthotopic intracranial tumor model, mice were placed in a stereotaxic instrument, then 1×10^7 U87MG-luc cells (10 μl) were performed stereotaxically at coordinates AP −2.0 mm and ML +0.7 mm relative to bregma and DV −3.0 mm from the dural surface. The needle was retained on site for 5 min before it was removed slowly. The mice were placed on a heating pad until they began to recover from the surgery. After surgery for 7 days, the mice were examined with an *in vivo* imaging system (IVIS) to validate tumor formation and then were randomly divided into three groups (n = 8). The mice in the above two models were administered TIZ (i.p., 5 mg/kg and 15 mg/kg) or a control agent three times per week for 3 weeks. After the drug treatment, mice in the intracranial model were euthanized and analyzed by MRI (Liu et al., 2019), after which samples were collected for subsequent studies. Bodyweight changes in mice were monitored throughout dosing and blood was collected to assess possible side effects of TIZ. The animal experiments were carried out following the Guiding Principles of the Animal Ethics Committee of the Second Xiangya Hospital of Central South University.

Immunohistochemistry and Hematoxylin-Eosin Staining

Formalin-fixed samples were embedded in paraffin and sliced into 5 μm-thick sections. The sections were stained with a standard H&E staining protocol (Fischer et al., 2008). For IHC staining, the sections were treated with 0.3% hydrogen peroxide for 10 min followed by incubation with anti-Ki67 and anti-p-CDK1 Thr161 at 4°C overnight. After a brief wash, the brain tissue slices were incubated with a biotinylated secondary antibody and visualized by using a DAB substrate Kit for 10 min. The slices were then counterstained with hematoxylin, and pictures were captured on a microscope (BX51TF, Olympus, Tokyo, Japan). For quantification of positive cells and image analysis, set a proper threshold for the binarization of the selected color image by ImageJ software. The average optical density (AOD) was calculated according to a reported method (Chlipala et al., 2020). The conditions of the analysis were blinded to the investigator.

Determination of TIZ in Glioma

The concentration of TIZ in glioma was determined by referring to the method previously reported (Guo et al., 2020). In brief, glioma tissue with 10 μl standard stock solution of TIZ and topiramate (internal standard, 5 μg/ml) was homogenized in cold acetonitrile (1:5, m/v) in a Tissuelyser ball mill (Servicebio, Wuhan, China), then sonicated for 5 min and centrifuged for 15 min at 4°C. 200 μl of supernatant of samples was removed and dried utilizing flowing nitrogen. Residual samples were reconstituted in 100 μl of acetonitrile containing 10% *N, N*-dimethylformamide (DMF) and analyzed on an HPLC system (Shimadzu, Kyoto, Japan) connected to an AB Sciex 4000 QTRAP mass spectrometer (AB Sciex, MA, USA). The compounds were separated on a Cosmosil $5C_{18}$-MS-II column (4.6 × 150 mm, 5 μm) with the temperature of the column oven was 30°C. The mobile phase was composed of acetonitrile and deionized water mixed with 10 mM ammonium formate (pH 3.0) according to a gradient volume ratio (60:40 to 80:20 to 60:40) with a flow rate of 0.8 ml/min. TIZ was detected in the positive mode by comparing the retention time and m/z ratio of the TIZ standard. Final concentrations of TIZ were adjusted for the weight of each glioma tissue.

Predictive Target Collection, Gene Ontology, Pathway Enrichment, and Bioinformatic Analyses

The potential target collection of TIZ was performed using Seaware software, the Swiss Target Prediction database (http://www.swisstargetprediction.ch) and the Bioinformatics & Evolutionary Genomics database (http://bioinformatics.psb.ugent.be/webtools/Venn). The GeneCards database (https://www.genecards.org) and CTD database (http://ctdbase.org) were used to obtain the currently reported genes related to glioma. The DAVID database (https://david.ncifcrf.gov, Version 6.8) was used to perform gene ontology and pathway enrichment analyses. GO analysis annotated and classified genes according to biological process (BP), molecular function (MF), and cellular location (CC). The enriched biological pathways were determined with the KEGG datasets. Bioinformatic data analysis was obtained from the TCGA data portal (https://cancergenome.nih.gov/dataportal/data/about) and GEPIA (http://gepia.cancer-pku.cn).

Molecular Docking

MOE2019 software was used to perform molecular docking. CDK1 (ID 6GU6) (Wood et al., 2019a), CDK2 (ID 6Q4G) (Wood et al., 2019b) and CDK4 (ID 4GCJ) (Schonbrunn et al., 2013) were obtained from Protein Data Bank. The 2D structure of TIZ was drawn in ChemDraw and converted to a 3D structure in MOE through energy minimization. Before docking, the force field of AMBER10: EHT and the implicit solvation model of Reaction Field (R-field) were applied to model molecular mechanics minimizations. MOE-Dock was used for molecular docking simulations of the TIZ with proteins. The "induced fit" protocol was selected, in which the side chains of the binding site in the receptor were allowed to move according to ligand conformations, and a constraint was applied on their positions. The weight used for tethering side-chain atoms to their original positions was 10. Firstly, all docked poses were ranked by the London dG scoring function, then force field refinement was applied to the top 30 poses followed by a rescoring of the GBVI/WSA dG scoring function. The conformation with the lowest binding free energy was finally identified as the best probable binding mode.

Statistical Analysis

All data are presented as the mean ± SD from three or more independent experiments. Histological data were analyzed using either Student's *t*-test or one-way ANOVA with Tukey's multiple-comparisons test. The threshold for significance for all experiments was set $^{*}p < 0.05$, and smaller p values are represented as $^{**}p < 0.01$ and $^{\#}p < 0.001$.

RESULTS

TIZ Inhibits Glioma Cell Proliferation and Induces ROS Damage

To investigate the role of TIZ in the proliferation of glioma cells, CCK-8 assays were carried out to determine cell viability. Three human glioma cells lines, U87MG, U118MG, and A172, were treated with different concentrations of TIZ ranging from 0.01 to 10 μM for 24, 48, and 72 h. The results demonstrated that TIZ dose-dependently inhibited cell proliferation regardless of the number of treatment days (**Figure 1A**). The 48 h IC_{50} of TIZ for U87MG cells was 1.10 μM, that for U118MG cells was 2.31 μM, and that for A172 cells was 0.73 μM. Meanwhile, colony formation assays were performed to examine the effect of TIZ on the formation of glioma colonies. The results showed that TIZ significantly decreased the colony formation of all three cell lines, especially at a TIZ concentration of 10 μM (**Figure 1B**). Quantitative analysis of the colony-forming efficiency mirrored these discoveries (**Figure 1C**). Furthermore, to explore whether the ROS levels are correlated with the antiglioma effect of TIZ, we examined ROS production using the fluorescent probe 2,7-dichlorodihydrofluorescein diacetate (DCFH-DA) (Zhao et al., 2021). An increase in ROS production was observed in U87MG cells after TIZ treatment compared with the vehicle group, significantly diminished by ROS scavenger NAC (**Figures 1D,E**). In particular, the nuclear ROS levels were augmented sharply in the 10 μM TIZ group, which suggested that damage to biological behavior in the nucleus might be involved in the antiglioma mechanism of TIZ. Fluorescence intensity analysis by flow cytometry confirmed the conclusion obtained by the microscopy (**Figure 1F**). Therefore, these data suggested that TIZ suppressed the viability and proliferation of human glioma cells, and the intranuclear activities might be disrupted in this process.

Cyclin-Dependent Kinases Are Potential Targets of TIZ Against Glioma

To explore the potential targets of TIZ in GBM, we performed target-binding predictions using SEAware software and Swiss Target Prediction based on the structure of TIZ (**Figure 2A**) and obtained a total of 35 corresponding potential target genes (**Supplementary Table S1**). A total of 20492 genes related to glioma were also collected in the GeneCards and CTD databases (data not shown).

Comparing the data of the two groups by using bioinformatics & evolutionary genomics, 32 promising antiglioma targets of TIZ were encapsulated, as shown in **Figure 2B**. The results from the Gene ontology enrichment analyses of the top 20 target genes showed that the genes enriched in the biological processes (BP) category involved protein autophosphorylation, cell proliferation, and apoptotic processing (**Supplementary Figure S1A**). In the molecular function (MF) category, the target genes were mainly involved in protein binding (**Supplementary Figure S1B**). In the cell components (CC) category, both the cytosol and nucleus contained these targets (**Supplementary Figure S1C**). KEGG pathway enrichment analysis showed an enhanced cell cycle of pathways in cancer (**Figure 2C**). A detailed p value analysis is provided in **Supplementary Table S2**.

To further anchor the potential targets, a top10 gene network was constructed using the cytoHubba module in Cytoscape, and the node's degree and related parameters were analyzed by Network Analyzer (**Figure 2D**). Cyclin-dependent kinases (CDKs) 1, 4, 5, and 2 ranked at the top of the score,

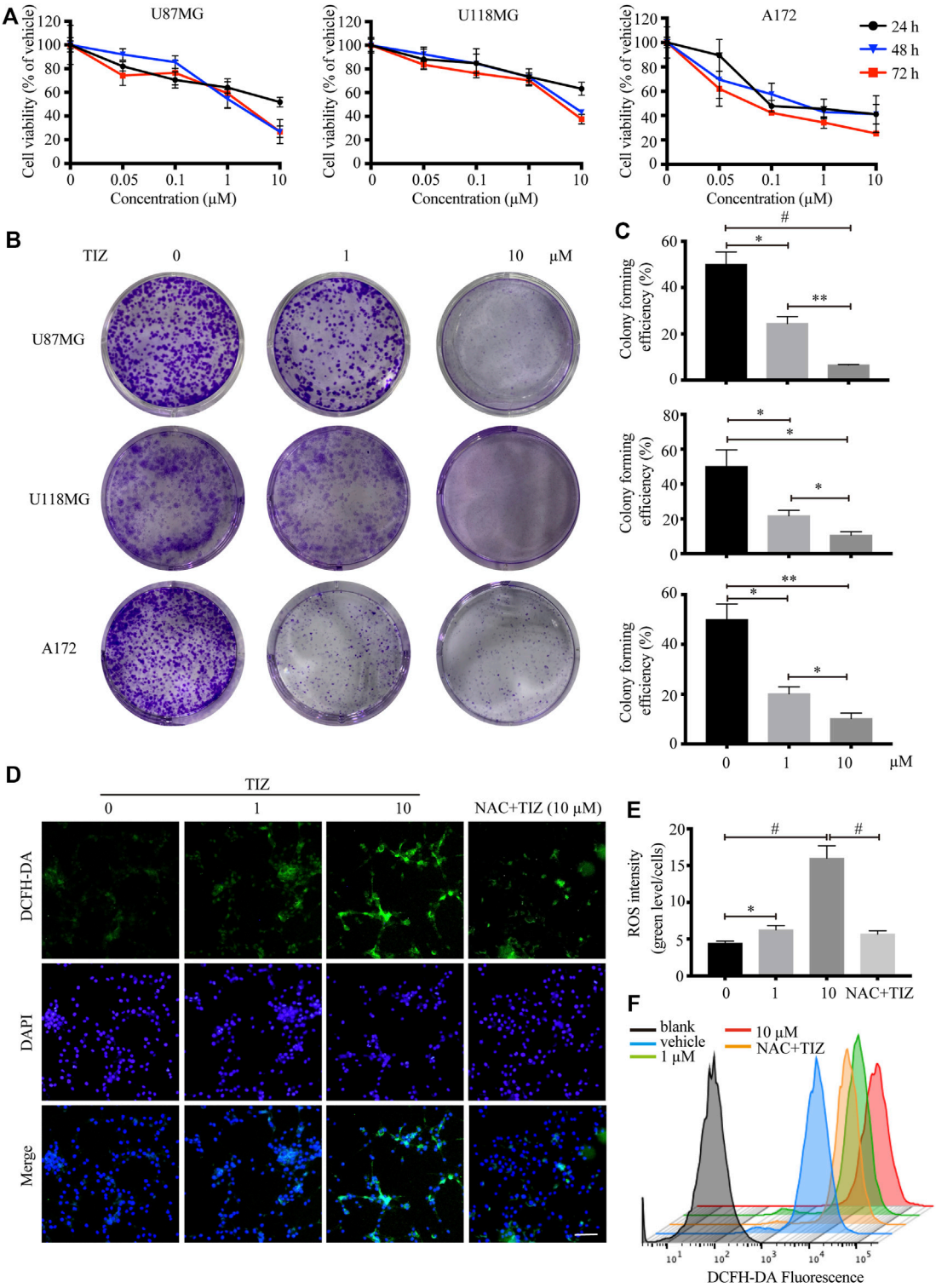

FIGURE 1 | TIZ inhibits GBM cell growth and upregulates ROS levels *in vitro*. **(A)** The cell viability of U87MG, U118 MG, and A172 cells was determined by CCK-8 assays after 24, 48, and 72 h of TIZ treatment. **(B)** Representative images of U87MG colony, U118 MG colony, and A172 colony after the treatment with different concentrations of TIZ. **(C)** Quantification of colony area in colony formation assays (n = 3). **(D)** Representative images of ROS levels in various U87MG cells after the treatment with the indicated concentrations of TIZ for 24 h, NAC (5 mM) was pretreated for 2 h before TIZ treatment. ROS-positive cells were detected by the indicator dye DCFH-DA. Scale bar = 100 μm. **(E)** Quantification of ROS intensities using the ratio of fluorescent intensity and cell numbers (n = 5). **(F)** Flow cytometric measurements of the average fluorescence intensity of U87MG cells. The experiments were repeated three times independently. Data are presented as the mean ± SD ($^{*}p < 0.05$, $^{**}p < 0.01$, $^{\#}p < 0.001$).

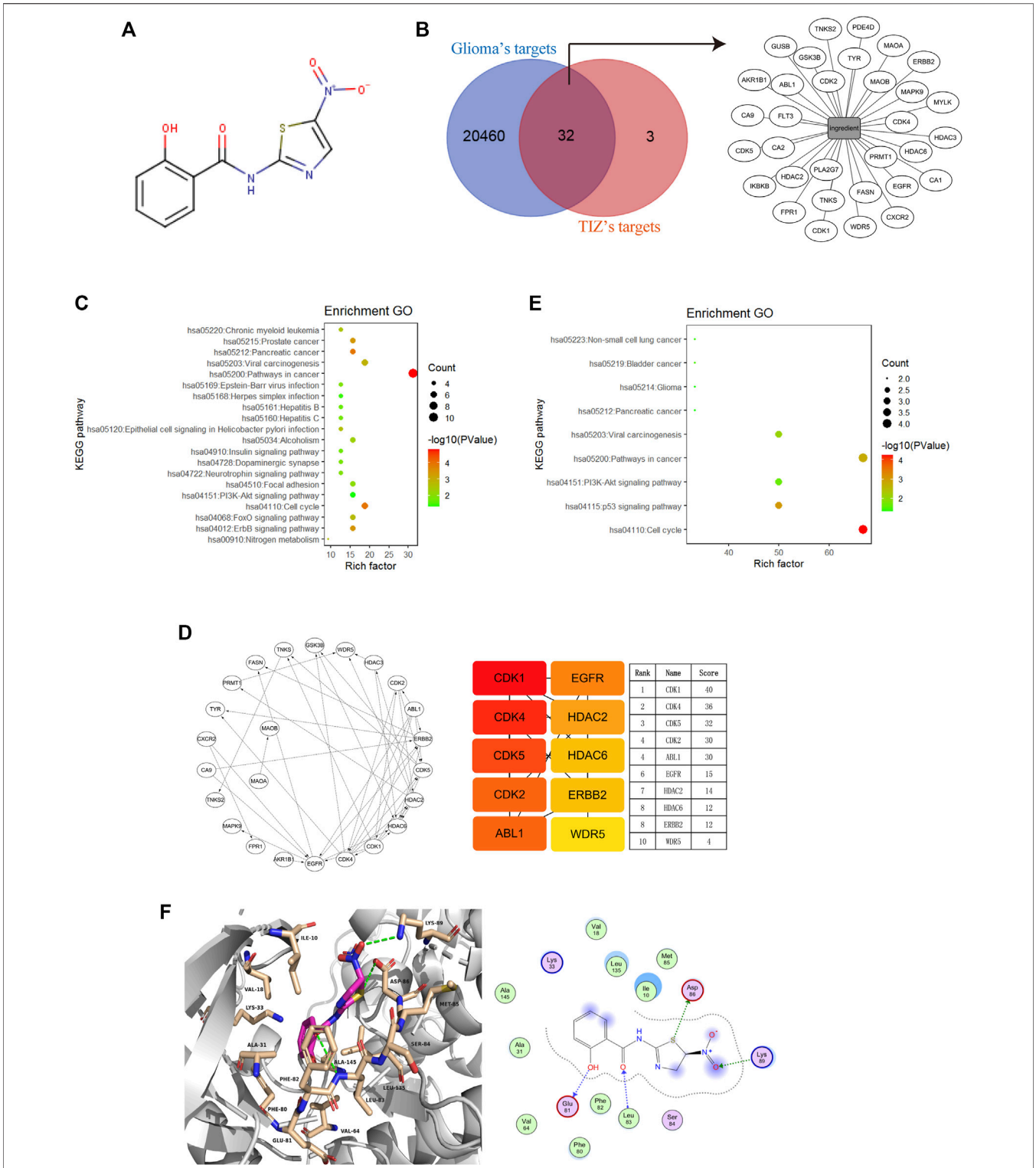

FIGURE 2 | Cyclin-dependent kinases are potential targets of TIZ against glioma. **(A)** The structure of TIZ. **(B)** Venn diagram of the shared targets and the TIZ-target network. The related targets of GBM and TIZ were obtained from GeneCards and SEAware, respectively. **(C)** KEGG pathway enrichment analysis of the top 20 target genes. **(D)** Schematic diagram of target network connections and the top 10 targets and their scores. NetworkAnalyzer was employed to analyze the node's degree and related parameters. The color of nodes changed from orange to red, which indicates that the affinity degree gradually increases from weak to strong. **(E)** KEGG pathway enrichment analysis of targets whose score was greater than 15. **(F)** Docking diagram of CDK1 and TIZ. Key interactions include hydrogen bonds formed by multiple atoms of TIZ with ASP86, Lys89, Glu81, and Leu83.

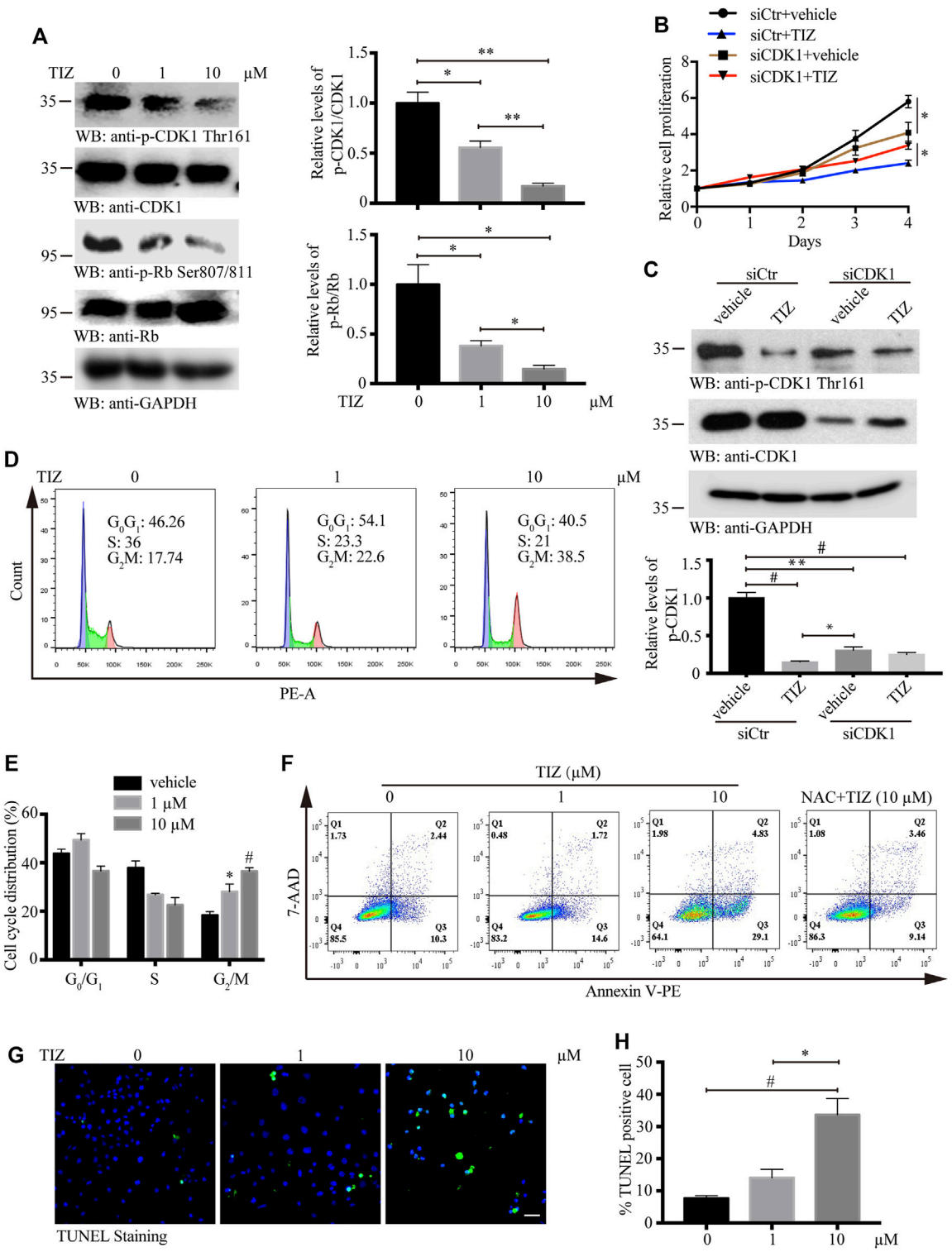

FIGURE 3 | TIZ arrests the cell cycle at the G2/M phase and induces apoptosis of GMB by inhibiting the activities of CDK1. **(A)** TIZ inhibits the activity of CDKs. U87MG cells were treated for 48 h with the indicated concentration of TIZ. Cell lysates were immunoblotted with anti-phospho CDK1 Thr161, a marker of activated CDK1, and anti-phospho Rb Ser807/811, a marker of cellular CDK activity. Right, Quantification of the relative levels of p-CDK1 Thr161 and p-Rb Ser807/811 ($n = 3$). **(B)** CCK-8 assay of U87MG cells treated with TIZ (10 μM) or siCDK1 or their combination for up to 4 days. **(C)** Western blot analysis of U87MG cells treated with TIZ (10 μM), siCDK1, or their combination for 48 h. Down, quantification of the relative levels of CDK1 ($n = 3$). **(D)** Flow cytometric analysis of cycle distribution showed that TIZ arrested the cell cycle of U87MG cells at the G2/M phase. **(E)** Quantification of cycle distribution confirmed G2/M phase arrest ($n = 3$). **(F)** Flow cytometric analysis of apoptosis in cells double-stained with Annexin V-PE and 7-AAD. **(G)** TUNEL staining of U87MG cells after the treatment with the indicated concentration of TIZ for 48 h. Scale bar = 50 μm. **(H)** Quantification of TUNEL-positive cells ($n = 5$). Blot data are representative of three independent experiments. Data are presented as the mean ± SD ($^{*}p < 0.05$, $^{**}p < 0.01$, $^{\#}p < 0.001$).

indicating that TIZ may act directly on these proteins to inhibit the cell cycle of glioma cells. KEGG pathway enrichment analysis of targets with scores greater than 15 mirrored the conclusion that the cell cycle was probably involved in the pharmacological mechanism of TIZ (**Figure 2E**). A detailed *p* value is provided in **Supplementary Table S3**.

To gain insight into the role of CDKs in human GBM, we analyzed a dataset from The Cancer Genome Atlas (TCGA) featuring expression and the corresponding clinical data of the selected GBM patient samples. Notably, when compared with the normal brain tissues, in addition to CDK5, the mRNA expression of CDK1, CDK2, and CDK4 was highly expressed in GBM patient samples (**Supplementary Figure S1D**). Next, we performed docking to elucidate the binding mode of TIZ with CDK1 (PDB ID: 6GU6). From the generated docking model, we found that TIZ was located in the active pocket of CDK1 with a calculated binding free energy of −36 kcal/mol by the GBVI/WSA dG scoring function, and formed multiple hydrogen bonds with ASP86, Lys89, Glu81, and Leu83 (**Figure 2F**). In parallel, the binding free energy of TIZ with CDK2 (PDB ID: 6Q4G) and CDK4 (PDB ID: 4GCJ) was calculated to be −25 kcal/mol and −19 kcal/mol, respectively (**Supplementary Figures S1E,F**). Although all calculated binding forces of TIZ with these three target proteins were smaller than those of TIZ with the ligand dinaciclib in the 6GU6 crystal (**Supplementary Figure S1G**, −41 kcal/mol), the docking results showed that TIZ has an affinity for CDKs, especially CDK1. Thus, these findings suggested that CDKs are potential targets of TIZ against GBM.

TIZ Arrests the Cell Cycle at G2/M Phase and Induces Apoptosis of GMB by Inhibiting the Activities of CDK1

During the embryonic breeding period, CDK1 binds to all cyclins, resulting in the phosphorylation of the retinoblastoma protein (pRb), and embryos fail to develop to the morula and blastocyst stages in the absence of CDK1. CDK1 was identified as the only essential cell cycle CDK and could execute all the events that are required to drive cell division (Santamaría et al., 2007). To validate whether CDK1 is the core target of TIZ, U87MG cells were treated with different concentrations of TIZ (1 and 10 μM) for 24 h, and cell lysates were immunoblotted with anti-CDK1 Thr161, a marker of activated CDK1, and anti-Rb Ser807/811, a marker of cellular CDK activity. As expected, the phosphorylation levels of these two proteins were significantly inhibited by TIZ (**Figure 3A**). To examine whether CDK1 is a direct molecular target of TIZ responsible for its antiproliferative effect, we treated U87MG cells with either siRNA control or CDK1-specific siRNA, followed by treatment with vehicle or TIZ for 4 days and monitoring of cell proliferation. Notably, the depletion of CDK1 reduced cell proliferation but compared with cells transfected with control siRNA, depletion of CDK1 attenuated the inhibitory effect of TIZ, which indicated that the inhibition of CDK1 is involved in the antiproliferative effect of TIZ (**Figure 3B**). Western blotting confirmed the successful knockdown of CDK1 and reflected the levels of p-CDK1 Thr161 (**Figure 3C**). Together, these data showed that CDK1 is the main cellular target of TIZ.

Inspired by the target determination process, flow cytometric analysis by propidium iodide was performed to investigate whether the observed TIZ effect on glioma cell viability was due to cell cycle arrest. As shown in **Figure 3D**, the percentage of cells in the S phase was reduced from 36% to approximately 22%, but notably, the cell rates in G2/M phase were augmented from 17.7% to 38.5% after the TIZ treatment at 1 and 10 μM, respectively. Quantitative analysis of cell cycle distribution mirrored these discoveries (**Figure 3E**). Based on cell cycle analysis, we quantitatively analyzed the apoptotic effect of TIZ using apoptosis-Annexin V/PE and 7AAD double-fluorescence staining by flow cytometry. The results indicated that the 48 h TIZ treatment significantly induced concentration-dependent apoptosis in U87MG cells. As shown in **Figure 3F**, the early apoptosis rate increased from 14.6% to 29.1% when the concentration increased from 1 to 10 μM, whereas the proportion of apoptotic cells was only 10.3% and 9.14% in the vehicle control and NAC pretreatment, respectively. We used another method to further confirm the proapoptotic effect of TIZ by a TUNEL staining. The results showed that TIZ also induced late apoptosis due to DNA damage in U87MG cells (**Figures 3G,H**). Therefore, our results indicated that TIZ arrests the cell cycle at the G2/M phase to induce apoptosis of GMB by inhibiting the activities of CDK1.

TIZ Inhibits GBM Progression in Subcutaneous Xenograft in Nude Mice and Exhibits Preliminary Safety

To evaluate the antiglioma activity and preliminary safety of TIZ *in vivo*, a subcutaneous xenograft model was established by inoculating U87MG nude mice and intraperitoneally treating the mice with 5 or 15 mg/kg of TIZ or vehicle three times per week for 3 weeks after the tumor volume reached approximately 100 mm^3 (**Figure 4A**). Representative photographs of mice from each group were taken at the endpoint (**Figure 4B**). Consistent with the gross observations, TIZ significantly reduced tumor volumes compared to the rapidly growing tumors in the vehicle group (**Figure 4C**). Next, we checked the related protein expression levels in the tumor tissue samples. Consistent with the *in vitro* results, the phosphorylation levels of CDK1 Thr161 and Rb Ser807/811 were inhibited, and active caspase 3 was increased by TIZ in a dose-dependent manner. CCNB1 (Cyclin B1), a protein that can form a complex with CDK1 in the G2/M phase, was accordingly reduced. However, the expression levels of CCNA1 (Cyclin A1) showed no obvious change between the experimental groups (**Figure 4D**). H&E staining demonstrated no obvious lesions in the heart, liver, spleen, lung, or kidney (**Figure 4E**). Together with the analysis results of RBCs and WBCs from the whole blood, as well as ALT, AST, and CREA from serum, we found that the side effects of TIZ were modest (**Supplementary Figure S2**), which suggested that TIZ does not have detectable systemic toxicity.

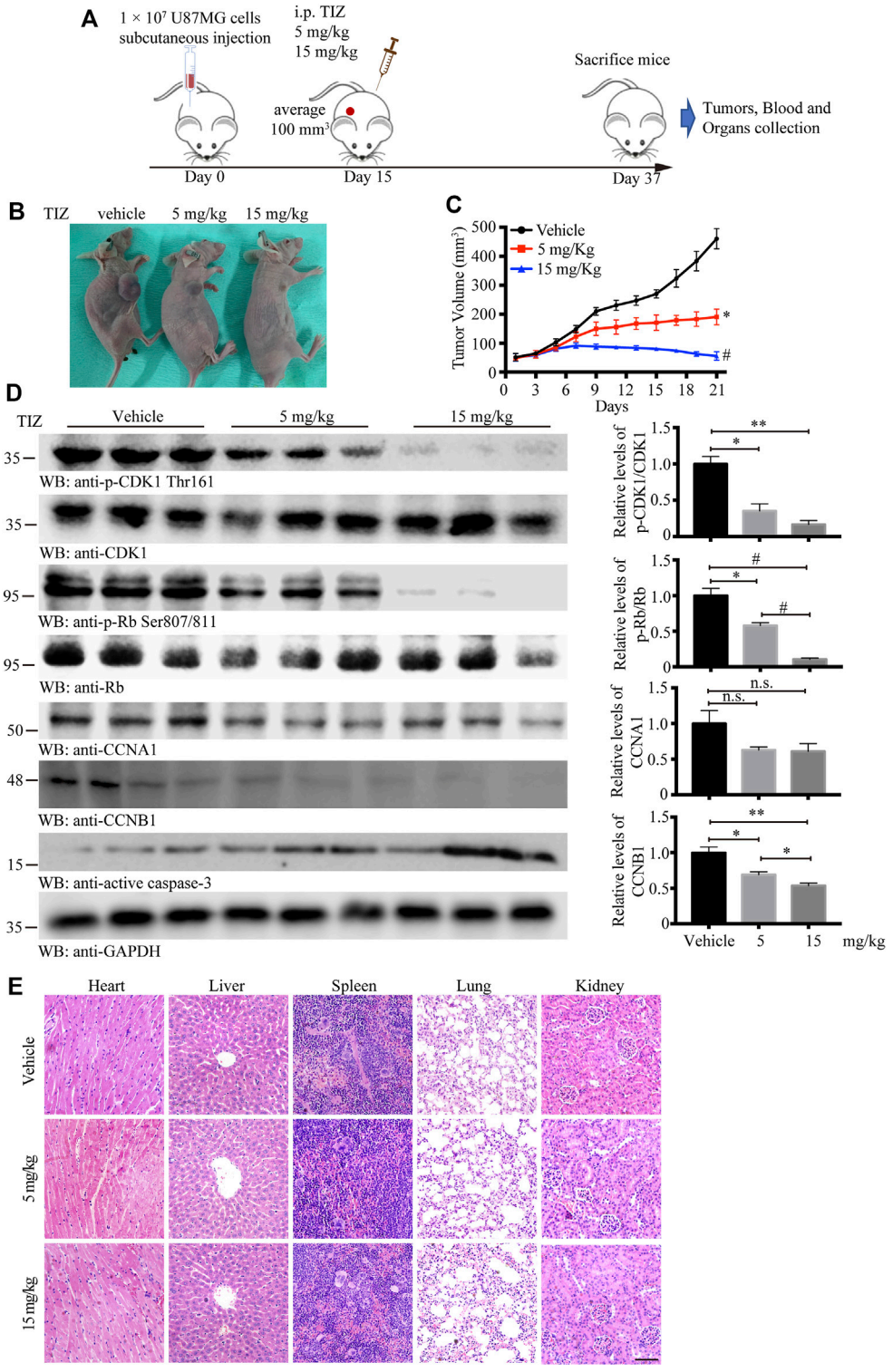

FIGURE 4 | TIZ inhibits GBM growth in a subcutaneous xenograft nude mouse model. **(A)** Schematic of xenograft mouse model establishment and TIZ administration. **(B)** Representative images of GBM growth after different dosages of TIZ administration. **(C)** TIZ inhibited GBM growth as measured by tumor volume (n = 6). **(D)** Western blot analysis of tumor lysates with various indicated antibodies. Quantifications of relative protein levels are shown in the right panel (n = 3). Blot data are representative of three independent experiments. **(E)** TIZ administration displayed no detectable toxicity. Histological analysis of H&E-stained tissue sections of representative mice in the TIZ or vehicle-treated group. Scale bar, 100 μm. Data are presented as the mean ± SD (n.s. means no significance, $^{*}p < 0.05$, $^{**}p < 0.01$, $^{\#}p < 0.001$).

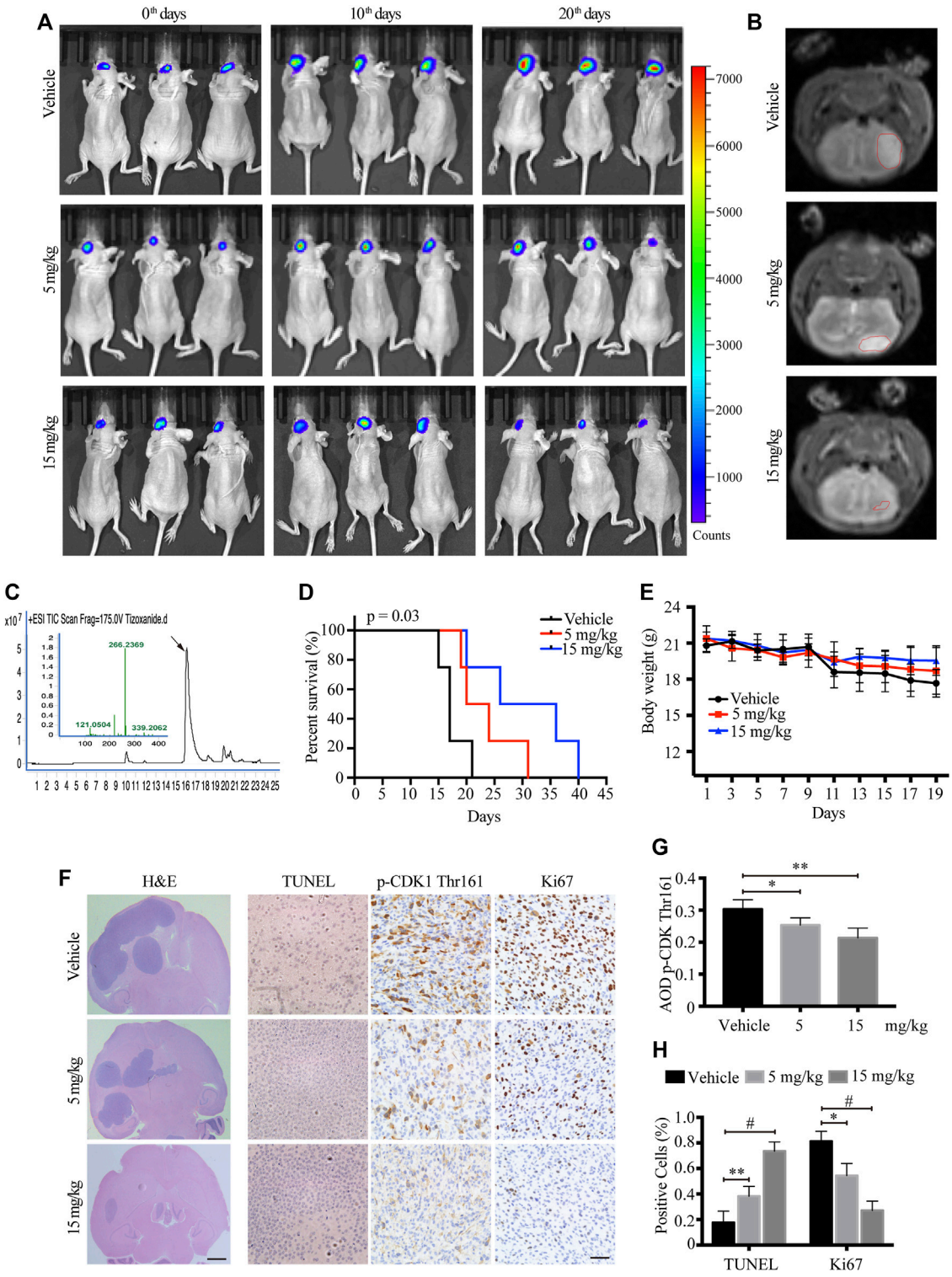

FIGURE 5 | TIZ suppresses the intracranial growth of GBM and elongates mouse survival. **(A)** IVIS analysis of fluorescence signal intensity in the brain at different stages of TIZ administration (*n* = 12 mice per group). **(B)** Representative images of brain tumor volume scan by the small animal MRI system. **(C)** Representative HPLC-MS chromatograms of the concentration analysis of TIZ in the glioma homogenate samples. **(D)** The survival curves of mice bearing glioma in the brain. **(E)** Bodyweight curves of nude mice during TIZ treatment. **(F)** H&E, TUNEL, and p-CDK1 Thr161 and Ki67 IHC staining of tumor slices in various groups. Scale bar = 1 mm (left) and 50 μm (right). Quantification of IHC staining of p-CDK1 Thr161 **(G)** and positive TUNEL and Ki67 staining **(H)** (*n* = 5).

TIZ Suppresses the Intracranial Growth of GBM and Prolongs Mouse Survival

To monitor the therapeutic effect of TIZ on GBM in greater detail, we further used a murine intracranial xenograft model *in situ* by stereotaxically injecting U87MG-luc cells into the brain. After confirming tumor formation by IVIS, each group of nude mice was administered TIZ with the same schedule of subcutaneous mode. Representative images monitored by IVIS were captured on the 0th,10th, and 20th days and showed that TIZ attenuated the growth of tumors (**Figure 5A**). A week after drug treatment, mice were subjected to magnetic resonance imaging (MRI) and mirrored the IVIS results (**Figure 5B**). To investigate the efficiency and blood-brain barrier (BBB) permeability of TIZ, we determined the concentration of TIZ in glioma after intraperitoneal injections of 5 and 15 mg/kg using HPLC-MS (**Figure 5C**). The results showed that TIZ can cross BBB and the average concentration reached 6.978 μg/kg and 20.084 μg/kg, respectively (**Supplementary Table S4**). The median survival compared by Kaplan-Meier analysis showed that TIZ at 15 mg/kg enhanced mouse survival (**Figure 5D**), and the body weight of mice in the drug group remained relatively stable compared with the weight loss in the vehicle group (**Figure 5E**). Furthermore, we harvested and sliced brains after sacrificing nude mice and performed histological staining (**Figure 5F**). Tumor size tracked by H&E staining of the entire brain slice confirmed that TIZ significantly suppressed the growth of GBM, especially at the dosage of 15 mg/kg (**Figure 5F**, left). As expected, the TUNEL assay showed extensive apoptosis in the TIZ-treated groups, and IHC staining for Ki67 indicated an almost 55% reduction in the number of proliferating cells in the 15 mg/kg TIZ group compared to the vehicle group, which was in alignment with the p-CDK1 Thr161 staining (**Figure 5F** right). Quantification of IHC staining confirmed these findings (**Figures 5G,H**). Thus, the data supported our previous observations that TIZ significantly blocks GBM growth by suppressing cell proliferation and inducing apoptosis by inhibiting the activity of CDK1 *in vivo*.

DISCUSSION

The deregulated proliferation and inhibition of apoptosis lie at the heart of all tumor development, which presents two definite directions for therapeutic intervention in all cancers. Thus, the capability to induce cell cycle arrest and promote apoptosis is a common criterion of potential chemotherapeutic agents (Liu et al., 2012). The augmentation of cell proliferation is largely due to tumor cells suffering defects that derail the cell cycle machinery. Such defects can target either mutation of upstream signaling cascades, such as mitogen protein tyrosine kinase (PTK) and G-protein signal transducers, or elements of the cell cycle itself that both eventually converge to trigger cell cycle deregulation (Malumbres and Carnero, 2003). In the present study, we identified TIZ as a novel inhibitor of the cell cycle and induced apoptosis in GBM. Although NTZ was first reported as an autophagy inhibitor and induced cell cycle arrest in GBM by upregulating ING1 (p33) expression (Wang et al., 2018), it is intrinsically linked with our finding that CDK1 is a target of TIZ. Because CDK1 and checkpoint kinase 1 (CHK1) can phosphorylate $p33^{ING1b}$ at Ser-126 in non-stress and DNA damage conditions, respectively, which increases the stability of $p33^{ING1b}$ (Garate et al., 2007). Thus, it can be speculated that when CDK1 activity is inhibited by TIZ, CHK1 replay predominantly phosphorylates $p33^{ING1b}$ at Ser-126 followed by the upregulation of $p33^{ING1b}$. Meanwhile, we identified CDK1 as a direct affinity target of TIZ and found that the antiglioma efficiency of TIZ was more robust than that of NTZ by referring to the previously reported data (Wang et al., 2018). NTZ has been reported to spontaneously hydrolyzes to TIZ once it dissolves in water and reaches equilibrium in 10 h (Qu et al., 2018), which could provide a plausible explanation for the antitumor advantages of TIZ.

In the process of finding a target for TIZ, we took a strategy based on network pharmacological disease target analysis together with computerized compound-target seeking technology, which is frequently used in the initial stage of innovative drug development (Gu et al., 2020). We obtained a series of candidate direct-binding proteins of TIZ, including CDK1, CDK4, CDK5, CDK2, and ABL1, which were ranked in the top five (**Figure 2**). In terms of CDKs, unlike unicellular organisms such as yeasts, only a single cyclin-dependent kinase, CDK1, is required to drive cell division (Michowski et al., 2020). Mammalian cells are traditionally believed to require the sequential activation of CDKs, such as CDK1, CDK2, CDK3, CDK4, and CDK6, to push interphase proceeding through mitosis (Malumbres and Barbacid, 2005). However, a report published in 2007 indicated that CDK1 is the only essential cell cycle CDK; in the absence of interphase CDKs, CDK1 can execute all the events that are required to drive cell division (Santamaría et al., 2007). Following this point of view, although the results of molecular docking supported the existence of affinity potential of TIZ with CDK1, CDK2, and CDK4, we only performed siRNA targeting CDK1 to verify the inhibitory effect of TIZ on the proliferation of gliomas. In addition, the CDK family comprises 21 phosphotransfer enzymes (CDK1-21) with diverse cellular functions, the development of CDK inhibitors with isozyme selectivity is technically challenging due to the catalytic pocket across the CDK enzyme family being highly conserved. Five cell-permeable energy transfer probes were tested to comprehensively profile CDK engagement in live cells (Wells et al., 2020). However, these probes are still on the way to commercialization, and we expect to get more accurate data about TIZ selectivity for CDK1-21 in the future and not just limited to CDK1, 2, 4, and 5 that are focused in our research. Tyrosine-protein kinase ABL1, targeting mitochondria in the response to oxidative stress and thereby mediating mitochondrial dysfunction and cell death, was disclosed as a target against *Entamoeba histolytica*, whereas NTZ is a classical drug for parasitic amoeba infection (Gilles and Hoffman, 2002; Sauvey et al., 2021). It will be interesting to verify the role of these TIZ direct binding proteins in different contexts.

An intriguing finding in the present study is that the downregulated expression of cyclin A1 is less desensitized than

that of cyclin B1 after the GBM cells were treated with TIZ. Reviewing the entire mitotic process of mammalian cells, each meiotic, as well as mitotic G2 phase to M phase is initialized through the activation of a complex of enzymatic subunit CDK1 and the regulatory cyclin B1 (Masui, 2001). The stability and activity of CDK1/cyclin B1 are tightly regulated by the phosphorylation state of CDK1, both by activating phosphorylation at Thr161 and inhibitory phosphorylation at Thr14 and Tyr15 (Timofeev et al., 2010; Shi and Feng, 2021). When complex inactivation occurs, cyclin B1 dissociates from CDK1 and becomes polyubiquitinated and targeted by the proteasome, and cyclin B1 degradation is crucial for long-term CDK1/cyclin B1 inactivation, whereas cyclin A1 is expressed during meiosis and embryogenesis and plays a critical role in S phase progression as a complex with CDK2 (Kubiak et al., 2003; Hirayama et al., 2020). Because TIZ could directly inhibit CDK1 phosphorylation at Thr161 and inhibit the stability of CDK1/cyclin B1 to trigger cyclin B1 degradation, the downregulation of cyclin B1 was more sensitive than that of cyclin A1, which might be attributed to the mechanism by which TIZ caused G2/M arrest.

Reactive oxygen species (ROS) play an important role in controlling certain stages of the cell cycle. For instance, CDK1/cyclin B1 is inactivated by oxidation; conversely, the complex itself seems concomitant with ROS leakage at the G2/M transition (Wang et al., 2014; Chang et al., 2021). ROS levels have been observed to peak in mitosis, resulting in mitotic accumulation of oxidized protein cysteine residues (Patterson et al., 2019). The results of several studies suggested the possibility of ROS-mediated oxidative DNA damage in the cell cycle process (Mittal and Pandey, 2014; Xie et al., 2018). In this study, a dose-dependent augmentation in ROS levels, especially in the nucleus, was observed after TIZ treatment, together with NAC significantly attenuated the ROS levels and apoptosis induced by TIZ treatment (**Figures 1D**, **3F**), implying damage to the DNA synthesis process. Mechanistically, our studies indicate that TIZ induces apoptosis of GBM mainly through ROS accumulation during G2/M arrest.

Drug repurposing refers to the reuse of clinical drugs to treat non-indication diseases. It has been a hot spot in drug development in recent years due to the compounds that have already been tested in humans and have demonstrated an acceptable level of safety and tolerability (Levin et al., 2020). NTZ is generally well tolerated, and adverse events have been mild and transient, and principally related to the gastrointestinal tract. Although in the subcutaneous xenograft mice, there was an unexplained rise in WBCs after TIZ administration (**Supplementary Figure S2B**), no significant adverse events have been noted in human trials as a new thiazolide antiparasitic agent (Fox and Saravolatz, 2005). NTZ is a FAD-approved drug that is used to treat infections by protozoa, helminths, anaerobic bacteria, microaerophilic bacteria, and viruses. The ADMET properties have been elucidated in the development process. The ADMET properties of TIZ could deeply refer to these of NTZ. Our results regarding the preliminary safety of TIZ as an antitumor candidate partially support the possibility of transitioning it into clinical research for a chemotherapy drug. Meanwhile, one situation we are facing is the continuation of the coronavirus disease 2019 (COVID-2019) pandemic, which has created panic and alarm across the globe. NTZ, as a first-in-class broad-spectrum antiviral agent, is widely reported to have the potential to treat COVID-2019 (Mahmoud et al., 2020; Rocco et al., 2020). To date, 10 clinical trial protocols focusing on evaluating the effects of NTZ in the treatment of COVID-19 have been registered at ClinicalTrials.gov, but preliminary results have not yet been reported (Martins-Filho et al., 2020).

CONCLUSION

In summary, our results show that TIZ, a novel CDK1 inhibitor, has favorable efficacy in inhibiting GBM *in vitro* and *in vivo*. It promotes apoptosis in glioma cells by inducing G2/M cell cycle arrest by inhibiting the phosphorylation of CDK1 and the activity of the CDK1/cyclin B1 complex. Both *in vivo* subcutaneous and intracranial orthotopic xenograft models showed that TIZ could inhibit the growth of GBM and prolong the survival of nude mice. Moreover, TIZ has shown good safety profiles. Taken together, the results indicate that TIZ is a favorable small-molecule antiglioma drug candidate, and its further repurposing investigations are warranted.

DATA AVAILABILITY STATEMENT

The original contributions presented in the study are included in the article/**Supplementary Material**, further inquiries can be directed to the corresponding author.

ETHICS STATEMENT

The animal study was reviewed and approved by the Second Xiangya Hospital of Central South University.

AUTHOR CONTRIBUTIONS

SL: Conceived the project, designed the experiments, analyzed the data, and wrote the manuscript. SH and JX: Performed most of the experiments. JW: Facilitated animal experiments. JL: Performed an MRI scan for nude mice. XF: Provides flow cytometry and fluorescence analysis platform. CY: Raises the nude mice. DX: Assisted with data analysis and critically read the manuscript. All the authors have read and approved the final manuscript before submission.

FUNDING

The research was supported by the Research funds of Natural Science Foundation of Hunan Province (No. 2020JJ9009, SL).

ACKNOWLEDGMENTS

Thank Zhihong Liu from Sun Yatsen University for providing the fore-mentioned docking software and Wecomput Technology for providing compound-target search consulting.

SUPPLEMENTARY MATERIAL

The Supplementary Material for this article can be found online at: https://www.frontiersin.org/articles/10.3389/fphar.2022.895573/full#supplementary-material

Supplementary Figure S1 | Bioinformatic analysis of the potential targets of TIZ and target-TIZ docking results. **(A)** Gene ontology (GO) biological process enrichment analysis of top20 target genes. **(B)** GO molecular function enrichment analysis of top20 target genes. **(C)** GO cellular component analysis of top20 target genes. **(D)** The mRNA expression of CDK1, CDK2, CDK4, and CDK5 were collected from The Cancer Genome Atlas (TCGA) and Gene Expression Profiling Interactive Analysis (GEPIA) databases. T, tumor; N, normal. **(E)** Docking diagram of CDK4 and TIZ. Key interactions include hydrogen bonds formed by a hydrogen atom of TIZ with Asp86. **(G)** Docking result of CDK1 and itself ligand Dinaciclib. Dinaciclib is a novel potent small-molecule inhibitor of CDK1, CDK2, CDK5, and CDK9. It is being evaluated in clinical trials for various cancer indications.

Supplementary Figure S2 | Analysis of blood biochemical parameters in nude mice after TIZ administration The results of RBC **(A)**, ALT **(C)**, AST **(D)**, and CREA **(E)** showed that Red blood cells and hepatic and renal function in mice have no obvious changes between the vehicle and TIZ -treated groups. The reason for the increase in white blood cells might be that an inflammatory response was stimulated during TIZ administration **(B)**. Data are presented as the mean ± SD ($n = 5$, $^{*}p < 0.05$, $^{**}p < 0.01$, $^{\#}p < 0.001$).

REFERENCES

Anderson, V. R., and Curran, M. P. (2007). Nitazoxanide: a Review of its Use in the Treatment of Gastrointestinal Infections. *Drugs* 67 (13), 1947–1967. doi:10.2165/00003495-200767130-00015

Batash, R., Asna, N., Schaffer, P., Francis, N., and Schaffer, M. (2017). Glioblastoma Multiforme, Diagnosis and Treatment; Recent Literature Review. *Curr. Med. Chem.* 24 (27), 3002–3009. doi:10.2174/0929867324666170516123206

Chang, J. G., Tien, N., Chang, Y. C., Lin, M. L., and Chen, S. S. (2021). Oxidative Stress-Induced Unscheduled CDK1-Cyclin B1 Activity Impairs ER-Mitochondria-Mediated Bioenergetic Metabolism. *Cells* 10 (6), 1280. doi:10.3390/cells10061280

Chlipala, E., Bendzinski, C. M., Chu, K., Johnson, J. I., Brous, M., Copeland, K., et al. (2020). Optical Density-Based Image Analysis Method for the Evaluation of Hematoxylin and Eosin Staining Precision. *J. Histotechnol.* 43 (1), 29–37. doi:10.1080/01478885.2019.1708611

Di Santo, N., and Ehrisman, J. (2014). A Functional Perspective of Nitazoxanide as a Potential Anticancer Drug. *Mutat. Res.* 768, 16–21. doi:10.1016/j.mrfmmm.2014.05.005

Fischer, A. H., Jacobson, K. A., Rose, J., and Zeller, R. (20082008). Hematoxylin and Eosin Staining of Tissue and Cell Sections. *CSH Protoc.* 2008 (5), pdb.prot4986. doi:10.1101/pdb.prot4986

Fox, L. M., and Saravolatz, L. D. (2005). Nitazoxanide: a New Thiazolide Antiparasitic Agent. *Clin. Infect. Dis.* 40 (8), 1173–1180. doi:10.1086/428839

Garate, M., Campos, E. I., Bush, J. A., Xiao, H., and Li, G. (2007). Phosphorylation of the Tumor Suppressor p33(ING1b) at Ser-126 Influences its Protein Stability and Proliferation of Melanoma Cells. *FASEB J.* 21 (13), 3705–3716. doi:10.1096/fj.07-8069com

Gilles, H. M., and Hoffman, P. S. (2002). Treatment of Intestinal Parasitic Infections: a Review of Nitazoxanide. *Trends Parasitol.* 18 (3), 95–97. doi:10.1016/s1471-4922(01)02205-x

Gu, L., Lu, J., Li, Q., Wu, N., Zhang, L., Li, H., et al. (2020). A Network-Based Analysis of Key Pharmacological Pathways of Andrographis Paniculata Acting on Alzheimer's Disease and Experimental Validation. *J. Ethnopharmacol.* 251, 112488. doi:10.1016/j.jep.2019.112488

Guo, S., Li, F., Wang, B., Zhao, Y., Wang, X., Wei, H., et al. (2020). Analysis of Tizoxanide, Active Metabolite of Nitazoxanide, in Rat Brain Tissue and Plasma by UHPLC-MS/MS. *Biomed. Chromatogr.* 34 (2), e4716. doi:10.1002/bmc.4716

Hirayama, M., Wei, F. Y., Chujo, T., Oki, S., Yakita, M., Kobayashi, D., et al. (2020). FTO Demethylates Cyclin D1 mRNA and Controls Cell-Cycle Progression. *Cell Rep.* 31 (1), 107464. doi:10.1016/j.celrep.2020.03.028

Johnson, B. E., Mazor, T., Hong, C., Barnes, M., Aihara, K., McLean, C. Y., et al. (2014). Mutational Analysis Reveals the Origin and Therapy-Driven Evolution of Recurrent Glioma. *Science* 343 (6167), 189–193. doi:10.1126/science.1239947

Kubiak, J. Z., Ciemerych, M. A., Hupalowska, A., Sikora-Polaczek, M., and Polanski, Z. (2003). On the Transition from the Meiotic to Mitotic Cell Cycle during Early Mouse Development. *Int. J. Dev. Biol.* 52 (2-3), 201–217. doi:10.1387/ijdb.072337jk

Lee, S. Y. (2016). Temozolomide Resistance in Glioblastoma Multiforme. *Genes Dis.* 3 (3), 198–210. doi:10.1016/j.gendis.2016.04.007

Levin, J. M., Oprea, T. I., Davidovich, S., Clozel, T., Overington, J. P., Vanhaelen, Q., et al. (2020). Artificial Intelligence, Drug Repurposing and Peer Review. *Nat. Biotechnol.* 38 (10), 1127–1131. doi:10.1038/s41587-020-0686-x

Liu, H., Zhou, B. H., Qiu, X., Wang, H. S., Zhang, F., Fang, R., et al. (2012). T63, a New 4-arylidene Curcumin Analogue, Induces Cell Cycle Arrest and Apoptosis through Activation of the Reactive Oxygen Species-FOXO3a Pathway in Lung Cancer Cells. *Free Radic. Biol. Med.* 53 (12), 2204–2217. doi:10.1016/j.freeradbiomed.2012.10.537

Liu, J., Li, Y., Zhang, J., Cai, Y., Shang, Q., Ma, C., et al. (2019). Comparison of Anesthesia and Tumor Implantation Methods for Establishing Rabbit VX2 Hepatocarcinoma. *Am. J. Transl. Res.* 11 (11), 7157–7165.

Mahmoud, D. B., Shitu, Z., and Mostafa, A. (2020). Drug Repurposing of Nitazoxanide: Can it Be an Effective Therapy for COVID-19? *J. Genet. Eng. Biotechnol.* 18 (1), 35. doi:10.1186/s43141-020-00055-5

Malumbres, M., and Barbacid, M. (2005). Mammalian Cyclin-dependent Kinases. *Trends biochem. Sci.* 30 (11), 630–641. doi:10.1016/j.tibs.2005.09.005

Malumbres, M., and Carnero, A. (2003). Cell Cycle Deregulation: a Common Motif in Cancer. *Prog. Cell Cycle Res.* 5, 5–18.

Martins-Filho, P. R., Barreto-Alves, J. A., and Fakhouri, R. (2020). Potential Role for Nitazoxanide in Treating SARS-CoV-2 Infection. *Am. J. Physiol. Lung Cell Mol. Physiol.* 319 (1), L35–l36. doi:10.1152/ajplung.00170.2020

Masui, Y. (2001). From Oocyte Maturation to the *In Vitro* Cell Cycle: the History of Discoveries of Maturation-Promoting Factor (MPF) and Cytostatic Factor (CSF). *Differentiation* 69 (1), 1–17. doi:10.1046/j.1432-0436.2001.690101.x

Melendez, B., Garcia-Claver, A., Ruano, Y., Campos-Martin, Y., and Mollejo, M. (2011). "Copy Number Alterations in Glioma Cell Lines," in *Glioma - Exploring its Biology and Practical Relevance* (London, UK: intechopen). doi:10.5772/22768

Michowski, W., Chick, J. M., Chu, C., Kolodziejczyk, A., Wang, Y., Suski, J. M., et al. (2020). Cdk1 Controls Global Epigenetic Landscape in Embryonic Stem Cells. *Mol. Cell* 78 (3), 459–e13. e413. doi:10.1016/j.molcel.2020.03.010

Mittal, S., and Pandey, A. K. (2014). Cerium Oxide Nanoparticles Induced Toxicity in Human Lung Cells: Role of ROS Mediated DNA Damage and Apoptosis. *BioMed Res. Int.* 2014. doi:10.1155/2014/891934

Müller, J., and Hemphill, A. (2011). Drug Target Identification in Intracellular and Extracellular Protozoan Parasites. *Curr. Top. Med. Chem.* 11 (16), 2029–2038. doi:10.2174/156802611796575876

Patterson, J. C., Joughin, B. A., van de Kooij, B., Lim, D. C., Lauffenburger, D. A., and Yaffe, M. B. (2019). ROS and Oxidative Stress Are Elevated in Mitosis during Asynchronous Cell Cycle Progression and Are Exacerbated by Mitotic Arrest. *Cell Syst.* 8 (2), 163–e2. doi:10.1016/j.cels.2019.01.005

Qu, Y., Olsen, J. R., Yuan, X., Cheng, P. F., Levesque, M. P., Brokstad, K. A., et al. (2018). Small Molecule Promotes β-catenin Citrullination and Inhibits Wnt Signaling in Cancer. *Nat. Chem. Biol.* 14 (1), 94–101. doi:10.1038/nchembio.2510

Rocco, P. R., Silva, P. L., Cruz, F. F., Junior, M. A. C., Tierno, P. F., Moura, M. A., et al. (2020). Early Use of Nitazoxanide in Mild Covid-19 Disease: Randomised,

Placebo-Controlled Trial. *Eur. Respir. J.* 58 (1), 2003725. doi:10.1183/13993003.03725-2020

Rossignol, J. F. (2014). Nitazoxanide: a First-In-Class Broad-Spectrum Antiviral Agent. *Antivir. Res.* 110, 94–103. doi:10.1016/j.antiviral.2014.07.014

Santamaría, D., Barrière, C., Cerqueira, A., Hunt, S., Tardy, C., Newton, K., et al. (2007). Cdk1 Is Sufficient to Drive the Mammalian Cell Cycle. *Nature* 448 (7155), 811–815.

Sauvey, C., Ehrenkaufer, G., Shi, D., Debnath, A., and Abagyan, R. (2021). Antineoplastic Kinase Inhibitors: A New Class of Potent Anti-amoebic Compounds. *PLoS Negl. Trop. Dis.* 15 (2), e0008425. doi:10.1371/journal.pntd.0008425

Schonbrunn, E., Betzi, S., Alam, R., Martin, M. P., Becker, A., Han, H., et al. (2013). Development of Highly Potent and Selective Diaminothiazole Inhibitors of Cyclin-dependent Kinases. *J. Med. Chem.* 56 (10), 3768–3782. doi:10.1021/jm301234k

Shakya, A., Bhat, H. R., and Ghosh, S. K. (2018). Update on Nitazoxanide: a Multifunctional Chemotherapeutic Agent. *Curr. Drug Discov. Technol.* 15 (3), 201–213. doi:10.2174/1570163814666170727130003

Shi, F., and Feng, X. (2021). Decabromodiphenyl Ethane Exposure Damaged the Asymmetric Division of Mouse Oocytes by Inhibiting the Inactivation of Cyclin-dependent Kinase 1. *FASEB J.* 35 (4), e21449. doi:10.1096/fj.202002585R

Timofeev, O., Cizmecioglu, O., Settele, F., Kempf, T., and Hoffmann, I. (2010). Cdc25 Phosphatases Are Required for Timely Assembly of CDK1-Cyclin B at the G2/M Transition. *J. Biol. Chem.* 285 (22), 16978–16990. doi:10.1074/jbc.M109.096552

Wang, X., Shen, C., Liu, Z., Peng, F., Chen, X., Yang, G., et al. (2018). Nitazoxanide, an Antiprotozoal Drug, Inhibits Late-Stage Autophagy and Promotes ING1-Induced Cell Cycle Arrest in Glioblastoma. *Cell Death Dis.* 9 (10), 1032–1047. doi:10.1038/s41419-018-1058-z

Wang, Z., Fan, M., Candas, D., Zhang, T. Q., Qin, L., Eldridge, A., et al. (2014). Cyclin B1/Cdk1 Coordinates Mitochondrial Respiration for Cell-Cycle G2/M Progression. *Dev. Cell* 29 (2), 217–232. doi:10.1016/j.devcel.2014.03.012

Wells, C. I., Vasta, J. D., Corona, C. R., Wilkinson, J., Zimprich, C. A., Ingold, M. R., et al. (2020). Quantifying CDK Inhibitor Selectivity in Live Cells. *Nat. Commun.* 11 (1), 2743. doi:10.1038/s41467-020-16559-0

Wood, D. J., Korolchuk, S., Tatum, N. J., Wang, L. Z., Endicott, J. A., Noble, M. E. M., et al. (2019a). Differences in the Conformational Energy Landscape of CDK1 and CDK2 Suggest a Mechanism for Achieving Selective CDK Inhibition. *Cell Chem. Biol.* 26 (1), 121–e5. doi:10.1016/j.chembiol.2018.10.015

Wood, D. J., Lopez-Fernandez, J. D., Knight, L. E., Al-Khawaldeh, I., Gai, C., Lin, S., et al. (2019b). FragLites-Minimal, Halogenated Fragments Displaying Pharmacophore Doublets. An Efficient Approach to Druggability Assessment and Hit Generation. *J. Med. Chem.* 62 (7), 3741–3752. doi:10.1021/acs.jmedchem.9b00304

Xiao, H., Tian, M., Ge, J., Wei, X., Li, Z., Li, X., et al. (2009). The Role of CDK1 siRNA Interference in Cell Cycle and Cell Apoptosis. *Front. Med. China* 3 (4), 384–389. doi:10.1007/s11684-009-0070-1

Xie, C., Yi, J., Lu, J., Nie, M., Huang, M., Rong, J., et al. (2018). N-acetylcysteine Reduces ROS-Mediated Oxidative DNA Damage and PI3K/Akt Pathway Activation Induced by helicobacter Pylori Infection. *Oxid. Med. Cell Longev.* 2018, 1874985. doi:10.1155/2018/1874985

Zhao, J., Li, P., Zhu, H., Ge, F., Liu, J., Xia, J., et al. (2021). 7,8-Dihydroxyflavone Suppresses Proliferation and Induces Apoptosis of Human Osteosarcoma Cells. *Acta Biochim. Biophys. Sin. (Shanghai)* 53 (7), 903–911. doi:10.1093/abbs/gmab060

Conflict of Interest: The authors declare that the research was conducted in the absence of any commercial or financial relationships that could be construed as a potential conflict of interest.

Publisher's Note: All claims expressed in this article are solely those of the authors and do not necessarily represent those of their affiliated organizations, or those of the publisher, the editors and the reviewers. Any product that may be evaluated in this article, or claim that may be made by its manufacturer, is not guaranteed or endorsed by the publisher.

frontiers | Frontiers in Oncology

ORIGINAL RESEARCH
published: 13 July 2022
doi: 10.3389/fonc.2022.903536

Stable *CDK12* Knock-Out Ovarian Cancer Cells Do Not Show Increased Sensitivity to Cisplatin and PARP Inhibitor Treatment

Rosaria Chilà[1†‡], *Michela Chiappa*[1‡], *Federica Guffanti*[1], *Nicolò Panini*[2], *Donatella Conconi*[3], *Andrea Rinaldi*[4], *Luciano Cascione*[4,5], *Francesco Bertoni*[4,6], *Maddalena Fratelli*[7] *and Giovanna Damia*[1*]

[1] *Laboratory of Experimental Oncology, Department of Oncology, Istituto di Ricerche Farmacologiche Mario Negri Istituito di Ricovero e Cura a Carattere Scientifico (IRCCS), Milan, Italy,* [2] *Laboratory of Cancer Pharmacology, Department of Oncology, Istituto di Ricerche Farmacologiche Mario Negri IRCCS, Milan, Italy,* [3] *School of Medicine and Surgery, University of Milano-Bicocca, Monza, Italy,* [4] *Institute of Oncology Research, Faculty of Biomedical Sciences, USI, Bellinzona, Switzerland,* [5] *SIB Swiss Institute of Bioinformatics, Lausanne, Switzerland,* [6] *Oncology Institute of Southern Switzerland (IOSI), Bellinzona, Switzerland,* [7] *Department of Biochemistry, Istituto di Ricerche Farmacologiche Mario Negri IRCCS, Milan, Italy*

Cyclin-dependent kinase 12 (CDK12) is a serine/threonine kinase involved in the regulation of RNA polymerase II and in the transcription of a subset of genes involved in the DNA damage response. *CDK12* is one of the most mutated genes in ovarian carcinoma. These mutations result in loss-of-function and can predict the responses to PARP1/2 inhibitor and platinum. To investigate the role of CDK12 in ovarian cancer, CRISPR/Cas9 technology was used to generate a stable *CDK12* knockout (KO) clone in A2780 ovarian carcinoma cells. This is the first report on a *CDK12* null cell line. The clone had slower cell growth and was less clonogenic than parental cells. These data were confirmed *in vivo*, where *CDK12* KO transplanted cells had a much longer time lag and slightly slower growth rate than CDK12-expressing cells. The slower growth was associated with a higher basal level of apoptosis, but there were no differences in the basal level of autophagy and senescence. While cell cycle distribution was similar in parental and knockout cells, there was a doubling in DNA content, with an almost double modal number of chromosomes in the *CDK12* KO clone which, however did not display any increase in γH2AX, a marker of DNA damage. We found partial down-regulation of the expression of DNA repair genes at the mRNA level and, among the down-regulated genes, an enrichment in the G2/M checkpoint genes. Although the biological features of *CDK12* KO cells are compatible with the function of CDK12, contrary to some reports, we could not find any difference in the sensitivity to cisplatin and olaparib between wild-type and *CDK12* KO cells.

Keywords: CDK12, ovarian carcinoma, PARP inhibitor, cisplatin, DNA damage

OPEN ACCESS

Edited by:
Arianna Palladini, University of Pavia, Italy

Reviewed by:
Kamal Eltayeb, University of Parma, Italy
Carmen Blanco Aparicio, Spanish National Cancer Research Center (CNIO), Spain

***Correspondence:**
Giovanna Damia
giovanna.damia@marionegri.it

[†]***Present address:***
Rosaria Chilà, IFOM-the FIRC Institute of Molecular Oncology, Milan, Italy

[‡]*These authors have contributed equally to this work*

Specialty section:
This article was submitted to Pharmacology of Anti-Cancer Drugs, a section of the journal Frontiers in Oncology

Received: *25 March 2022*
Accepted: *24 May 2022*
Published: *13 July 2022*

Citation:
Chilà R, Chiappa M, Guffanti F, Panini N, Conconi D, Rinaldi A, Cascione L, Bertoni F, Fratelli M and Damia G (2022) Stable CDK12 Knock-Out Ovarian Cancer Cells Do Not Show Increased Sensitivity to Cisplatin and PARP Inhibitor Treatment. Front. Oncol. 12:903536. doi: 10.3389/fonc.2022.903536

INTRODUCTION

Cyclin-dependent kinase 12 (CDK12) is a serine/threonine kinase involved in the regulation of RNA polymerase II and mRNA processing (1–3). CDK12 is important for the maintenance of genomic stability as it regulates the transcription of a subset of genes involved in the DNA damage response (DDR) (4, 5). In murine embryonic cells, CDK12 sustains self-renewal and its knock-down reduces the expression of self-renewal genes and increases the expression of differentiation markers (6). *CDK12* knockout (KO) mice are not viable, as *CDK12* deletion is fatal during the peri-implantation stage, when *CDK12*-/- blastocysts fail to undergo inner cell mass outgrowth and do not survive *in vitro* due to the induction of apoptosis (5).

CDK12 mutations and amplifications have been reported in different tumor types (7, 8). Not only it is one of the most mutated genes in ovarian carcinoma (9), but its mutations have been correlated with alterations of its catalytic activity, leading to genomic instability, downregulation of genes in the homologous recombination (HR) repair pathway (10, 11) and increased sensitivity to platinum agents and PARP inhibitors (PARPi) (12, 13). HR genes have multiple intronic to poly-adenylation sites that are susceptible to CDK12 inhibition, leading to decreases in their expression (14, 15). In addition, CDK12 inhibition induces an RNA Pol II elongation defect with the subsequent use of proximal poly(A) sites that leads to premature cleavage and polyadenylation especially in DDR gene, known to have longer lengths (16).

High-grade serous ovarian carcinomas (HGSOC) with mutated *CDK12* present a unique signature of genomic instability characterized by tens to hundreds of large tandem duplications scattered throughout the genome, probably due to defects in DNA repair (17). In breast cancer *CDK12* amplification co-occurs with *ERBB2* amplification (18, 19) and its over-expression has been associated with aggressive disease (18). The absence of CDK12 protein, however, correlates with the triple negative phenotype and with reduced expression of some DDR proteins, but not with lower DDR mRNA levels (20). *CDK12* mutations in primary and castration-resistant prostate cancer have also been reported, mutually exclusive with other mutations in DNA repair genes (21–23).

With the aim of understanding the role of CDK12 in tumor growth and response to therapy better, we used CRISPR/Cas9 technology to generate a *CDK12* knock-out system in A2780 ovarian cancer cell lines.

MATERIALS AND METHODS

CDK12 KO Clone

The ovarian carcinoma cell line A2780 was obtained from the American Type Culture Collection (ATCC) and was authenticated by the authors within the last six months. Cell lines were maintained in RPMI culture medium supplemented with 10% FBS and 1% glutamine, at 37°C with 5% CO_2. A2780 cells were initially transfected with CRISPR/Cas9 plasmid directed against exon 1 of CDK12 (U6gRNA-Cas9-2A-GFP, Sigma-Aldrich). After 48 hours, cells were seeded at very low density in order to isolate, expand and analyze single clones by western blot and DNA sequencing. We obtained only a CDK12 heterozygous KO clone, out of about 150 clones screened. On this clone, we ran a second round of transfection and selection and obtained an A2780 homozygous KO clone (A2780 KO).

DNA Sequencing

Total DNA was purified from cells (Maxwell Total DNA Purification Kit, Promega) and the selected *CDK12* locus was amplified with a polymerase chain reaction (PCR) (**Supplementary Table 1**). Amplified DNAs were separated through electrophoresis, and Sanger-sequenced.

Cell Growth

Growth curves were obtained seeding the cells at 15000 cells/mL in six-well plates and counting them at different time points with a cell counter (Multisizer 3, Beckman Coulter). For clonogenic assay in six-well plates, cells were seeded at 125 cells/mL; colonies were left to grow for about ten days then stained with Gram's Crystal Violet solution (Merck). For the limiting dilution assay, cells were seeded at 0.5 cells/well in 96-well plates and colonies were left to grow for about 30 days.

Flow Cytometry Analysis of DNA Content

Exponentially growing cells were washed twice in ice-cold PBS, fixed in ice-cold 70% ethanol, washed in PBS, re-suspended in 2 mL of a solution containing 25 μg/mL of propidium iodide in PBS and 25 μL of RNase 1 mg/mL in water, and stained overnight at 4°C in the dark. We used the FACS Calibur (Becton Dickinson) for cell cycle analysis.

Chromosome Analysis

Exponentially growing A2780, and A2780 *CDK12* KO cells were treated for 6 hours with colcemid (Roche) 0.2 μg/mL in order to block them in metaphase, then treated with hypotonic solution (75 mM KCl) and fixed with 3:1 (vol/vol) methanol:acetic acid. We karyotyped 19 metaphases for A2780 and fifteen for A2780 *CDK12* KO cells lines. Chromosome preparations were analyzed by QFQ banding (Q-Bands by Fluorescence using Quinacrine) according to routine procedures and the karyotype was described using the International System for Chromosome Nomenclature 2016.

Cell Death Analysis

To investigate apoptosis in the cells, we used a caspase 3/7 luminescence-based assay (Promega) and the β-galactosidase staining assay (Cell Signaling Technology) for the detection of senescent cells.

Western Blotting

Proteins were extracted and processed as already described (24). The primary antibodies used are listed in **Supplementary Table 2**. All the protein blots for western analysis have been cropped before antibody hybridization to be able to detect in the same filter different proteins.

Real-Time (RT)-PCR

Total RNA from cell lines was purified with the Maxwell 16 Total RNA Purification Kit (Promega) and reverse transcribed with the cDNA Archive Kit (Applied Biosystems). mRNA expression of the genes was detected using Sybr Green assays (Applied Biosystems). Reactions were run in a total volume of 20 µL containing 10 ng of cDNA with Sybr Green and the forward and reverse primers of the gene, in triplicate (**Supplementary Table 1**). All the data were normalized to the levels of the cyclophillin gene and expressed as the -fold increase over the wild type *CDK12* cells.

Gene Expression

As already described (25), NEBNext Ultra Directional RNA Library Prep Kit for Illumina (New England BioLabs Inc., Ipswich, MA, USA) was used for RNA-seq experiments and the NEBNext Multiplex Oligos for Illumina (New England BioLabs Inc.) for cDNA synthesis. The pre-pool sequencing was done using the NextSeq 500 (Illumina, San Diego, CA, USA) with the NextSeq 500/550 High Output Kit v2.5 (75 cycles; Illumina) and for all the samples we used stranded, single-ended 75bp-long sequencing reads.

Drugs and Treatments

Cisplatin was purchased from Sigma Aldrich; paclitaxel from ChemieTek; olaparib from LC Laboratories; VE822, MK1775 and KU55933 from Axon Medchem; THZ1 and THZ1 hydrochloride were from Insight Biotechnology Limited; ET-743 from PharmaMar and PF-00477736 from Pfizer. For cytotoxicity experiments, cell lines were seeded in 96-well plates and were treated after 48 hours with different concentrations of the drugs. After 72 hours cell viability was examined with the MTS assay (Promega) and absorbance was acquired using a plate reader (Infinite M200, TECAN). Drug concentrations inhibiting growth in 50% of the cells (IC50s) were calculated for each cell line, with the interpolation method.

Chemotaxis and Chemo-Invasion Tests

The cell lines were tested for their ability to migrate through a Nucleopore Track-Etch Membrane (pore size 8 µm, Whatman International), coated with Matrigel Basement Membrane Matrix for chemo-invasion, using Boyden chambers. We added 05 to 2 x 10^4 cells, re-suspended in DMEM culture medium with 0.1% FBS, to each well of the upper chamber for chemotaxis and chemo-invasion tests; DMEM+0.1% FBS (control wells) or 3T3 cell line supernatant (chemo-attractive agent) were added to the lower chamber. The chambers were incubated at 37°C overnight, then the cells from the upper side of the filter were removed and filters were fixed in methanol and stained for nuclear and cytoplasmic detection. Cells that had migrated the lower side of the filters were quantified by brightfield microscopy using a 40× objective, and the average number of cells per field was calculated.

In Vivo Studies

NCr-nu/nu mice (five-week-old females) were from Harlan S.p.a Italy and maintained under standard pathogen-free conditions. The Istituto di Ricerche Farmacologiche Mario Negri IRCCS adheres to national and international laws, regulations, and policies on the maintenance, care and use of laboratory animals, as already reported (26). The *in vivo* experiments were approved by an institutional review board and the Italian Ministry of Health (Authorization no. 705/2016-PR). Exponentially growing A2780 and A2780 *CDK12* KO cells (approximately 7.5 x 10^6 cells per mouse) were injected subcutaneously in the flank of four mice per group. A Vernier caliper was used to measure tumor diameters, and tumor volumes were calculated following the formula: [(smallest diameter)^2 x biggest diameter]/2. Tumor and body weights were recorded at different time points from implant and mice were euthanized by carbon dioxide (CO2) overdose when tumors reached 10% of the animal's body weight.

Statistical Analyses

Statistical analyses were done with GraphPad Prism software. We used a *t-test* to compare cell growth, colony formation, IC50s of cytotoxic experiments and chemo-attraction and chemo-invasion data between the *CDK12* wild type (WT) and *CDK12* KO cell lines. To compare the activation of apoptosis between *CDK12* WT and *CDK12* KO cells we used two-way ANOVA followed by a Bonferroni test.

RNA-Seq was analyzed as previously described (27). Briefly, after quality control using fastqc and mapping against the human GRCh38 genome build, alignment was done with STAR, reads counted with HTSeq-Count, and differently expressed transcripts defined with the voom/limma R package. Genes were considered up-regulated or down-regulated if the adjusted p-value was <0.05 and log2 (KO vs WT) was respectively >1 or <-1. Genes deregulated in both cell lines were analyzed for enrichment in cancer hallmarks using the web-based tool of the Molecular Signaling Database (MsigDB, http://software.broadinstitute.org/gsea/msigdb), filtering for a false discovery rate (FDR) <0.05.

RESULTS

CDK12 KO Ovarian Cancer Cell Lines

A2780 cells were selected to generate KO clones for *CDK12* with the CRISPR/Cas9 gene editing tool. As already reported (28), this was not very successful as we obtained only one clone from A2780 (A2780 KO). Sequencing of genomic DNA showed the A2780 KO clone was homozygous in exon 1 of *CDK12*, carrying one allele harboring a deletion of 30 base pairs and one containing an insertion of 270 base pairs (**Figure 1A**). These data were confirmed by the cDNA sequencing of the *CDK12* KO cells (data not shown).

We tested whether our guide RNAs could be directed against other genes besides *CDK12* (off-target genes). We used the online CRISPR Design tool by Zhang laboratory (http://crispr.mit.edu/) and found no off-target sequence in other genes.

Alterations in *CDK12* sequence are predicted to code for probably non-functional proteins. In fact, deletion in one allele (30 bp deletion) would produce a protein lacking 10 AA; the other allele has a 270 bp insertion that causes a number of stop codons,

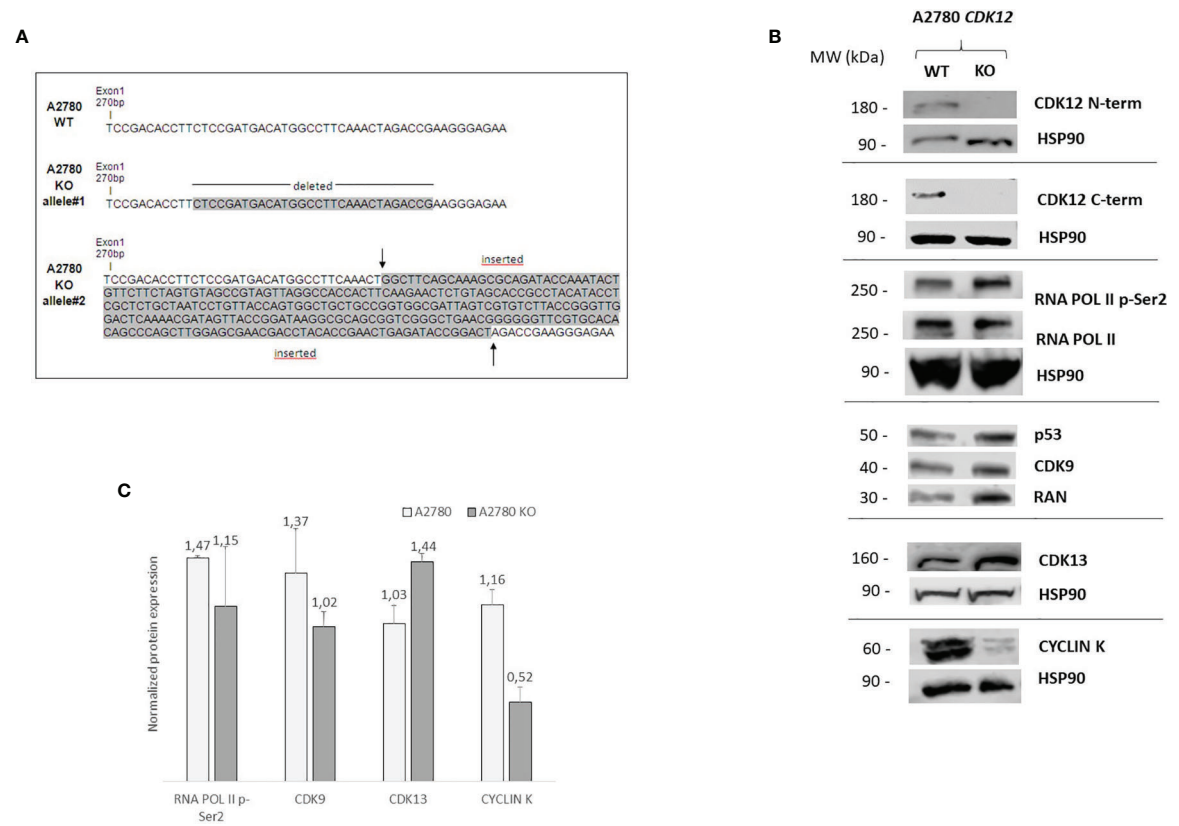

FIGURE 1 | Molecular characterization of A2780 and A2780 *CDK12* KO cells. **(A)** Nucleotide sequences of the loci targeted by CRISPR/Cas9 in exon 1 of *CDK12*, generating *CDK12* KO clones. Upper panel: nucleotide sequences of A2780 *CDK12* WT and KO; shaded nucleotides were deleted and inserted in KO clone allele #1 and #2, respectively. **(B)** Western blot analysis showing *CDK12*, HSP90, RNA pol II p-Ser2, RNA pol II, p53, CDK9, cyclin K, CDK13, RAN protein levels in A2780 and A2780 *CDK12* KO cell lines. All the protein blots for western analysis have been cropped before antibody hybridization to be able to detect in the same filter different proteins. **(C)** Quantification of the western blot data by densitometric analyses. Values are normalized by actin and are the mean+SD of three replicates.

implying that no full protein should be formed. No expression of CDK12 protein in A2780 KO cells was observed, using both a C-terminal and a N-terminal epitope directed CDK12 antibody (**Figure 1B**). We carefully checked for extra bands (possibly CDK12) with different sizes, but we never found any. Considering that one allele is predicted to produce a protein lacking 10 AA, the fact that we could not find any CDK12 protein by western blot suggests that the encoded protein is very unstable.

We checked the levels of a number of proteins that have been associated and regulated by CDK12 (7, 29). We found that the basal level of RNA polymerase II phosphorylation was similar in WT and KO *CDK12*, while slightly lower levels of the CDK12 cyclin partner cyclin K (**Figures 1B, C**). The levels of CDK9, the other transcriptional CDK involved in Ser2 RNA polymerase II phosphorylation, were not changed, nor were those of CDK13 (**Figure 1B**). p53 protein levels were similar in A2780 and the corresponding CDK12 KO clone (**Figure 1B**).

Biological Characterization of the *CDK12* KO Ovarian Cancer Cells

CDK12 KO cells were morphologically indistinguishable from their parental counterparts (data not shown). We characterized the clone for its proliferation rate and clonogenicity. KO clones had slower growth than their parental cells (**Figure 2A**). Colony and limiting dilution assays suggested that A2780 *CDK12* KO cells had lower clonogenic ability than parental cells. *CDK12* KO cells did have less colony formation ability (**Figure 2B**) and less single cell growth in the limiting dilution assay (**Figure 2C**). We wondered whether the absence of CDK12 led to an increase in cell death that could partly explain the differences in cell growth. As shown in **Figure 2D**, the percentage of cells undergoing apoptosis was higher in *CDK12* KO cells than in their parental cell line at different times. There was no activation of autophagy, as demonstrated by the absence of a cleaved form of LC3 protein and the increase in p62 (**Supplementary Figure 1A**), or senescence, as indicated by the absence of β-galactosidase staining (**Supplementary Figure 1B**) in *CDK12* KO cells.

A2780 and *CDK12* KO cells were analyzed for their DNA content and distribution in the different phases of the cell cycle. A2780 and A2780 *CDK12* KO cells were regularly distributed in the different phases of the cell cycle (**Figure 3A**). However, A2780 *CDK12* KO cells had a twice DNA content as compared to parental cells.

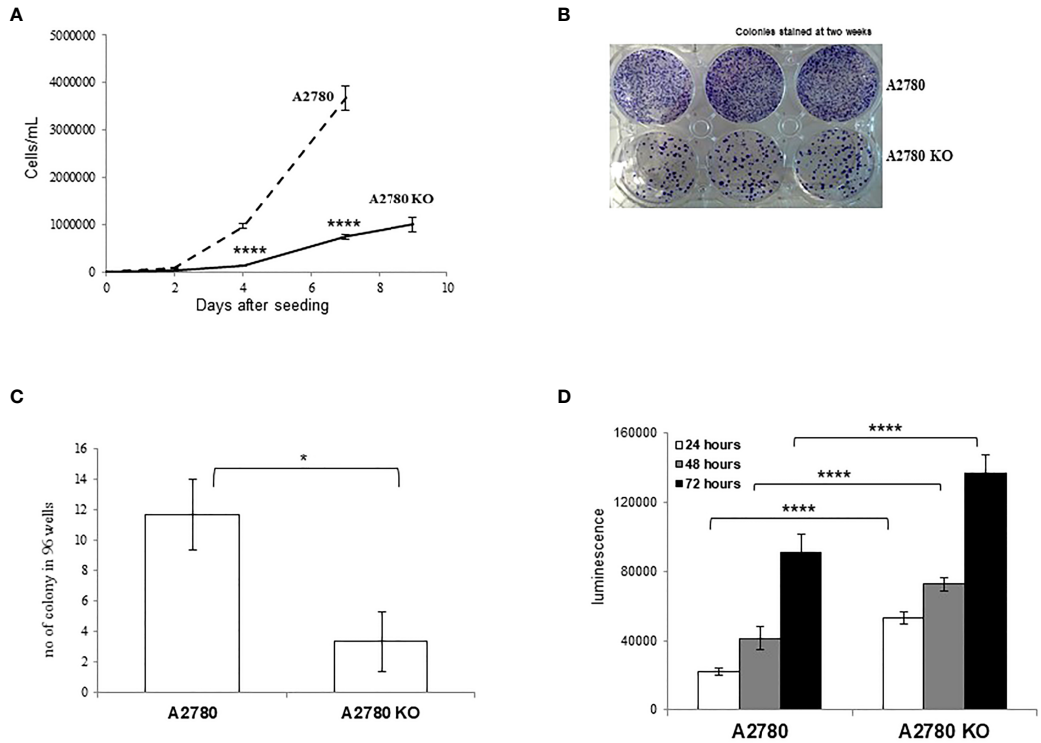

FIGURE 2 | Biological characterization of A2780 and A2780 *CDK12* KO cells. **(A)** Growth curves for cells/mL (— A2780 cells; — — A2780 *CDK12* KO cells) at different times from seeding. Data are the mean ± SD of three replicates and each experiment was performed three times. t-test was used for statistical analysis (****p < 0.0001). **(B)** Colony assays performed in six-wells plates of *CDK12* WT (upper wells) and KO (lower wells) cell lines. Cells were stained two weeks after seeding. The results shown are representative of three independent experiments. **(C)** Number of colonies in 96-wells plates. Data are the mean ± SD of three replicates done three times (*= p<0.0082). **(D)** Apoptotic signals 24 (white), 48 (grey) and 72 (black) hours from the seeding. Data are the mean ± SD of six replicates done three times. For statistical analysis, two-way ANOVA, followed by Tukey's test was used to compare *CDK12* KO with the WT cell line at each time (****p < 0.0001).

Considering the recent report of an association of bi-allelic inactivation of *CDK12* with tandem duplication (17), we analyzed the karyotype of the cells to investigate the number and structure of the chromosomes. The composite reconstructions of WT and KO karyotypes (**Figure 3B**) showed that structural rearrangements of A2780 were maintained in A2780 *CDK12* KO cells, but duplicated. The A2780 cell line (upper panel) showed a modal number of 46 chromosomes, ranging from 44 to 47 corresponding to a diploid DNA content. Its composite karyotype is 44~47,XX,-1x2,+der (1) dup (1q),+del(1)(p36.3p32),+der(1)t(1);?(q11);?x2,-4,der(6)t(1;6)(q21.2;q22),7, der(7)add(7)(q32), der (12)t(?;12),del(14)(q23),der (21)add(21)(q22). The A2780 CDK12 KO cells line had a modal number of 90 chromosomes, ranging from 88 to 95 (lower panel), in line with the doubled DNA content shown by FACS analysis. Its composite karyotype is 88~95,XXXX,-1x4, +der(1)dup(1q)x3, +del (1)(p36.3p32)x2,+der(1)t(1);?(q11);?x4,+3,-4,+4,+5,der(6)t(1;6)(q21.2;q22)x2,-7x2,der(7) add (7) (q32) x 2, -10, der (12) t (?;12) x 2, -13x2, der (13;14)(q10;q10),-14,del(14)(q23)x2,-17,-18,-19,-21, der (21)add(21)(q22)x2.

CDK12 KO Effect on Tumor Growth *In Vivo*

We transplanted parental and *CDK12* KO cells in nude mice and examined their tumor take and tumor growth. The A2780 KO tumor lag was much longer than A2780, all the mice having a palpable tumor by day 135, while all the animals transplanted with A2780 cells were dead with tumors by day 25 (**Table 1**). Tumor growth rates of A2780 *CDK12* KO cells were slightly lower than A2780 cells (**Supplementary Figure 2**).

CDK12 KO Effect on Invasiveness

CDK12 was reported to modulate the alternative splicing of specific genes, increasing the tumorigenicity and aggressiveness of breast cancer cells (30). We therefore investigated whether *CDK12* KO cells showed a difference in migrating from their parental cells. In chemotaxis experiments (**Supplementary Figure 3**) there was no difference in migration between parental and *CDK12* KO clone. In wound healing assay, we found no differences in the ability to repair the wound in *CDK12* KO cells compared to the parental cells (data not shown).

CDK12 KO Effect on DNA Damage and Repair

CDK12 down-regulation has been reported to be associated with lower mRNA and protein levels of DNA repair genes (4). We investigated the levels of a number of DNA damage genes in *CDK12* KO cells compared to those in parental cells. **Figure 4A**

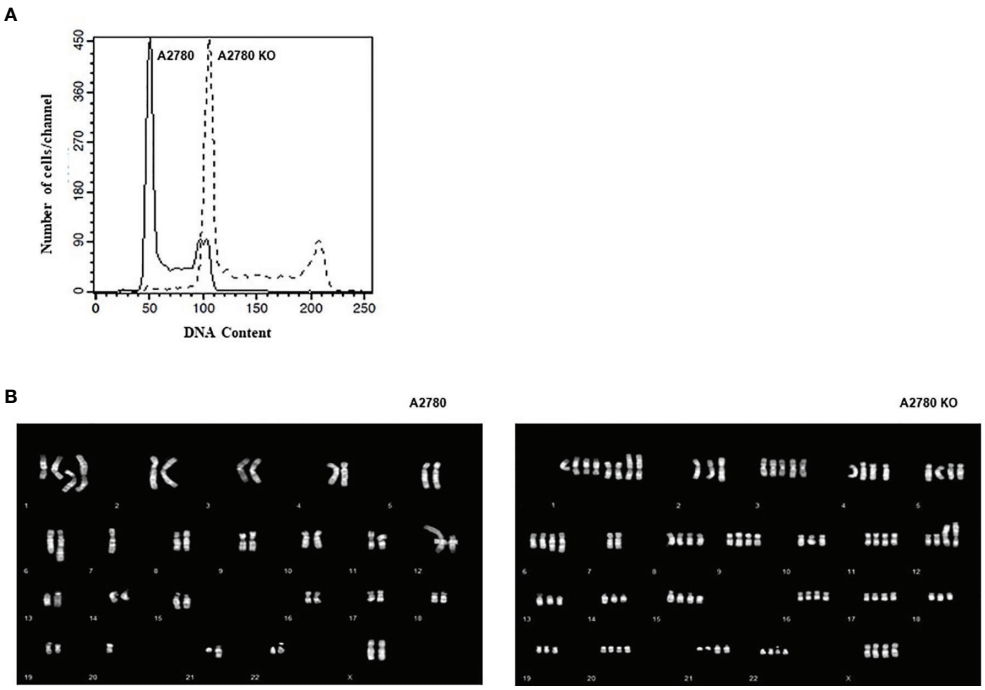

FIGURE 3 | **(A)** Flow cytometric analysis of DNA content of the cell lines. **–**: *CDK12* WT cell lines, - - : *CDK12* KO cell lines. **(B)** Composite karyotypes of A2780 cell line (left panel) and of A2780 *CDK12* KO (right panel).

shows the relative mRNA levels of some of the genes acting in DNA damage and repair, expressed as the fold of increase over the parental cells. There was a partial downregulation of *BRCA1, CHK1*, and *WEE1* in A2780 KO cells, while *PARP1* was downregulated. Protein levels of the same genes (**Figures 4B, D**) assessed by western blot, confirmed the downregulation of PARP1, while no significant change of BRCA1, CHK1, and WEE1 protein levels. We then checked for the level of endogenous DNA damage evaluating the activation of H2AX, a *bone fide* marker of this. No increase in p-Ser139 H2AX was detected in *CDK12* KO cells compared to the WT cells, suggesting no greater DNA damage in *CDK12* KO cells (**Figure 4C**).

Considering the reported role of the cyclin K/CDK12 complex in eukaryotic gene expression and to gain a broader picture of changes in gene expression, we compared the baseline gene expression profiles in KO versus WT cells, as described in Materials and Methods. In *CDK12* KO cells, 6.8% of genes were up-regulated in A2780 KO and 7.6% were down-regulated (**Supplementary Table 3**). We did not find the reported (4) enrichment in DNA repair genes in A2780 CDK12 KO cells. However, among the up-regulated genes there was significant enrichment of genes involved in apoptosis, in agreement with the experimental data (**Figure 2D**) (**Supplementary Table 4**).

TABLE 1 | No of mice tumor/no of transplanted mice with A2780 and *CDK12 KO* A2780 cells.

Days after tumor implant	A2780 xenograph	*CDK12* KOA2780 xenograph
10	0/4	0/4
25	04/04	0/4
15		01/04
45		02/04
75		03/04
135		04/04

CDK12 KO Effect on Sensitivity to Anticancer Drugs

Recent reports suggest that cells with *CDK12* mutations and/or transient downregulation with small interference RNA are more sensitive to alkylating agents, PARP inhibitors and irinotecan (11, 12, 31). We pharmacologically characterized A2780 *CDK12* KO cells compared to parental cells using agents with different mechanisms of action; DNA interfering agents: cisplatin (DDP), ET-743, olaparib (OLA); antitubulin agents: paclitaxel (PTX), and agents targeting the DNA damage response pathway: ATR inhibitor (VE822), ATM inhibitor (KU55933), CHK1 inhibitor (PF477736), WEE1 inhibitor (MK1775) and CDK7/CDK12 inhibitors (THZ1 and THZ1 HYDRO). Contrary to some reports, KO clones were not more sensitive to DDP and OLA; the patterns of sensitivity were also similar with ET-743, PTX, KU55933, PF477736 and MK1775. *CDK12* KO cells showed the same sensitivity to THZ1 and THZ1 HYDRO as WT cells (**Figure 5**). Interestingly, *CDK12* KO cells were five fold more resistant to the ATR inhibitor VE822 with an IC50 value of 1.99 + 0.81μM versus 0.39 + 0.07 μM (**Figure 5**; **Supplementary Table 5**).

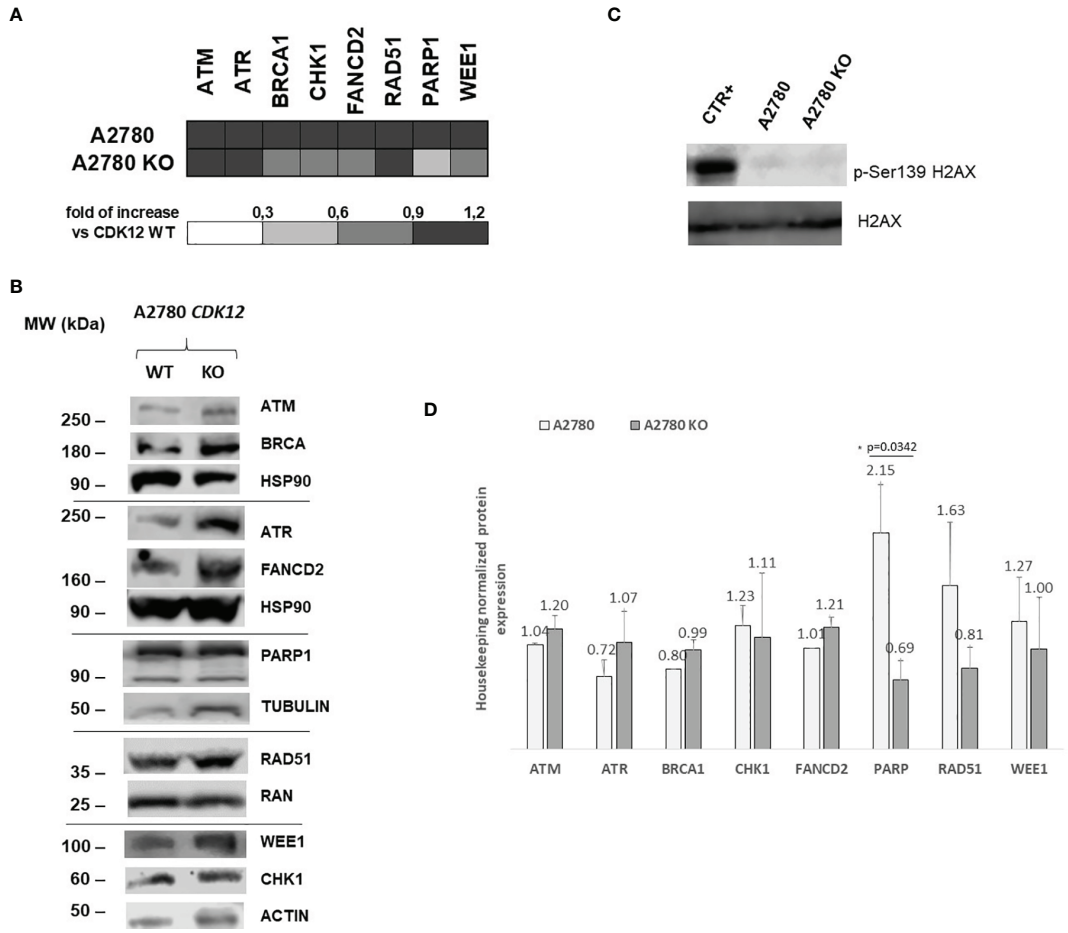

FIGURE 4 | DNA repair gene expression in A2780 and A2780 CDK12 KO cells. **(A)** mRNA levels of *ATM, ATR, BRCA1, CHK1, FANCD2, RAD51, PARP1, WEE1* in A2780 and A2780 *CDK12* KO cell lines obtained by RT-PCR. Values are the mean+SD of three independent experiments, done in triplicates and are expressed as the fold of change over the *CDK12* WT cell line. **(B)** Western blot analysis showing ATM, HSP90, ATR, FANCD2, BRCA1, PARP1, RAD51, β tubulin, CHK1, WEE1, ACTIN, p-Ser139 H2AX, H2AX protein levels in A2780 and A2780 *CDK12* KO cells lines. All the protein blots for western analysis have been cropped before antibody hybridization to be able to detect in the same filter different proteins. **(C)** Western blot analysis showing p-Ser139 H2AX, H2AX protein levels in A2780 and A2780 *CDK12* KO cells. All the protein blots for western analysis have been cropped before antibody hybridization to be able to detect in the same filter different proteins. **(D)** Quantification of the western blot data by densitometric analyses. Values are normalized by actin and are the mean+SD of three replicates.*p = 0.0342.

To see whether the cells' sensitivities to DDP and VE822 were due to some changes in apoptosis, we ran an apoptosis test 24, 48 and 72 hours after treatment with different drug concentrations. **Supplementary Figure 4** shows the apoptotic levels of treated and untreated A2780 and A2780 *CDK12* KO cells. There were no differences in DDP-induced apoptosis between the WT and *CDK12* KO cells, while VE822 caused weaker induction of apoptosis in KO than in WT cells. These data suggest that the lower sensitivity of A2780 *CDK12* KO to VE822 than A2780 may be partly due to a lower induction of apoptosis.

DISCUSSION

Cyclin-dependent kinase 12 (CDK12) has been reported to favor the maintenance of genomic stability as it promotes the transcription of a subset of genes involved in the DNA damage response (4, 5). *CDK12* inactivation causes downregulation of genes involved in DNA repair (10, 11) and increases sensitivity to platinum agents and PARP inhibitors (12, 13). Mutations in *CDK12* have been reported in different tumor types (7, 8) and it is one of the most mutated genes in ovarian carcinoma (9). Recently, we reported that CDK12 mRNA levels were predictive of platinum response in a xenobank of patient-derived ovarian carcinomas (32). To understand CDK12's role in tumor growth and response to therapy better, we here generated ovarian cancer cells knocked out for *CDK12*.

The very low rate of success in obtaining *CDK12* KO clones using the effective CRISPR/Cas9 tool suggests CDK12 is important for cell viability (5, 28). To the best of our knowledge, no stable *CDK12* KO cells have been described; only an analog sensitive *CDK12* cellular system has been published (28), a single HeLa cell clone in which the only functional copy of *CDK12* was selectively

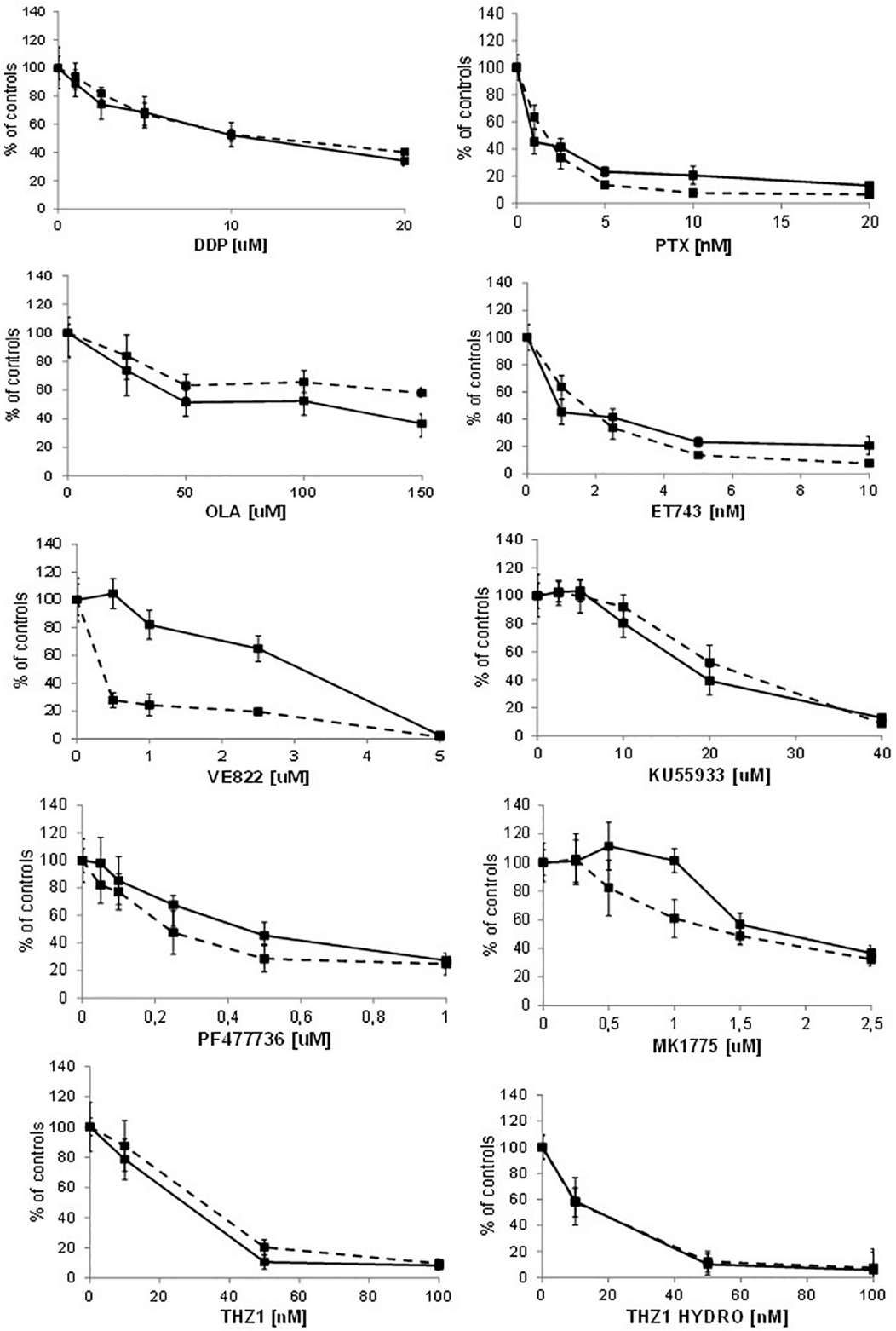

FIGURE 5 | Drug dose-response curves. Dose-response curves of A2780 - - -■- - - and A2780 KO ▬▬■▬▬ to cisplatin, paclitaxel, olaparib, ET-743, VE822, KU55933, PF477736, MK1775, THZ1, THZ1 hydrocloride. Data are expressed as survival percentages over controls (+ standard error) of least three experiments done in quintuplicate.

inhibited by a cell-permeable adenine analog. In this system, CDK12 inhibition resulted in an arrest in cell proliferation and perturbation of the phosphorylation pattern of RNA polymerase II CTD. The cell growth of *CDK12* KO cells confirmed this, as the lack of CDK12 delayed cell growth and reduced the clonogenic ability of the *CDK12* KO cells. The data were also partially confirmed *in vivo*, where A2780 KO tumors were as tumorigenic as A2780 cells. However, their time lags were almost 9-13 times those of A2780 cells, and their growth rates were slightly lower than the parental cells. These data seem to contrast with the reported evidence of CDK12 as tumor suppressor. However, as recently suggested (33), if important events in oncogenesis depend on the loss of CDK12 catalytic activity leading, among others to deregulation of DDR, we did not observed in our experimental setting an impairment of response to damage in *CDK12* KO cells. As regards CDK12's implication in tumor invasiveness and aggressiveness (30), we did not find any differences in migration capacity between WT and KO clones.

The absence of the CDK12 protein is not associated with any clear decrease in RNA pol II p-Ser2 phosphorylation, probably because CDK9 and CDK13 levels-which induce the same phosphorylation- were unchanged (34). Of note, CDK13 is evolutionarily and structurally related to CDK12 kinase, sharing the same cognate cyclin K and biochemical assays reported similar kinase activity and phosphorylation of Ser2 of the CTD heptad sequence (33). Even some studies support gene selective modulation and non-overlapping function for CDK12 and CDK13, evidence have recently been put forward on a significant redundancy between these two kinases and on the fact that both are key regulators of global POLII processivity (35). There was a slight decrease in cyclin K levels, never reaching statistical significance in *CDK12* KO cells. The pre-replicative assembly complex (licensing) is a requisite for DNA replication and sustains cell proliferation (36). Cyclin K is essential to promote efficient licensing in G1 phase and *CDK12* knockdown prevents the pre-replicative complex assembly in G1 (37). This might explain a DNA replication defect in *CDK12* KO cells, leading to slower growth.

Contributing to the slower growth in *CDK12* KO cells is the significant downregulation of genes involved in the G2/M checkpoint observed with gene expression analysis, and the higher basal level of apoptosis in *CDK12* KO than WT cells. In A2780 *CDK12* KO cells we did not find any increase in DNA damage, as demonstrated by the comparable levels of γH2AX phosphorylation in contrast to the reports in reduced licensing conditions (38) and in *CDK12*-null embryos (4, 5), suggesting a more complex picture.

CDK12 KO cells have double the DNA content of WT cells, even with regular distribution in the cell cycle, with doubling of the chromosomes and retention of the structural rearrangements seen in the parental WT cells. It has been recently demonstrated that ovarian cancers with inactivating mutations of *CDK12* present genomic instability characterized by hundreds of tandem duplications of up to ten megabases (MB) in size (*CDK12* TD-plus phenotype) (17). In prostate cancer, the bi-allelic inactivation of *CDK12* is associated with a large number of focal copy-number gains dispersed across the genome (39). This phenotype was mutually exclusive with *BRCA1/2* mutations (germline and/or somatic) and with *BRCA1* promoter methylation and was not associated with genomic homologous recombination deficiency, partially contrasting with the data suggesting a decrease in the expression of genes involved in homologous recombination repair (4, 40). It was also reported that large genes (including the DNA repair genes) were not markedly abundant among the downregulated ones.

Given the role of CDK12 in regulating the expression of genes involved in DNA repair, we investigated the levels of some of these genes in our *CDK12* KO cells. There was a slight tendency to mRNA downregulation of some genes involved in DNA repair (i.e. BRCA1, CHK1, WEE1 and PARP1) not always supported by a downregulation at protein level. This apparently inconsistency could be due to other level of regulation at protein level, such as post-translation modifications interfering with their stability (41). As we focused on a limited number of DNA repair genes (those whose mRNAs were downregulated in CDK12 transient KO conditions), we might not have captured the whole spectrum of altered transcription. However, a wide gene expression analysis indicated a certain proportion of deregulated genes (both up- and down-regulated), but we did not find any clear enrichment in DNA repair genes among the downregulated transcripts as reported elsewhere (4, 40). However, the fact that *CDK12* KO cells have double DNA content suggests that the two-fold increase in DNA repair genes copy number could potentially lead to an increase in their transcripts, even in the absence of CDK12. A detailed gene copy number analysis coupled with transcriptome of the clones would help clarify this issue.

Although the biological and molecular characterization of our *CDK12* KO clones is compatible with the known function of CDK12 in cells, we could not find any differences in the sensitivity of CDK12 KO cells to cisplatin, PARP inhibitor olaparib, ET-743, KU55933 (an ATM inhibitor) and paclitaxel compared to WT cells. The ATR inhibitor VE822 was less active in *CDK12* KO clones than in WT cells.

These results partially contrast with reports of increased sensitivity to platinum-based drugs and olaparib in cells transiently transfected with shRNA and siRNA against CDK12 (11, 31, 42). Possible explanations can be offered: i) the experimental settings are quite different, as our *CDK12* KO cells had a stable, not transient, loss of CDK12, and may have developed some mechanisms of adaptation to survive cells; ii) given the functional redundancy between CDK12 and CDK13 (35), it could be that CDK13 can compensate for CDK12 loss; iii) our *CDK12* KO cells have double the DNA content and no significant decrease in DDR proteins. The lower sensitivity to ATR inhibitor in CDK12 KO cells - partly explained by the less induction of apoptosis - would be due to the fact that these cells are less dependent on the ATR-CHK1 axis. Finally, the similar sensitivity to the reported CDK12 inhibitors in A2780 CDK12 KO cells would suggest that these inhibitors are not specific for CDK12.

In conclusion, here we report for the first time a *CDK12* null cell line. We realize that all the data here rely on only one clone, but nevertheless all are compatible with the known function of CDK12 and support its role for survival in tumor cells too. *CDK12* KO cells showed a duplication of DNA, with doubling of the chromosomal

number, corroborating the role of CDK12 in genomic maintenance. *CDK12* KO cells had reduced cell growth, no increase in endogenous DNA damage levels and no major downregulation of DNA repair genes, reported to be downregulated in transient *CDK12* KO cells. The lack of DDR gene downregulation might be partially explained by the doubling of DNA content and could justify the lack of increase sensitivity to platinum and PARPi. Detailed genome molecular study coupled with a global gene expression profile will help us understand better what kind of selection this KO clone has undergone and explain the differences from the transient *CDK12* downregulation experimental setting.

DATA AVAILABILITY STATEMENT

All data will be available at the National Center for Biotechnology Information (NCBI) Gene Expression Omnibus (GEO) (http://www.ncbi.nlm.nih.gov/geo) database; GSE183041.

ETHICS STATEMENT

The animal study was reviewed and approved by the Italian Ministry of Health Institutional Review Board. The IRB also approved all the *in vivo* experiments performed with PDXs (Authorization n.705/2016-PR).

AUTHOR CONTRIBUTIONS

RC performed research, collected data, analysed and interpreted data, performed statistical analyses and wrote the manuscript; MC and FG performed the western blots, interpret the data and performed statistical analyses; NP collected data and analysed and interpreted data; DC performed research, analysed and interpreted data; AR and LC performed research, analysed and interpreted data, performed statistical analysis; FB and MF analysed and interpreted data, performed statistical analysis and wrote the manuscript; GD designed experiments, analysed and interpreted data; wrote and reviewed the manuscript. All authors reviewed the manuscript. All authors contributed to the article and approved the submitted version.

FUNDING

The research was supported by a grant from the The Italian Association for Cancer Research (GD IG 19797).

ACKNOWLEDGMENTS

The generous contribution of AIRC (The Italian Association for Cancer Research) is gratefully acknowledged.

SUPPLEMENTARY MATERIAL

The Supplementary Material for this article can be found online at: https://www.frontiersin.org/articles/10.3389/fonc.2022.903536/full#supplementary-material

REFERENCES

1. Lim S, Kaldis P. Cdks, Cyclins and CKIs: Roles Beyond Cell Cycle Regulation. *Development* (2013) 140(15):3079–93. doi: 10.1242/dev.091744
2. Cheng SW, Kuzyk MA, Moradian A, Ichu TA, Chang VC, Tien JF, et al. Interaction of Cyclin-Dependent Kinase 12/CrkRS With Cyclin K1 Is Required for the Phosphorylation of the C-Terminal Domain of RNA Polymerase II. *Mol Cell Biol* (2012) 32(22):4691–704. doi: 10.1128/MCB.06267-11
3. Liang K, Gao X, Gilmore JM, Florens L, Washburn MP, Smith E, et al. Characterization of Human Cyclin-Dependent Kinase 12 (CDK12) and CDK13 Complexes in C-Terminal Domain Phosphorylation, Gene Transcription, and RNA Processing. *Mol Cell Biol* (2015) 35(6):928–38. doi: 10.1128/MCB.01426-14
4. Blazek D, Kohoutek J, Bartholomeeusen K, Johansen E, Hulinkova P, Luo Z, et al. The Cyclin K/Cdk12 Complex Maintains Genomic Stability *via* Regulation of Expression of DNA Damage Response Genes. *Genes Dev* (2011) 25(20):2158–72. doi: 10.1101/gad.16962311
5. Juan HC, Lin Y, Chen HR, Fann MJ. Cdk12 is Essential for Embryonic Development and the Maintenance of Genomic Stability. *Cell Death Differ* (2016) 23(6):1038–48. doi: 10.1038/cdd.2015.157
6. Dai Q, Lei T, Zhao C, Zhong J, Tang YZ, Chen B, et al. Cyclin K-Containing Kinase Complexes Maintain Self-Renewal in Murine Embryonic Stem Cells. *J Biol Chem* (2012) 287(30):25344–52. doi: 10.1074/jbc.M111.321760
7. Chila R, Guffanti F, Damia G. Role and Therapeutic Potential of CDK12 in Human Cancers. *Cancer Treat Rev* (2016) 50:83–8. doi: 10.1016/j.ctrv.2016.09.003
8. Paculova H, Kramara J, Simeckova S, Fedr R, Soucek K, Hylse O, et al. BRCA1 or CDK12 Loss Sensitizes Cells to CHK1 Inhibitors. *Tumour Biol* (2017) 39 (10):1010428317727479. doi: 10.1177/1010428317727479
9. Cancer Genome Atlas Research N. Integrated Genomic Analyses of Ovarian Carcinoma. *Nature* (2011) 474(7353):609–15. doi: 10.1038/nature10166
10. Ekumi KM, Paculova H, Lenasi T, Pospichalova V, Bosken CA, Rybarikova J, et al. Ovarian Carcinoma CDK12 Mutations Misregulate Expression of DNA Repair Genes *via* Deficient Formation and Function of the Cdk12/CycK Complex. *Nucleic Acids Res* (2015) 43(5):2575–89. doi: 10.1093/nar/gkv101
11. Joshi PM, Sutor SL, Huntoon CJ, Karnitz LM. Ovarian Cancer-Associated Mutations Disable Catalytic Activity of CDK12, A Kinase That Promotes Homologous Recombination Repair and Resistance to Cisplatin and Poly (ADP-Ribose) Polymerase Inhibitors. *J Biol Chem* (2014) 289(13):9247–53. doi: 10.1074/jbc.M114.551143
12. Bajrami I, Frankum JR, Konde A, Miller RE, Rehman FL, Brough R, et al. Genome-Wide Profiling of Genetic Synthetic Lethality Identifies CDK12 as a Novel Determinant of PARP1/2 Inhibitor Sensitivity. *Cancer Res* (2014) 74 (1):287–97. doi: 10.1158/0008-5472.CAN-13-2541
13. Natrajan R, Wilkerson PM, Marchio C, Piscuoglio S, Ng CK, Wai P, et al. Characterization of the Genomic Features and Expressed Fusion Genes in Micropapillary Carcinomas of the Breast. *J Pathol* (2014) 232(5):553–65. doi: 10.1002/path.4325
14. Dubbury SJ, Boutz PL, Sharp PA. CDK12 Regulates DNA Repair Genes by Suppressing Intronic Polyadenylation. *Nature* (2018) 564(7734):141–5. doi: 10.1038/s41586-018-0758-y
15. Krajewska M, Dries R, Grassetti AV, Dust S, Gao Y, Huang H, et al. CDK12 Loss in Cancer Cells Affects DNA Damage Response Genes Through Premature Cleavage and Polyadenylation. *Nat Commun* (2019) 10(1):1757. doi: 10.1038/s41467-019-09703-y
16. Bayles I, Krajewska M, Pontius WD, Saiakhova A, Morrow JJ, Bartels C, et al. Ex Vivo Screen Identifies CDK12 as a Metastatic Vulnerability in

Osteosarcoma. *J Clin Invest* (2019) 129(10):4377–92. doi: 10.1172/JCI127718
17. Popova T, Manie E, Boeva V, Battistella A, Goundiam O, Smith NK, et al. Ovarian Cancers Harboring Inactivating Mutations in CDK12 Display a Distinct Genomic Instability Pattern Characterized by Large Tandem Duplications. *Cancer Res* (2016) 76(7):1882–91. doi: 10.1158/0008-5472.CAN-15-2128
18. Capra M, Nuciforo PG, Confalonieri S, Quarto M, Bianchi M, Nebuloni M, et al. Frequent Alterations in the Expression of Serine/Threonine Kinases in Human Cancers. *Cancer Res* (2006) 66(16):8147–54. doi: 10.1158/0008-5472.CAN-05-3489
19. Kauraniemi P, Kuukasjarvi T, Sauter G, Kallioniemi A. Amplification of a 280-Kilobase Core Region at the ERBB2 Locus Leads to Activation of Two Hypothetical Proteins in Breast Cancer. *Am J Pathol* (2003) 163(5):1979–84. doi: 10.1016/S0002-9440(10)63556-0
20. Naidoo K, Wai PT, Maguire SL, Daley F, Haider S, Kriplani D, et al. Evaluation of CDK12 Protein Expression as a Potential Novel Biomarker for DNA Damage Response-Targeted Therapies in Breast Cancer. *Mol Cancer Ther* (2018) 17(1):306–15. doi: 10.1158/1535-7163.MCT-17-0760
21. Grasso CS, Wu YM, Robinson DR, Cao X, Dhanasekaran SM, Khan AP, et al. The Mutational Landscape of Lethal Castration-Resistant Prostate Cancer. *Nature* (2012) 487(7406):239–43. doi: 10.1038/nature11125
22. Robinson D, Van Allen EM, Wu YM, Schultz N, Lonigro RJ, Mosquera JM, et al. Integrative Clinical Genomics of Advanced Prostate Cancer. *Cell* (2015) 161(5):1215–28. doi: 10.1016/j.cell.2015.06.053
23. Zehir A, Benayed R, Shah RH, Syed A, Middha S, Kim HR, et al. Mutational Landscape of Metastatic Cancer Revealed From Prospective Clinical Sequencing of 10,000 Patients. *Nat Med* (2017) 23(6):703–13. doi: 10.1038/nm.4333
24. Restelli V, Vagni M, Arribas AJ, Bertoni F, Damia G, Carrassa L. Inhibition of CHK1 and WEE1 as a New Therapeutic Approach in Diffuse Large B Cell Lymphomas With MYC Deregulation. *Br J Haematol* (2018) 181(1):129–33. doi: 10.1111/bjh.14506
25. Mensah AA, Spriano F, Sartori G, Priebe V, Cascione L, Gaudio E, et al. Study of the Antilymphoma Activity of Pracinostat Reveals Different Sensitivities of DLBCL Cells to HDAC Inhibitors. *Blood Adv* (2021) 5(10):2467–80. doi: 10.1182/bloodadvances.2020003566
26. Guffanti F, Alvisi MF, Caiola E, Ricci F, De Maglie M, Soldati S, et al. Impact of ERCC1, XPF and DNA Polymerase Beta Expression on Platinum Response in Patient-Derived Ovarian Cancer Xenografts. *Cancers (Basel)* (2020) 12 (9):2398–3411. doi: 10.3390/cancers12092398
27. Cascione L, Rinaldi A, Bruscaggin A, Tarantelli C, Arribas AJ, Kwee I, et al. Novel Insights Into the Genetics and Epigenetics of MALT Lymphoma Unveiled by Next Generation Sequencing Analyses. *Haematologica* (2019) 12, e558–61. doi: 10.3324/haematol.2018.214957
28. Bartkowiak B, Yan C, Greenleaf AL. Engineering an Analog-Sensitive CDK12 Cell Line Using CRISPR/Cas. *Biochim Biophys Acta* (2015) 1849(9):1179–87. doi: 10.1016/j.bbagrm.2015.07.010
29. Choi SH, Kim S, Jones KA. Gene Expression Regulation by CDK12: A Versatile Kinase in Cancer With Functions Beyond CTD Phosphorylation. *Exp Mol Med* (2020) 52(5):762–71. doi: 10.1038/s12276-020-0442-9
30. Tien JF, Mazloomian A, Cheng SG, Hughes CS, Chow CCT, Canapi LT, et al. CDK12 Regulates Alternative Last Exon mRNA Splicing and Promotes Breast Cancer Cell Invasion. *Nucleic Acids Res* (2017) 45(11):6698–716. doi: 10.1093/nar/gkx187
31. Quereda V, Bayle S, Vena F, Frydman SM, Monastyrskyi A, Roush WR, et al. Therapeutic Targeting of CDK12/CDK13 in Triple-Negative Breast Cancer. *Cancer Cell* (2019) 36(5):545–58.e7. doi: 10.1016/j.ccell.2019.09.004
32. Guffanti F, Fratelli M, Ganzinelli M, Bolis M, Ricci F, Bizzaro F, et al. Platinum Sensitivity and DNA Repair in a Recently Established Panel of Patient-Derived Ovarian Carcinoma Xenografts. *Oncotarget* (2018) 9(37):24707–17. doi: 10.18632/oncotarget.25185
33. Greenleaf AL. Human CDK12 and CDK13, Multi-Tasking CTD Kinases for the New Millenium. *Transcription* (2019) 10(2):91–110. doi: 10.1080/21541264.2018.1535211
34. Franco LC, Morales F, Boffo S, Giordano A. CDK9: A Key Player in Cancer and Other Diseases. *J Cell Biochem* (2018) 119(2):1273–84. doi: 10.1002/jcb.26293
35. Fan Z, Devlin JR, Hogg SJ, Doyle MA, Harrison PF, Todorovski I, et al. CDK13 Cooperates With CDK12 to Control Global RNA Polymerase II Processivity. *Sci Adv* (2020) 6(18):eaaz5041. doi: 10.1126/sciadv.aaz5041
36. Falaschi A, Abdurashidova G, Biamonti G. DNA Replication, Development and Cancer: A Homeotic Connection? *Crit Rev Biochem Mol Biol* (2010) 45 (1):14–22. doi: 10.3109/10409230903365608
37. Lei T, Zhang P, Zhang X, Xiao X, Zhang J, Qiu T, et al. Cyclin K Regulates Prereplicative Complex Assembly to Promote Mammalian Cell Proliferation. *Nat Commun* (2018) 9(1):1876. doi: 10.1038/s41467-018-04258-w
38. McIntosh D, Blow JJ. Dormant Origins, the Licensing Checkpoint, and the Response to Replicative Stresses. *Cold Spring Harb Perspect Biol* (2012) 4(10): a012955. doi: 10.1101/cshperspect.a012955
39. Wu YM, Cieslik M, Lonigro RJ, Vats P, Reimers MA, Cao X, et al. Inactivation of CDK12 Delineates a Distinct Immunogenic Class of Advanced Prostate Cancer. *Cell* (2018) 173(7):1770–82.e14. doi: 10.1016/j.cell.2018.04.034
40. Zhang T, Kwiatkowski N, Olson CM, Dixon-Clarke SE, Abraham BJ, Greifenberg AK, et al. Covalent Targeting of Remote Cysteine Residues to Develop CDK12 and CDK13 Inhibitors. *Nat Chem Biol* (2016) 12(10):876–84. doi: 10.1038/nchembio.2166
41. Keenan EK, Zachman DK, Hirschey MD. Discovering the Landscape of Protein Modifications. *Mol Cell* (2021) 81(9):1868–78. doi: 10.1016/j.molcel.2021.03.015
42. Johnson SF, Cruz C, Greifenberg AK, Dust S, Stover DG, Chi D, et al. CDK12 Inhibition Reverses *De Novo* and Acquired PARP Inhibitor Resistance in BRCA Wild-Type and Mutated Models of Triple-Negative Breast Cancer. *Cell Rep* (2016) 17(9):2367–81. doi: 10.1016/j.celrep.2016.10.077

Conflict of Interest: The authors declare that the research was conducted in the absence of any commercial or financial relationships that could be construed as a potential conflict of interest.

Publisher's Note: All claims expressed in this article are solely those of the authors and do not necessarily represent those of their affiliated organizations, or those of the publisher, the editors and the reviewers. Any product that may be evaluated in this article, or claim that may be made by its manufacturer, is not guaranteed or endorsed by the publisher.

frontiers | Frontiers in Oncology

TYPE Original Research
PUBLISHED 22 July 2022
DOI 10.3389/fonc.2022.942341

OPEN ACCESS

EDITED BY
Tong-Chuan He,
University of Chicago Medicine,
United States

REVIEWED BY
Fei-Ting Hsu,
China Medical University, Taiwan
Ibrahim C. Haznedaroglu,
Hacettepe University Hospital, Turkey

*CORRESPONDENCE
Silvia La Monica
silvia.lamonica@unipr.it
Andrea Cavazzoni
andrea.cavazzoni@unipr.it

†These authors have contributed equally to this work

SPECIALTY SECTION
This article was submitted to Pharmacology of Anti-Cancer Drugs, a section of the journal Frontiers in Oncology

RECEIVED 12 May 2022
ACCEPTED 29 June 2022
PUBLISHED 22 July 2022

CITATION
Digiacomo G, Fumarola C, La Monica S, Bonelli M, Cavazzoni A, Galetti M, Terenziani R, Eltayeb K, Volta F, Zoppi S, Bertolini P, Missale G, Alfieri R and Petronini PG (2022) CDK4/6 inhibitors improve the anti-tumor efficacy of lenvatinib in hepatocarcinoma cells. *Front. Oncol.* 12:942341. doi: 10.3389/fonc.2022.942341

CDK4/6 inhibitors improve the anti-tumor efficacy of lenvatinib in hepatocarcinoma cells

Graziana Digiacomo[1†], Claudia Fumarola[1†], Silvia La Monica[1*], Mara Bonelli[1], Andrea Cavazzoni[1*], Maricla Galetti[2], Rita Terenziani[1], Kamal Eltayeb[1], Francesco Volta[1], Silvia Zoppi[1], Patrizia Bertolini[3], Gabriele Missale[1,4], Roberta Alfieri[1] and Pier Giorgio Petronini[1]

[1]Department of Medicine and Surgery, University of Parma, Parma, Italy, [2]Department of Occupational and Environmental Medicine, Epidemiology and Hygiene, INAIL - Italian Workers' Compensation Authority, Rome, Italy, [3]Paediatric Hematology Oncology Unit, University Hospital of Parma, Parma, Italy, [4]Unit of Infectious Diseases and Hepatology, University Hospital of Parma, Parma, Italy

Hepatocellular carcinoma (HCC) is the most frequent primary liver cancer with a poor prognosis and limited treatment options. Considering that alterations of the CDK4/6-cyclin D-Rb pathway occur frequently in HCC, we tested the efficacy of two CDK4/6 inhibitors, abemaciclib and ribociclib, in combination with lenvatinib, a multi-kinase inhibitor approved as first-line therapy for advanced HCC, in a panel of HCC Rb-expressing cell lines. The simultaneous drug combinations showed a superior anti-proliferative activity as compared with single agents or sequential schedules of treatment, either in short or in long-term experiments. In addition, the simultaneous combination of abemaciclib with lenvatinib reduced 3D cell growth, and impaired colony formation and cell migration. Mechanistically, these growth-inhibitory effects were associated with a stronger down-regulation of c-myc protein expression. Depending on the HCC cell model, reduced activation of MAPK, mTORC1/p70S6K or src/FAK signaling was also observed. Abemaciclib combined with lenvatinib arrested the cells in the G1 cell cycle phase, induced p21 accumulation, and promoted a stronger increase of cellular senescence, associated with elevation of β-galactosidase activity and accumulation of ROS, as compared with single treatments. After drug withdrawal, the capacity of forming colonies was significantly impaired, suggesting that the anti-tumor efficacy of abemaciclib and lenvatinib combination was persistent.

Our pre-clinical results demonstrate the effectiveness of the simultaneous combination of CDK4/6 inhibitors with lenvatinib in HCC cell models, suggesting that this combination may be worthy of further investigation as a therapeutic approach for the treatment of advanced HCC.

KEYWORDS

hepatocarcinoma (HCC), CDK4/6 inhibition, abemaciclib, lenvatinib, senescence

Introduction

Hepatocellular carcinoma (HCC) is the sixth most common malignant tumor and the fourth leading cause of cancer-related death (1). HCC is a highly heterogenic disease, and a significant proportion of HCC patients show intermediate/advanced disease at the time of clinical diagnosis, thus reducing the opportunity for a radical cure (2). In these patients, systemic therapy remains the only available therapeutic option.

Sorafenib has been the first drug approved as standard first-line treatment for advanced HCC; however, during the last 4 years, other treatments reached the Food and Drug Administration (FDA) approval, including new molecular targeted agents and immune checkpoint inhibitors (ICIs) (3–5)

The IMbrave150 trial (6) demonstrated that the combination of atezolizumab, an ICI directed against PD-L1, with the anti-angiogenic drug bevacizumab improved the overall survival of HCC patients as compared to sorafenib. Atezolizumab plus bevacizumab has become the standard of care for the treatment of patients with unresectable locally advanced or metastatic HCC (5) However, 20% of patients do not respond to this therapy and the median progression-free survival is only 6.8 months. In addition, there is a portion of patients who cannot be treated with atezolizumab/bevacizumab, for whom the therapy options available remain sorafenib or lenvatinib. Lenvatinib is a multi-kinase inhibitor approved in 2018 as first-line treatment for advanced HCC (7), exerting its inhibitory activity against vascular endothelial growth factor receptors (VEGFR1-3), fibroblast growth factor receptors (FGFR1-4), platelet-derived growth factor receptor alpha (PDGFR-α), c-KIT, and RET (8). Targeting the FGF receptors and inhibiting the FGF signaling pathway distinguishes lenvatinib from sorafenib.

Preclinical studies demonstrated that the combination of lenvatinib with pembrolizumab is effective in HCC, resulting in increased antitumor activity as compared to monotherapy in a mouse model of HCC (9). Interestingly, such combination showed promising antitumor activity with a tolerable safety profile also in patients with unresectable HCC (10).

In patients who failed first-line therapy, the treatment choices in second-line include the multi-tyrosin kinases inhibitors (TKIs) regorafenib and cabozantinib, and the monoclonal anti-VEGF2 antibody ramucirumab (11).

Cell cycle dysregulation is a hallmark of cancer and alterations in genes regulating cell proliferation have been frequently reported in HCC cells. Among them, alterations of the cyclin D-CDK4/6-Rb pathways frequently occur in HCC: CDK4 overexpression has been described in more than 70% of cases (12), whereas the inactivation of *CDKN2A/ARF* gene, encoding for the cell cycle inhibitor $p16^{INK4a}$, has been found in over 50% of patients (13, 14). In addition, the oncosuppressor Rb gene has been found inactivated in around 20% of patients (13, 15).

To date, the CDK4/6 inhibitors palbociclib (PD-0332991), ribociclib (LEE011), and abemaciclib (LY835219) are approved for the treatment of Estrogen Receptor positive advanced or metastatic breast cancer in association with endocrine therapy (16). Interestingly, a number of preclinical studies have demonstrated their efficacy also in Rb-expressing HCC cells (17). Accordingly, our recent findings demonstrated that HCC cell lines harboring *CDKN2A/ARF* gene loss and expressing a functional Rb protein were sensitive to palbociclib, and proved the efficacy of CDK4/6 inhibition in combination with regorafenib, thus suggesting a novel approach for the treatment of HCC patients (18).

Based on these positive findings, we investigated the anti-tumor activity of the combination of CDK4/6 inhibitors with lenvatinib in a panel of HCC cell lines. We focused in particular on abemaciclib, because of its highest potency; in addition, abemaciclib is more potent against CDK4 than CDK6, which is involved in the differentiation of hematologic precursor cells, implying a reduced hematological toxicity in the clinical setting (19). Our results demonstrated that the simultaneous drug combination inhibited cell proliferation in either two or three-dimensional (2D, 3D) cell models, impaired colony formation and cell migration, and induced cellular senescence more strongly than single treatments. Interestingly, the growth-inhibitory effect of the drug combination was maintained even after drug removal, providing a pre-clinical rationale for the combination of abemaciclib with lenvatinib as a therapeutic strategy for advanced HCC.

Material and methods

Cell culture

Human HCC cell lines (HUH7, SNU398, HepG2) were obtained from the American Type Culture Collection (ATCC, Manassas, VA); ATCC authenticates the phenotypes of these cell lines on a regular basis. The cells were cultured in Dulbecco's Modified Eagle Medium (DMEM) supplemented with 2 mM glutamine, 10% Fetal Bovine serum (FBS), and 100 U/ml penicillin,100 µg/ml streptomycin, and incubated at 37°C in a humidified atmosphere of 5% CO_2 in air.

Drug treatments

Abemaciclib (S5716), ribociclib (S7740), and lenvatinib (S1164) were purchased from Selleckchem (Houston, TX). All drugs were dissolved in DMSO. DMSO concentration never exceeded 0.1% (v/v); equal amounts of the solvent were added to control cells.

Western blotting

Western blot analysis was performed as previously described (20). Antibodies against p-Rb^{Ser780}, Rb, cyclin D1, CDK6, p-ERK1/2$^{Thr202/Tyr204}$, ERK1/2, p-AKT^{Ser473}, AKT, p-p70S6K^{Thr389}, p70S6K, p-FAK^{Tyr925}, FAK, p-SrcTyr^{416}, Src, PDGFRα, FGFR1, FGFR2, cKIT, *c*-Myc, p21, p-MDM2 and MDM2 were from Cell Signaling Technology, Incorporated (Danvers, MA); anti-p-CDK6^{Tyr24}, FGFR4 were from Santa Cruz Biotechnology, Incorporated (Dallas, TX). The antibody against CDKN2A/p16^{INK4a} was from Abcam (Cambridge, UK). Anti-β-actin (clone B11V08) was from BioVision (Milpitas, CA). Horseradish peroxidase-conjugated secondary antibodies and the chemiluminescence system were from Millipore (Millipore, MA). Reagents for electrophoresis and blotting analysis were from BIO-RAD Laboratories (Hercules, CA). The chemiluminescent signal was acquired by C-DiGit R Blot Scanner and the bands were quantified by Image Studio^{TM}Software, LI-COR Biotechnology (Lincoln, NE).

Drug combination studies

The nature of the interaction between CDK4/6 inhibitors and lenvatinib was calculated by combination index (CI) determination. CIs were calculated with Calcusyn software (Biosoft), which is based on the method of Chou and Talalay. In this method, a CI < 0.8 is considered as synergistic, 0.8 < CI < 1.2 additive and CI > 1.2 antagonistic (21).

Colony and clonogenic assay

Cells were seeded in 12-well culture plates at a low density and were incubated at 37°C in 5% CO_2 incubator. After 6 days of treatment, cells were fixed with ice-cold methanol, stained with 0.1% crystal violet (Sigma Aldrich). The unbound dye was removed by washing with water. The bound crystal violet was solubilized with 0.2% TritonX-100 in PBS and the absorbance of the solution was measured at a wavelength of 570 nm (22). In the experiments of clonogenic assay, after 6 days of treatment, viable cells were harvested, reseeded in 6-well culture plates at a density of 400 cells per well, and cultured for additional 15 days in the absence of drugs. After the recovery time, colonies were fixed with methanol, stained with crystal violet and counted. Data were given as colony number (23).

Analysis of spheroid cell growth

Spheroids from HCC cells were generated using LIPIDURE®-COAT PLATE A-U96 (NOF Corporation, Japan) according to the manufacturer's instructions. Briefly, 3 days after seeding, the spheroids were formed and treated with drugs or vehicles for 6 or 12 days. The effects of the drugs were evaluated in terms of volume changes using the Nikon Eclipse E400 Microscope with digital Net camera. The volume of spheroids [D=(Dmax+Dmin)/2; V=4/3π(D/2)3] was measured using SpheroidSizer, a MATLAB-based and open-source software application (24).

Migration

The migration assay was carried out using Transwell chambers with 6.5-mm diameter polycarbonate filters (8μm pore size, BD Biosciences, Erembodegem, Belgium) as previously described (25).

β-Galactosidase staining

The evaluation of Senescence Associated β-Galactosidase (SA-β-Gal) expression was performed using the Senescence β-Galactosidase Staining kit (Cell Signaling Technology Inc.). Briefly, cells were seeded in 6-well plates in complete medium for 24 h and then treated with drugs or vehicles. At the end of the treatments, a fixative solution was added for 15 min at room temperature. The plates were washed twice with PBS and then the β-Gal staining solution was added. After overnight incubation at 37°C without CO_2, the number of SA-β-Gal positive cells (blue stained) was evaluated by cell counting in ten randomly chosen microscope fields (100× magnification) (26).

Reactive oxygen species detection

Intracellular ROS production was assessed by oxidation of the cell-permeable fluorescent probes 5-(and-6)-chloromethyl-20,70-dichlorodihydrofluorescein diacetate, acetyl ester (CM-H2DCFDA, Molecular Probes®). At the end of the drug treatments, the cells were harvested, centrifuged, resuspended in PBS containing the probe at 1 μM, and incubated in the dark at 37°C. After 30 minutes, the cells were washed, resuspended in PBS, and analyzed on a Beckman-Coulter Cytoflex flow cytometer.

Statistical analysis

Statistical analyses were carried out using Graph-Pad Prism version 6.0 software (GraphPad Software, San Diego, CA). Statistical significance of differences among data was estimated by analysis of variance (ANOVA) followed by Tukey's post-test. p values are indicated where appropriate in the figures and in their legends. p values less than 0.05 were considered significant.

Results

Effects of abemaciclib alone or combined with lenvatinib in HCC cell lines

Firstly, we demonstrated that abemaciclib was effective at inhibiting cell proliferation in a panel of HCC cell lines (Figure 1A). As previously demonstrated for HUH7 and HepG2 cells (18), SNU398 cells also expressed a functional Rb protein and were negative for $p16^{INK4a}$ expression (Figure S1A), molecular features that have been previously correlated with sensitivity to CDK4/6 inhibition (20, 27). In these cells, abemaciclib decreased CDK6 phosphorylation and downregulated both p-Rb and Rb levels (Figure 1B), in accordance with data from literature showing that CDK4/6 inhibitors reduce Rb phosphorylation and concomitantly decrease the expression of total Rb protein in multiple cancer models (28). In addition, abemaciclib increased cyclin D1 levels (Figure 1B), an effect that we had previously observed with palbociclib treatment (18).

Then, we investigated whether abemaciclib treatment could potentiate the anti-tumor activity of lenvatinib. To this end, we firstly analyzed the effects of lenvatinib alone in HCC cells and demonstrated that it inhibited cell proliferation, with a stronger efficacy observed in HUH7 cells compared with HepG2 and SNU398 cells (Figure S1B), confirming results from previous studies (29). All three cell models expressed one or more TK receptors targeted by lenvatinib (Figure S1C): in particular, FGFR1, FGFR2, and FGFR4 were expressed in all cell lines, although to a different extent, c-KIT was absent in SNU398, while PDGFR-α was detected only in HUH7 cells, presumably contributing to their greater sensitivity to lenvatinib. These data confirm that lenvatinib, in addition to its anti-angiogenic activity, exerts direct anti-tumor effects in cells expressing its targets.

The combination of abemaciclib with lenvatinib was evaluated by comparing a simultaneous treatment with sequential schedules (abemaciclib followed by lenvatinib; lenvatinib followed by abemaciclib; abemaciclib or lenvatinib followed by the simultaneous drug combination). In all cell lines analyzed, the simultaneous combination induced a greater inhibition of cell proliferation compared with single agents, and was more efficacious than the sequential schedules, after one or two cycles of treatment (Figure 1C). Actually, some of the sequential schedules were even less effective than single-agent treatments. Based on these findings, we chose the simultaneous combined treatment with abemaciclib and lenvatinib for the subsequent experiments.

To identify the type of interaction between abemaciclib and lenvatinib, we calculated the combination index (CI). As shown in Figure 2A, we demonstrated that this combination resulted in synergistic anti-proliferative effects in HUH7, SNU398, and HepG2 cells.

The superior efficacy of abemaciclib combined with lenvatinib was also demonstrated by a cell colony formation assay, showing that the combination reduced the colony formation more strongly than single-agent treatments in all three cell models analyzed (Figure 2B).

Effects of ribociclib alone or combined with lenvatinib in HCC cell lines

Then, we evaluated whether the same increased anti-tumor activity demonstrated by abemaciclib in combination with lenvatinib could be achieved by inhibiting CDK4/6 with ribociclib. Ribociclib inhibited cell proliferation in the HCC cell models, downregulating p-CDK6 and p-Rb, while cyclin D1 levels were increased as shown for abemaciclib (Figures 3A, B).

The simultaneous combination with lenvatinib produced synergistic anti-proliferative effects, (Figure 3C) and was more effective than single treatments in reducing the colony formation (Figure 3D). It is worth noting that the IC_{50} value for ribociclib was higher than that determined for abemaciclib in all three cell models; actually abemaciclib shows a higher potency in comparison to the other CDK4/6 inhibitors (19). Therefore, we decided to continue using abemaciclib to investigate the effects of CDK4/6 inhibition in combination with lenvatinib.

The combination of abemaciclib with lenvatinib inhibits spheroid cell growth, impairs cell migration, and induces cell cycle arrest and senescence

The greater efficacy of the simultaneous combined treatment with abemaciclib and lenvatinib over individual agents was further confirmed in a 3D system using HUH7 cells (Figure 4A). Indeed, both drugs alone inhibited spheroid cell growth but were significantly more effective when used in combination.

Interestingly, abemaciclib combined with lenvatinib significantly impaired the ability of SNU398 cells to migrate (Figure 4B).

The simultaneous combination induced cell cycle arrest (Figure 4C), with an increased percentage of cells accumulating in the G1 phase in comparison with abemaciclib or lenvatinib alone. No significant induction of cell death was observed (not shown). Interestingly, abemaciclib but not lenvatinib significantly induced senescence, as demonstrated by the induction of β-gal activity in HUH7 cells, and the percentage of senescent cells was further increased after the simultaneous treatment (70% versus 40%) (Figure 4D). Mechanistically, the combination induced significant higher levels of p21 protein (Figure 4E), which is known to play a key role in the initiation of senescence-mediated

A

CELL LINE	Abemaciclib (IC_{50} μM)
HUH7	0.11 ± 0.07
SNU398	0.24 ± 0.01
HepG2	0.05 ± 0.015

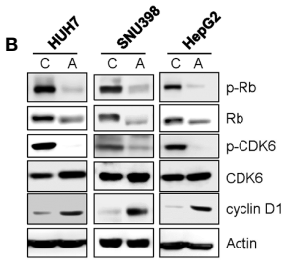

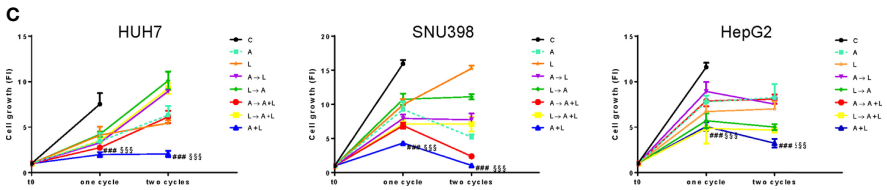

FIGURE 1
The simultaneous combined treatment of abemaciclib and lenvatinib inhibits cell proliferation more strongly than single agents and sequential schedules in HCC cells. **(A)** After 24h from seeding, HUH7, SNU398, and HepG2 cells were treated with increasing concentrations of abemaciclib (A) for 6 days. Cell proliferation was evaluated by CV assay and the IC_{50} values were calculated using GraphPad Prism 6.00 software. **(B)** HCC cells were untreated (Control, C) or treated with 1 μM A for 24h. The cells were lysed and the expression of the indicated proteins was evaluated by Western blot analysis. **(C)** HUH7, SNU398, and HepG2 cells were treated with A or L at their corresponding IC50 values for 6 days (one cycle), or 12 days (two cycles), alone or with different combinations of the two drugs: A for 72h followed by L for 72h (A→L), L for 72h followed by A for 72h (L→A), A for 72h followed by A+L for 72h (A→A+L), L for 72h followed by A+L for 72h (L→A+L), or a simultaneous combination for 6 days (A+L) for each cycle. The growth medium with drugs was refreshed every 3 days. Cell proliferation was evaluated by CV assay. Data are expressed as Fold Increase (FI). The FI index was calculated as the ratio between cell proliferation after 6 or 12 days and cell proliferation at T_0 (T_0 = 24h after seeding). $^{###}p<0.001$ vs A; $^{§§§}p<0.001$, vs L. Data in A are mean values ± SD of three independent experiments. Data in B-C are representative of two independent experiments.

growth arrest (30). Since HUH7 cells express a Y220C-mutated form of p53 (31), we investigated the mechanisms responsible for p21 accumulation, analyzing the activation/expression of MDM2, which has been demonstrated to negatively regulate p21, activating its proteasomal-mediated degradation independently of p53 (32). As shown in Figure 4E, MDM2 phosphorylation and total protein expression were significantly downregulated by abemaciclib/lenvatinib combination, providing a mechanism for p21 induction. Since a variety of evidence indicates that accumulation of intracellular ROS contributes to senescence (33), we evaluated whether the emergence of the senescent phenotype in abemaciclib/lenvatinib-treated cells was related to increased ROS levels. To this end, we measured ROS production by using the fluorescent probe CM-H2DCFDA and demonstrated that the drug combination effectively promoted a stronger increase in ROS levels compared with single-agent treatments (Figure 4F).

The combination of abemaciclib with lenvatinib has different modulatory effects on intracellular signaling pathways depending on the cell model

Then, we investigated the molecular mechanisms underlying the superior efficacy of the drug combination (Figure 5). Rb phosphorylation was reduced not only by abemaciclib but also by lenvatinib, although to a lesser extent, in all three HCC cell lines; interestingly, a further downregulation was induced by the combination, resulting in a stronger inhibition of c-myc expression, whose transcriptional modulation by E2F is well-recognized (34). In addition, the combination significantly reduced the abemaciclib-mediated increase of cyclin D1 expression levels. While the inhibitory effects on the expression of cell cycle regulatory proteins were comparable in the three cell lines, the impact of abemaciclib/lenvatinib combination on the activation status of survival/proliferation intracellular signaling pathways varied significantly depending on the cell model.

In HUH7 cells, the phosphorylation of the mTORC1 substrate p70S6K was reduced by both abemaciclib and lenvatinib, and further downregulated by the combined treatment, even though p-AKT levels were not affected. These inhibitory effects were a consequence of the inhibition of the MAPK pathway, which can modulate the mTORC1/p70S6K signaling independently of AKT (35), as confirmed by using the selective MEK1/2 inhibitor trametinib (Figure S2A). The drug combination downregulated the MAPK pathway also in SNU398 cells, although without affecting the mTORC1/p70S6K signaling; p-AKT levels did not change. Accordingly, trametinib did not inhibit p70S6K phosphorylation in these cells

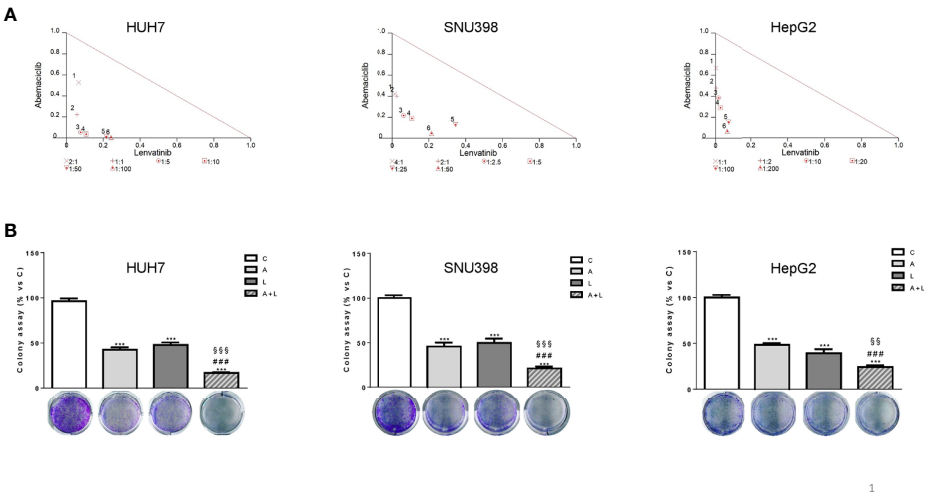

FIGURE 2
Abemaciclib and lenvatinib combination exerts additive anti-proliferative effects in HCC cells and inhibits colony formation more strongly than single agents. **(A)** Cells were treated with A, L or the combination. The growth medium with drugs was refreshed every 3 days. After 6 days, cell proliferation was assessed by CV assay. Combination indexes were calculated with Calcusyn software. **(B)** HUH7, SNU398, and HepG2 cells were treated with A or L at their corresponding IC_{50} values alone or in combination. After 6 days, colony formation was assessed by CV assay. Representative images of crystal violet staining of colonies are shown. ***p<0.001 vs C, $^{###}$p<0.001 vs A; §§p< 0.01, §§§p<0.001 vs L. Data in A are representative of three independent experiments. Data in B are mean values ± SD of three independent experiments.

(Figure S2B), suggesting that the AKT-independent mechanism of mTORC1 modulation by the MAPK pathway is cell type-specific. In HepG2 cells, abemaciclib alone downregulated p-p70S6K levels, supporting the finding that CDK4/6 inhibition reduces mTORC1 activity in some cancer models (36); however, no further decrease was observed with the combination. AKT phosphorylation was unchanged, while p-ERK1/2 levels were increased by lenvatinib alone or in combination. Interestingly, a significant downregulation of src/FAK signaling was promoted by abemaciclib and lenvatinib combination in SNU398 and HepG2 cells. Due to the key role of this pathway in the control of cell migration (37), its inhibition was presumably responsible for the impairment of cell migration observed in SNU398 cells.

The anti-proliferative effects of abemaciclib with lenvatinib are maintained after drug removal

To evaluate whether the anti-tumor effects of abemaciclib and lenvatinib combination were persistent, we performed long-term experiments in HUH7 cells. After 6 days of treatment with the drugs alone or combined, the cells were harvested, counted, reseeded at low density, and cultured in drug-free medium for additional 15 days to test their capacity to form colonies. As shown in Figure 6, colony formation was significantly impaired in cells previously treated with abemaciclib, whereas the inhibitory effects of lenvatinib were almost completely lost. Most importantly, in the culture of cells previously exposed to the drug combination, very few and small colonies were detected, suggesting that the superior efficacy of the combined treatment is maintained even after drug removal.

Discussion

Despite the recent advances in the management of advanced HCC, this malignant disease remains difficult to treat and the development of more effective therapies is warranted. In this regard, different strategies are currently under evaluation, including approaches exploring the anti-cancer properties of compounds normally used for other medical purposes (38), or combinatorial approaches aimed at improving the efficacy of the therapies used in the clinical practice (5).

In this study, we provide evidence that the simultaneous combination of the CDK4/6 inhibitors abemaciclib and ribociclib with lenvatinib is effective in Rb-proficient, $p16^{INK4}$ negative HCC cells, producing synergistic anti-proliferative effects that persisted even after drug withdrawal. These findings are in accordance with our previous results showing that palbociclib, another CDK4/6 inhibitor, improved the efficacy of regorafenib in HCC cells (18), suggesting that CDK4/6 targeting may represent a valuable strategy for enhancing the anti-tumor activity of the anti-angiogenic drugs currently used in the clinic for advanced HCC treatment.

Despite the efficacy of both abemaciclib/lenvatinib and ribociclib/lenvatinib combinations, HCC cells, especially

10.3389/fonc.2022.942341

A

CELL LINE	Ribociclib (IC_{50} μM)
HUH7	0.19 ± 0.08
SNU398	1.87 ± 1.2
HepG2	0.28 ± 0.08

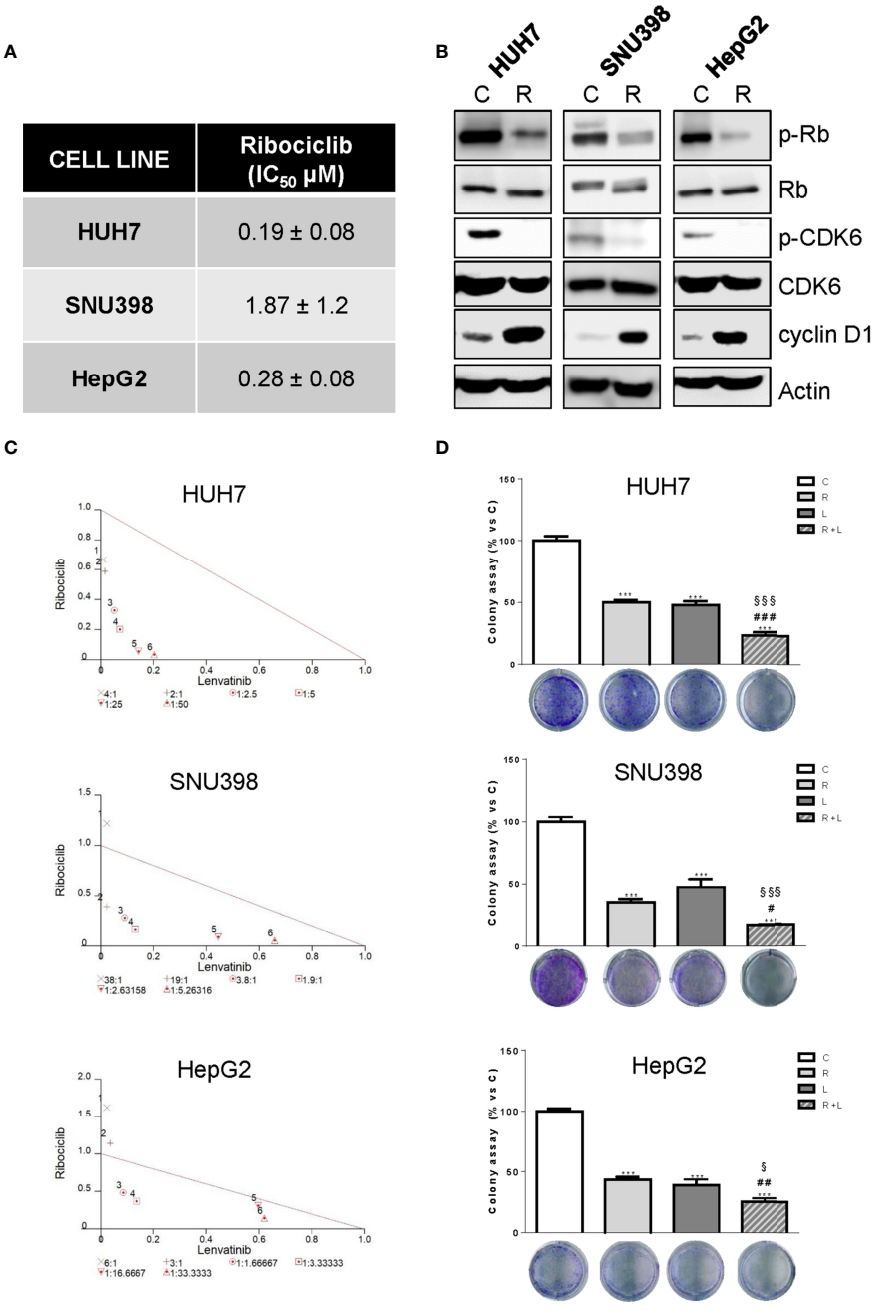

FIGURE 3
Ribociclib and lenvatinib combination exerts additive anti-proliferative effects in HCC cells and inhibits colony formation more strongly than single agents. **(A)** After 24h from seeding, HUH7, SNU398, and HepG2 cells were treated with increasing concentrations of ribociclib (R) for 6 days. Cells proliferation was evaluated by CV assay and the IC_{50} values were calculated using GraphPad Prism 6.00 software. **(B)** HCC cells were untreated (C) or treated with 1 μM R for 24h. The cells were lysed and the expression of the indicated proteins was evaluated by Western blot analysis. **(C)** Cells were treated with R, L or the combination. The growth medium with drugs was refreshed every 3 days. After 6 days, cell proliferation was assessed by CV assay. Combination indexes were calculated with Calcusyn software. **(D)** HUH7, SNU398, and HepG2 cells were treated with R or L at their corresponding IC_{50} values alone or in combination. After 6 days, colony formation was assessed by CV assay. Representative images of crystal violet staining of colonies are shown. ***p<0.001 vs C; $^{\#}$p<0.05, $^{\#\#}$p<0.01 $^{\#\#\#}$p<0.001 vs R; §p< 0.05, §§§p<0.001 vs L. Data in A are mean values ± SD of three independent experiments. Data in B-C are representative of two independent experiments. Data in D are mean values ± SD of two independent experiments.

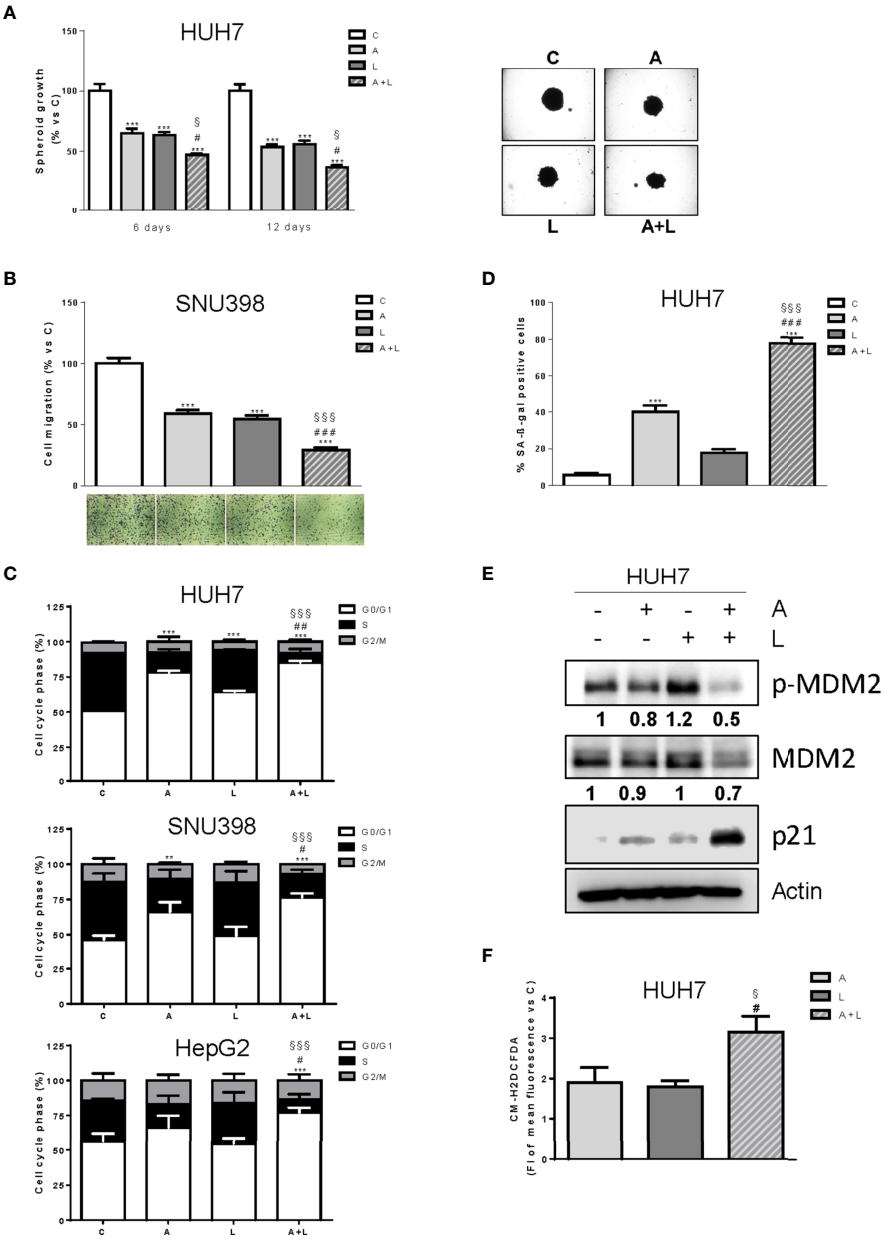

FIGURE 4
Abemaciclib combined with lenvatinib reduces 3D cell growth, inhibits cell migration, and induces G1 cell cycle arrest associated with senescence. **(A)** The growth of spheroids from HUH7 was analyzed after 6 or 12 days of treatment with 0.1 μM A and 0.5 μM L alone or in combination. The data are expressed as percent of spheroid growth versus control. Representative images of spheroids after 12 days of culture are shown. ***p<0.001 vs C; $^{\#}$p<0.05 vs A; §p<0.05 vs L. **(B)** SNU398 cells were treated with 0.2 μM A or 2 μM L as single treatment or in combination for 20h. Migrated cells were then counted. Data are expressed as percent versus control. Representative fields of migration are shown (magnification of 4x). ***p<0.001 vs C; $^{\#\#\#}$p<0.001 vs A; §§§p<0.001 vs L. **(C)** HUH7, SNU398, and HepG2 cells were untreated (C) or treated with 0.1, 0.2 μM and 0.05 μM A and 0.5, 2 or 6.5 μM L for HUH7, SNU398 and HepG2, respectively, as single treatment or in combination for 24h. After 24h the cells were stained with propidium iodide and cell-cycle-phase distribution was determined by flow cytometry. Data are expressed as percentage of cells in each cell-cycle phase. **p<0.01, ***p<0.001 vs C; $^{\#}$p<0.05, $^{\#\#}$p<0.01 vs A; §§§p<0.001 vs L. **(D)** HUH7 cells were treated with 0.1 μM A and 0.5 L alone or in combination for 6 days. Histograms represent the percentage of senescent cells positive for SA-β-Gal expression. ***p<0.001 vs C; $^{\#\#\#}$p<0.001 vs A; §§§p<0.001 vs L. **(E)** HUH7 was treated with 0.1 μM A and 0.5 L alone or in combination for 3 days. The cells were lysed and the expression of the indicated proteins was evaluated by Western blot analysis. **(F)** HUH7 were treated with 0.1 μM A and 0.5 L alone or in combination. After 6 days, the cells were incubated with 1 μM CM-H2DCFDA probe and analyzed by flow cytometry. $^{\#}$p<0.05 vs A; §p<0.05 vs L. Experiments in A-E are representative of two independent experiments. Data in **(B, C)** are mean values ± SD of two independent experiments. Data in D are mean values ± SD of three independent experiments. Data in F are mean values ± SD of three independent experiments.

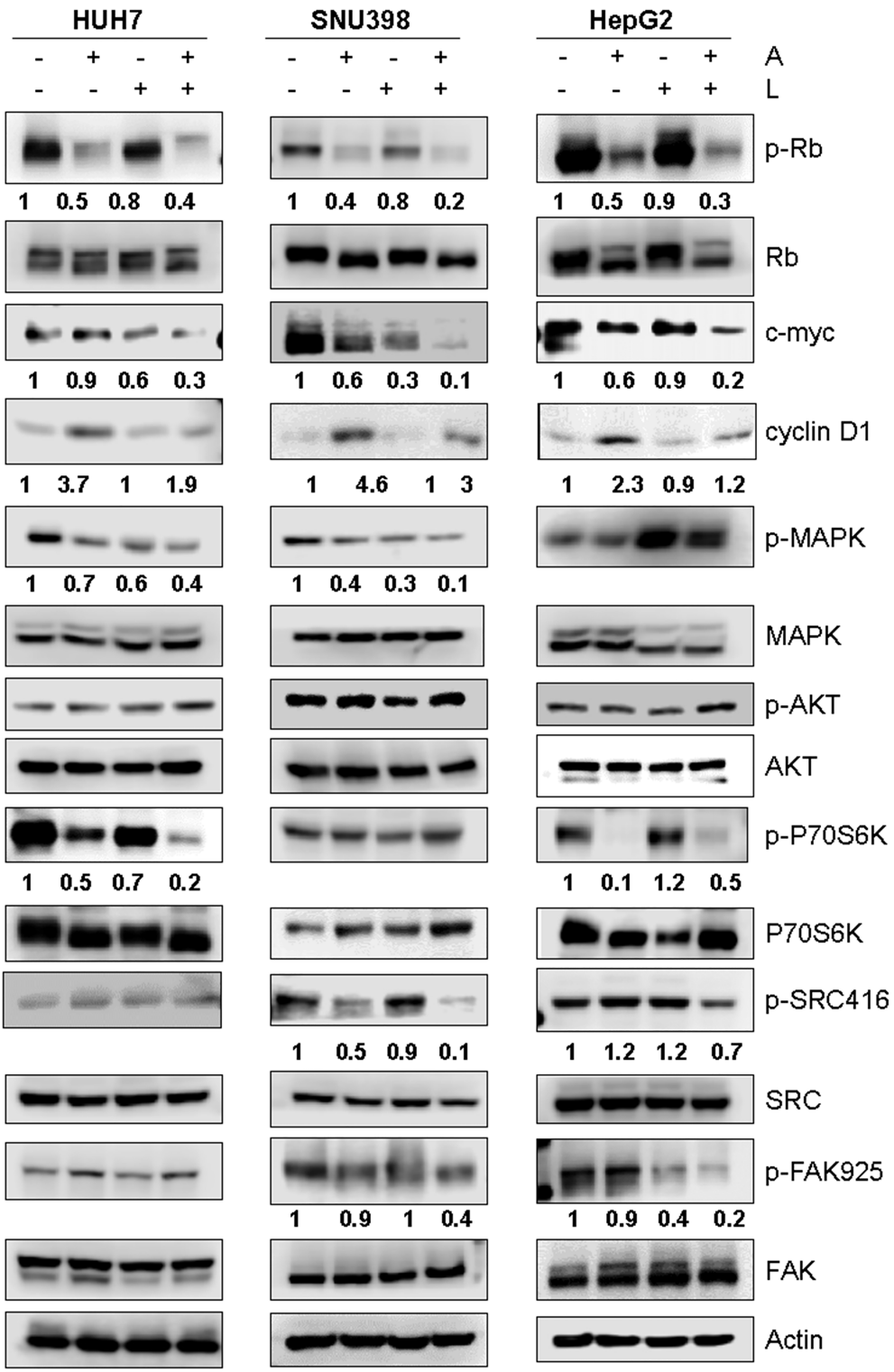

FIGURE 5
Effects of the simultaneous combination of abemaciclib and lenvatinib on intracellular signaling pathways. Cells were treated with 1 μM A and 0.5, 2, or 6.5 μM L for HUH7, SNU398, and HepG2, respectively, alone or in combination for 24 h. The cells were lysed and the expression of the indicated proteins was evaluated by Western blot analysis. Data are representative of two independent experiments.

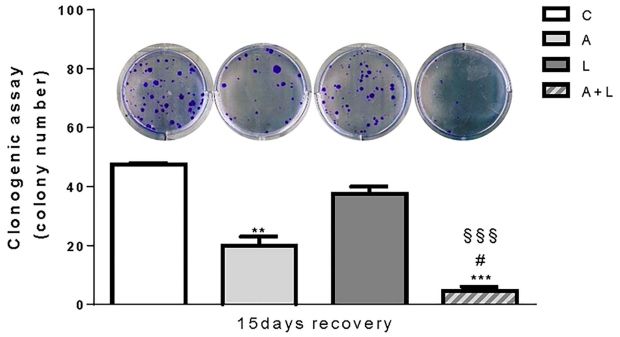

FIGURE 6
The anti-proliferative effects of abemaciclib and lenvatinib combination persisted after drug withdrawal. HUH7 after 6 days of drug treatments, the cells were harvested, seeded at low density, and cultured for additional 15 days in the absence of the drugs (recovery). Representative images of crystal violet staining of colonies are shown. **p<0.01,***p<0.001 vs C; #p<0.05 vs A; §§§p<0.001 vs L. Data are mean values ± SD of two independent experiments.

SNU398 cells, were relatively less sensitive to ribociclib than abemaciclib, confirming literature data showing that abemaciclib is the most potent CDK4/6 inhibitor (19). Therefore, in this study we mainly focused on the effects of abemaciclib in combination with lenvatinib.

Comparing different schedules of treatment, we demonstrated that the best strategy for combining abemaciclib with lenvatinib was represented by the simultaneous treatment, whereas the sequential schedules (abemaciclib before or after lenvatinib, or pre-treatment with single drugs followed by the combination) in some cases were even less effective than single-agent treatments. It is worth noting that, in contrast with palbociclib, whose current clinical regimen requires a week of drug holiday, the lower toxicity of abemaciclib allows for continuous dosing (39), suggesting that combined treatment with abemaciclib and lenvatinib is potentially feasible in the clinic. In this context, it is of interest to note that a phase II clinical trial is currently ongoing to evaluate the combination of abemaciclib with nivolumab, an ICI directed against PD-1, in HCC patients (NCT03781960).

Mechanistically, the effectiveness of abemaciclib/lenvatinib combination was associated with a stronger dephosphorylation/activation of Rb in comparison with single treatments, which resulted in a significant downregulation of c-myc protein, a known transcriptional target of E2F (34). This effect was observed in all cell models analyzed. In contrast, inhibition of other survival/proliferation signaling pathways contributed to the anti-cancer activity of the drug combination in a cell type-dependent fashion. Indeed, only HUH7 and SNU398 cells showed a marked downregulation of ERK1/2 signaling. In a recent study, lenvatinib was shown to activate feedback signaling through EGFR-PAK2-ERK1/2 and EGFR-PAK2-ERK5 pathways in EGFR expressing HCC cell lines (40). Combining lenvatinib with EGFR inhibitors prevented the activation of this feedback mechanism, ensuring a more complete inhibition of MEK and ERK phosphorylation, which resulted in potentiated anti-proliferative effects both *in vitro* and *in vivo*. The src/FAK signaling was downregulated by abemaciclib and lenvatinib combination only in SNU398 and HepG2 cells. Interestingly, previous studies indicate that FAK represents a valuable druggable target in HCC, being frequently overexpressed in this type of cancer (41).

A variety of evidence indicates that inhibition of CDK4/6, after arresting the cell cycle in the G1 phase, can induce quiescence, senescence, or apoptosis, depending on the cell context, cell type, and duration of the inhibition (42–44).

Here we show that abemaciclib and lenvatinib combination in HUH7 cells promoted senescence in a significant proportion of the cell population (~70%), as demonstrated by the induction of SA-β-gal activity. The molecular mechanism underlying this phenomenon involves the induction of p21, whose role in the positive regulation of senescence is well known (45). Abemaciclib/lenvatinib combination may promote the induction of p21 through two possible mechanisms: downregulation of c-myc protein, which inhibits p21 transcription through direct binding to its promoter (46), and downregulation of MDM2, which acts as a negative regulator of p21 favoring its degradation independently of both p53 and ubiquitination (32). Interestingly, a study by Kovatcheva et al. (47) demonstrated that MDM2 degradation was required for CDK4/6 inhibition to mediate the transition from quiescence to senescence in multiple cell models, including liposarcoma, breast, glioma, and lung cancer cell lines. CDK4/6 inhibition enhanced MDM2 proteasome-dependent turnover through a p53-independent mechanism requiring E3 ligase activity of MDM2 and ATRX expression. It is important to stress that these regulatory processes occur independently of p53, since HUH7 cells are p53 mutant (31). The combination of abemaciclib with lenvatinib significantly reduced the phosphorylation of MDM2 at Ser166. Phosphorylation at this site, required for MDM2 stabilization and inhibition of its self-

ubiquitination, is generally attributed to AKT (48); however, in normal liver and HCC cells it was shown to be mediated by MEK-ERK signaling (49). Therefore, downregulation of the MAPK pathway by abemaciclib/lenvatinib combination may contribute to the reduced phosphorylated and total MDM2 levels observed in HUH7 cells.

HUH7 abemaciclib/lenvatinib-treated cells showed a significant increase in ROS levels in comparison with single-agent treatments. ROS have an established role in senescence and their increased production has been shown to be mediated by p21 independently of p53 (50, 51). Therefore, in our experimental system, p21 may induce senescence through a mechanism involving ROS accumulation. It is worth noting that lenvatinib alone induced p21 accumulation, confirming previous findings in thyroid cancer (52), and promoted ROS production, without inducing senescence. ROS were previously shown to play a role in lenvatinib-mediated anti-tumor effects in HUH7 cells, and their accumulation by lenvatinib, as well as by sorafenib and regorafenib, was associated with Keap1-mediated downregulation of Nrf2, a transcription factor playing a key role in the control of antioxidant responses (53).

Growing evidence indicates that induction of senescence exerts anti-tumor effects in HCC (54). For example, inhibition of Sirtuin 6 reduced the tumorigenicity of HCC cells by inducing cellular senescence *via* upregulation of p21 (55). In another study, dual-specificity phosphatase 16 (DUSP16) was shown to play a role in the growth of HCC cells by inactivating p53 and Rb and promoting cell escape from senescence. Accordingly, DUSP16 expression levels were found upregulated in liver cancer and positively correlated with the tumor cell proliferation index (56). It is worth underlining that the aberrant persistence of senescent cells may have detrimental effects with a negative impact on long-term patient outcome. However, induction of senescence can be exploited *in vivo* as a tool for preparing the conditions for subsequent elimination of cancer cells by recruited immune cells (57). In this regard, it is interesting to note that a mechanism contributing to the anti-tumor activity of lenvatinib involves the enhancement of tumor infiltration by NK cells (58). Therefore, we can speculate that, in the therapeutic strategy proposed in our study, lenvatinib may favor the elimination of senescent cells induced by abemaciclib/lenvatinib combination by stimulating the recruitment of tumor-infiltrating NK cells *in vivo*; this may help avoid senescence-related side effects and minimize the risk of regression.

Data availability statement

The raw data supporting the conclusions of this article will be made available by the authors, without undue reservation.

Author contributions

Conception and design: GD, CF, MB, PP. Cebnll biology and molecular biology experiments: GD, CF, SM, RT, KE, SZ. Statistical analysis: FV, MG. writing of the manuscript: CF, GD. review of the manuscript: SL, AC, RA, PB. Study supervision: PP, GM. All the authors contributed to revising the manuscript and approved the final version for publication.

Funding

This work was supported by Associazione Noi per Loro onlus (Parma), Grant "New therapeutic strategies for hepatocarcinoma"; Associazione Noi per Loro onlus (Parma), Project "Andrea Spadola" fellowship to Graziana Digiacomo.

Conflict of interest

The authors declare that the research was conducted in the absence of any commercial or financial relationships that could be construed as a potential conflict of interest.

Publisher's note

All claims expressed in this article are solely those of the authors and do not necessarily represent those of their affiliated organizations, or those of the publisher, the editors and the reviewers. Any product that may be evaluated in this article, or claim that may be made by its manufacturer, is not guaranteed or endorsed by the publisher.

Supplementary material

The Supplementary Material for this article can be found online at: https://www.frontiersin.org/articles/10.3389/fonc.2022.942341/full#supplementary-material

References

1. Hatanaka T, Naganuma A, Kakizaki S. Lenvatinib for hepatocellular carcinoma: A literature review. *Pharm (Basel)* (2021) 14(1). doi: 10.3390/ph14010036

2. Petrick JL, Florio AA, Znaor A, Ruggieri D, Laversanne M, Alvarez CS, et al. International trends in hepatocellular carcinoma incidence, 1978-2012. *Int J Cancer* (2020) 147(2):317–30. doi: 10.1002/ijc.32723

3. Villanueva A. Hepatocellular carcinoma. *N Engl J Med* (2019) 380(15):1450–62. doi: 10.1056/NEJMra1713263

4. Huang A, Yang XR, Chung WY, Dennison AR, Zhou J. Targeted therapy for hepatocellular carcinoma. *Signal Transduct Target Ther* (2020) 5(1):146. doi: 10.1038/s41392-020-00264-x

5. Zhang H, Zhang W, Jiang L, Chen Y. Recent advances in systemic therapy for hepatocellular carcinoma. *biomark Res* (2022) 10(1):3. doi: 10.1186/s40364-021-00350-4

6. Finn RS, Qin S, Ikeda M, Galle PR, Ducreux M, Kim TY, et al. Atezolizumab plus bevacizumab in unresectable hepatocellular carcinoma. *N Engl J Med* (2020) 382(20):1894–905. doi: 10.1056/NEJMoa1915745

7. Kudo M, Ueshima K, Yokosuka O, Ogasawara S, Obi S, Izumi N, et al. Sorafenib plus low-dose cisplatin and fluorouracil hepatic arterial infusion chemotherapy versus sorafenib alone in patients with advanced hepatocellular

carcinoma (Silius): a randomised, open label, phase 3 trial. *Lancet Gastroenterol Hepatol* (2018) 3(6):424–32. doi: 10.1016/S2468-1253(18)30078-5

8. Zhao Y, Zhang YN, Wang KT, Chen L. Lenvatinib for hepatocellular carcinoma: From preclinical mechanisms to anti-cancer therapy. *Biochim Biophys Acta Rev Cancer* (2020) 1874(1):188391. doi: 10.1016/j.bbcan.2020.188391

9. Kimura T, Kato Y, Ozawa Y, Kodama K, Ito J, Ichikawa K, et al. Immunomodulatory activity of lenvatinib contributes to antitumor activity in the Hepa1-6 hepatocellular carcinoma model. *Cancer Sci* (2018) 109(12):3993–4002. doi: 10.1111/cas.13806

10. Finn RS, Ikeda M, Zhu AX, Sung MW, Baron AD, Kudo M, et al. Phase ib study of lenvatinib plus pembrolizumab in patients with unresectable hepatocellular carcinoma. *J Clin Oncol* (2020) 38(26):2960–70. doi: 10.1200/JCO.20.00808

11. Llovet JM, Kelley RK, Villanueva A, Singal AG, Pikarsky E, Roayaie S, et al. Hepatocellular carcinoma. *Nat Rev Dis Primers* (2021) 7(1):6. doi: 10.1038/s41572-020-00240-3

12. Lu JW, Lin YM, Chang JG, Yeh KT, Chen RM, Tsai JJ, et al. Clinical implications of deregulated Cdk4 and cyclin D1 expression in patients with human hepatocellular carcinoma. *Med Oncol* (2013) 30(1):379. doi: 10.1007/s12032-012-0379-5

13. Azechi H, Nishida N, Fukuda Y, Nishimura T, Minata M, Katsuma H, et al. Disruption of the P16/Cyclin D1/Retinoblastoma protein pathway in the majority of human hepatocellular carcinomas. *Oncology* (2001) 60(4):346–54. doi: 10.1159/000058531

14. Zhou Y, Wang XB, Qiu XP, Shuai Z, Wang C, Zheng F. Cdkn2a promoter methylation and hepatocellular carcinoma risk: A meta-analysis. *Clin Res Hepatol Gastroenterol* (2018) 42(6):529–41. doi: 10.1016/j.clinre.2017.07.003

15. Totoki Y, Tatsuno K, Covington KR, Ueda H, Creighton CJ, Kato M, et al. Trans-ancestry mutational landscape of hepatocellular carcinoma genomes. *Nat Genet* (2014) 46(12):1267–73. doi: 10.1038/ng.3126

16. Sobhani N, D'Angelo A, Pittacolo M, Roviello G, Miccoli A, Corona SP, et al. Updates on the Cdk4/6 inhibitory strategy and combinations in breast cancer. *Cells* (2019) 8(4). doi: 10.3390/cells8040321

17. Bollard J, Miguela V, Ruiz de Galarreta M, Venkatesh A, Bian CB, Roberto MP, et al. Palbociclib (Pd-0332991), a selective Cdk4/6 inhibitor, restricts tumour growth in preclinical models of hepatocellular carcinoma. *Gut* (2017) 66(7):1286–96. doi: 10.1136/gutjnl-2016-312268

18. Digiacomo G, Fumarola C, La Monica S, Bonelli MA, Cretella D, Alfieri R, et al. Simultaneous combination of the Cdk4/6 inhibitor palbociclib with regorafenib induces enhanced anti-tumor effects in hepatocarcinoma cell lines. *Front Oncol* (2020) 10:563249. doi: 10.3389/fonc.2020.563249

19. Braal CL, Jongbloed EM, Wilting SM, Mathijssen RHJ, Koolen SLW, Jager A. Inhibiting Cdk4/6 in breast cancer with palbociclib, ribociclib, and abemaciclib: Similarities and differences. *Drugs* (2021) 81(3):317–31. doi: 10.1007/s40265-020-01461-2

20. Cretella D, Ravelli A, Fumarola C, La Monica S, Digiacomo G, Cavazzoni A, et al. The anti-tumor efficacy of Cdk4/6 inhibition is enhanced by the combination with Pi3k/Akt/Mtor inhibitors through impairment of glucose metabolism in tnbc cells. *J Exp Clin Cancer Res* (2018) 37(1):72. doi: 10.1186/s13046-018-0741-3

21. Van Der Steen N, Leonetti A, Keller K, Dekker H, Funel N, Lardon F, et al. Decrease in phospho-Pras40 plays a role in the synergy between erlotinib and crizotinib in an egfr and cmet wild-type squamous non-small cell lung cancer cell line. *Biochem Pharmacol* (2019) 166:128–38. doi: 10.1016/j.bcp.2019.05.014

22. La Monica S, Fumarola C, Cretella D, Bonelli M, Minari R, Cavazzoni A, et al. Efficacy of the Cdk4/6 dual inhibitor abemaciclib in egfr-mutated nsclc cell lines with different resistance mechanisms to osimertinib. *Cancers (Basel)* (2020) 13 (1). doi: 10.3390/cancers13010006

23. Cavazzoni A, Alfieri RR, Carmi C, Zuliani V, Galetti M, Fumarola C, et al. Dual mechanisms of action of the 5-benzylidene-hydantoin upr1024 on lung cancer cell lines. *Mol Cancer Ther* (2008) 7(2):361–70. doi: 10.1158/1535-7163.MCT-07-0477

24. Fumarola C, Bozza N, Castelli R, Ferlenghi F, Marseglia G, Lodola A, et al. Expanding the arsenal of fgfr inhibitors: a novel chloroacetamide derivative as a new irreversible agent with anti-proliferative activity against fgfr1-amplified lung cancer cell lines. *Front Oncol* (2019) 9:179. doi: 10.3389/fonc.2019.00179

25. La Monica S, Caffarra C, Saccani F, Galvani E, Galetti M, Fumarola C, et al. Gefitinib inhibits invasive phenotype and epithelial-mesenchymal transition in drug-resistant nsclc cells with met amplification. *PloS One* (2013) 8(10):e78656. doi: 10.1371/journal.pone.0078656

26. Bonelli MA, Digiacomo G, Fumarola C, Alfieri R, Quaini F, Falco A, et al. Combined inhibition of Cdk4/6 and Pi3k/Akt/Mtor pathways induces a synergistic anti-tumor effect in malignant pleural mesothelioma cells. *Neoplasia* (2017) 19 (8):637–48. doi: 10.1016/j.neo.2017.05.003

27. Finn RS, Dering J, Conklin D, Kalous O, Cohen DJ, Desai AJ, et al. Pd 0332991, a selective cyclin d kinase 4/6 inhibitor, preferentially inhibits proliferation of luminal estrogen receptor-positive human breast cancer cell lines in vitro. *Breast Cancer Res* (2009) 11(5):R77. doi: 10.1186/bcr2419

28. Pan Q, Sathe A, Black PC, Goebell PJ, Kamat AM, Schmitz-Draeger B, et al. Cdk4/6 inhibitors in cancer therapy: A novel treatement strategy for bladder cancer. *Bladder Cancer* (2017) 3(2):79–88. doi: 10.3233/BLC-170105

29. Matsuki M, Hoshi T, Yamamoto Y, Ikemori-Kawada M, Minoshima Y, Funahashi Y, et al. Lenvatinib inhibits angiogenesis and tumor fibroblast growth factor signaling pathways in human hepatocellular carcinoma models. *Cancer Med* (2018) 7(6):2641–53. doi: 10.1002/cam4.1517

30. Kumari R, Jat P. Mechanisms of cellular senescence: Cell cycle arrest and senescence associated secretory phenotype. *Front Cell Dev Biol* (2021) 9:645593. doi: 10.3389/fcell.2021.645593

31. Hsu IC, Tokiwa T, Bennett W, Metcalf RA, Welsh JA, Sun T, et al. P53 gene mutation and integrated hepatitis b viral DNA sequences in human liver cancer cell lines. *Carcinogenesis* (1993) 14(5):987–92. doi: 10.1093/carcin/14.5.987

32. Zhang Z, Wang H, Li M, Agrawal S, Chen X, Zhang R. Mdm2 is a negative regulator of P21waf1/Cip1, independent of P53. *J Biol Chem* (2004) 279(16):16000–6. doi: 10.1074/jbc.M312264200

33. Lu T, Finkel T. Free radicals and senescence. *Exp Cell Res* (2008) 314 (9):1918–22. doi: 10.1016/j.yexcr.2008.01.011

34. Oswald F, Lovec H, Moroy T, Lipp M. E2f-dependent regulation of human myc: trans-activation by cyclins d1 and a overrides tumour suppressor protein functions. *Oncogene* (1994) 9(7):2029–36.

35. Bahrami BF, Ataie-Kachoie P, Pourgholami MH, Morris DL. P70 ribosomal protein S6 kinase (Rps6kb1): An update. *J Clin Pathol* (2014) 67(12):1019–25. doi: 10.1136/jclinpath-2014-202560

36. Goel S, Wang Q, Watt AC, Tolaney SM, Dillon DA, Li W, et al. Overcoming therapeutic resistance in her2-positive breast cancers with cdk4/6 inhibitors. *Cancer Cell* (2016) 29(3):255–69. doi: 10.1016/j.ccell.2016.02.006

37. Westhoff MA, Serrels B, Fincham VJ, Frame MC, Carragher NO. Src-mediated phosphorylation of focal adhesion kinase couples actin and adhesion dynamics to survival signaling. *Mol Cell Biol* (2004) 24(18):8113–33. doi: 10.1128/MCB.24.18.8113-8133.2004

38. Nenni M, Oncul S, Ercan A, Celebier M, Suslu I, Haznedaroglu IC. Exposure of hepatocellular carcinoma cells to ankaferd blood stopper® alters cell death signaling networks confirmed by oncoproteomic and genomic profiling studies. *Curr Traditional Med* (2021) 7(2):8. doi: 10.2174/2215083806666200117093815

39. Onesti CE, Jerusalem G. Cdk4/6 inhibitors in breast cancer: differences in toxicity profiles and impact on agent choice. a systematic review and meta-analysis. *Expert Rev Anticancer Ther* (2021) 21(3):283–98. doi: 10.1080/14737140.2021.1852934

40. Jin H, Shi Y, Lv Y, Yuan S, Ramirez CFA, Lieftink C, et al. Egfr activation limits the response of liver cancer to lenvatinib. *Nature* (2021) 595(7869):730–4. doi: 10.1038/s41586-021-03741-7

41. Romito I, Porru M, Braghini MR, Pompili L, Panera N, Crudele A, et al. Focal adhesion kinase inhibitor tae226 combined with sorafenib slows down hepatocellular carcinoma by multiple epigenetic effects. *J Exp Clin Cancer Res* (2021) 40(1):364. doi: 10.1186/s13046-021-02154-8

42. Klein ME, Kovatcheva M, Davis LE, Tap WD, Koff A. Cdk4/6 inhibitors: The mechanism of action may not be as simple as once thought. *Cancer Cell* (2018) 34(1):9–20. doi: 10.1016/j.ccell.2018.03.023

43. Blagosklonny MV. Geroconversion: irreversible step to cellular senescence. *Cell Cycle* (2014) 13(23):3628–35. doi: 10.4161/15384101.2014.985507

44. Yoshida A, Diehl JA. Cdk4/6 inhibitor: From quiescence to senescence. *Oncoscience* (2015) 2(11):896–7. doi: 10.18632/oncoscience.256

45. Bonelli M, La Monica S, Fumarola C, Alfieri R. Multiple effects of cdk4/6 inhibition in cancer: from cell cycle arrest to immunomodulation. *Biochem Pharmacol* (2019) 170:113676. doi: 10.1016/j.bcp.2019.113676

46. Gartel AL, Ye X, Goufman E, Shianov P, Hay N, Najmabadi F, et al. Myc represses the P21(Waf1/Cip1) promoter and interacts with Sp1/Sp3. *Proc Natl Acad Sci U.S.A.* (2001) 98(8):4510–5. doi: 10.1073/pnas.081074898

47. Kovatcheva M, Liu DD, Dickson MA, Klein ME, O'Connor R, Wilder FO, et al. Mdm2 turnover and expression of atrx determine the choice between quiescence and senescence in response to cdk4 inhibition. *Oncotarget* (2015) 6 (10):8226–43. doi: 10.18632/oncotarget.3364

48. Feng J, Tamaskovic R, Yang Z, Brazil DP, Merlo A, Hess D, et al. Stabilization of Mdm2 *Via* decreased ubiquitination is mediated by protein kinase B/Akt-dependent phosphorylation. *J Biol Chem* (2004) 279(34):35510–7. doi: 10.1074/jbc.M404936200

49. Malmlof M, Roudier E, Hogberg J, Stenius U. Mek-Erk-Mediated phosphorylation of Mdm2 at ser-166 in hepatocytes. *Mdm2 Is Activated*

Response to Inhibited Akt Signaling J Biol Chem (2007) 282(4):2288–96. doi: 10.1074/jbc.M604953200

50. Macip S, Igarashi M, Fang L, Chen A, Pan ZQ, Lee SW, et al. Inhibition of P21-mediated ros accumulation can rescue P21-induced senescence. *EMBO J* (2002) 21(9):2180–8. doi: 10.1093/emboj/21.9.2180

51. Masgras I, Carrera S, de Verdier PJ, Brennan P, Majid A, Makhtar W, et al. Reactive oxygen species and mitochondrial sensitivity to oxidative stress determine induction of cancer cell death by P21. *J Biol Chem* (2012) 287(13):9845–54. doi: 10.1074/jbc.M111.250357

52. Kim SY, Kim SM, Chang HJ, Kim BW, Lee YS, Park CS, et al. Solat (Sorafenib lenvatinib alternating treatment): A new treatment protocol with alternating sorafenib and lenvatinib for refractory thyroid cancer. *BMC Cancer* (2018) 18(1):956. doi: 10.1186/s12885-018-4854-z

53. Zheng A, Chevalier N, Calderoni M, Dubuis G, Dormond O, Ziros PG, et al. Crispr/Cas9 genome-wide screening identifies keap1 as a sorafenib, lenvatinib, and regorafenib sensitivity gene in hepatocellular carcinoma. *Oncotarget* (2019) 10 (66):7058–70. doi: 10.18632/oncotarget.27361

54. Liu P, Tang Q, Chen M, Chen W, Lu Y, Liu Z, et al. Hepatocellular senescence: Immunosurveillance and future senescence-induced therapy in hepatocellular carcinoma. *Front Oncol* (2020) 10:589908. doi: 10.3389/fonc.2020.589908

55. Feng XX, Luo J, Liu M, Yan W, Zhou ZZ, Xia YJ, et al. Sirtuin 6 promotes transforming growth factor-beta1/h2o2/hocl-mediated enhancement of hepatocellular carcinoma cell tumorigenicity by suppressing cellular senescence. *Cancer Sci* (2015) 106(5):559–66. doi: 10.1111/cas.12632

56. Zhang H, Zheng H, Mu W, He Z, Yang B, Ji Y, et al. Dusp16 ablation arrests the cell cycle and induces cellular senescence. *FEBS J* (2015) 282(23):4580–94. doi: 10.1111/febs.13518

57. Wang C, Vegna S, Jin H, Benedict B, Lieftink C, Ramirez C, et al. Inducing and exploiting vulnerabilities for the treatment of liver cancer. *Nature* (2019) 574 (7777):268–72. doi: 10.1038/s41586-019-1607-3

58. Zhang Q, Liu H, Wang H, Lu M, Miao Y, Ding J, et al. Lenvatinib promotes antitumor immunity by enhancing the tumor infiltration and activation of nk cells. *Am J Cancer Res* (2019) 9(7):1382–95.

frontiers | Frontiers in Oncology

TYPE Review
PUBLISHED 08 August 2022
DOI 10.3389/fonc.2022.957844

OPEN ACCESS

EDITED BY
Arianna Palladini,
University of Pavia, Italy

REVIEWED BY
Cecilia Garofalo,
Veneto Institute of Oncology (IRCCS), Italy
Marianna Carrabotta,
Rizzoli Orthopedic Institute (IRCCS), Italy

*CORRESPONDENCE
Hiroyuki Tsuchiya
tsuchi@med.kanazawa-u.ac.jp
Robert M Hoffman
all@anticancer.com

SPECIALTY SECTION
This article was submitted to Pharmacology of Anti-Cancer Drugs, a section of the journal Frontiers in Oncology

RECEIVED 31 May 2022
ACCEPTED 15 July 2022
PUBLISHED 08 August 2022

CITATION
Higuchi T, Igarashi K, Yamamoto N, Hayashi K, Kimura H, Miwa S, Bouvet M, Tsuchiya H and Hoffman RM (2022) Review: Precise sarcoma patient-derived orthotopic xenograft (PDOX) mouse models enable identification of novel effective combination therapies with the cyclin-dependent kinase inhibitor palbociclib: A strategy for clinical application. *Front. Oncol.* 12:957844. doi: 10.3389/fonc.2022.957844

Review: Precise sarcoma patient-derived orthotopic xenograft (PDOX) mouse models enable identification of novel effective combination therapies with the cyclin-dependent kinase inhibitor palbociclib: A strategy for clinical application

Takashi Higuchi[1,2,3], Kentaro Igarashi[3], Norio Yamamoto[3], Katsuhiro Hayashi[3], Hiroaki Kimura[3], Shinji Miwa[3], Michael Bouvet[2], Hiroyuki Tsuchiya[3]* and Robert M. Hoffman[1,2]*

[1]AntiCancer, Inc., San Diego, CA, United States, [2]Department of Surgery, University of California San Diego, San Diego, CA, United States, [3]Department of Orthopaedic Surgery, Graduate School of Medical Sciences, Kanazawa University, Kanazawa, Japan

Introduction: Sarcomas are rare heterogeneous malignant tumors that originate and develop in soft tissue or bone. Effective treatment for sarcomas is still limited to traditional chemotherapy and surgery that are often ineffective for recurrent disease. Cyclin-dependent kinases (CDKs) promote abnormal cell cycling and cell division in many cancers including sarcomas. Therefore, our hypothesis was that CDK inhibitors may be useful candidates for sarcoma treatment. Patient-derived orthotopic xenograft (PDOX) mouse models mimic the clinical disease for all major cancer types and have identified effective treatments that hold much clinical promise. The present report reviews sarcoma PDOX models that we have established for their potential to discover effective combination treatments based on CDK inhibitors for recalcitrant sarcoma.

Methods: We have previously reported six sarcoma PDOX studies evaluating the CDK inhibitor palbociclib on sarcoma, including osteosarcoma, Ewing sarcoma, de-differentiated liposarcoma, and peritoneal metastatic leiomyosarcoma.

Results: Palbociclib monotherapy significantly inhibited, but not regressed, the PDOX growth of osteosarcoma, Ewing sarcoma, de-differentiated liposarcoma, and peritoneal metastatic leiomyosarcoma. A combination of palbociclib and a mammalian target of rapamycin (mTOR) inhibitor, everolimus,

significantly inhibited, but did not regress, the PDOX growth of osteosarcoma. Combinations of palbociclib with a multikinase inhibitor, sorafenib, and palbociclib combined with recombinant methioninase were effective and regressed the osteosarcoma and de-differentiated liposarcoma PDOX models, respectively.

Conclusions: Novel effective drug combinations using the CDK inhibitor palbociclib were identified in PDOX models of the major types of sarcomas. Methionine restriction effected by methioninase increased the efficacy of palbociclib. Combination therapy with palbociclib is a promising future strategy for improved sarcoma therapy in the clinic.

KEYWORDS

patient-derived orthotopic xenograft (PDOX), sarcoma, CDK4/6 inhibitor, palbociblib, osteosarcoma, soft-tissue sarcoma, combination therapy, methioninase

Introduction

Sarcomas are rare heterogeneous malignant tumors that originate and develop in connective tissue, such as muscle, adipose, vascular, nerve, and bone (1). Their rarity and heterogeneous features have limited the development of more effective therapies (2). Cyclin-dependent kinases (CDKs) regulate cell cycle progression and abnormal activation, or overexpression of CDKs results in altered cell cycle behavior in many cancers (3, 4). Recent studies suggest that CDKs are major drivers of sarcomagenesis (5). Therefore, our hypothesis was that CDK inhibitors may be useful candidates for sarcoma treatment.

Our laboratory developed the patient-derived orthotopic xenograft (PDOX) mouse model for all major cancer types (6). The PDOX models mimic the clinical disease, including the malignant behavior of sarcoma, due to their natural tumor microenvironment (7–11). The PDOX models, established from patients with many cancer types, including sarcoma, have identified effective treatments that hold much clinical promise (1, 12). The present report reviews sarcoma PDOX models thus far established and their potential to discover effective combination treatment, based on CDK inhibitors, for recalcitrant sarcoma.

The cyclin-dependent kinase 4/6 inhibitor, palbociclib, inhibits a cyclin-dependent kinase inhibitor 2A-deletion Ewing sarcoma in a patient-derived orthotopic xenograft model

The efficacy of a CDK inhibitor, palbociclib, was evaluated in a PDOX model established from a chest-wall Ewing sarcoma patient who had undergone conventional chemotherapy including doxorubicin, vincristine, and cyclophosphamide (13). Ewing sarcoma is the second most common sarcoma of bone in children and young adults comprising poorly differentiated small round cells (13, 14).

Palbociclib is the first selective CDK4/6 inhibitor approved for cancer treatment and is used for estrogen receptor-positive/human epidermal growth factor receptor-2 (HER2)-negative metastatic breast cancer (15). Since deletion of cyclin-dependent kinase inhibitor 2A (CDKN2A), which is a tumor-suppressor gene and a negative regulator of CDK4/6, was found in this Ewing sarcoma patient's tumor, the efficacy of palbociclib was tested on the PDOX model of this tumor (13).

The Ewing sarcoma PDOX model was established using the surgical orthotopic implantation (SOI) technique that we developed (6), implanting a single tumor fragment orthotopically into the right chest wall of nude mice (Figure 1A) (13). Histological features of the PDOX tumor were similar to those of the original patient, demonstrating small round cells. Palbociclib (100 mg/kg) was orally administered to the Ewing sarcoma PDOX models for 21 consecutive days. Palbociclib significantly inhibited PDOX tumor growth, while first-line treatment doxorubicin did not affect the growth of PDOX. It has been reported that 10%–22% of Ewing sarcoma and 20% of all sarcoma types have a CDKN2A deletion (16–18). This study demonstrated that palbociclib appears to be a clinically promising agent for Ewing sarcoma and possibly other sarcomas that have a CDKN2A deletion. Three clinical trials investigating the efficacy of palbociclib for Ewing sarcoma are ongoing (ClinicalTrials.gov).

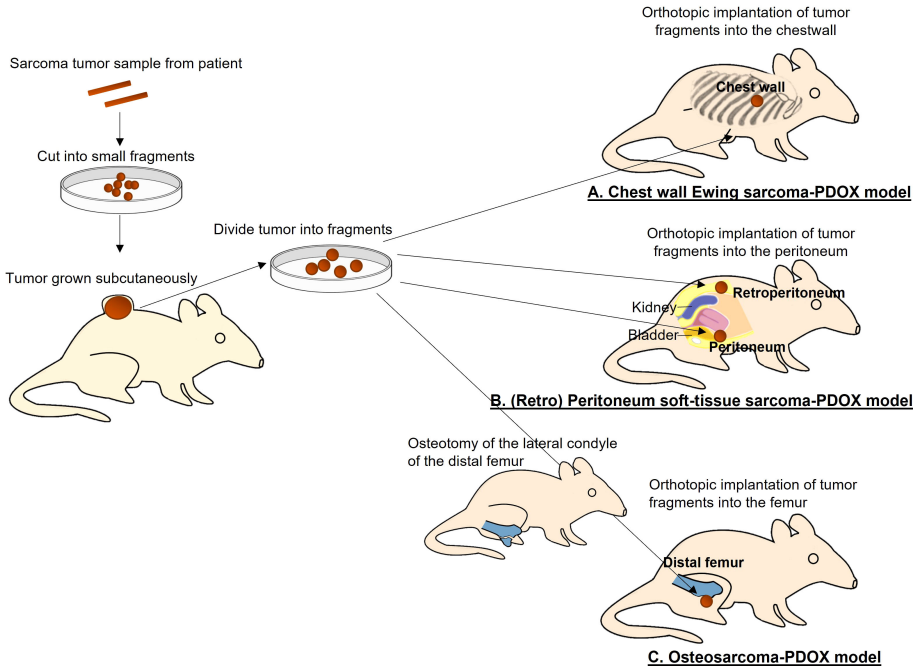

FIGURE 1
Establishment of a patient-derived orthotopic xenograft (PDOX) models of sarcoma. **(A)** Chest-wall Ewing sarcoma PDOX model. **(B)** Peritoneum and retroperitoneum soft-tissue sarcoma PDOX models. **(C)** Osteosarcoma PDOX model.

Palbociclib in soft-tissue sarcoma patient-derived orthotopic xenograft models

The efficacy of palbociclib was next evaluated on recalcitrant soft-tissue sarcoma PDOX models. Liposarcoma and leiomyosarcoma are two of the most common subtypes of soft-tissue sarcoma. Almost half of high-grade soft-tissue sarcoma patients develop local or distal recurrence and their prognosis is poor, with a median overall survival of 20 months (19, 20).

Leiomyosarcoma, which frequently occurs in the extremities, the retroperitoneal space, and uterus, has a high risk of metastasis and local recurrence with a 5-year recurrence rate of 40%, leading to high mortality (21). Doxorubicin as first-line treatment and ifosfamide, gemcitabine and docetaxel, eribulin, pazopanib, and trabectedin as second-line treatment have long been used for leiomyosarcoma with limited efficacy (19). Palbociclib has been shown to be effective for leiomyosarcoma, which may be due to a CDKNA2 deletion being found in 11%–32% of leiomyosarcoma patients who have a worse prognosis (22, 23). Clinical trials examining the efficacy of CDK4/6 inhibitor monotherapy in leiomyosarcoma have not been published.

A peritoneal-metastatic leiomyosarcoma PDOX model was established using SOI to implant a tumor fragment on the dome of the urinary bladder of nude mice (Figure 1B) (21). Palbociclib was administered to this recurrent leiomyosarcoma PDOX model for 21 days. Palbociclib showed significant efficacy on the PDOX growth, compared to the control group with a decreased number of cancer cells found in the treated tumor shown by histological analysis. The combination of gemcitabine and docetaxel was more effective (21). This report indicated moderate efficacy of palbociclib as a monotherapy in leiomyosarcoma. The status of CDKNA2 in this leiomyosarcoma PDOX tumor will be analyzed in a future study.

Dedifferentiated liposarcoma, which often occurs in the extremities and the retroperitoneal space, is a subtype of liposarcoma, with the lowest survival rate among liposarcomas (24). Amplification of CDK4 and murine double minute 2 (MDM2) is observed in 90% of dedifferentiated liposarcoma, suggesting the usefulness of palbociclib (25). Several clinical trials investigating the efficacy of CDK4/6 inhibitors for dedifferentiated liposarcoma have been performed or are

ongoing (16). However, it should be noted that many of these clinical trials have analyzed dedifferentiated and well-differentiated liposarcomas together, which can have totally different clinical outcomes. When limited to dedifferentiated liposarcoma, interim analysis of a phase II study of abemaciclib, a CDK4/6 inhibitor, in patients with dedifferentiated liposarcoma demonstrated favorable outcomes (30.4 months in median progression-free survival) (26).

A retroperitoneal dedifferentiated liposarcoma PDOX model was established using SOI, by implanting the tumor into the retroperitoneum of nude mice by splitting the obliquus externus abdominis muscle (Figure 1B) (27). Palbociclib was administered to this liposarcoma PDOX model for 14 days. Palbociclib showed significant efficacy on PDOX growth compared to that of the control group. The tumor treated with palbociclib showed altered cancer cell shapes with an area of necrotic cells and fibrosis shown by histological analysis (27).

This report suggests that palbociclib is only moderately effective as monotherapy even in dedifferentiated liposarcoma that usually has CDK4 amplification.

Combination treatment using palbociclib in soft-tissue sarcoma patient-derived orthotopic xenograft models

We tested combination treatment with palbociclib for increased efficacy on sarcoma. Recent studies have shown a synergy of CDK inhibitors with other chemotherapy drugs (16, 28). A phase II study of the combination of ribociclib, a CDK4/6 inhibitor, and everolimus, a mammalian target of rapamycin (mTOR) inhibitor, in patients with dedifferentiated liposarcoma and leiomyosarcoma is currently ongoing (ClinicalTrials.gov).

We have developed recombinant methioninase to restrict methionine in cancer cells (29). Methionine addiction is a fundamental and general hallmark of cancer and is termed the Hoffman effect (30). Methionine addiction appears to be caused by excess transmethylation reactions in cancer cells. Therefore, methionine restriction has been shown to be effective in many cancer types (29–32). Methionine-restricted cancer cells selectively arrest in late S/G2 of the cell cycle that may elicit a synergistic efficacy with palbociclib (32).

A methioninase and palbociclib combination was administered to the dedifferentiated liposarcoma PDOX model, described above, for 14 days. While monotherapy with palbociclib showed only moderate efficacy, similar to the study described above, the combination of methioninase and palbociclib regressed the PDOX tumor with extensive tumor necrosis. This report suggests that although palbociclib as a single agent is effective in treating drug-resistant soft-tissue sarcoma, the combination of palbociclib and other anticancer agents, including experimental drugs, may more effectively regress the tumors.

Combination treatment using palbociclib in sarcoma patient-derived orthotopic xenograft models

Osteosarcoma is the most common malignant primary bone tumor (12). Resistance to traditional first-line chemotherapy drugs, such as doxorubicin and cisplatinum, leads to local and distance recurrence that is often fatal to patients, which are mostly adolescents and young adults (12). Osteosarcoma tends to have abnormal cell cycle control regulators, including CDKN2A and CDK4 (16). It has been reported that upregulated CDK4 expression in osteosarcoma patients correlates with the incidence of metastasis and poor prognosis, suggesting that palbociclib can be effective for osteosarcoma (33). However, prospective clinical trials investigating the efficacy of CDK4/6 inhibitors on osteosarcoma have not yet been performed (16).

The osteosarcoma PDOX model was established using SOI by implanting a tumor fragment into a space made by cutting the lateral condyle of the distal femur of nude mice (Figure 1C) (12). The patient tumor used for this osteosarcoma PDOX model was from a fresh biopsy sample of a pelvic osteosarcoma (34). Palbociclib either alone or combined with sorafenib was administered to the osteosarcoma PDOX model for 14 days (Figure 2) (35). Monotherapy with palbociclib significantly, but moderately, inhibited osteosarcoma PDOX growth and decreased cancer cell density (Figure 2). The combination of palbociclib and sorafenib significantly inhibited and regressed the osteosarcoma PDOX and extensively induced tumor necrosis with non-viable cells and degenerative changes in the stroma (Figure 2). Sorafenib is an oral multikinase inhibitor approved for the treatment of renal cell carcinoma, hepatocellular carcinoma, and thyroid cancer (36). The combination of sorafenib and palbociclib has been reported to have synergy against pancreatic carcinoma and hepatocellular carcinoma (35). The efficacy of the sorafenib–palbociclib combination to regress the osteosarcoma PDOX tumor indicates future clinical efficacy.

Another osteosarcoma PDOX was treated with palbociclib combined with everolimus, which is an mTOR inhibitor approved for breast and renal cell cancer (37). The patient tumor used for this osteosarcoma PDOX model was from a fresh surgical sample of femoral osteosarcoma (38). Monotherapy with palbociclib moderately inhibited the PDOX growth compared to that of the control (38). The combination of palbociclib and everolimus significantly inhibited tumor growth and induced cancer necrosis (38). This was the first report demonstrating the efficacy of the

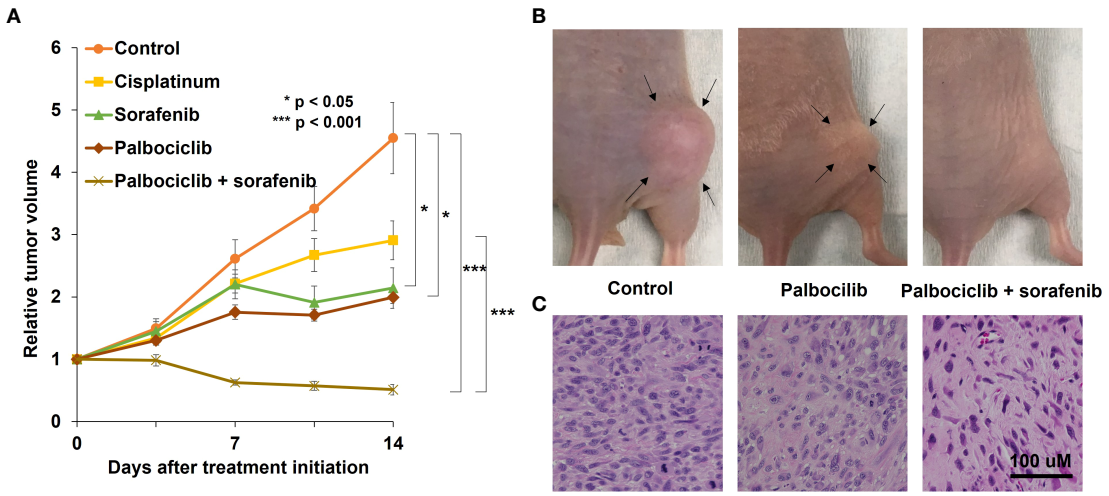

FIGURE 2
A representative osteosarcoma patient-derived orthotopic xenograft (PDOX) study identifying effective combination treatment with palbociclib. **(A)** The line graphs indicate the tumor volume at each time point after treatment start relative to the initial tumor volume for each group. *p < 0.05; ***p < 0.001. Error bar: ± standard error of the mean. **(B)** Representative photographs of the control, palbociclib-treated, or palbociclib–sorafenib combination-treated osteosarcoma PDOX models. Arrows indicate the tumor margins. **(C)** Hematoxylin and eosin-stained sections of control, palbociclib-treated, or palbociclib–sorafenib combination-treated tumors. Scale bar: 100 μm. Modified after Higuchi et al. (35).

palbociclib–everolimus combination for osteosarcoma, suggesting promising clinical efficacy (38). CDK4/6 inhibition was reported to downregulate the downstream mediators of the mTOR pathway in several cancer types, predicting synergy of a CDK4/6 inhibitor combined with an mTOR inhibitor (39). The efficacy of this combination *in vitro* and *in vivo* was also shown in breast cancer, malignant pleural mesothelioma, and glioblastoma (39).

Message to the reader

Sarcoma is a rare and heterogeneous group of cancers. Many molecular-targeted drugs have been developed for major cancers. However, prospective trials evaluating these drugs are limited in sarcoma due to its rarity and heterogeneity. Sarcomas have a poor prognosis when they are resistant to first-line chemotherapy. Therefore, discovering more effective treatment in sarcoma is mandatory.

The sarcoma PDOX model presents an opportunity to discover candidate unproven therapeutics for sarcoma, including the CDK4/6 inhibitor palbociclib. CDK4/6 inhibitors represent a potential breakthrough in cancer treatment. Although many sarcoma types have alterations in the CDK4/6 pathway, so far, no CDK4/6 inhibitor is approved for sarcoma treatment. We have reported six studies evaluating palbociclib as a candidate for sarcoma treatment using sarcoma PDOX models (Table 1). Palbociclib in combination with other agents effectively arrested the growth of all sarcoma PDOX tumors, showing that a CDK4/6 inhibitor is active against sarcoma. To regress the sarcoma PDOX tumors, palbociclib was used with other chemotherapy drugs, including an mTOR inhibitor, a multikinase inhibitor, and methioninase.

CDK inhibitors are used preferentially in combination with other chemotherapy drugs that target dual genomic derangements and convert temporary cell cycle inhibition into permanent cell growth arrest or cell death (40). Although none of the nude mouse PDOX models used in the studies reviewed in the present report had significant toxicity such as significant weight loss or mouse death, combination chemotherapy in the clinic may have toxicity issues. Pharmacogenomic biomarkers are expected to identify effective drugs for sarcoma patients, thereby avoiding unnecessary drug toxicity (41). However, there are still no established biomarkers for each sarcoma subtype due to tremendous heterogeneity of this class of diseases. Further genetic and molecular biological analysis combined with drug–response studies using the PDOX model should contribute to the establishment of pharmacogenomic biomarkers in sarcoma patients.

Since the sarcoma PDOX model behaves similarly to the sarcoma in the patient, the results obtained here are directly relevant to clinical outcome (1). The present review demonstrated that a CDK inhibitor is active in the major types of sarcomas and that treatment using the CDK4/6 inhibitor palbociclib especially in combination with methionine

TABLE 1 Summary of efficacy of CDK4/6 inhibitors in the sarcoma PDOX studies.

Sarcoma type (Ref)	Presentation	SOI	Tested drugs (Standard chemotherapy and palbociclib)	Result
Ewing sarcoma (13)	Primary	Chest wall	Doxorubicin	Total resistance
			Linsitinib (not approved for sarcoma)	Highly inhibited
			Palbociclib	Arrested
Leiomyosarcoma (21)	Metastatic	Peritoneum	Doxorubicin	Mildly inhibited
			Gemcitabine + docetaxel	Regressed
			Pazopanib	Mildly inhibited
			Palbociclib	Mildly inhibited
De-differentiated liposarcoma (27)	Recurrent	Retroperitoneum	Doxorubicin	Total resistance
			Pazopanib	Mildly inhibited
			Gemcitabine + docetaxel	Mildly inhibited
			Trabectedin	Mildly inhibited
			Eribulin	Regressed
			Palbociclib	Mildly inhibited
De-differentiated liposarcoma (32)	Recurrent	Retroperitoneum	Doxorubicin	Total resistance
			rMETase (experimental)	Mildly inhibited
			Palbociclib	Mildly inhibited
			Palbociclib + methioninase	Regressed
Osteosarcoma (35)	Primary	Femur	Cisplatinum	Total resistance
			Sorafenib (not approved for sarcoma)	Highly inhibited
			Palbociclib	Highly inhibited
			Palbociclib + sorafenib	Regressed
Osteosarcoma (38)	Primary	Femur	Doxorubicin	Total resistance
			Everolimus (not approved for sarcoma)	Mildly inhibited
			Palbociclib	Mildly inhibited
			Palbociclib + everolimus	Arrested

CDK, cyclin-dependent kinase; PDOX, patient-derived orthotopic xenograft; SOI, surgical orthotopic implantation.

restriction by methioninase or with a multikinase inhibitor is a promising strategy for sarcoma treatment in the clinic.

Author contributions

Conception and design: TH and RMH. Acquisition, analysis, and interpretation of data: TH, KI, NY, KH, HK, SM, and MB. Writing, review, and revision of the article: TH, HT, and RMH. All authors contributed to the article and approved the submitted version.

Funding

This work was supported in part by the Japan Society for the Promotion of Science (JSPS) KAKENHI Grant Number JP20K22802 and the Robert M. Hoffman Foundation for Cancer Research.

Conflict of interest

Authors TH and RH are unpaid associates of AntiCancer, Inc.

The remaining authors declare that the research was conducted in the absence of any commercial or financial relationships that could be construed as a potential conflict of interest.

Publisher's note

References

1. Igarashi K, Kawaguchi K, Murakami T, Miyake K, Kiyuna T, Miyake M, et al. Patient-derived orthotopic xenograft models of sarcoma. *Cancer Lett* (2020) 469:332–9. doi: 10.1016/j.canlet.2019.10.028

2. Ehnman M, Larsson O. Microenvironmental targets in sarcoma. *Front Oncol* (2015) 5:248. doi: 10.3389/fonc.2015.00248

3. Shapiro GI. Cyclin-dependent kinase pathways as targets for cancer treatment. *J Clin Oncol* (2006) 24:1770–83. doi: 10.1200/jco.2005.03.7689

4. Thoma OM, Neurath MF, Waldner MJ. Cyclin-dependent kinase inhibitors and their therapeutic potential in colorectal cancer treatment. *Front Pharmacol* (2021) 12:757120. doi: 10.3389/fphar.2021.757120

5. Kohlmeyer JL, Gordon DJ, Tanas MR, Monga V, Dodd RD, Quelle DE. CDKs in sarcoma: mediators of disease and emerging therapeutic targets. *Int J Mol Sci* (2020) 21:3018. doi: 10.3390/ijms21083018

6. Hoffman RM. Patient-derived orthotopic xenografts: better mimic of metastasis than subcutaneous xenografts. *Nat Rev Cancer* (2015) 15:451–2. doi: 10.1038/nrc3972

7. Hiroshima Y, Maawy A, Zhang Y, Murakami T, Momiyama M, Mori R, et al. Metastatic recurrence in a pancreatic cancer patient derived orthotopic xenograft (PDOX) nude mouse model is inhibited by neoadjuvant chemotherapy in combination with fluorescence-guided surgery with an anti-CA 19-9-conjugated fluorophore. *PLoS One* (2014) 9:e114310. doi: 10.1371/journal.pone.0114310

8. Hiroshima Y, Maawy A, Zhang Y, Zhang N, Murakami T, Chishima T, et al. Patient-derived mouse models of cancer need to be orthotopic in order to evaluate targeted anti-metastatic therapy. *Oncotarget* (2016) 7:71696–702. doi: 10.18632/oncotarget.12322

9. Hiroshima Y, Zhang Y, Zhang N, Maawy A, Mii S, Yamamoto M, et al. Establishment of a patient-derived orthotopic xenograft (PDOX) model of HER-2-positive cervical cancer expressing the clinical metastatic pattern. *PLoS One* (2015) 10:e0117417. doi: 10.1371/journal.pone.0117417

10. Hoffman RM. Patient-derived orthotopic xenograft (pdox) models of melanoma. *Int J Mol Sci* (2017) 18:1875. doi: 10.3390/ijms18091875

11. Suetsugu A, Hoffman RM. Color-coded imaging of the tumor microenvironment (tme) in human patient-derived orthotopic xenograft (pdox) mouse models. *Adv Exp Med Biol* (2021) 1329:163–79. doi: 10.1007/978-3-030-73119-9_9

12. Higuchi T, Igarashi K, Yamamoto N, Hayashi K, Kimura H, Miwa S, et al. Osteosarcoma patient-derived orthotopic xenograft (pdox) models used to identify novel and effective therapeutics: a review. *Anticancer Res* (2021) 41:5865–71. doi: 10.21873/anticanres.15406

13. Murakami T, Singh AS, Kiyuna T, Dry SM, Li Y, James AW, et al. Effective molecular targeting of CDK4/6 and IGF-1R in a rare FUS-ERG fusion CDKN2A-deletion doxorubicin-resistant ewing's sarcoma patient-derived orthotopic xenograft (PDOX) nude-mouse model. *Oncotarget* (2016) 7:47556–64. doi: 10.18632/oncotarget.9879

14. Chang WI, Lin C, Liguori N, Honeyman JN, DeNardo B, El-Deiry W. Molecular targets for novel therapeutics in pediatric fusion-positive non-cns solid tumors. *Front Pharmacol* (2021) 12:747895. doi: 10.3389/fphar.2021.747895

15. Dhillon S. Palbociclib: first global approval. *Drugs* (2015) 75:543–51. doi: 10.1007/s40265-015-0379-9

16. Hsu JY, Seligson ND, Hays JL, Miles WO, Chen JL. Clinical utility of cdk4/6 inhibitors in sarcoma: successes and future challenges. *JCO Precis Oncol* (2022) 6: e2100211. doi: 10.1200/PO.21.00211

17. Bui N, Przybyl J, Million L, Rijn MVD, Ganjoo KN. CDKN2A deletion as a prognostic marker: A clinico-genomic analysis of sarcoma patients. *J Clin Oncol* (2018) 36:11543. doi: 10.1200/JCO.2018.36.15_suppl.11543

18. Lerman DM, Monument MJ, McIlvaine E, Liu XQ, Huang D, Monovich L, et al. Tumoral TP53 and/or CDKN2A alterations are not reliable prognostic biomarkers in patients with localized Ewing sarcoma: a report from the children's oncology group. *Pediatr Blood Cancer* (2015) 62:759–65. doi: 10.1002/pbc.25340

19. Phillips E, Jones RL, Huang P, Digklia A. Efficacy of eribulin in soft tissue sarcomas. *Front Pharmacol* (2022) 13:869754. doi: 10.3389/fphar.2022.869754

20. Tap WD, Wagner AJ, Schöffski P, Martin-Broto J, Krarup-Hansen A, Ganjoo KN, et al. Effect of doxorubicin plus olaratumab vs doxorubicin plus placebo on survival in patients with advanced soft tissue sarcomas: the announce randomized clinical trial. *JAMA* (2020) 323:1266–76. doi: 10.1001/jama.2020.1707

21. Miyake K, Kiyuna T, Miyake M, Kawaguchi K, Zhang Z, Wangsiricharoen S, et al. Gemcitabine combined with docetaxel precisely regressed a recurrent leiomyosarcoma peritoneal metastasis in a patient-derived orthotopic xenograft (PDOX) model. *Biochem Biophys Res Commun* (2019) 509:1041–6. doi: 10.1016/j.bbrc.2019.01.046

22. Kawaguchi K, Oda Y, Saito T, Yamamoto H, Tamiya S, Takahira T, et al. Mechanisms of inactivation of the p16INK4a gene in leiomyosarcoma of soft tissue: decreased p16 expression correlates with promoter methylation and poor prognosis. *J Pathol* (2003) 201:487–95. doi: 10.1002/path.1419

23. Elvin JA, Gay LM, Ort R, Shuluk J, Long J, Shelley L, et al. Clinical benefit in response to palbociclib treatment in refractory uterine leiomyosarcomas with a common cdkn2a alteration. *Oncologist* (2017) 22:416–21. doi: 10.1634/theoncologist.2016-0310

24. McGovern Y, Zhou CD, Jones RL. Systemic therapy in metastatic or unresectable well-differentiated/dedifferentiated liposarcoma. *Front Oncol* (2017) 7:292. doi: 10.3389/fonc.2017.00292

25. Assi T, Kattan J, Rassy E, Nassereddine H, Farhat F, Honore C, et al. Targeting CDK4 (cyclin-dependent kinase) amplification in liposarcoma: A comprehensive review. *Crit Rev Oncol Hematol* (2020) 153:103029. doi: 10.1016/j.critrevonc.2020.103029

26. Dickson MA, Koff A, D'Angelo SP, Gounder MM, Keohan ML, Kelly CM, et al. Phase 2 study of the CDK4 inhibitor abemaciclib in dedifferentiated liposarcoma. *J Clin Oncol* (2019) 37:11004. doi: 10.1200/JCO.2019.37.15_suppl.11004

27. Igarashi K, Kawaguchi K, Kiyuna T, Miyake K, Higuchi T, Yamamoto N, et al. Eribulin regresses a doxorubicin-resistant dedifferentiated liposarcoma in a patient-derived orthotopic xenograft mouse model. *Cancer Genomics Proteomics* (2020) 17:351–8. doi: 10.21873/cgp.20194

28. Rampioni Vinciguerra GL, Sonego M, Segatto I, Dall'Acqua A, Vecchione A, Baldassarre G, et al. CDK4/6 inhibitors in combination therapies: better in company than alone: a mini review. *Front Oncol* (2022) 12:891580. doi: 10.3389/fonc.2022.891580

29. Hoffman RM. Development of recombinant methioninase to target the general cancer-specific metabolic defect of methionine dependence: a 40-year odyssey. *Expert Opin Biol Ther* (2015) 15:21–31. doi: 10.1517/14712598.2015.963050

30. Kaiser P. Methionine Dependence of Cancer. *Biomolecules* (2020) 10:568. doi: 10.3390/biom10040568

31. Yamamoto J, Aoki Y, Inubushi S, Han Q, Hamada K, Tashiro Y, et al. Extent and instability of trimethylation of histone h3 lysine increases with degree of malignancy and methionine addiction. *Cancer Genomics Proteomics* (2022) 19:12–8. doi: 10.21873/cgp.20299

32. Igarashi K, Kawaguchi K, Kiyuna T, Miyake K, Miyaki M, Yamamoto N, et al. Metabolic targeting with recombinant methioninase combined with palbociclib regresses a doxorubicin-resistant dedifferentiated liposarcoma. *Biochem Biophys Res Commun* (2018) 506:912–7. doi: 10.1016/j.bbrc.2018.10.119

33. Zhou Y, Shen JK, Yu Z, Hornicek FJ, Kan Q, Duan Z. Expression and therapeutic implications of cyclin-dependent kinase 4 (CDK4) in osteosarcoma. *Biochim Biophys Acta Mol Basis Dis* (2018) 1864:1573–82. doi: 10.1016/j.bbadis.2018.02.004

34. Higuchi T, Yamamoto J, Sugisawa N, Tashiro Y, Nishino H, Yamamoto N, et al. PPARγ agonist pioglitazone in combination with cisplatinum arrests a chemotherapy-resistant osteosarcoma pdox model. *Cancer Genomics Proteomics* (2020) 17:35–40. doi: 10.21873/cgp.20165

35. Higuchi T, Sugisawa N, Miyake K, Oshiro H, Yamamoto N, Hayashi K, et al. Sorafenib and palbociclib combination regresses a cisplatinum-resistant osteosarcoma in a pdox mouse model. *Anticancer Res* (2019) 39:4079–84. doi: 10.21873/anticanres.13565

36. Huang A, Zeng P, Li Y, Lu W, Lai Y. LY294002 is a promising inhibitor to overcome sorafenib resistance in flt3-itd mutant aml cells by interfering with pi3k/akt signaling pathway. *Front Oncol* (2021) 11:782065. doi: 10.3389/fonc.2021.782065

37. Porta C, Paglino C, Mosca A. Targeting PI3K/Akt/mTOR signaling in cancer. *Front Oncol* (2014) 4:64. doi: 10.3389/fonc.2014.00064

38. Oshiro H, Tome Y, Miyake K, Higuchi T, Sugisawa N, Kanaya F, et al. Combination of cdk4/6 and mtor inhibitors suppressed doxorubicin-resistant osteosarcoma in a patient-derived orthotopic xenograft mouse model: a translatable strategy for recalcitrant disease. *Anticancer Res* (2021) 41:3287–92. doi: 10.21873/anticanres.15115

39. Cretella D, Ravelli A, Fumarola C, La Monica S, Digiacomo G, Cavazzoni A, et al. The anti-tumor efficacy of CDK4/6 inhibition is enhanced by the combination with PI3K/AKT/mTOR inhibitors through impairment of glucose metabolism in TNBC cells. *J Exp Clin Cancer Res* (2018) 37:72. doi: 10.1186/s13046-018-0741-3

40. Bollard J, Miguela V, Ruiz de Galarreta M, Venkatesh A, Bian CB, Roberto MP, et al. Palbociclib (PD-0332991), a selective CDK4/6 inhibitor, restricts tumour growth in preclinical models of hepatocellular carcinoma. *Gut* (2017) 66:509. doi: 10.3389/fonc.2020.00509

41. Caruso C, Garofalo C. Pharmacogenomics biomarkers of soft tissue sarcoma therapies. *Front Oncol* (2020) 10:509:509. doi: 10.3389/fonc.2020.00509

frontiers | Frontiers in Pharmacology

TYPE Original Research
PUBLISHED 08 August 2022
DOI 10.3389/fphar.2022.958443

OPEN ACCESS

EDITED BY
Andrea Cavazzoni,
University of Parma, Italy

REVIEWED BY
Kamal Eltayeb,
University of Parma, Italy
Martin Perez-Santos,
Benemérita Universidad Autónoma de Puebla, Mexico

*CORRESPONDENCE
Manzoor Ahmad Mir,
drmanzoor@kashmiruniversity.ac.in

SPECIALTY SECTION
This article was submitted to Pharmacology of Anti-Cancer Drugs, a section of the journal Frontiers in Pharmacology

RECEIVED 31 May 2022
ACCEPTED 04 July 2022
PUBLISHED 08 August 2022

CITATION
Mehraj U, Wani NA, Hamid A, Alkhanani M, Almilaibary A and Mir MA (2022), Adapalene inhibits the growth of triple-negative breast cancer cells by S-phase arrest and potentiates the antitumor efficacy of GDC-0941. *Front. Pharmacol.* 13:958443. doi: 10.3389/fphar.2022.958443

Adapalene inhibits the growth of triple-negative breast cancer cells by S-phase arrest and potentiates the antitumor efficacy of GDC-0941

Umar Mehraj[1], Nissar Ahmad Wani[2], Abid Hamid[2], Mustfa Alkhanani[3], Abdullah Almilaibary[4] and Manzoor Ahmad Mir[1]*

[1]Department of Bioresources, School of Biological Sciences, University of Kashmir, Srinagar, J&K, India, [2]Department of Biotechnology, School of Life Sciences, Central University of Kashmir, Ganderbal, J&K, India, [3]Biology Department, College of Science, University of Hafr Al Batin, Hafr Al Batin, Saudi Arabia, [4]Department of Family and Community Medicine, Albaha University, Albaha, Saudi Arabia

Although advances in diagnostics and therapeutics have prolonged the survival of triple-negative breast cancer (TNBC) patients, metastasis, therapeutic resistance, and lack of targeted therapies remain the foremost hurdle in the effective management of TNBC. Thus, evaluation of new therapeutic agents and their efficacy in combination therapy is urgently needed. The third-generation retinoid adapalene (ADA) has potent antitumor activity, and using ADA in combination with existing therapeutic regimens may improve the effectiveness and minimize the toxicities and drug resistance. The current study aimed to assess the anticancer efficacy of adapalene as a combination regimen with the PI3K inhibitor (GDC-0941) in TNBC *in vitro* models. The Chou–Talalay's method evaluated the pharmacodynamic interactions (synergism, antagonism, or additivity) of binary drug combinations. Flow cytometry, Western blotting, and *in silico* studies were used to analyze the mechanism of GDC–ADA synergistic interactions in TNBC cells. The combination of GDC and ADA demonstrated a synergistic effect in inhibiting proliferation, migration, and colony formation of tumor cells. Accumulation of reactive oxygen species upon co-treatment with GDC and ADA promoted apoptosis and enhanced sensitivity to GDC in TNBC cells. The findings indicate that ADA is a promising therapeutic agent in treating advanced BC tumors and enhance sensitivity to GDC in inhibiting tumor growth in TNBC models while reducing therapeutic resistance.

KEYWORDS

Breast cancer, triple-negative breast cancer, adapalene, combination therapy, Chou–Talalay, GDC-0941

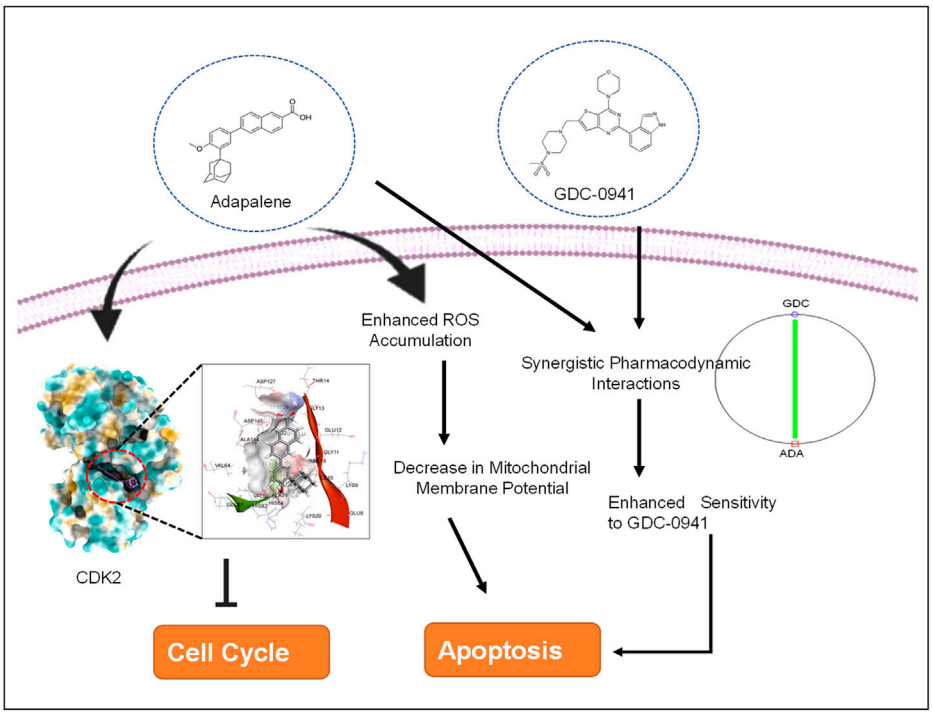

Graphical Abstract

Introduction

Breast cancer (BC) is one of the most frequent malignancies diagnosed in women worldwide, with the highest incidence and mortality rates (Siegel et al., 2021; Sung et al., 2021). TNBC, an aggressive and invasive subtype of BC, constitutes 20% of all breast malignancies (Hon et al., 2016). TNBC tumors are large, less differentiated, and prone to brain metastasis. Owing to the absence of hormonal receptors (ER and PR) and *HER2* amplification, conventional chemotherapeutic agents continue to be the primary therapeutic approach (Yin et al., 2020). TNBC patients respond favorably to chemotherapy; however, the development of therapeutic resistance limits the prognosis and is associated with poor survival (Yin et al., 2020; Mehraj et al., 2021a; Mehraj et al., 2021b). The need for effective treatment options and treatment strategies, as a result, has become urgent.

Due to the intrinsic instability of tumor cells, which makes therapeutic resistance common, aggressive malignancies such as TNBC cannot be efficiently treated with a single treatment. As a result, combining therapeutic drugs may be more helpful in treating the condition (Lebert et al., 2018; Mir et al., 2020; Yin et al., 2020). In addition, by concurrently targeting different signaling cascades implicated in tumor development in a parallel or linear manner, combination therapy minimizes the chance of chemoresistance and toxicity while retaining or even enhancing the effectiveness of each agent at lower dosages (Lu et al., 2013; Mir et al., 2020). Moreover, combination therapy is a promising technique that can alter the long-term strategy for developing a more effective treatment option for TNBC patients (Mir et al., 2020).

The PI3K/AKT/mTOR signaling cascade is critical for cell biology functions such as metabolism, growth, survival, and genomic stability and has been found aberrant in several malignancies, including BC (Mishra et al., 2021). As a result, inhibitors targeting PI3K/AKT/mTOR signaling are studied extensively (Ellis and Ma, 2019; Mishra et al., 2021). Previously, studies have established that TNBC cells show resistance to GDC-0941, a pan-PI3K inhibitor (Tzeng et al., 2015). Given the lack of targeted medicines for TNBC, modulating current therapy regimens appear to be a potential strategy for developing effective therapies (Ellis and Ma, 2019; Elwakeel et al., 2019; Mehraj et al., 2021c).

Adapalene (ADA), a third-generation retinoid clinically used to treat acne vulgaris on a topical basis, was the second chemical we investigated (Rusu et al., 2020). Numerous research studies on the pharmacological features of ADA have proven its low toxicity and good stability compared to other retinoids. *In vitro* and *in vivo*, it inhibits the proliferation of Hela, CC-531, and HepG2 cells and various cancers (Ocker et al., 2003; Shi et al., 2015; Wang et al., 2019; Ghosalkar et al., 2018; Rusu et al., 2020; Mehraj et al., 2022a). Repurposing ADA for cancer therapy is a promising approach. Herein, we evaluated the therapeutic

potential of ADA in TNBC models for improving TNBC cell sensitivity to GDC-0941 (GDC). This is the first study to assess the pharmacodynamic interactions of GDC and ADA in TNBC *in vitro* models.

Materials and methods

Chemicals and reagents

Cayman Chemical (Ann Arbor, Michigan 48108, United States) supplied GDC-0941 (Cat. No. 1160) and adapalene (Cat. No. 13655) (Ann Arbor, Michigan 48108, United States). Dulbecco's modified Eagle medium (DMEM), Roswell Park Memorial Institute medium (RPMI-1640), and fetal bovine serum (FBS) were procured from Gibco, Thermo Fisher Scientific, United States. All the reagents used were of molecular biology or cell culture grade.

Cell culture

TNBC cell lines (MDA-MB-231 and MDA-MB-468) and ER + cell line MCF-7 were procured from the Cell Repository, National Centre for Cell Science (NCCS) Pune, India. Prof. Annapoorni Rangarajan (IISC, India) graciously provided the murine TNBC cell line 4T1. MDA-MB-231, MCF-7, and MDA-MB-468 cells were cultured in DMEM with 10% FBS and 1% penicillin–streptomycin. The murine TNBC cell line, 4T1, was cultured in RPMI-1640 with FBS (10%) and penicillin–streptomycin (1%). The BC cell lines were maintained at 37°C in a humidified CO_2 incubator (5%).

Single-drug cytotoxicity assay

Cell viability assay was used to assess the potency of ADA and GDC and to generate a dose–response curve required for the Chou–Talalay model for designing binary drug combinations (Chou, 2006; Zhang et al., 2016). In 96-well plates, BC cells (MDA-MB-468, 4T1, MDA-MB-231, and MCF-7) were cultured at 3×10^3 cells/well. Seven distinct concentrations of GDC, ADA, or drug vehicle (DMSO), each with four replicates, were given the next day. After 72 h of incubation, the drug solutions were replaced with a fresh media containing 5 mg/ml MTT (Invitrogen), and the growth inhibition was evaluated using the following equation (Eq. 1):

$$\%\ \text{Inhibition} = \left[1 - \left(\frac{\text{OD treated Cells}}{\text{OD vehicle control Cells}}\right)\right] \times 100, \quad (1)$$

where "OD-treated cells" defines the mean absorbance of cells incubated with therapeutics, "OD vehicle control" implies the mean absorbance of cells treated with a complete cell culture medium containing 0.1% DMSO.

Constant ratio cytotoxicity test for binary drug combinations

The cytotoxicity assay of single drugs in BC models laid the groundwork for the combined evaluation of GDC and ADA. Six distinct equipotent GDC–ADA combinations were constructed using the IC_{50s} values of the two drugs and evaluated in four repetitions in different cell lines. As Chou and Talalay recommended, the equipotent constant ratio method was used for all combinations. In this method, the amount of each agent in the combination is the same (Chou, 2006; 2010). Following a 72-hr treatment period, the cytotoxic effects of drugs as individual agents or in combination were assessed. As indicated in Eq. 1, the percentage inhibition for each combination was calculated.

Adoption of the Chou–Talalay approach for calculating the combination index and DRI

The combination index (CI) value—a dimensionless variable used to identify and quantify pharmacological interaction—was generated for binary combinations using CompuSyn software application, implementing the combination index equation (Eq. 2). When the CI value equals one, an additive impact is obtained. Synergistic interaction is observed when CI < 1 and antagonistic interaction when CI > 1.

$$(\text{CI})^2 = \frac{(\text{D})_1}{(\text{Dy})_1} + \frac{(\text{D})_2}{(\text{Dy})_2} = \frac{(\text{D})_1}{(\text{Dm})_1\,[\text{fa}\,/\,(1-\text{fa})]^{1/\text{m1}}} + \frac{(\text{D})_2}{(\text{Dm}_2)\,[\text{fa}/\,(1-\text{fa})]^{1/\text{m2}}}, \quad (2)$$

where (Dx)1 is the concentration of drug 1 that alone reduces cell viability by x percent, (Dx)2 is the drug 2 concentration that alone reduces cell viability by x percent, and (D)1 and (D)2 are the concentrations of drug 1 (D1) and drug 2 (D2) taken together that reduce cell viability by x percent. The values of (Dx)1 and (Dx)2 can be easily obtained by rearrangement of the median-effect equation (Sung et al., 2021) as follow.

$$D = Dm\left[\frac{fa}{1-fa}\right]^{1/m}.$$

The dimensionless function, dose reduction index or DRI, evaluates and indicates the magnitude, by which the concentration of the individual agent in a drug combination may be lowered compared to the doses of

each drug alone at a given fractional inhibition. It was generated automatically by the CompuSyn program for experimental drug combinations based on the DRI equations (Chou, 2006) as follows:

$$(DRI)_1 = \frac{(Dx)_1}{D1}, (DRI)_2 = \frac{(Dx)_2}{D2}, (DRI)_3 = \frac{(Dx)_3}{D3} \ldots \text{etc.}$$

DRI greater than one implies a desirable dosage decrease, DRI less than one suggests a detrimental dose reduction, and DRI equal to one indicates zero dose reduction (Chou, 2006).

Proliferation assay

After evaluating pharmacodynamic interactions, we examined the effect of the synergistic drug combination of GDC and ADA on cell proliferation time-dependently. In a 96-well plate, the cells were seeded (3×10^3 cells/well) and treated with ADA or GDC alone or in combination at concentrations below the IC_{50} values. After 24–72 h of incubation, according to the manufacturer's instructions, the proliferation of cells was determined using the Vybrant Proliferation Kit (Thermo Fisher Scientific, United States). GraphPad Prism 8.4.3 and a two-way ANOVA were employed for statistical analysis, followed by a Tukey test for multiple comparisons.

Colony formation assay

To assess the impact of ADA, GDC, and their combined effect on the colony formation of cells, cells were seeded in six-well plates at a density of 1,000–1,500 cells per well (Elbaz et al., 2015). After 48 h, the media was replaced with a fresh medium, supplemented with therapeutics. The assay was performed for 14–18 days. The medium containing therapeutics was replenished every 3 days, and colonies were observed in the wells using an inverted microscope. Once substantial colonies were formed, they were fixed with 3.7 percent paraformaldehyde (in PBS) and stained with crystal violet (0.05%). The plates were photographed, and the colonies were counted using the ImageJ program. Each cell type and treatment combination was subjected to the experiment thrice.

Wound healing assay

We utilized the Wound Healing Assay Kit (Cell Biolabs, Inc. United States) to investigate the impact of GDC and ADA and their combination on the migration of the highly invasive TNBC cell lines MDA-MB-231 and 4T1. On a 24-well plate, cells were seeded at 70% confluency and allowed to attach overnight with implanted scratch inserts. After 24 h, the scratch inserts were gently removed, and the cells were rinsed with PBS. Fresh media with therapeutics was added, and cell migration was assessed after 48 h of treatment. The cells were fixed in 3.7% paraformaldehyde (in PBS) and stained with Giemsa stain (in PBS). The cells were photographed, and the migration of cells into the wound region was analyzed and quantified using ImageJ software (Pijuan et al., 2019).

Mammosphere formation assay

MDA-MB-231 cells (1×10^4) were seeded as a single-cell suspension in 2-ml DMEM/F12 (Gibco, 11320033), supplemented with 1x B27 supplement (Invitrogen, 17504044) and SingleQuot™ (Lonza, CC-4136) into each well of ultralow attachment 6-well plates (Corning, 3471) (Klopp et al., 2010). The next day, the cells were treated with therapeutics as single agents or in combination, and the cells were cultured for 5–10 days later with media added every 3 days. Spheres were imaged under an inverted phase-contrast microscope (Nikon).

Reactive oxygen species measurement assay

MDA-MB-231 cells were grown in 24-well culture plates and treated with ADA, GDC, or both for 24 h. Next, the cells were stained with 10-μM 2′,7′-dichlorofluorescin diacetate (DCFDA) (Sigma-Aldrich) for 30 min in the dark, and fluorescence intensity was measured using a fluorometer.

Mitochondrial membrane potential analysis

Rhodamine 123 (Rh 123) staining was used to assess changes in mitochondrial membrane potential. The transition of mitochondria from a polarized to a depolarized state during the induction of apoptosis results in leakage of the dye, consequently resulting in a decrease in Rh 123 fluorescence intensity. The cells were grown in 24-well plates and treated with GDC, ADA, or both for 24 h. The cells were collected and incubated with 10-μM Rh 123 for 15 min at 37°C in the dark. Next, the cells were resuspended in PBS and analyzed immediately using an Agilent fluorescence spectrophotometer.

Annexin V assay

To investigate the mechanism behind the antitumor activity of ADA, GDC, and their combination, we utilized a

BD Biosciences Annexin V apoptosis detection kit. MDA-MB-231 was treated with GDC, ADA, or both for 24 and 48 h. All the cells were collected, including free-floating and adherent cells, and stained with the fluorescent dyes FITC-Annexin V and 7-AAD as recommended by the manufacturer. Flow cytometry was performed at the Department of Biotechnology, National Institute of Technology, Rourkela, Odisha, India, on a BD Accuri™ C6 flow cytometer (Mehraj et al., 2022b).

Molecular docking

To further investigate the molecular target of ADA in breast tumor cells, we utilized the molecular docking technique to validate the targets. Previous studies have demonstrated that ADA selectively targets CDK2 in cancer cells. As CDK2 is highly upregulated in BC patients, targeting CDK2 in combination with conventional therapy is a promising approach. Autodock v 4.2.6 was used to perform docking investigations of ADA and CDK2. The predetermined co-crystallized X-ray structure of CDK2 (5NEV) from the RCSB PDB was used to calculate the binding cavity of proteins. The co-crystallized ligand was used to compute the residue locations within the 4-Å radius. As part of the cavity selection process, chimera (https://www.cgl.ucsf.edu/chimera/) was used to remove co-crystallized ligands, and then the energy was minimized using the steepest descent and conjugate gradient algorithms. Both receptor and target compound were then saved in pdbqt format after combining non-polar hydrogens. Molecular docking was performed within a grid box dimension 14 × 14 × 13 Å. It was necessary to design grid boxes with particular dimensions and 0.3 Å spacing. Docking experiments of the protein–ligand complex were carried out following the Lamarckian genetic algorithm (LGA). There were three replicates of molecular docking investigations, each of which included 50 solutions, a population size of 500, 2,500,000 evaluations, a maximum generational number of 27, and all other parameters were left at their default values. Once the docking was complete, the RMSD clustering maps were generated by re-clustering with the clustering tolerances of 0.25, 0.50, and 1 to find the best cluster with the lowest energy score and the most populations.

Molecular dynamics simulation

The Desmond 2020.1 from Schrödinger, LLC was used to run MD simulations on dock complexes for CDK2 with ADA. SPC water molecules and the OPLS-2005 force field were utilized in this system (Jorgensen et al., 1983) in a period boundary salvation box of 10 × 10 × 10 Å dimensions. Na^+ ions were supplied to the system to neutralize the charge, and 0.15 M of NaCl solution was added to replicate the physiological environment. When retraining with the complex CDK2-ADA, the system was first equilibrated using an NVT ensemble for 100 ns. After the preceding phase, a 12-ns NPT ensemble run was used to perform a quick equilibration and reduction. The NPT ensemble was set up using the Nose–Hoover chain coupling approach (Li et al., 2003) and run at 27°C for 1.0 ps under a pressure of 1 bar throughout the study. A time step of 2 fs was employed in this experiment. With a relaxation duration of 2 ps, the Martyna–Tuckerman–Klein barostat method was utilized for pressure control. Ewald's particle mesh approach was used to calculate long-range electrostatic interactions; the radius for coulomb interactions was fixed at 9 nm. The bonded forces were calculated using the RESPA integrator with a time step of 2 fs for each trajectory. Calculations were made to track the stability of MD simulations using parameters such as the root mean square deviation (RMSD), gyroradius, root mean square fluctuation (RMSF), number of hydrogen atoms (H-bonds), and solvent accessible surface area (SASA).

Western blotting

Cells were grown in 6-cm dishes and treated with ADA for 24 h. After the drug treatment, the cells were lysed with lysis buffer NP40 (Invitrogen, Thermo Fisher Scientific), supplemented with protease and phosphatase inhibitors. Next, protein concentrations were determined using the BCA assay kit (Pierce™ BCA Protein Assay Kit, Cat No. 23227, Thermo Scientific). Equal amounts of protein were separated by electrophoresis on SDS-polyacrylamide gels and electroblotted onto polyvinylidene difluoride membranes. BSA (5%) was used to block non-specific binding for 1 h at room temperature. Protein bands were probed using specific primary antibodies, viz., CDK2 (78B2) rabbit mAb (CST, Cat No. 2546, dilution-1:1000) and horseradish peroxidase-conjugated secondary antibodies and visualized using an ECL kit (Bio-Rad, Hercules, CA). ImageJ software analyzed the intensity of immunoreactive protein bands and normalized them with GAPDH (CST, Cat No 2118, dilution-1:1000) as the loading control.

Cell cycle analysis

MDA-MB-231 cells were seeded in 12-well plates at 50% confluency and allowed to adhere overnight, followed by serum starvation for cell cycle synchronization. Next, the cells were treated for 24 and 48 h with ADA, GDC, and a combination of ADA and GDC. After treatment, the cells were trypsinized and fixed in 75% ethanol. After washing, the cells were stained with a

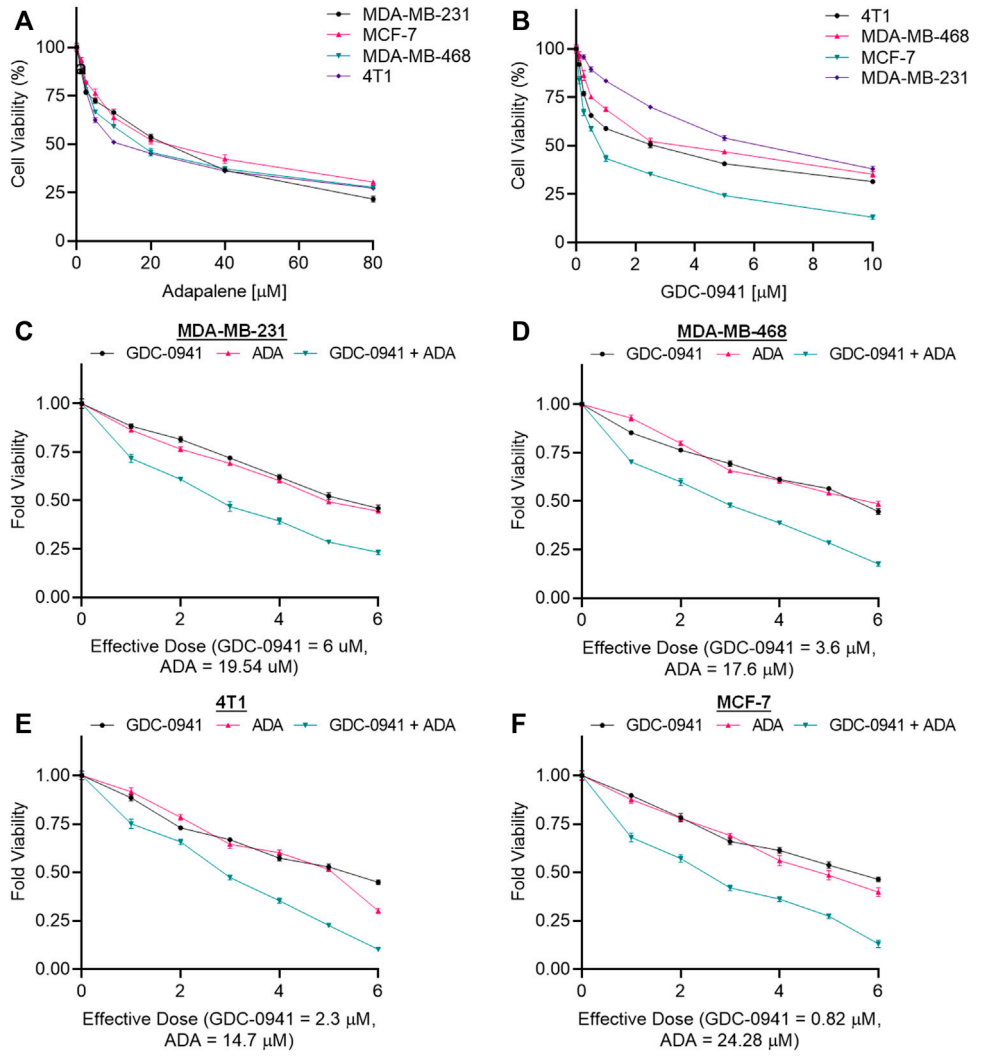

FIGURE 1
Adapalene and GDC reduce TNBC cell growth *in vitro*. Single-drug cytotoxicity assays of **(A)**. adapalene and **(B)** GDC-0941 in TNBC cell lines and MCF-7 cells. Both ADA and GDC inhibited tumor growth in a dose-dependent manner. The IC_{50} values were calculated using GrpahPad Prism V8.4.3. Combination treatment shows an enhanced reduction in cell growth in **(C)**. MDA-MB-231 **(D)**. MDA-MB-468 **(E)**. 4T1 and **(F)** MCF-7 cells. Enhanced reduction in cell viability was observed upon combination treatment with ADA and GDC, indicating positive pharmacodynamic interactions.

solution containing PI (0.5 mg/ml) and RNase A (10 mg/ml). The cells were filtered prior to flow cytometry, using a 70-m cell strainer. Flow cytometry was performed at the NIT Rourkela, India (Mehraj et al., 2022b).

Statistics

IC_{50s} values were calculated using non-linear regression analysis in GraphPad Prism. The statistical significance was analyzed using the one-way or two-way ANOVA in GraphPad Prism V 8.43, followed by Tukey multiple comparisons test. $p < 0.05$ was considered significant.

Results

Cytotoxicity assay for each single drug

The cell viability assay using MTT reagent was carried out to evaluate the cytotoxicity of GDC and ADA alone against BC cell lines, and GraphPad Prism 8 was used to generate dose–effect curves and obtain IC_{50} values for single drugs (Figures 1A,B). GDC and ADA were both cytotoxic to all breast cancer cell lines dose-dependently. The IC_{50} values of GDC in MDA-MB-231, MCF-7, MDA-MB-468, and 4T1 were 6.0, 0.82, 3.6, and 2.3 μM, respectively. GDC-0941 demonstrated high cytotoxicity in ER + MCF-7 cells, while

TABLE 1 Experimental design and data summary of the dose–effect curve and Chou–Talalay parameters of GDC-0941 and adapalene drug combinations against breast cancer cell lines after 72 h treatment period.

Cell line	GDC-0941 (G) (μM)	Adapalene (A) (μM)	Fraction affected (Fa)	Parameters					
				m	Dm	r	CI	DRI	
MDA-MB-231	0.1 * IC_{50}	0.1 * IC_{50}	0.28	0.83	9.4	0.98	0.53	G = 4.15	A = 3.42
	0.25 * IC_{50}	0.25 * IC_{50}	0.39				0.74	G = 2.90	A = 2.50
	0.5 * IC_{50}	0.5 * IC_{50}	0.53				0.75	G = 2.80	A = 2.54
	0.75 * IC_{50}	0.75 * IC_{50}	0.60				0.77	G = 2.66	A = 2.49
	IC_{50} (6)	**IC_{50} (19.5)**	0.71				0.57	G = 3.49	A = 3.42
	1.25 * IC_{50}	1.25 * IC_{50}	0.76				0.51	G = 3.85	A = 3.87
MDA-MB-468	0.1 * IC_{50}	0.1 * IC_{50}	0.29	0.88	7.2	0.95	0.46	G = 3.87	A = 4.77
	0.25 * IC_{50}	0.25 * IC_{50}	0.40				0.67	G = 2.91	A = 2.99
	0.5 * IC_{50}	0.5 * IC_{50}	0.52				0.76	G = 2.86	A = 2.41
	0.75 * IC_{50}	0.75 * IC_{50}	0.61				0.73	G = 3.21	A = 2.33
	IC_{50} (3.6)	**IC_{50} (17.6)**	0.71				0.58	G = 4.56	A = 2.75
	1.25 * IC_{50}	1.25 * IC_{50}	0.82				0.35	G = 8.75	A = 4.10
4T1	0.1 * IC_{50}	0.1 * IC_{50}	0.24	1.22	6.3	0.98	0.95	G = 1.86	A = 2.39
	0.25 * IC_{50}	0.25 * IC_{50}	0.34				0.91	G = 2.16	A = 2.22
	0.5 * IC_{50}	0.5 * IC_{50}	0.52				0.89	G = 2.38	A = 2.08
	0.75 * IC_{50}	0.75 * IC_{50}	0.64				0.79	G = 2.89	A = 2.23
	IC_{50} (2.3)	**IC_{50} (14.7)**	0.77				0.54	G = 4.63	A = 3.06
	1.25 * IC_{50}	1.25 * IC_{50}	0.89				0.36	G = 7.65	A = 4.35
MCF-7	0.1 * IC_{50}	0.1 * IC_{50}	0.31	0.82	7.58	0.98	0.45	G = 4.77	A = 4.13
	0.25 * IC_{50}	0.25 * IC_{50}	0.42				0.66	G = 3.27	A = 2.77
	0.5 * IC_{50}	0.5 * IC_{50}	0.57				0.67	G = 3.26	A = 2.69
	0.75 * IC_{50}	0.75 * IC_{50}	0.63				0.77	G = 2.88	A = 2.35
	IC_{50} (0.82)	**IC_{50} (24.2)**	0.72				0.65	G = 3.42	A = 2.74
	1.25 * IC_{50}	1.25 * IC_{50}	0.86				0.49	G = 4.57	A = 3.59

m, Median; Dm, IC50; r, linear correlation coefficient CI, Combinational Index.

TNBC cells showed resistance to GDC, with MDA-MB-231 showing the highest resistance. ADA showed an IC_{50} of 17.57, 19.54, 24.28, and 14.7 μM in MDA-MB-468, MDA-MB-231, MCF-7, and 4T1, respectively. ADA demonstrated high cytotoxicity in murine TNBC cells (4T1). The ER + cell line was responsive to ADA, while TNBC showed high sensitivity toward ADA.

Cytotoxicity assay of binary drug combination

The conditions of the Chou–Talalay method were met by the results of the single-drug cytotoxicity experiment, so the *in vitro* pharmacodynamic drug interaction study could begin. We analyzed a constant ratio combination design to examine all potential binary drug combinations. After 72 h of treatment, cell viability was evaluated Figures 1C–F. The combination of GDC and ADA showed an enhanced reduction in cell viability of BC cells at very low doses, demonstrating positive drug–drug interactions of GDC and ADA in BC cell lines. CompuSyn software was further utilized to calculate the CI, DRI values, and dose–inhibition curve parameters (Table 1). For MCF-7, MDA-MB-468, and MDA-MB-231, a flat sigmoidal (m < 1) curve was observed with an r-value (linear correlation coefficient) of approximately 0.95. 4T1 cells had a sigmoidal curve (m > 1) with approximately 0.95 for *r*. Also, the CompuSyn-calculated CI values could achieve synergistic interactions as demonstrated with the CI less than one at precise combinations (Table 1; Figure 2A). The median-effect blots of all tested drug combinations are shown in Figure 2C.

CompuSyn software's computer simulation

Utilizing the median effect and the combination index equations and the automation capabilities of the CompuSyn program, an algorithm was developed to simulate the computed CI and DRI values at various fraction affected (Fa) levels other than actual dosage. The simulated CI at different Fa levels was significantly synergistic, further validating *in vitro* results. The program generated the simulated Fa-Log CI plot, Fa-DRI plot, and isobolograms for each drug combination (Supplementary Figures S1–S4). The simulated CI and DRI values at 50, 75, 90, and 95% fraction affected are shown in Table 2. Apart from that, polygonograms of drug combinations at 50% Fa levels were designed to provide a visual comparison of the kind and magnitude of drug interactions (Figure 2B). The continuous line represents synergistic interaction, whereas the dashed line represents antagonistic interaction. The width of the

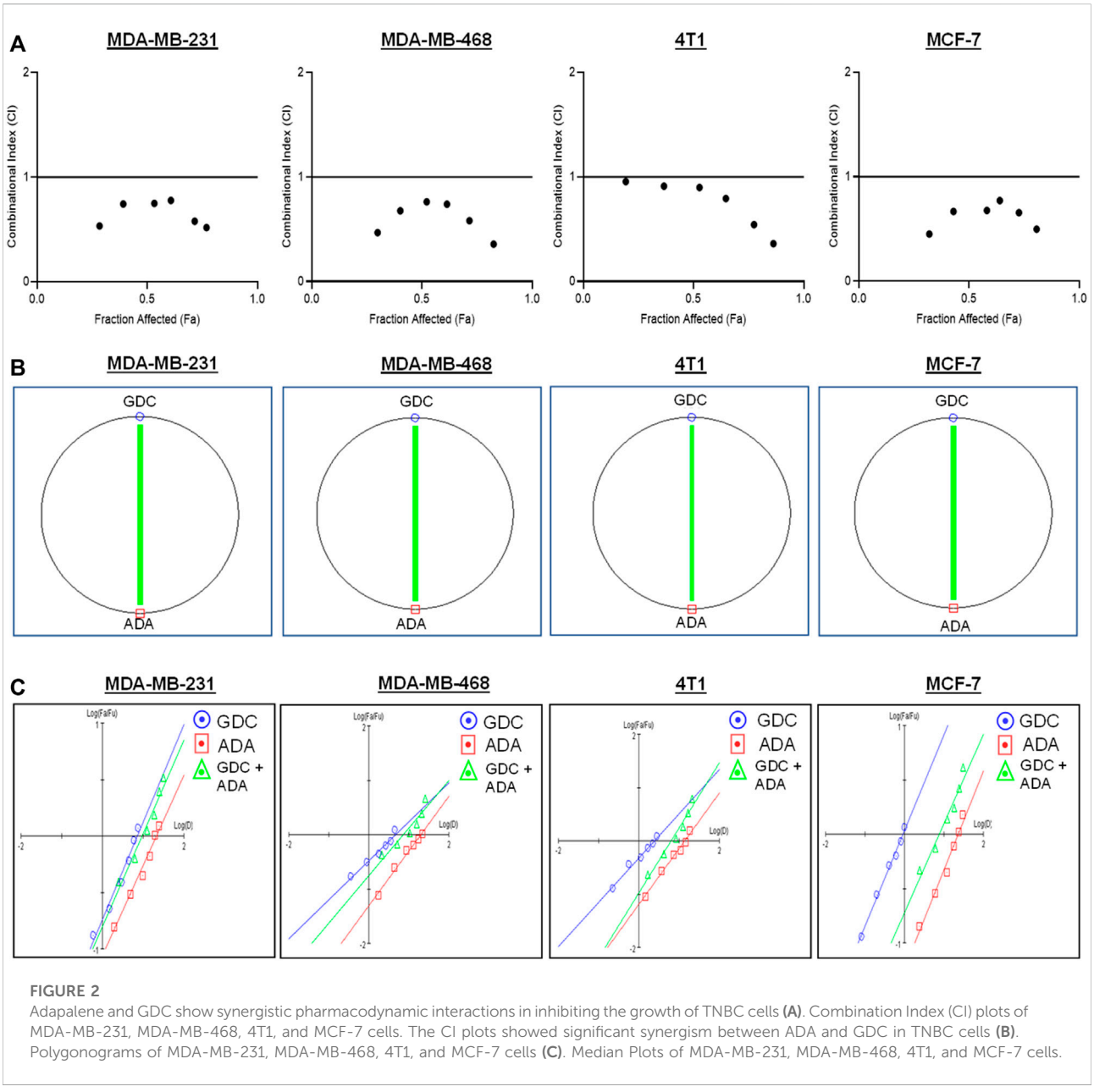

FIGURE 2
Adapalene and GDC show synergistic pharmacodynamic interactions in inhibiting the growth of TNBC cells **(A)**. Combination Index (CI) plots of MDA-MB-231, MDA-MB-468, 4T1, and MCF-7 cells. The CI plots showed significant synergism between ADA and GDC in TNBC cells **(B)**. Polygonograms of MDA-MB-231, MDA-MB-468, 4T1, and MCF-7 cells **(C)**. Median Plots of MDA-MB-231, MDA-MB-468, 4T1, and MCF-7 cells.

line indicates the level of synergy or competition. Based on the simulated CI and DRI, it was confirmed that all tested combinations demonstrated synergistic interactions of various inhibitory magnitudes, demonstrating that ADA and GDC interact synergistically.

Adapalene enhances sensitivity to GDC-0941 in triple-negative breast cancer cells

We further evaluated the synergetic drug combination of GDC and ADA in a time-dependent manner. We proceeded with a single synergistic drug combination below individual IC_{50} value among several drug combinations designed earlier. The cell viability was analyzed at 24, 48, and 72 h using the Vybrant cell proliferation kit (Invitrogen, Thermo Fisher, United States), following the manufacturer's protocol. Combinatorial treatment significantly reduced cell viability compared to single-agent treatment (Figure 3). The results demonstrate that GDC and ADA in combination enhance the antiproliferative effect of each other synergistically. Moreover, the sensitivity of TNBC cells toward GDC significantly increased upon co-treatment with ADA. The trend was seen in all three time periods.

TABLE 2 Summary of CompuSyn simulated CI and DRI values for GDC-0941 and adapalene combination in breast cancer cell lines at 50, 75, 90, and 95% growth inhibition.

Cell line	Drug combination GDC (G) + ADA (A)	CI values at inhibition of				DRI values at inhibition of			
		50%	75%	90%	95%	50%	75%	90%	95%
MDA-MB-231	G + A	0.63	0.64	0.64	0.65	G = 2.20 A = 7.18	G = 8.25 A = 26.89	G = 30.92 A = 100.71	G = 75.91 A = 247.21
MDA-MB-468	G + A	0.57	0.56	0.58	0.61	G = 1.23 A = 6.01	G = 4.31 A = 21.07	G = 15.09 A = 73.78	G = 35.39 A = 173.02
4T1	G + A	0.75	0.57	0.44	0.37	G = 0.85 A = 5.49	G = 2.10 A = 13.46	G = 5.17 A = 33.05	G = 9.52 A = 60.87
MCF-7	G + A	0.59	0.66	0.73	0.79	G = 0.24 A = 7.34	G = 0.94 A = 27.91	G = 3.58 A = 106.14	G = 8.89 A = 263.29

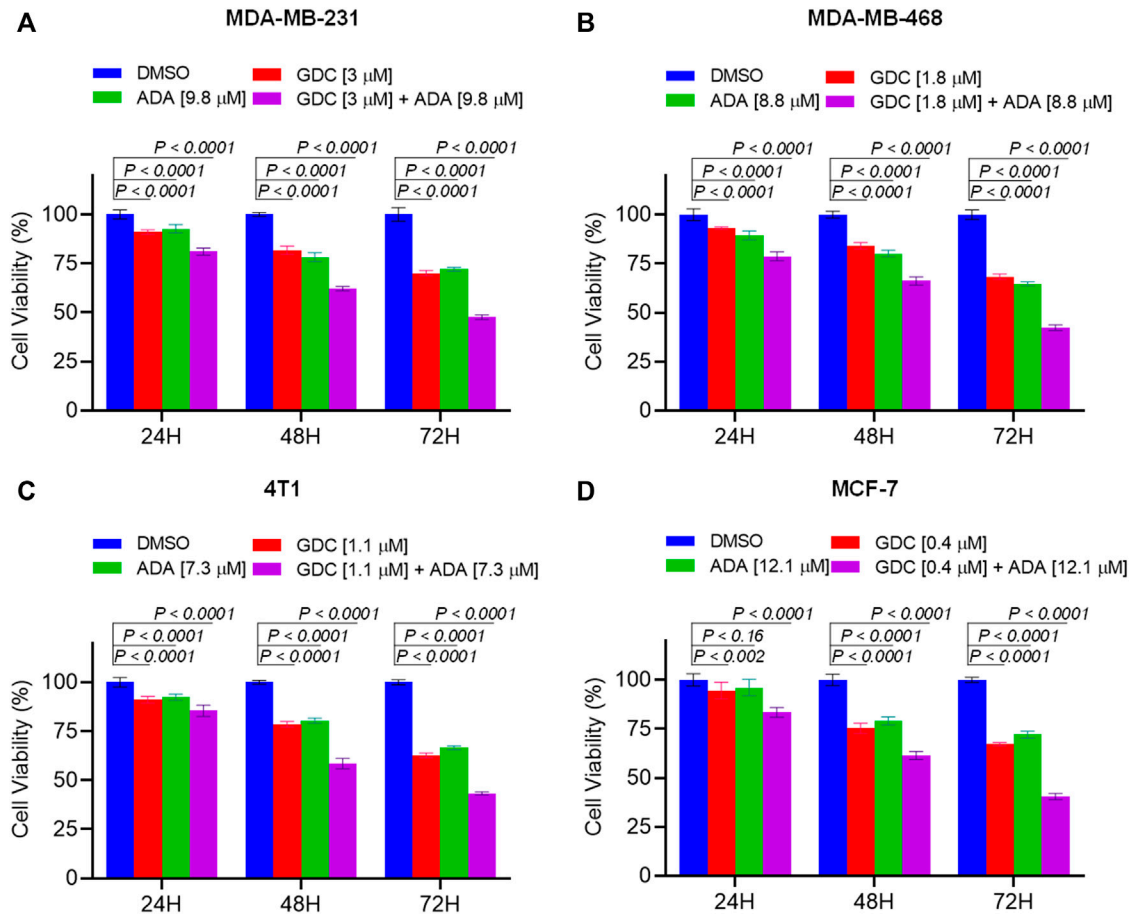

FIGURE 3
Combination of GDC-0941 and adapalene reduces tumor cell proliferation. The combination of GDC and ADA inhibited proliferation of **(A)**. MDA-MB-231 **(B)**. MDA-MB-468 **(C)**. 4T1 **(D)**. MCF-7 in a synergistic manner. Data are mean ± SD. *p*-values were determined by two-way ANOVA followed by Tukey's multiple comparisons test. Significant reduction in cell viability was observed when treated in a time-dependent manner with combined treatment of GDC and ADA showing a maximal effect.

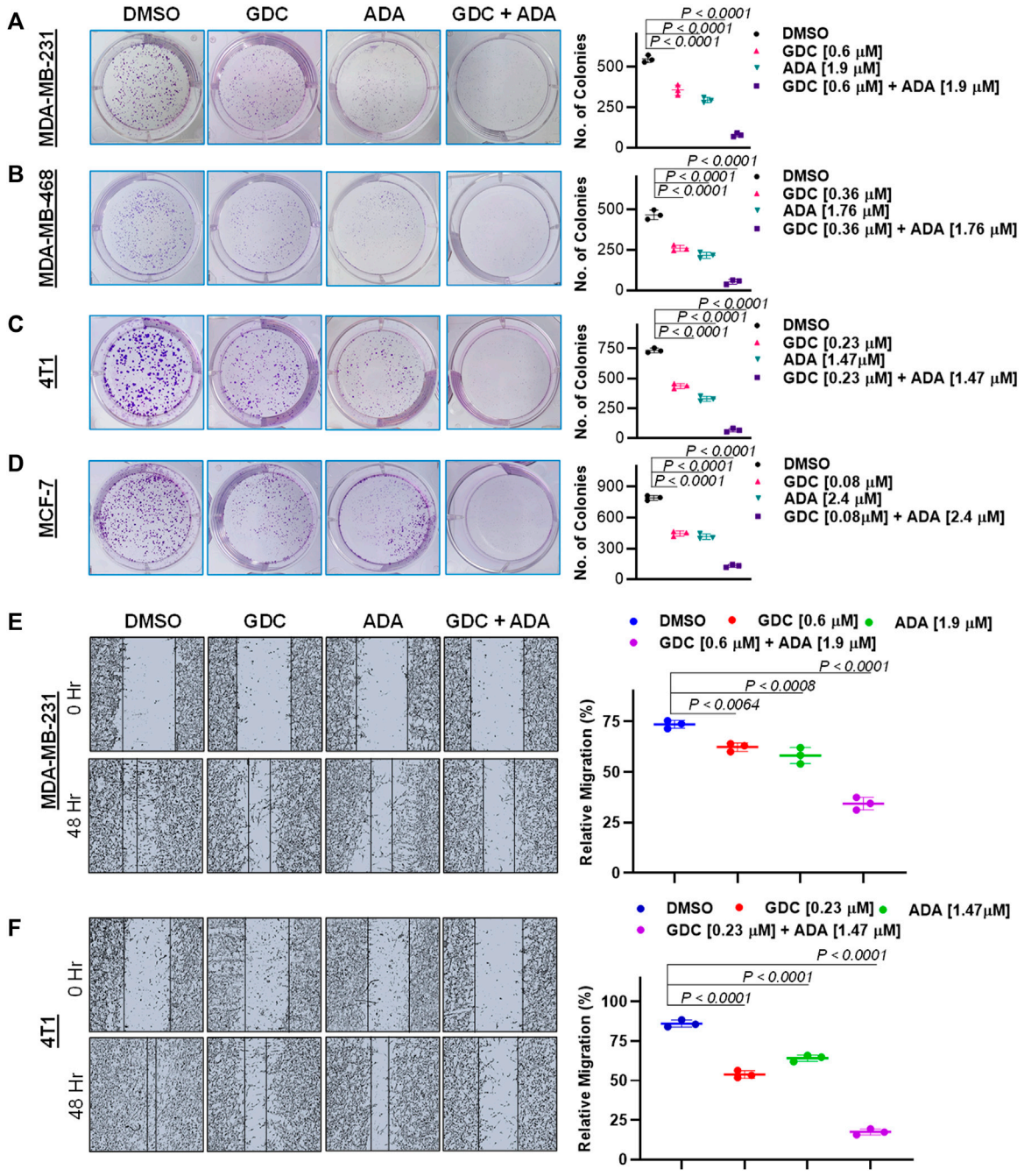

FIGURE 4
Combination of GDC-0941 and adapalene reduces colony formation and migration potential of TNBC cells. Representative images and quantification of colony formation assay data of **(A)**. MDA-MB-231, **(B)**. MDA-MB-468, **(C)**. 4T1 and, **(D)**. MCF-7 cells are treated with drug vehicle (DMSO), GDC, ADA, or a combination of GDC & ADA. The right panels show the quantification of colonies formed under each treatment condition described in the left panels. Data are mean ± SD. P values were determined by one-way ANOVA followed by Tukey's multiple comparisons test. Representative images and quantification of migration assay data of **(E)**. MDA-MB-231, **(F)**. 4T1. The right panels show the relative migration under control, single treatment and combination of GDC and ADA described in the left panels. Data are mean ± SD. *p*-values were determined by one-way ANOVA followed by Tukey's multiple comparisons test. Data are representative of at least three independent experiments.

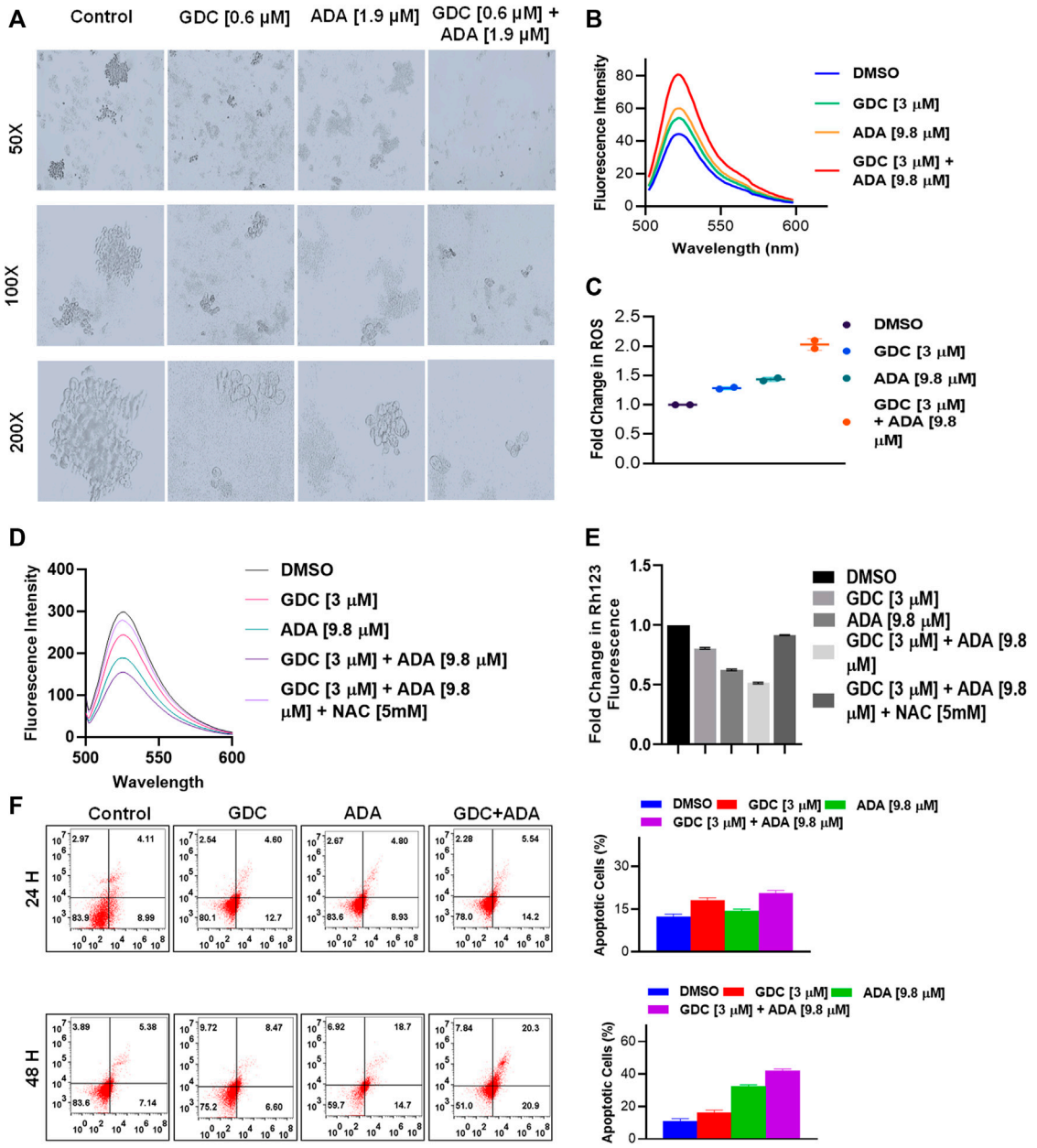

FIGURE 5
GDC-0941 and adapalene affect the anchorage-independent growth of MDA-MB-231 cells and enhance apoptosis. **(A)**. Representative images of the spheroid assay. Treatment with the combination of GDC and ADA significantly reduced the growth of TNBC cells in ultra-low attachment plates. **(B)**. Fluorescence intensity and **(C)**. fold change in ROS levels in MDA-MB-231 cells treated with ADA (9.8 μM) and GDC (3 μM) alone or in combination for 24 hrs. **(D)**. fluorescence intensity and **(E)**. fold change in Rh123 staining levels in MDA-MB-231 cells treated with ADA or GDC alone or in combination both showing decrease in mitochondrial membrane potential upon treatment. **(F)**. Annexin V & &-AAD staining showed increased apoptotic cells in plates treated with the combination of GDC and ADA after 24 h or 48 hr periods.

Combination of GDC-0941 and adapalene reduces colony formation and migration of triple-negative breast cancer cells

Experiments with colony formation in BC cell lines were utilized to confirm and assess the synergistic interactions of ADA and GDC. While treatment with GDC and ADA alone decreased colony formation, treatment with the combination of GDC and ADA resulted in an enhanced decrease in colony formation compared to individual drug treatments. Also, the number of colonies in each treated cell line was almost equivalent when treated alone; however, the number of colonies was significantly

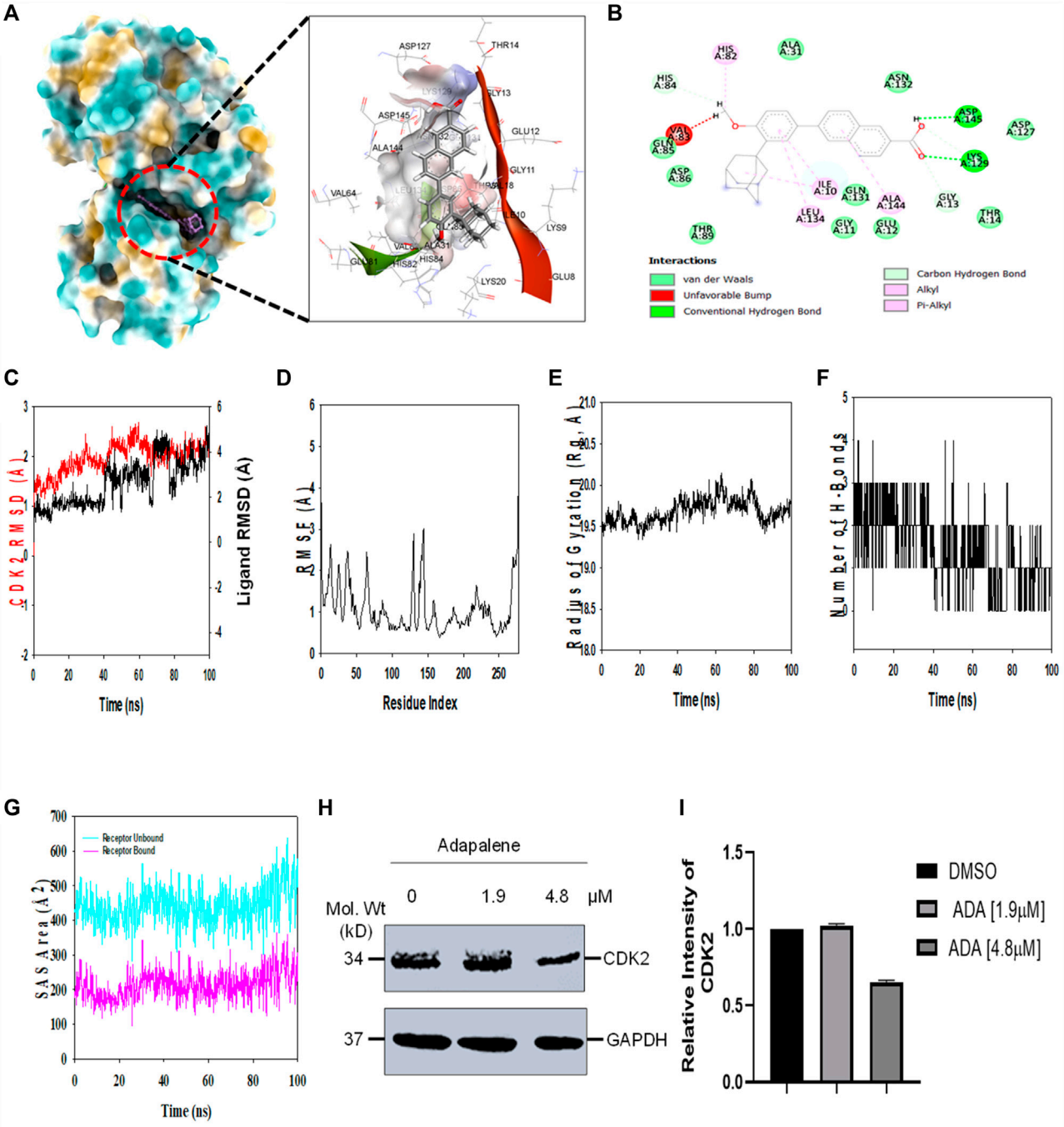

FIGURE 6
ADA shows high binding affinity and stability with CDK2 **(A)**. Analysis of the binding pose of ADA at the binding cavity of CDK2 on the left panel and 3D cavity interaction of residues with ADA **(B)**. 2D interaction of ADA showing various interactions at the binding cavity of CDK2 **(C)**. RMSD plot displaying the molecular vibration of Cα backbone of CDK2 (red) and ADA (black) **(D)**. RMSF plot showing the fluctuations of respective amino acids throughout the simulation time 100 ns for CDK2-ADA **(E)**. The radius of the gyration plot to deduce the compactness of CDK2 bound to ADA **(F)**. The number of hydrogen bonds formed between CDK2-ADA during the 100 ns simulation time scale **(G)**. Solvent accessible surface area (SAS Area) displays the unbound area at the binding pocket (cyan) and bound ADA with CDK2 **(H)**. Immunoblot of CDK2 upon treatment with ADA. ADA reduced CDK2 in a dose-dependent manner **(I)**. Relative intensity of CDK2 protein levels upon treatment with ADA.

reduced when treated in combination. The study demonstrated that ADA as a single agent reduces tumor cell growth, inhibiting the colony formation of breast tumor cells (Figures 4A–D).

To colonize distant organs, cancer cells must penetrate the ECM and undergo the multistep phenomena of metastasis (Neophytou et al., 2018). As a result, inhibiting cell migration may be vital for limiting metastasis. This investigation sought to examine the effect of the GDC–ADA combination on the motility of tumor cells. CytoSelect™ 24-Well Wound Healing Experiment Kit was used to perform the assay in 24-well plates. MDA-MB-231 and 4T1 cells were treated for 48 h with GDC and ADA alone or in combination, and cell movement was assessed using ImageJ software. ADA showed a high reduction in migration of MDA-MB-231 and 4T1 cells. The combination of GDC and ADA significantly reduced migration compared to control cells or cells treated with GDC or ADA alone (Figures 4E,F).

Also, GDC and ADA, in combination, significantly repressed the anchorage-independent growth of MDA-MB-231 cells (Figure 5A) and suppressed mammosphere formation. These results further support that GDC and ADA have significant tumor-reducing activity in TNBC.

Combined treatment with GDC-0941 and adapalene disrupts mitochondrial membrane potential and enhances reactive oxygen species production, triggering apoptosis of triple-negative breast cancer cells

Next, we set out to investigate the mechanisms underlying the anticancer activity of ADA and the synergistic effect of GDC and ADA. Therefore, we measured the intracellular ROS levels after ADA and GDC co-treatment and individual treatment. The results indicated that the combined treatment significantly increased ROS levels in MDA-MB-231. In addition, we found that the treatment with ADA and GDC alone induced ROS generation. However, ROS levels were higher in ADA treated, but the combined treatment resulted in a two-fold increase in ROS levels (Figures 5B,C). ROS generation is associated with mitochondrial membrane potential (MMP) disruption, a critical event in apoptosis initiation, which can be measured by Rh 123 staining. We found that the percentage of cells treated with ADA, GDC, or both showed low Rh 123 fluorescence intensities compared to untreated controls. Moreover, the membrane disruption decreased upon exposure to NAC for 2 h before co-treatment of GDC and ADA, further validating the involvement of ROS in the synergistic interaction of GDC–ADA. These results suggest that oxidative injury, resulting in disruption of mitochondrial membrane potential, may significantly enhance lethality induced by the combined treatment of MDA-MB-231 cells with ADA and GDC (Figures 5D,E).

Furthermore, we utilized Annexin V and 7-AAD staining to assess the apoptosis induction potential of ADA/GDC or a combination of both. MDA-MB-231 cells were treated for 24 and 48 h, followed by staining with Annexin V and 7-AAD. Flow cytometry analysis revealed that ADA induction tumor cell death *via* induction of apoptosis and apoptosis enhanced significantly upon combination treatment (Figure 5D). GDC also showed apoptosis, but apoptosis in combination treatment was highly significant compared to single-agent treatments.

Molecular docking showed high binding of adapalene with CDK2

Molecular docking studies were performed to decipher the binding aspects of CDK2 with ADA. The images of docked complexes, molecular surfaces, and 2D and 3D interactive plots for ADA with the CDK2 are shown in Figures 6A,B. Molecular docking studies revealed that ADA bound significantly with protein CDK2, with the lowest binding energy of −9 kcal/mol and an inhibitory concentration (Ki) of 21 μM. Also, ADA formed pi-alkyl interaction with Ile10, Leu134, and Ala144, conventional hydrogen bond with Lys19 and Asp145 residues as shown in Figure 6B. Other non-bonded interactions, such as van der Waals interactions involved with Gly11, Glu12, Thr14, Ala31, His84, Gln85, Asp86, Gln131, and Asn132, were also found between CDK2 and ADA. All the binding energy scores are calculated from the best cluster (95%), which falls within the lowest RMSD 0.25 Å. Therefore, from the docking studies, it can be suggested that ADA has a high affinity for CDK2 and was considered for further MD simulation studies.

Molecular dynamics and simulation

Molecular dynamics and simulation (MD) studies were carried out to determine the stability and convergence of CDK2 with ADA. Simulation of 100 ns displayed stable conformation while comparing the root mean square deviation (RMSD) values. The RMSD of the Cα-backbone of CDK2 bound to ADA exhibited a deviation of 0.5 Å (Figure 6C). Stable RMSD plots during simulation signify a good convergence and stable conformations (Hollingsworth and Dror, 2018). Therefore, it can be suggested that ADA bound to CDK2 is relatively stable in complex due to the higher affinity of the ligand. The plot for root mean square fluctuations (RMSF) displayed small spikes of fluctuation in CDK2 protein except at residues 135 and 146 might be due to the higher flexibility of the residues conformed to the loop region.

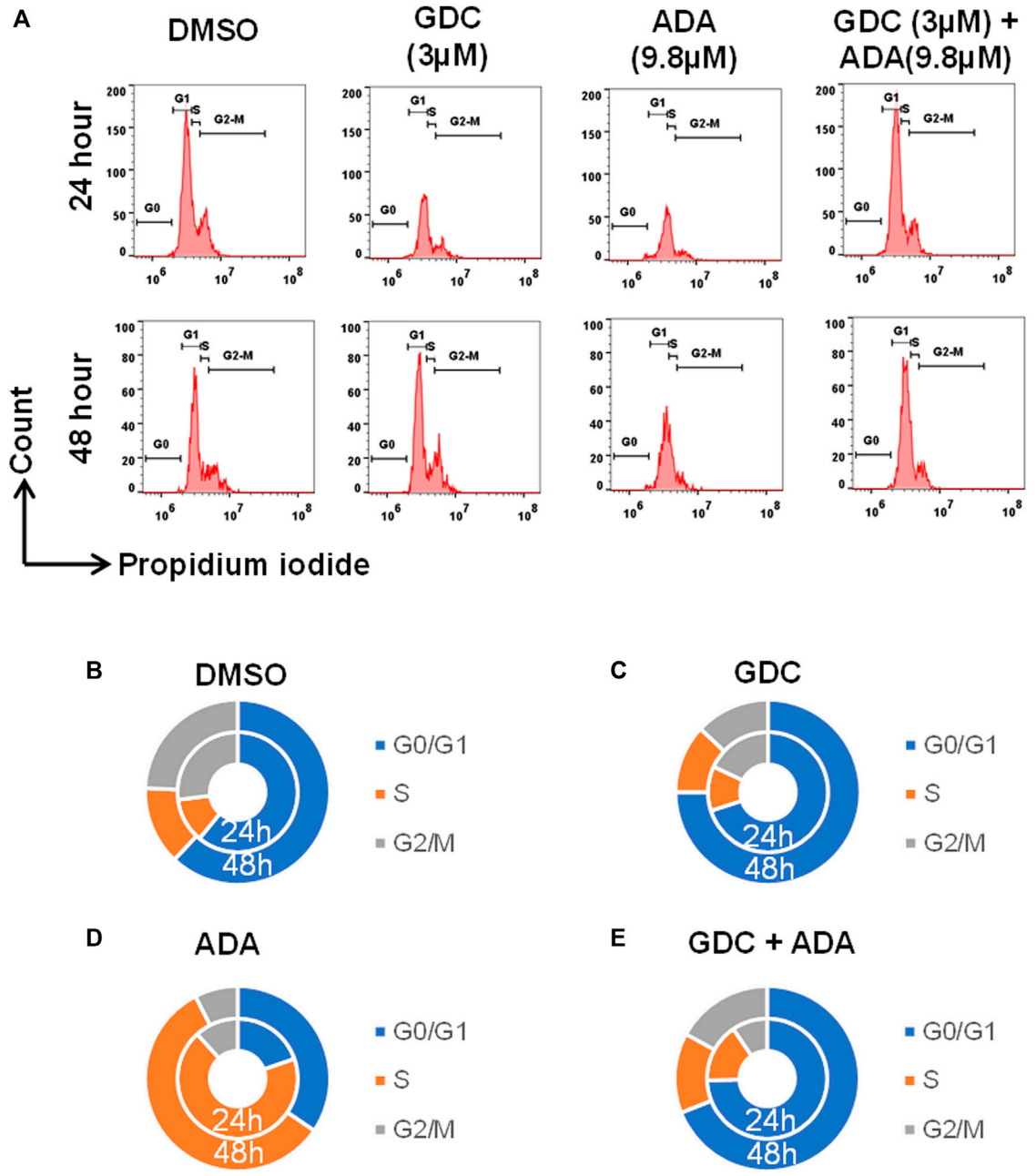

FIGURE 7
GDC-0941 and adapalene promoted cell cycle arrest of MDA-MB-231 cells **(A–E)** ADA upon treatment showed S-phase arrest of MDA-MB-231 cells, while GDC showed the arrest of MDA-MB-231 cells in the G2/M phase of the cell cycle. Upon combination treatment with GDC and ADA, the arrest of cells enhanced in the S-phase.

In contrast, the rest of the residues fluctuated less during the entire 100 ns simulation, and Figure 6D indicates the stable amino acid conformations during the simulation time. Moreover, all these RMSF values are in the acceptable region. Therefore, from the RMSF plot, it can be suggested that the structure of CDK2 is stable during simulation in ligand-bound conformation (Hollingsworth and Dror, 2018). The radius of gyration (Rg) measures the compactness of the protein. Here, in this study, CDK2 Cα-backbone bound to ADA displayed a stable radius of gyration (Rg) from 19.5 to 19.7 Å (Figure 6E). Significantly, stable gyration (Rg) indicates a highly compact protein orientation in the ligand-bound state (Mosquera-Yuqui

et al., 2020). The number of hydrogen bonds between protein and ligand suggests the significant interaction and stability of the complex, and we observed a high number of H-bonds between CDK2 with ADA throughout the simulation time of 100 ns (Figure 6F). Following Rg analysis, similar patterns were observed in a solvent accessible surface area (SASA) in both ligand-bound and ligand-unbound states. In the unbound state of ADA, CDK2 displayed high surface area accessible to solvent (Figure 6G). The SASA value lowered significantly in the bound state with CDK2 as compared to the unbound state. The overall study of Rg signifies that the binding of ADA to CDK2 compels the protein to become more compact and less flexible.

Adapalene inhibits CDK2 and promotes S-phase cell arrest

In addition, we evaluated the effect of ADA on CDK2 protein levels. It was found that ADA significantly reduced CDK2 protein levels dose-dependent. Moreover, reduced CDK2 protein levels confirm the *in silico* docking and molecular simulation results (Figures 6H,I).

We also evaluated the effect of ADA, GDC, and both on the cell cycle. The cell cycle analysis was performed, following the treatment for 24 and 48 h using flow cytometry. Flow cytometry results demonstrated that ADA induced S-phase cell cycle arrest in MDA-MB-231, while GDC promoted the arrest of MDA-MB-231 cells in the G1 phase. In combination, GDC and ADA enhanced the arrest of cells in the G1 phase (Figure 7). Flow cytometry results are in tandem with *in silico* and *in vitro* results, validating that ADA inhibits CDK2, thereby promoting the arrest of cells.

Discussion

BC is currently one of the most common malignancies and the leading cause of tumor-related mortality in women globally (Siegel et al., 2021; Sung et al., 2021). TNBC is one of the aggressive subtypes of breast cancer, and it has a more aggressive clinical course than the other types of breast cancer (Dai et al., 2016; Mehraj et al., 2022c). Since presently available endocrine and *HER2*-directed medications are inadequate in treating TNBC, chemotherapy has traditionally been the backbone of systemic treatment for the disease (Waks and Winer, 2019; Mehraj et al., 2022d). The PI3K inhibitor, GDC-0941 (Pictilisib), is an orally accessible compound that binds to and competes with the ATP-binding pocket in the PI3K signaling and blocks the signaling cascade (Yamamoto et al., 2017; Han et al., 2019). Patients with advanced NSCLC in Japan reported that it had a superior tolerance and safety profile (Yamamoto et al., 2017). GDC-0941 revealed modest antitumor efficacy in clinical studies, and a tolerable safety profile and combination with paclitaxel improved the antitumor response (Sarker et al., 2015; Schmid et al., 2016). While inhibiting PI3K provides significant therapeutic advantages, there has been some apprehension about the sometimes significant toxicity connected with its usage (Greenwell et al., 2017). As a result, there is an urgent need to investigate innovative therapeutics that will allow for a reduction in the dose of GDC-0941 while simultaneously increasing its antitumor efficacy.

Adapalene, a third-generation retinoid currently used to treat acne, binds to nuclear retinoic acid receptors and has been reported to possess potent antitumor activity (Rusu et al., 2020). ADA possesses high comedolytic, anti-inflammatory, antiproliferative, and immunomodulatory properties. Also, its safety profile is superior to other retinoids (Rusu et al., 2020). Several recent studies established the antitumor potential of ADA in solid malignancies, including HCC, colon cancer, melanoma, ovarian cancer, and prostate cancer (Shi et al., 2015; Ghosalkar et al., 2018; Li et al., 2019; Wang et al., 2019; Nong et al., 2022). Also, in our recent study, we demonstrated the antitumor potential of ADA in TNBC *in vitro* models. We reported that ADA promotes tumor cell apoptosis and acts synergistically with doxorubicin. Herein, we aimed to evaluate the therapeutic potential of ADA in combination with GDC-0941.

Our results demonstrate that ADA is an effective therapeutic agent combined with GDC in inhibiting proliferation, migration, and colonization capacity. We found that the combination of ADA and GDC resulted in a marked increase in cell death in TNBC cancer cells and reduced GDC resistance. ADA enhanced ROS generation and demonstrated a synergistic effect in ROS production and decreased MMP with GDC. Elucidation of the underlying mechanisms warrants further study.

Our findings demonstrate that both ADA alone and in combination with GDC exerts anticancer efficacy by inducing apoptosis in tumor cells. In addition, the synergistic combination of GDC and ADA resulted in considerable dosage reductions for both GDC and ADA, as shown in Tables 1, 2. As shown in Figure 2B, the combination of GDC and ADA showed a synergistic relationship, as depicted by the thickness of the line connecting polygonograms. In addition, it was observed that ADA alone or in combination with GDC inhibited TNBC cell colony formation and migration. Colony numbers and sizes decreased considerably when cells were treated with ADA and GDC in combination.

Cancer cells often produce and sustain larger reactive oxygen species (ROS) levels than normal cells. Increased ROS levels make cancer cells susceptible to ROS-generating agents (Trachootham et al., 2009; Gorrini et al., 2013). As a result, stimulating ROS is a possible therapeutic method for cancer. Numerous studies have shown that increasing ROS production in cancer cells inhibits development and induces apoptosis (Yang et al., 2017; Liu et al., 2018; Baptista Moreno Martin et al., 2020). We found that enhanced ROS levels accumulated upon combined treatment with ADA and GDC and promoted

tumor cell apoptosis. Also, in our previous study, we reported that ADA promoted Erk1/2 activation by ROS generation and apoptosis. Previously, Erk1/2 activation has been reported to promote therapeutic resistance, including GDC-0941, how hyperactivation of Erk1/2 by ROS generation prompts apoptotic role of Erk1/2. The previous reports and the present findings indicate that high ROS accumulation upon co-treatment with GDC and ADA reduced GDC resistance *via* modulation of the signaling cascades involved in GDC resistance in TNBC cells. Also, Annexin V/7-AAD labeling revealed that ADA causes apoptosis in MDA-MB-231 cells and that synergistic drug interactions occurred during apoptosis. Apoptosis increased from 24.2 to 40.3 percent in cells treated with the combination of GDC and ADA. These findings suggest that co-treatment with ADA and GDC increases BC cells sensitivity to GDC and that substantial tumor inhibition may be obtained with moderate dosages of both drugs, hence decreasing the risks associated with GDC-0941.

In addition, it was further found that ADA selectively binds CDK2 and induces S-phase cell cycle arrest. The results were validated both *in silico* and *in vitro*. CDK2 is upregulated in breast tumors, and its vital role in cell cycle regulation makes CDK2 an attractive therapeutic target (Sofi et al., 2022a; Mehraj et al., 2022e; Mehraj et al., 2022f). Together, these results demonstrate that ADA has high potential in reducing tumor growth and colonization of TNBC cells. A recent study demonstrated that ADA-mediated tumor growth suppression occurs due to DNA damage and apoptotic pathway activation (Nong et al., 2022). Also, Wang et al. (2019) demonstrated that ADA reduced the growth of ovarian cancer cells by inhibiting glutamic-oxaloacetic transaminase 1. ADA also effectively reduced the growth of colorectal carcinoma, melanoma cells, prostate cancer cells, and hepatoma cells (Ocker et al., 2004; Shi et al., 2015; Li et al., 2019; Nong et al., 2022). These previous studies and the present study's findings demonstrate that ADA is a promising therapeutic agent across a wide range of tumors with TNBC, prostate tumors, and melanoma cells more responsive toward ADA treatment.

In addition to its enhanced ability to inhibit proliferation and promote tumor cell apoptosis, ADA may offer numerous advantages over conventional retinoic acid derivatives *in vivo*, such as increased stability, more prolonged comedolytic action, enhanced anti-inflammatory activity, and a favorable safety profile (Ocker et al., 2003; Shi et al., 2015; Ghosalkar et al., 2018; Rusu et al., 2020; Sofi et al., 2022b).

In conclusion, our results indicate that the combination of ADA and GDC is effective against BC cells by augmenting the induction of apoptosis. Existing chemotherapy agents are associated with highly unpleasant side effects, but ADA has the potential to be an effective anticancer treatment with far reduced toxicity. Even though our results were verified *in vitro*, they paved the way for further exploration of the synergistic therapeutic combination of GDC and ADA *in vivo* and with other TNBC models and cancer hallmarks.

Data availability statement

The raw data supporting the conclusion of this article will be made available by the authors, without undue reservation.

Author contributions

MM designed and supervised the study. UM performed the experiments and wrote the manuscript. MM, MA, AA, NW, and AH performed the analysis and critically revised the manuscript. All authors read and approved the manuscript.

Funding

The study was funded by the Jammu Kashmir Science Technology & Innovation Council (JKST&IC), Govt of J&K vide grant No. JKST&IC/SRE/885-87 to MM.

Acknowledgments

UM is a senior research fellowship (SRF) recipient from UGC-CSIR, Governmentt of India. NW is the recipient of the Ramalinga Swami Fellowship from DBT Government of India. The authors are thankful to Prof. Rohan Dhiman and Ashish Kumar NIT Rourkela, for performing flow cytometry studies. MA would like to express his gratitude to University of Hafr Al Batin, Saudi Arabia for providing funding to this study.

Conflict of interest

The authors declare that the research was conducted in the absence of any commercial or financial relationships that could be construed as a potential conflict of interest.

Publisher's note

Supplementary material

The Supplementary Material for this article can be found online at: https://www.frontiersin.org/articles/10.3389/fphar.2022.958443/full#supplementary-material

References

Baptista Moreno Martin, A. C., Tomasin, R., Luna-Dulcey, L., Graminha, A. E., Araújo Naves, M., Teles, R. H. G., et al. (2020). [10]-Gingerol improves doxorubicin anticancer activity and decreases its side effects in triple negative breast cancer models. *Cell Oncol.* 43 (5), 915–929. doi:10.1007/s13402-020-00539-z

Chou, T-C. (2006). Theoretical basis, experimental design, and computerized simulation of synergism and antagonism in drug combination studies. *Pharmacol. Rev.* 58 (3), 621–681. doi:10.1124/pr.58.3.10

Chou, T. C. (2010). Drug combination studies and their synergy quantification using the Chou-Talalay method. *Cancer Res.* 70 (2), 440–446. doi:10.1158/0008-5472.CAN-09-1947

Dai, X., Xiang, L., Li, T., and Bai, Z. (2016). Cancer hallmarks, biomarkers and breast cancer molecular subtypes. *J. Cancer* 7 (10), 1281–1294. doi:10.7150/jca.13141

Elbaz, M., Nasser, M. W., Ravi, J., Wani, N. A., Ahirwar, D. K., Zhao, H., et al. (2015). Modulation of the tumor microenvironment and inhibition of EGF/EGFR pathway: novel anti-tumor mechanisms of Cannabidiol in breast cancer. *Mol. Oncol.* 9 (4), 906–919. doi:10.1016/j.molonc.2014.12.010

Ellis, H., and Ma, C. X. (2019). PI3K inhibitors in breast cancer therapy. *Curr. Oncol. Rep.* 21 (12), 11. doi:10.1007/s11912-019-0846-7

Elwakeel, A., Soudan, H., Eldoksh, A., Shalaby, M., Eldemellawy, M., Ghareeb, D., et al. (2019). Implementation of the Chou-Talalay method for studying the *in vitro* pharmacodynamic interactions of binary and ternary drug combinations on MDA-MB-231 triple negative breast cancer cells. *Synergy* 8, 100047. doi:10.1016/j.synres.2019.100047

Ghosalkar, J., Iyer, S., Malhotra, G., and Joshi, K. (2018). *In vitro* and *in vivo* anticancer potential of adapalene, a third-generation retinoid against bladder cancer. *Cancer Res.* 78, 2316. doi:10.1158/1538-7445.AM2018-2316

Gorrini, C., Harris, I. S., and Mak, T. W. (2013). Modulation of oxidative stress as an anticancer strategy. *Nat. Rev. Drug Discov.* 12 (12), 931–947. doi:10.1038/nrd4002

Greenwell, I. B., Ip, A., and Cohen, J. B. (2017). PI3K inhibitors: understanding toxicity mechanisms and management. *Oncology* 31 (11), 821–828.

Han, N., Jiang, Y., Gai, Y., Liu, Q., Yuan, L., Wang, Y., et al. (2019). 11C-Labeled pictilisib (GDC-0941) as a molecular tracer targeting phosphatidylinositol 3-kinase (PI3K) for breast cancer imaging. *Contrast Media Mol. Imaging* 2019, 1760184. doi:10.1155/2019/1760184

Hollingsworth, S. A., and Dror, R. O. (2018). Molecular dynamics simulation for all. *Neuron* 99 (6), 1129–1143. doi:10.1016/j.neuron.2018.08.011

Hon, J. D. C., Singh, B., Sahin, A., Du, G., Wang, J., Wang, V. Y., et al. (2016). Breast cancer molecular subtypes: from TNBC to QNBC. *Am. J. Cancer Res.* 6 (9), 1864–1872.

Jorgensen, W. L., Chandrasekhar, J., Madura, J. D., Impey, R. W., and Klein, M. L. (1983). Comparison of simple potential functions for simulating liquid water. *J. Chem. Phys.* 79 (2), 926–935. doi:10.1063/1.445869

Klopp, A. H., Lacerda, L., Gupta, A., Debeb, B. G., Solley, T., Li, L., et al. (2010). Mesenchymal stem cells promote mammosphere formation and decrease E-cadherin in normal and malignant breast cells. *PloS one* 5 (8), e12180. doi:10.1371/journal.pone.0012180

Lebert, J. M., Lester, R., Powell, E., Seal, M., and McCarthy, J. (2018). Advances in the systemic treatment of triple-negative breast cancer. *Curr. Oncol.* 25 (s1), S142–S150. doi:10.3747/co.25.3954

Li, J., Ngan, A. H. W., and Gumbsch, P. (2003). Atomistic modeling of mechanical behavior. *Acta Mater.* 51 (19), 5711–5742. doi:10.1016/j.actamat.2003.08.002

Li, H., Wang, C., Li, L., Bu, W., Zhang, M., Wei, J., et al. (2019). Adapalene suppressed the proliferation of melanoma cells by S-phase arrest and subsequent apoptosis via induction of DNA damage. *Eur. J. Pharmacol.* 851, 174–185. doi:10.1016/j.ejphar.2019.03.004

Liu, N., Wang, K. S., Qi, M., Zhou, Y. J., Zeng, G. Y., Tao, J., et al. (2018). Vitexin compound 1, a novel extraction from a Chinese herb, suppresses melanoma cell growth through DNA damage by increasing ROS levels. *J. Exp. Clin. Cancer Res.* 37 (1), 269. doi:10.1186/s13046-018-0897-x

Lu, D. Y., Lu, T. R., and Cao, S. (2013). Drug combinations in cancer treatment. *Clin. Exp. Pharmacol.* 3 (4), 134. doi:10.4172/2167-1052.1000e124

Mehraj, U., Ganai, R. A., Macha, M. A., Hamid, A., Zargar, M. A., Bhat, A. A., et al. (2021). The tumor microenvironment as driver of stemness and therapeutic resistance in breast cancer: new challenges and therapeutic opportunities. *Cell Oncol.* 44, 1209–1229. doi:10.1007/s13402-021-00634-9

Mehraj, U., Dar, A. H., Wani, N. A., and Mir, M. A. (2021). Tumor microenvironment promotes breast cancer chemoresistance. *Cancer Chemother. Pharmacol.* 87, 147–158. doi:10.1007/s00280-020-04222-w

Mehraj, U., Qayoom, H., and Mir, M. A. (2021). Prognostic significance and targeting tumor-associated macrophages in cancer: new insights and future perspectives. *Breast Cancer* 28, 539–555. doi:10.1007/s12282-021-01231-2

Mehraj, U., Alshehri, B., Khan, A. A., Bhat, A. A., Bagga, P., Wani, N. A., et al. (2022). Expression pattern and prognostic significance of chemokines in breast cancer: an integrated bioinformatics analysis. *Clin. Breast Cancer*. doi:10.1016/j.clbc.2022.04.008

Mehraj, U., Mir, I. A., Ul Hussain, M., Alkhanani, M., Wani, N. A., and Mir, M. A. (2022). Adapalene and doxorubicin synergistically promote apoptosis of TNBC Cells by hyperactivation of the ERK1/2 pathway through ROS induction. *Front. Oncol.* 12, 1–16. doi:10.3389/fonc.2022.938052

Mehraj, U., Mushtaq, U., Mir, M. A., Saleem, A., Macha, M. A., Lone, M. N., et al. (2022). Chemokines in triple-negative breast cancer heterogeneity: new challenges for clinical implications. *Seminars Cancer Biol.* doi:10.1016/j.semcancer.2022.03.008

Mehraj, U., Qayoom, H., Sofi, S., Farhana, P., Asdaq, S. M. B., and Mir, M. A. (2022). Cryptolepine targets TOP2A and inhibits tumor cell proliferation in breast cancer cells-an *in vitro* and *in silico* study. *Anti-cancer Agents Med. Chem.* doi:10.2174/1871520622666220419135547

Mehraj, U., Sofi, S., Alshehri, B., and Mir, M. A. (2022). Expression pattern and prognostic significance of CDKs in breast cancer: an integrated bioinformatic study. *Cancer Biomark.* 34, 505–519. doi:10.3233/CBM-210186

Mehraj, U., Aisha, S., Sofi, S., and Mir, M. A. (2022). Expression pattern and prognostic significance of baculoviral inhibitor of apoptosis repeat-containing 5 (BIRC5) in breast cancer: a comprehensive analysis. *Adv. Cancer Biol. Metastasis* 4, 100037. doi:10.1016/j.adcanc.2022.100037

Mir, M. A., Qayoom, H., Mehraj, U., Nisar, S., Bhat, B., Wani, N. A., et al. (2020). Targeting different pathways using novel combination therapy in triple negative breast cancer. *Curr. Cancer Drug Targets* 20 (8), 586–602. doi:10.2174/1570163817666200518081955

Mishra, R., Patel, H., Alanazi, S., Kilroy, M. K., and Garrett, J. T. (2021). PI3K inhibitors in cancer: clinical implications and adverse effects. *Int. J. Mol. Sci.* 22 (7), 3464. doi:10.3390/ijms22073464

Mosquera-Yuqui, F., Lopez-Guerra, N., and Moncayo-Palacio, E. A. (2020). Targeting the 3CLpro and RdRp of SARS-CoV-2 with phytochemicals from medicinal plants of the andean region: molecular docking and molecular dynamics simulations. *J. Biomol. Struct. Dyn.* 40, 2010–2023. doi:10.1080/07391102.2020.1835716

Neophytou, C., Boutsikos, P., and Papageorgis, P. (2018). Molecular mechanisms and emerging therapeutic targets of triple-negative breast cancer metastasis. *Front. Oncol.* 8, 31. doi:10.3389/fonc.2018.00031

Nong, H. B., Zhang, Y. N., Bai, Y. G., Zhang, Q., Liu, M. F., Zhou, Q., et al. (2022). Adapalene inhibits prostate cancer cell proliferation *in vitro* and *in vivo* by inducing DNA damage, S-phase cell cycle arrest, and apoptosis. *Front. Pharmacol.* 13, 801624. doi:10.3389/fphar.2022.801624

Ocker, M., Herold, C., Ganslmayer, M., Hahn, E. G., and Schuppan, D. (2003). The synthetic retinoid adapalene inhibits proliferation and induces apoptosis in colorectal cancer cells *in vitro*. *Int. J. Cancer* 107 (3), 453–459. doi:10.1002/ijc.11410

Ocker, M., Herold, C., Ganslmayer, M., Zopf, S., Hahn, E. G., Schuppan, D., et al. (2004). Potentiated anticancer effects on hepatoma cells by the retinoid adapalene. *Cancer Lett.* 208 (1), 51–58. doi:10.1016/j.canlet.2003.12.026

Pijuan, J., Barceló, C., Moreno, D. F., Maiques, O., Sisó, P., Marti, R. M., et al. (2019). *In vitro* cell migration, invasion, and adhesion assays: from cell imaging to data analysis. *Front. Cell Dev. Biol.* 7, 107. doi:10.3389/fcell.2019.00107

Rusu, A., Tanase, C., Pascu, G. A., and Todoran, N. (2020). Recent advances regarding the therapeutic potential of adapalene. *Pharmaceuticals* 13 (9), 217. doi:10.3390/ph13090217

Sarker, D., Ang, J. E., Baird, R., Kristeleit, R., Shah, K., Moreno, V., et al. (2015). First-in-human phase I study of pictilisib (GDC-0941), a potent pan–class I phosphatidylinositol-3-kinase (PI3K) inhibitor, in patients with advanced solid tumors. *Clin. Cancer Res.* 21 (1), 77–86. doi:10.1158/1078-0432.CCR-14-0947

Schmid, P., Pinder, S. E., Wheatley, D., Macaskill, J., Zammit, C., Hu, J., et al. (2016). Phase II randomized preoperative window-of-opportunity study of the PI3K inhibitor pictilisib plus anastrozole compared with anastrozole alone in patients with estrogen receptor-positive breast cancer. *J. Clin. Oncol.* 34 (17), 1987–1994. doi:10.1200/JCO.2015.63.9179

Shi, X. N., Li, H., Yao, H., Liu, X., Li, L., Leung, K. S., et al. (2015). Adapalene inhibits the activity of cyclin-dependent kinase 2 in colorectal carcinoma. *Mol. Med. Rep.* 12 (5), 6501–6508. doi:10.3892/mmr.2015.4310

Siegel, R. L., Miller, K. D., Fuchs, H. E., and Jemal, A. (2021). Cancer statistics, 2021. *CA Cancer J. Clin.* 71 (1), 7–33. doi:10.3322/caac.21654

Sofi, S., Mehraj, U., Qayoom, H., Aisha, S., Almilaibary, A., Alkhanani, M., et al. (2022). Targeting cyclin-dependent kinase 1 (CDK1) in cancer: molecular docking and dynamic simulations of potential CDK1 inhibitors. *Med. Oncol.* 39 (9), 133. doi:10.1007/s12032-022-01748-2

Sofi, S., Mehraj, U., Qayoom, H., Aisha, S., Asdaq, S. M. B., Almilaibary, A., et al. (2022). Cyclin-dependent kinases in breast cancer: expression pattern and therapeutic implications. *Med. Oncol.* 39 (6), 106. doi:10.1007/s12032-022-01731-x

Sung, H., Ferlay, J., Siegel, R. L., Laversanne, M., Soerjomataram, I., Jemal, A., et al. (2021). Global cancer statistics 2020: GLOBOCAN estimates of incidence and mortality worldwide for 36 cancers in 185 countries. *CA Cancer J. Clin.* 71 (3), 209–249. doi:10.3322/caac.21660

Trachootham, D., Alexandre, J., and Huang, P. (2009). Targeting cancer cells by ROS-mediated mechanisms: a radical therapeutic approach? *Nat. Rev. Drug Discov.* 8 (7), 579–591. doi:10.1038/nrd2803

Tzeng, H-E., Yang, L., Chen, K., Wang, Y., Liu, Y-R., Pan, S-L., et al. (2015). The pan-PI3K inhibitor GDC-0941 activates canonical WNT signaling to confer resistance in TNBC cells: resistance reversal with WNT inhibitor. *Oncotarget* 6 (13), 11061–11073. doi:10.18632/oncotarget.3568

Waks, A. G., and Winer, E. P. (2019). Breast cancer treatment: a review. *JAMA* 321 (3), 288–300. doi:10.1001/jama.2018.19323

Wang, Q., Zhang, Q., Luan, S., Yang, K., Zheng, M., Li, K., et al. (2019). Adapalene inhibits ovarian cancer ES-2 cells growth by targeting glutamic-oxaloacetic transaminase 1. *Bioorg. Chem.* 93, 103315. doi:10.1016/j.bioorg.2019.103315

Yamamoto, N., Fujiwara, Y., Tamura, K., Kondo, S., Iwasa, S., Tanabe, Y., et al. (2017). Phase Ia/Ib study of the pan-class I PI3K inhibitor pictilisib (GDC-0941) administered as a single agent in Japanese patients with solid tumors and in combination in Japanese patients with non-squamous non-small cell lung cancer. *Invest. New Drugs* 35 (1), 37–46. doi:10.1007/s10637-016-0382-3

Yang, Y., Zhang, Y., Wang, L., and Lee, S. (2017). Levistolide A induces apoptosis via ROS-mediated ER stress pathway in colon cancer cells. *Cell. Physiol. Biochem.* 42 (3), 929–938. doi:10.1159/000478647

Yin, L., Duan, J-J., Bian, X-W., and Yu, S. C. (2020). Triple-negative breast cancer molecular subtyping and treatment progress. *Breast Cancer Res.* 22 (1), 61. doi:10.1186/s13058-020-01296-5

Zhang, N., Fu, J-N., and Chou, T-C. (2016). Synergistic combination of microtubule targeting anticancer fludelone with cytoprotective panaxytriol derived from panax ginseng against MX-1 cells *in vitro*: experimental design and data analysis using the combination index method. *Am. J. Cancer Res.* 6 (1), 97–104.

frontiers | Frontiers in Oncology

TYPE Review
PUBLISHED 19 January 2023
DOI 10.3389/fonc.2023.1095219

OPEN ACCESS

EDITED BY
Claudia Fumarola,
University of Parma, Italy

REVIEWED BY
Rossella Rota,
Bambino Gesù Children's Hospital (IRCCS), Italy
Michele Bernasconi,
University Children's Hospital Bern, Switzerland

*CORRESPONDENCE
Lorenzo D'Ambrosio
lorenzo.dambrosio@unito.it

†These authors share last authorship

SPECIALTY SECTION
This article was submitted to Pharmacology of Anti-Cancer Drugs, a section of the journal Frontiers in Oncology

RECEIVED 10 November 2022
ACCEPTED 03 January 2023
PUBLISHED 19 January 2023

CITATION
Merlini A, Pavese V, Manessi G, Rabino M, Tolomeo F, Aliberti S, D'Ambrosio L and Grignani G (2023) Targeting cyclin-dependent kinases in sarcoma treatment: Current perspectives and future directions. *Front. Oncol.* 13:1095219. doi: 10.3389/fonc.2023.1095219

Targeting cyclin-dependent kinases in sarcoma treatment: Current perspectives and future directions

Alessandra Merlini[1,2], Valeria Pavese[2], Giulia Manessi[2], Martina Rabino[2], Francesco Tolomeo[1], Sandra Aliberti[1], Lorenzo D'Ambrosio[2,3*†] and Giovanni Grignani[1†]

[1]Candiolo Cancer Institute, IRCCS-FPO, Turin, Italy, [2]Department of Oncology, University of Turin, Turin, Italy, [3]Medical Oncology, Azienda Ospedaliera Universitaria San Luigi Gonzaga, Turin, Italy

Effective treatment of advanced/metastatic bone and soft tissue sarcomas still represents an unmet medical need. Recent advances in targeted therapies have highlighted the potential of cyclin-dependent kinases (CDK) inhibitors in several cancer types, including sarcomas. CDKs are master regulators of the cell cycle; their dysregulation is listed among the "hallmarks of cancer" and sarcomas are no exception to the rule. In this review, we report both the molecular basis, and the potential therapeutic implications for the use of CDK inhibitors in sarcoma treatment. What is more, we describe and discuss the possibility and biological rationale for combination therapies with conventional treatments, target therapy and immunotherapy, highlighting potential avenues for future research to integrate CDK inhibition in sarcoma treatment.

KEYWORDS

sarcoma, cyclin dependent kinases (CDK), cdk inhibitors, target therapy, cell cycle

1 Introduction

Sarcomas are a heterogeneous group of rare, mesenchymal malignancies that add up to 1% of all adult cancers and 20% of pediatric cancers (1). The sarcoma family encompasses more than 100 histological subtypes, comprising bone sarcomas and soft tissue sarcomas (BSTS) (2). Standard treatment entails radical surgical resection with (neo)adjuvant radiation therapy and/or chemotherapy in high-risk patients for localized disease, and systemic chemotherapeutic treatment in advanced stages (3). However, prognosis in advanced/metastatic stages remains dismal for the vast majority of sarcoma patients (3, 4). Hence, finding novel, effective treatment strategies for advanced BSTS represents an unmet medical need. Indeed, differently from epithelial cancers, mesenchymal tumors have seldom benefitted from the advent of innovative therapeutic strategies, from targeted therapy to immunotherapy (5, 6). Both the rarity of sarcomas, and the variety of their molecular determinants (7, 8), have represented major challenges for the development of effective,

innovative therapeutic strategies in the field in past years. One of the first actionable molecular alterations discovered in sarcomas has been the amplification of the chromosomal region encoding the murine double minute 2 (MDM2) and cyclin dependent kinase 4 (CDK4) genes in a subset of liposarcomas (well-differentiated and dedifferentiated liposarcomas; WDLPS and DDLPS) (9, 10).

However, until recent years, the possibility to safely target master regulators of the cell cycle as MDM2 and CDK4 appeared difficult to translate in the clinical setting, for their potential off-tumor side effects in healthy tissues (11, 12). Targeting CDK4 seemed particularly attractive for WDLPS and DDLPS, in which it has a specific clinical and biological significance, with respect to MDM2 amplified-only liposarcomas. Indeed, CDK4-amplified WDLPS and DDLPS have been associated with worse prognosis with respect to those lacking CDK4 amplification (13). However, the CDK family is involved not only in WDLPS and DDLPS pathobiology, but in many different sarcoma types across BSTS (14). The comprehensive genomic analysis *via* The Cancer Genome Atlas (TCGA) has shown that approximately one quarter of all sarcomas harbor genetic alterations in the Cyclin-Dependent Kinase Inhibitor 2A (CDKN2A) - Cyclin D (CCND) - CDK4 - retinoblastoma (RB) axis (15, 16), providing strong rationale for targeting this crucial pathway in sarcomas. Hence, better understanding of the role of CDKs in cell biology and cancer, might provide novel avenues of treatment for advanced BSTS (14, 17).

2 CDKs in physiology and cancer

The cell cycle is divided into four distinct phases: a first growth phase (G1), a DNA replication or synthesis phase (S), a second growth phase (G2) and the mitotic phase (M). Cyclin-dependent kinases (CDKs) are members of the serine/threonine protein kinase family; as master regulators of cell cycle control, transcription, and RNA splicing, they are essential for tumor cell proliferation and growth. CDKs do not possess autonomous enzymatic activity and need to be bound to a cyclin subunit to function properly, hence their designation as cyclin-dependent kinases (18). Moreover, a few CDK family members play an important role in RNA transcription and pre-messenger RNA (mRNA) splicing.

The activity of CDKs is respectively up and down regulated by their cyclin partners and cyclin-dependent kinase inhibitors (CKIs). CDKs can phosphorylate the tumor suppressor protein retinoblastoma (Rb). This activity blocks the growth-inhibitory function of Rb: indeed, phospho-Rb (pRb) releases its grip, previously blocking the transactivation domain of the E2F transcription factors, allowing the transcription of genes which are crucial for cell cycle progression to the S-phase (19). In detail, cyclin D-CDK4/6 kinase complexes phosphorylate multiple Rb tumor suppressor protein residues (or its homologs, p107 and p130). As abovementioned, in its hypo-phosphorylated state, Rb actively suppresses G1-S progression by sequestering E2F transcription factors, which transcribe genes needed for DNA replication (20).

The human genome encodes 20 CDKs, divided into two subfamilies: cell cycle-associated CDKs (CDK1–7 and CDK14–18) and transcription-associated CDKs (CDK7–13, 19, and 20). Different CDKs interact with different cyclins to regulate numerous stages of the cell cycle in various cells or to perform other functions. CDK1 is the ancestor of all mitotic kinases; CDK2, CDK4, and CDK6 regulate progression through cell cycle phases. CDK7, instead, is peculiar in that it has been implicated in both transcription processes and cell cycle control (21). CDK8 and CDK9 control the RNA polymerase II (RNA Pol II)-dependent initiation and elongation of transcription (22). Other CDKs (5, 10, 11, 14–18, and 20) do not fit into either canonical roles, exhibiting different functions, often in a tissue-specific fashion. For example, CDK11 has multiple functions in mediating apoptosis, transcription, mitosis, hormone receptor signaling, and autophagy (23, 24). Likewise, CDK5 promotes neuron outgrowth and synaptogenesis in the nervous system, while in pancreatic β cells it reduces insulin secretion (25). As CDKs master fundamental processes required for cell survival and propagation, their hyperactivation (typically through mutation, gene amplification, or altered expression of their regulators) is frequently reported in cancer.

Until a few years ago, CKIs were also classified in two families of cell cycle inhibitors: the CDK family interacting with the CIP/KIP protein and the kinase inhibitor (INK) family. CIP/KIP family members are specific for CDK-cyclin complexes, such as CDK2-cyclin E, A and/or CDK1-cyclin B1, A and/or CDK2,4,6-cyclin D1, D2, D3. Members of the INK family bind CDK4,6 to inhibit formation of CDK4,6-cyclin D1, D2, D3 complexes (26, 27).

3 Partners in life, partners in crime: Key players in cell cycle function and dysregulation beyond CDKs

More recently, additional important regulatory proteins and mechanisms involved in cell cycle control have been discovered, such as members of CDK regulatory subunit (CKS) protein family and new cell cycle regulators. A recent addition to the family is the double homeobox 4 (DUX4) protein, which is of specific interest for sarcoma pathobiology. DUX4 is a transcription factor physiologically expressed during early embryonic development, and it is silenced by epigenetic pathways in most adult somatic cells. Studies revealed that DUX4 binds to CDK1, preventing the formation of CDK1-cyclin B1 complex, thus limiting its kinase activity (28). Aberrant expression of DUX4 in skeletal muscle leads to facioscapulohumeral dystrophy (26, 29). DUX4 rearrangements have been identified in specific types of pediatric B cell acute lymphoblastic leukemia (30, 31), in small round cell bone and soft tissue sarcomas – the so-called CIC-DUX4 rearranged family of sarcomas (32, 33), and rhabdomyosarcoma (34).

The dysregulation of CDK activity through activation of pathways enhancing CDK activity, or through the oncogene-induced inactivation of apoptosis, is a common occurrence in various cancers (35). Identifying and characterizing which cancer types require selected CDK activities for proliferation and survival, might enable to understand which subtypes could benefit more from specific CDK inhibitors (CDKi). However, weighing the importance of each CDK activity to cancer initiation, proliferation and progression is no trivial task, given the individual, multiple roles of each CDK and cyclin beyond cell cycle control (36).

In cancer, CDKs affect multiple targets and phosphorylate relevant transcription factors involved in tumorigenesis. What is more, their pathway can be altered at different stages in various

cancer subtypes; even within the same cancer type (and, most importantly, within the same patient), multiple CDK pathway alterations can co-exist and, in some cases, provide escape/resistance to CDK inhibition. Moreover, resistance almost invariably ensues with targeted treatments in cancer, due to both intratumor heterogeneity and tumor evolutionary dynamics, and CDKi treatment is no exception to the rule. The emergence of somatic RB mutations has been identified in the clinic as a relevant resistance mechanism in breast cancer patients treated with CDKi (37); RB mutation/deletion is a frequent event in sarcomas, with deep deletions detected in a significant proportion of STS in the TCGA sarcoma cohort (16).

Another commonly deleted key tumor suppressor gene is Cyclin Dependent Kinase Inhibitor 2A (CDKN2A). CDKN2A encodes two important cell cycle regulatory proteins, p16 (encoded by the INK4A gene) and, in an alternative reading frame, p14 (encoded by the Alternative Reading Frame – ARF - gene). CDKN2A deletions and inactivating mutations seem to have a negative prognostic role across different tumor types, including sarcomas (38–42). p16, a CDK inhibitor, inhibits Rb phosphorylation, while p14 inhibits MDM2, resulting in a positive regulation of p53. p16 expression increases gradually to a sustained, significantly high level in the later stages of cellular senescence.

Indeed, in murine cells, p19/p53 pathway inactivation is generally sufficient to escape senescence, while in human cells disruption of at least both the p53/p21 and the p16/pRb pathways is usually needed. Homozygous deletion of CDKN2A/ARF thus results in inactivation of two major tumor suppressing pathways, mainly acting through Rb and p53 (43).

Hence, a plethora of alterations beyond CDK4/6 genes emerges as highly relevant for sarcoma pathobiology, providing several potential actionable targets at various steps of the CDKN2A-CCND-CDK4-RB axis. Understanding which sarcoma subtypes are most affected by specific alterations in this axis, has provided the rational basis to select those sarcomas which could benefit more from CDK inhibition (14) (Figure 1).

4 Actionable targets in CDK signaling across different sarcoma subtypes

Despite the diversity in histotypes, age at presentation, risk of recurrence and prognosis, the most frequently altered genes in sarcomas precisely include genes involved in cell cycle regulation, namely TP53, CDKN2A, RB (44–46). Surprisingly, the only gene whose alterations were associated with worse overall survival across all types of STS was CDKN2A (39). These results confirm the biological importance of the p16INK4a-CDK4/6-pRb pathway and/or ARF signaling pathways in sarcoma (39). Indeed, pinpointing histotype-specific alterations might help to dissect the most appropriate therapeutic challenges and opportunities for each sarcoma subtype.

4.1 Undifferentiated pleomorphic sarcoma

UPS accounts for 15–20% of all STS. Typically, it occurs in the limbs and trunk of adults >40 years of age (47). The development of most UPS is sporadic, but approximately 3% of UPS develop in areas of the body that received radiation therapy to treat an unrelated disease after a median latency of 10 years, and are consequently classified as secondary (or, more appropriately, radiation-induced) UPS (48). The standard of care for patients with localized UPS is surgical resection with (neo)adjuvant chemo/radiotherapy in selected cases; for patients with unresectable or metastatic disease, systemic chemotherapy and/or radiotherapy may be considered with low to moderate response rates in patients with UPS. Remarkably, UPS are also among the most represented sarcoma histotypes with CDKN2A loss (39). About 30% of UPS show MDM2 and CDK4 up-regulation; MDM2 ubiquitinates the tumor suppressor p53 and promotes its proteasomal degradation, while MDM2 overexpression leads to downregulation of the CKI p21. P21 is a transcriptional target of p53, and its downregulation causes hyperactivation of CDKs (49). Up to 78% of UPS tumors carry RB gene deletions, due to losses of different regions within the long arm of chromosome 13 (8). TP53 is also very frequently deleted in UPS, and together with RB and ATRX, is among the few genes recurrently showing pathogenic missense mutations in UPS (16). Intriguingly, S phase kinase-associated protein 2 (Skp2) is required for survival of RB- and TP53-deficient UPS cells, in which it drives cell proliferation by degrading p21 and p27. Hence, the loss of both RB and TP53 renders UPS dependent on Skp2, which could provide the basis for innovative therapeutic strategies in this setting (50). However, there are no experimental studies ongoing or published so far, about the potential of CKIs in UPS patients.

4.2 Liposarcoma

Liposarcomas (LPS) account for a significant proportion (~13–20%) of adult STS (13-20%). LPS are subcategorized into three main groups, including WDLPS/DDLPS, characterized by a typical MDM2 and high-mobility group AT-hook 2 (HMGA2) gene amplification and an inconsistent CDK4 gene amplification (the 12q amplicon can span chromosomal regions from 12q12 up to 12q21); myxoid/round cell liposarcoma (M/RCLPS), carrying a typical t (12, 16)(q13;p111) translocation, and pleomorphic liposarcoma (PLPS), frequently showing TP53 and/or RB gene losses. Roughly 60% of LPS cases are WD/DDLPS, while PLPS is the rarest subtype (~5%). In WDLPS/DDLPS, the CDK4 gene (12q14.1) is within a distinct, inconsistent amplicon that is not present in about 10% of WDLPS/DDLPS (51), and its presence has been associated with a worse prognostic outcome (13). Moreover, patients carrying both gene amplifications (MDM2 and CDK4) have a much higher risk of local recurrence after surgery. The WDLPS/DDLPS genetic signature shows a complex pattern of expression for Cyclin D1, P16INK4a, P14ARF, and RB which is not dependent on CDK4 status. Finally, alterations in CDKN2A/CDKN2B/CDK4/CCND2 axis have been detected in almost all CDK4 amplification-negative WDLPS/DDLPS in a cohort of 104 WDLPS/DDLPS patients (52).

4.3 Malignant peripheral nerve sheath tumors

Malignant peripheral nerve sheath tumors (MPNSTs) add up to 3-10% of all STS diagnoses. They can arise sporadically or in patients

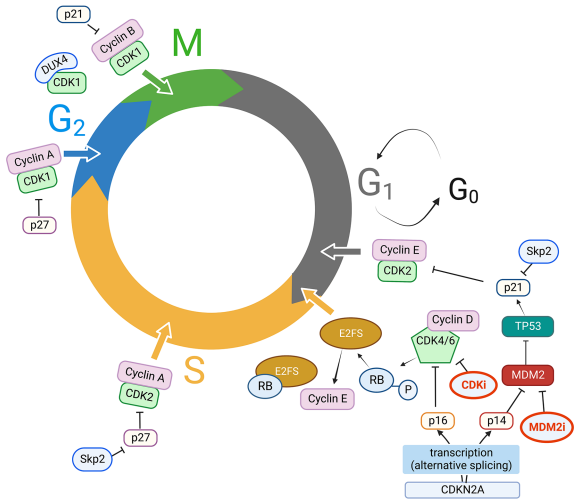

FIGURE 1
Key players in cell cycle dysregulation in STS. CDK, Cyclins, CKI, and other key molecular players in CDK activity/inhibition. Clockwise, starting from G1 to S phase progression: CDKN2A is transcribed by alternative splicing either into p16 or p14, which respectively inhibit CDK4/6/Cyclin D complexes and MDM2 activity. MDM2, an ubiquitin ligase, ubiquitinates p53 targeting it to the proteasome; p53 has p21 as a direct transcriptional target, and p21 in turn inhibits CDK2/Cyclin E complexes. Cyclin E expression is regulated by E2F transcription factor, which in turn is released from Rb protein grip (usually blocking its transactivation domain) when CDK4/6/Cyclin D complexes phosphorylate Rb, facilitating G1 to S phase progression. The ubiquitin ligase Skp2 targets p21 and p27 for proteasomal degradation, thus promoting CDK2/Cyclin E, CDK2/Cyclin A activity in S phase progression, CDK1/Cyclin A activity for G2 to M transition, which is also fostered by releasing p21 inhibitory activity on CDK1/Cyclin B; DUX4 can also bind CDK1, thus preventing CDK1/Cyclin B interaction. MDM2 activity can also be inhibited with MDM2 inhibitors (MDM2i), while CDK inhibitors (CDKi) currently in use in clinical practice are mainly CDK4/6 inhibitors. MDM2i and CDKi are highlighted in bold (red) in Figure 1. *Created with BioRender.com*

affected by neurofibromatosis type I (NF1). MPNSTs are very aggressive and the first cause of oncological death in patients affected by NF1. In those tumors, CDK2 and CDK 4/6 are overexpressed because of the loss of p16 and p27. This causes constant pRb phosphorylation, fostering cell cycle progression (53). Remarkably, up to 80% of MPNST show CDKN2A loss (54). This leads to the upregulation of CDK4/6 and sequentially the initiation of the S phase and promotion of mitosis. Hence, CDK4/6 inhibitors (CKIs) hold promise as a potential innovative treatment for advanced MPNST (55).

4.4 Synovial sarcoma

Synovial sarcoma typically arises in young adults, and is characterized by a typical translocation between chromosome X and chromosome 18 t(X,18;p11,q11), which generates a fusion between SS18 and SSX1/2 or SSX4, disrupting epigenetic regulation within the cancer cell (56, 57). CDKN2A deletion is a highly frequent event in synovial sarcomas (58); moreover, the translocation facilitates repression of CDKN2A activity (59) and increases the expression of CDK4 as well as multiple cyclins (D1, B1, A2, I, and F) (60).

4.5 Other soft tissue sarcomas

Leiomyosarcoma (LMS) accounts for 10-20% of all STS, and can arise at any body site. LMS is characterized by spindle-shaped cells resembling smooth muscle cells and are grouped among the so-called "complex karyotype" STS, as they are not driven by a single translocation or genetic alteration, but are characterized by multiple, various genetic abnormalities. Common genetic alterations include PTEN deletion and/or mutation, TP53 mutations and, importantly, RB loss (16, 61–63). One striking, recent finding is the high frequency of biallelic inactivation of the above mentioned by various mechanisms, in the vast majority of LMS samples analyzed in the study by *Chudasama P.* and colleagues (61). Rb inactivation casts some doubt on the clinical utility of CDK inhibition, as Rb inactivation affects the CDK pathway downstream of CDKs, presenting a potential mechanism of both primary and secondary resistance to CDKi in LMS, similarly to Rb-mediated resistance mechanisms in CDK-treated breast cancer patients (37).

Intimal sarcomas (INS) are rare STS which can be particularly aggressive also because of their site of origin, most frequently affecting the wall of large vessels or the heart (64–66). INS are characterized by the peculiar presence of large gains/amplifications in the 12q12-15 chromosomal region, encompassing MDM2 and/or CDK4. CDKN2A deletions are also very frequent in INS (65). Taken together, these recent molecular findings might provide the rationale for trials with CDKi in this set of STS patients burdened by very poor prognosis (67).

Rhabdomyosarcoma (RMS) is the most common STS in children and adolescents; alveolar rhabdomyosarcomas (ARMS) are characterized by either PAX3-FOXO1 or PAX7-FOXO1 fusion genes; ARMS with the former fusion most often carry additional 12q13-q14 amplifications, therefore including the CDK4 gene, which has been correlated with poor survival outcomes (68). Disappointingly, in fusion-positive RMS, CDK4 amplification has not been linked to increased sensitivity to CDKi, but, rather counterintuitively, to the opposite condition (resistance to CDKi), at least in *in vitro* studies (69).

4.6 Bone sarcomas

Osteosarcomas (OS) represent the most common primary malignant tumors of bone. They can arise at any skeletal site, but they more frequently develop in the long bones of the extremities. OS has a bimodal age distribution (adolescents between 14-18 years and older adults, > 40 years old) and, even though it is sensitive to chemotherapy, prognosis in advanced stages remains dismal (2, 70). Intriguingly, TP53 is inactivated in >90% of OS, contributing to cell cycle dysregulation; RB1 is also among genes most frequently mutated in OS (>50%) (71). Indeed, individuals affected by Li-Fraumeni and hereditary retinoblastoma syndromes have an increased risk of developing OS (72). Other genes commonly altered in OS and involved in cell cycle regulation include CDK4, MDM2, PTEN, CDKN2A, CCND3, and CCNE1 (14, 49, 73). The clinical utility of CDKi in OS has not yet been tested in dedicated clinical trials, but advanced osteosarcoma patients with CDK4 overexpression could be included in the phase II PalboSarc trial with the CDKi palbociclib (NCT03242382) (14).

5 Targeting CDKs in cancer

The history and success of CDKi in cancer have now come a long way, with more than 25 years of preclinical and clinical development (74). The first generation of CDKi was constituted by pan-CDKi (e.g. flavopiridol, olomucine, roscovitine) (75, 76), which were designed to halt cell cycle and cell proliferation by inhibiting CDK enzymatic activity. This first generation of pan-CDKi had limited selectivity and was burdened by high toxicity in normal cells, preventing their clinical development. For these reasons, almost all first generation CDKi failed to meet their endpoints in early-stage clinical trials (77, 78). Second-generation CDKi (e.g. dinaciclib, CYC065) have been developed with greater selectivity and fewer side effects (79). Finally, third-generation, selective CDK4/6 inhibitors were the first CDKi which received FDA approval in March 2017, for the treatment of postmenopausal women with hormone receptor (HR)-positive metastatic breast cancer, in combination with an aromatase inhibitor as initial endocrine-based therapy.

Currently, the three FDA- and EMA-approved CDK4/6 inhibitors are palbociclib, ribociclib and abemaciclib. While palbociclib is equally active against CDK4 and CDK6, ribociclib and abemaciclib show higher efficacy in CDK4 inhibition (80). Indeed, all these approved compounds act by inhibiting Rb phosphorylation, thus blocking cell cycle progression from G1 to S phase. However, their action extends beyond simple enzymatic inhibition, with likely direct effects on cell metabolism, senescence, and possibly immune modulation (81, 82).

5.1 Anti-CDK targeted therapy in sarcomas: Ongoing clinical trials and future perspectives

Sarcomas have been included in clinical studies on CDKi since early phase I trials; however, only very few CDKi trials enrolled exclusively BSTS, including an early-phase trial of flavopiridol in association with doxorubicin (14, 75). Among these, two studies are of peculiar interest. In particular, the study "PD0332991 (Palbociclib) in Patients with Advanced or Metastatic Liposarcoma", NCT01209598, demonstrated a favorable progression free survival (PFS) in a mixed WDLPS/DDLPS patient cohort, which included advanced/metastatic WDLPS/DDLPS patients who had received at least one line of systemic treatment (patients previously untreated for systemic disease were allowed to join the expansion cohort) (83). Another study, NCT02846987, still active although closed to enrollment, has investigated the role of abemaciclib monotherapy in advanced DDLPS, assuming that this novel, more potent CDK inhibitor might achieve better results in the sarcoma population. So far, the study has met its primary endpoint (12-week PFS ≥ 60%) and final results are awaited (84).

One highly attractive combination treatment opportunity in WDLPS/DDLPS is represented by the possibility to combine novel MDM2 inhibitors (85, 86) with CDKi. Preclinical studies demonstrated both evidence of synergism (87), and efficacy of MDM2 inhibitors in overcoming resistance to CDK4/6 inhibitors (88). However, the significant risk of unacceptable combined toxicities of MDM2 and CDK4 inhibitors - especially myelosuppression - casts some doubt over the clinical applicability of their combination.

Concerning other possible targeted treatment combinations, one interesting opportunity could be the association of CDKi with PI3K inhibitors. Indeed, PTEN downregulation and AKT increased phosphorylation were shown to be associated with increased CDK2/cyclin E2 expression in breast cancer cell lines resistant to CDKi, rendering PI3K inhibitors (capable of downregulating cyclin E2) an attractive partner to overcome resistance to CDKi (89).

Finally, studies on the association (combination/sequence) of CDKi with immunotherapy are currently ongoing in many cancer types, including sarcomas (e.g. study NCT04438824, listed in Table 1). Indeed, CDKi seem to have a relevant immune-priming effect (81). Preliminary data are not available yet for BSTS, but similar studies in breast cancer with combination of palbociclib, pembrolizumab and letrozole have yielded promising results (90).

In Table 1, a list of ongoing, actively recruiting clinical trials with CDKi (alone as monotherapy, or in combination) in BSTS is provided.

6 Conclusions

The presence of molecular alterations affecting the CDKN2A-CDK4-CCND1-RB axis is an important opportunity for innovative targeted treatments for patients with BSTS, typically burdened by dismal prognosis in advanced/metastatic stages. Knowledge of the fine-tuning of these pathways across different sarcoma subtypes is instrumental to develop rationally-based clinical trial proposals in this setting. Indeed, presence of multiple alterations in different steps of cell cycle regulation might provide primary/secondary resistance mechanisms to CDK inhibition; moreover, when present, CDK4 amplification is the main oncogenic driver of only a subset of CDK4-amplified sarcomas. Hence, thorough understanding of the

10.3389/fonc.2023.1095219

TABLE 1 Ongoing clinical trials with CDKi in BSTS (source: www.clinicaltrials.gov, accessed on October 20th, 2022).

ClinicalTrials.gov identifier	Study Title	Status	Interventions	Study Type, Phase
NCT03242382	Trial of Palbociclib in Second Line of Advanced Sarcomas with CDK4 Overexpression.	Recruiting	• Drug: Palbociclib	Study Type: Interventional Phase: Phase II
NCT04040205	Abemaciclib for Bone and Soft Tissue Sarcoma with Cyclin- Dependent Kinase (CDK) Pathway Alteration	Recruiting	• Drug: Abemaciclib	Study Type: Interventional Phase: Phase II
NCT03604783	Phase 1, First-in-human Study of Oral TP-1287 in Patients with Advanced Solid Tumors	Recruiting	• Drug: TP-1287	Study Type: Interventional Phase: Phase I
NCT05159518	A Study of PRT2527 in Patients with Advanced Solid Tumors	Recruiting	• Drug: PRT2527	Study Type: Interventional Phase: Phase I
NCT04941274	Abemaciclib in Patients With HIV-associated and HIV-negative Kaposi Sarcoma	Recruiting	• Drug: Abemaciclib	Study Type: Interventional Phase: Phase I-II
NCT02644460	Abemaciclib in Children with DIPG or Recurrent/Refractory Solid Tumors	Recruiting	• Drug: Abemaciclib	Study Type: Interventional Phase: Phase I
NCT04557449	Study to Test the Safety and Tolerability of PF-07220060 in Participants with Advance Solid Tumors	Recruiting	• Drug: PF-07220060	Study Type: Interventional Phase: Phase I
NCT04438824	Palbociclib and INCMGA00012 in People with Advanced Liposarcoma	Recruiting	• Drug: INCMGA00012	Study Type: Interventional Phase: Phase II
NCT03784014	Molecular Profiling of Advanced Soft-tissue Sarcomas	Recruiting	• Drug: Nilotinib • Drug: Ceritinib • Drug: Capmatinib • Drug: Lapatinib • Drug: Trametinib • Combination Product: Trametinib and Dabrafenib • Combination Product: Olaparib and Durvalumab • Drug: Palbociclib • Drug: Glasdegib • Drug: TAS-120 • Other: Next Generation sequencing exome	Study Type: Interventional Phase: Phase III
NCT05252416	(VELA) Study of BLU-222 in Advanced Solid Tumors	Recruiting	• Drug: BLU-222 • Drug: Carboplatin • Drug: Ribociclib • Drug: Fulvestrant	Study Type: Interventional Phase: Phase I-II
NCT03709680	Study Of Palbociclib Combined with Chemotherapy In Pediatric Patients With Recurrent/Refractory Solid Tumors	Recruiting	• Drug: Palbociclib	Study Type: Interventional Phase: Phase II
NCT04238819	A Study of Abemacicli (LY2835219) in Combination with Other Anti-Cancer Treatments in Children and Young Adult Participants With Solid Tumors, Including Neuroblastoma	Recruiting	• Drug: Abemaciclib	Study Type: Interventional Phase: Phase I-II

molecular basis of cell cycle dysregulation in each specific histotype, will be crucial for the development of tailored treatment combinations with CDK inhibitors and other innovative targeted therapies or immunotherapeutic strategies.

Author contributions

AM, LA, and GG contributed to conception and design of the review article. AM, VP, LA organized the literature data. AM, VP, LA and GG wrote the first draft of the manuscript. AM, VP, GM, MR, FT, SA, LA, GG wrote sections of the manuscript. All authors contributed to the article and approved the submitted version.

Funding

AIRC IG 2019-ID 23104, to GG.

Conflict of interest

AM: travel expenses from PharmaMar. LA received travel expenses from PharmaMar and Lilly. GG has received fees for consulting and advisory board roles from PharmaMar, Lilly, Novartis, GSK, Bayer, and Eisai.

The remaining authors declare that the research was conducted in the absence of any commercial or financial relationships that could be construed as a potential conflict of interest.

Publisher's note

References

1. Siegel RL, Miller KD, Fuchs HE, Jemal A. Cancer statistics, 2022. *CA Cancer J Clin* (2022) 72:7–33. doi: 10.3322/caac.21708

2. WHO Classification of Tumours Editorial Board. *Soft tissue and bone tumours. ed. 5th* Vol. vol. 3. . Lyon (France: WHO classification of tumours series (International Agency for Research on Cancer (2020).

3. Gronchi A, Miah AB, Dei Tos AP, Abecassis N, Bajpai J, Bauer S, et al. Soft tissue and visceral sarcomas: ESMO-EURACAN-GENTURIS clinical practice guidelines for diagnosis, treatment and follow-up. *Ann Oncol* (2021) 32:1348–65. doi: 10.1016/j.annonc.2021.07.006

4. Lochner J, Menge F, Vassos N, Hohenberger P, Kasper B. Prognosis of patients with metastatic soft tissue sarcoma: Advances in recent years. *Oncol Res Treat* (2020) 43:613–9. doi: 10.1159/000509519

5. Hall F, Villalobos V, Wilky B. Future directions in soft tissue sarcoma treatment. *Curr Probl Cancer* (2019) 43:300–7. doi: 10.1016/j.currproblcancer.2019.06.004

6. Rytlewski J, Milhem MM, Monga V. Turning 'Cold' tumors 'Hot': immunotherapies in sarcoma. *Ann Transl Med* (2021) 9:1039. doi: 10.21037/atm-20-6041

7. Barretina J, Taylor BS, Banerji S, Ramos AH, Lagos-Quintana M, Decarolis PL, et al. Subtype-specific genomic alterations define new targets for soft-tissue sarcoma therapy. *Nat Genet* (2010) 42:715–21. doi: 10.1038/ng.619

8. Taylor BS, Barretina J, Maki RG, Antonescu CR, Singer S, Ladanyi M. Advances in sarcoma genomics and new therapeutic targets. *Nat Rev Cancer* (2011) 11:541–57. doi: 10.1038/nrc3087

9. Sirvent N, Forus A, Lescaut W, Burel F, Benzaken S, Chazal M, et al. Characterization of centromere alterations in liposarcomas. *Genes Chromosomes Cancer* (2000) 29:117–29. doi: 10.1002/1098-2264(2000)9999:9999<::AID-GCC1014>3.0.CO;2-Q

10. Pilotti S, Della Torre G, Lavarino C, Di Palma S, Sozzi G, Minoletti F, et al. Distinct mdm2/p53 expression patterns in liposarcoma subgroups: implications for different pathogenetic mechanisms. *J Pathol* (1997) 181:14–24. doi: 10.1002/(SICI)1096-9896(199701)181:1<14::AID-PATH730>3.0.CO;2-O

11. Li Q, Lozano G. Molecular pathways: targeting Mdm2 and Mdm4 in cancer therapy. *Clin Cancer Res* (2013) 19:34–41. doi: 10.1158/1078-0432.CCR-12-0053

12. Jhaveri K, Burris Rd HA, Yap TA, Hamilton E, Rugo HS, Goldman JW, et al. The evolution of cyclin dependent kinase inhibitors in the treatment of cancer. *Expert Rev Anticancer Ther* (2021) 21:1105–24. doi: 10.1080/14737140.2021.1944109

13. Italiano A, Bianchini L, Gjernes E, Keslair F, Ranchere-Vince D, Dumollard JM, et al. Clinical and biological significance of CDK4 amplification in well-differentiated and dedifferentiated liposarcomas. *Clin Cancer Res* (2009) 15:5696–703. doi: 10.1158/1078-0432.CCR-08-3185

14. Hsu JY, Seligson ND, Hays JL, Miles WO, Chen JL. Clinical utility of CDK4/6 inhibitors in sarcoma: Successes and future challenges. *JCO Precis Oncol* (2022) 6: e2100211. doi: 10.1200/PO.21.00211

15. Burns J, Brown JM, Jones KB, Huang PH. The cancer genome atlas: Impact and future directions in sarcoma. *Surg Oncol Clin N Am* (2022) 31:559–68. doi: 10.1016/j.soc.2022.03.013

16. C. G. A. R. N. E. a. elizabeth.demicco@sinaihealthsystem.ca, C. G. A. R. Network. Comprehensive and integrated genomic characterization of adult soft tissue sarcomas. *Cell* (2017) 171:950–965.e928. doi: 10.1016/j.cell.2017.10.014

17. Thiel JT, Daigeler A, Kolbenschlag J, Rachunek K, Hoffmann S. The role of CDK pathway dysregulation and its therapeutic potential in soft tissue sarcoma. *Cancers (Basel)* (2022) 14(14):1–20. doi: 10.3390/cancers14143380

18. Lim S, Kaldis P. Cdks, cyclins and CKIs: roles beyond cell cycle regulation. *Development* (2013) 140:3079–93. doi: 10.1242/dev.091744

19. Giacinti C, Giordano A. RB and cell cycle progression. *Oncogene* (2006) 25:5220–7. doi: 10.1038/sj.onc.1209615

20. Burkhart DL, Sage J. Cellular mechanisms of tumour suppression by the retinoblastoma gene. *Nat Rev Cancer* (2008) 8:671–82. doi: 10.1038/nrc2399

21. Fisher RP. Secrets of a double agent: CDK7 in cell-cycle control and transcription. *J Cell Sci* (2005) 118:5171–80. doi: 10.1242/jcs.02718

22. Michowski W, Chick JM, Chu C, Kolodziejczyk A, Wang Y, Suski JM, et al. Cdk1 controls global epigenetic landscape in embryonic stem cells. *Mol Cell* (2020) 78:459–476.e413. doi: 10.1016/j.molcel.2020.03.010

23. Malumbres M. Cyclin-dependent kinases. *Genome Biol* (2014) 15:122. doi: 10.1186/gb4184

24. Zhou Y, Shen JK, Hornicek FJ, Kan Q, Duan Z. The emerging roles and therapeutic potential of cyclin-dependent kinase 11 (CDK11) in human cancer. *Oncotarget* (2016) 7:40846–59. doi: 10.18632/oncotarget.8519

25. Wood DJ, Endicott JA. Structural insights into the functional diversity of the CDK-cyclin family. *Open Biol* (2018) 8(9):1–26. doi: 10.1098/rsob.180112

26. Bury M, Le Calvé B, Ferbeyre G, Blank V, Lessard F. New insights into CDK regulators: Novel opportunities for cancer therapy. *Trends Cell Biol* (2021) 31:331–44. doi: 10.1016/j.tcb.2021.01.010

27. Sherr CJ, Roberts JM. CDK inhibitors: positive and negative regulators of G1-phase progression. *Genes Dev* (1999) 13:1501–12. doi: 10.1101/gad.13.12.1501

28. Bury M, Le Calvé B, Lessard F, Dal Maso T, Saliba J, Michiels C, et al. NFE2L3 controls colon cancer cell growth through regulation of DUX4, a CDK1 inhibitor. *Cell Rep* (2019) 29:1469–1481.e1469. doi: 10.1016/j.celrep.2019.09.087

29. Dib C, Zakharova V, Popova E, Kiseleva E, Chernyak B, Lipinski M, et al. DUX4 pathological expression: Causes and consequences in cancer. *Trends Cancer* (2019) 5:268–71. doi: 10.1016/j.trecan.2019.03.001

30. Tanaka Y, Kawazu M, Yasuda T, Tamura M, Hayakawa F, Kojima S, et al. Transcriptional activities of DUX4 fusions in b-cell acute lymphoblastic leukemia. *Haematologica* (2018) 103:e522–6. doi: 10.3324/haematol.2017.183152

31. Zhang J, McCastlain K, Yoshihara H, Xu B, Chang Y, Churchman ML, et al. Deregulation of DUX4 and ERG in acute lymphoblastic leukemia. *Nat Genet* (2016) 48:1481–9. doi: 10.1038/ng.3691

32. Gambarotti M, Benini S, Gamberi G, Cocchi S, Palmerini E, Sbaraglia M, et al. CIC-DUX4 fusion-positive round-cell sarcomas of soft tissue and bone: a single-institution morphological and molecular analysis of seven cases. *Histopathology* (2016) 69:624–34. doi: 10.1111/his.12985

33. Sbaraglia M, Righi A, Gambarotti M, Dei Tos AP. Ewing Sarcoma and Ewing-like tumors. *Virchows Arch* (2020) 476:109–19. doi: 10.1007/s00428-019-02720-8

34. Sirvent N, Trassard M, Ebran N, Attias R, Pedeutour F. Fusion of EWSR1 with the DUX4 facioscapulohumeral muscular dystrophy region resulting from t(4,22)(q35;q12) in a case of embryonal rhabdomyosarcoma. *Cancer Genet Cytogenet* (2009) 195:12–8. doi: 10.1016/j.cancergencyto.2009.06.011

35. Sherr CJ, Beach D, Shapiro GI. Targeting CDK4 and CDK6: From discovery to therapy. *Cancer Discovery* (2016) 6:353–67. doi: 10.1158/2159-8290.CD-15-0894

36. Otto T, Sicinski P. Cell cycle proteins as promising targets in cancer therapy. *Nat Rev Cancer* (2017) 17:93–115. doi: 10.1038/nrc.2016.138

37. Condorelli R, Spring L, O'Shaughnessy J, Lacroix L, Bailleux C, Scott V, et al. Polyclonal RB1 mutations and acquired resistance to CDK 4/6 inhibitors in patients with metastatic breast cancer. *Ann Oncol* (2018) 29:640–5. doi: 10.1093/annonc/mdx784

38. Merlini A, Centomo ML, Ferrero G, Chiabotto G, Miglio U, Berrino E, et al. DNA Damage response and repair genes in advanced bone and soft tissue sarcomas: An 8-gene signature as a candidate predictive biomarker of response to trabectedin and olaparib combination. *Front Oncol* (2022) 12:844250. doi: 10.3389/fonc.2022.844250

39. Bui NQ, Przybyl J, Trabucco SE, Frampton G, Hastie T, van de Rijn M, et al. A clinico-genomic analysis of soft tissue sarcoma patients reveals CDKN2A deletion as a biomarker for poor prognosis. *Clin Sarcoma Res* (2019) 9:12. doi: 10.1186/s13569-019-0122-5

40. Zhao R, Choi BY, Lee M-H, Bode AM, Dong Z. Implications of genetic and epigenetic alterations of CDKN2A (p16INK4a) in cancer. *EBioMedicine* (2016) 8:30–9. doi: 10.1016/j.ebiom.2016.04.017

41. Lu VM, O'Connor KP, Shah AH, Eichberg DG, Luther EM, Komotar RJ, et al. The prognostic significance of CDKN2A homozygous deletion in IDH-mutant lower-grade glioma and glioblastoma: a systematic review of the contemporary literature. *J Neurooncol* (2020) 148:221–9. doi: 10.1007/s11060-020-03528-2

42. Monzon J, Liu L, Brill H, Goldstein AM, Tucker MA, From L, et al. CDKN2A mutations in multiple primary melanomas. *New Engl J Med* (1998) 338:879–87. doi: 10.1056/NEJM199803263381305

43. Pyeritz R, Korf BGW. *Emery and rimoin's principles and practice of medical genetics and genomics*, *7th* ed. Academic Press (2020).

44. Chalmers ZR, Connelly CF, Fabrizio D, Gay L, Ali SM, Ennis R, et al. Analysis of 100,000 human cancer genomes reveals the landscape of tumor mutational burden. *Genome Med* (2017) 9:34. doi: 10.1186/s13073-017-0424-2

45. Cote GM, He J, Choy E. Next-generation sequencing for patients with sarcoma: A single center experience. *Oncologist* (2018) 23:234–42. doi: 10.1634/theoncologist.2017-0290

46. Tirrò E, Martorana F, Micale G, Inzerilli N, Carciotto R, Romano C, et al. Next generation sequencing in a cohort of patients with rare sarcoma histotypes: A single institution experience. *Pathol Res Pract* (2022) 232:153820. doi: 10.1016/j.prp.2022.153820

47. Carvalho SD, Pissaloux D, Crombé A, Coindre JM, Le Loarer F. Pleomorphic sarcomas: The state of the art. *Surg Pathol Clin* (2019) 12:63–105. doi: 10.1016/j.path.2018.10.004

48. Riad S, Biau D, Holt GE, Werier J, Turcotte RE, Ferguson PC, et al. The clinical and functional outcome for patients with radiation-induced soft tissue sarcoma. *Cancer* (2012) 118:2682–92. doi: 10.1002/cncr.26543

49. Kohlmeyer JL, Gordon DJ, Tanas MR, Monga V, Dodd RD, Quelle DE. CDKs in sarcoma: Mediators of disease and emerging therapeutic targets. *Int J Mol Sci* (2020) 21 (8):1–30. doi: 10.3390/ijms21083018

50. Li GZ, Okada T, Kim YM, Agaram NP, Sanchez-Vega F, Shen Y, et al. Rb And p53-deficient myxofibrosarcoma and undifferentiated pleomorphic sarcoma require Skp2 for survival. *Cancer Res* (2020) 80:2461–71. doi: 10.1158/0008-5472.CAN-19-1269

51. Italiano A, Bianchini L, Keslair F, Bonnafous S, Cardot-Leccia N, Coindre JM, et al. HMGA2 is the partner of MDM2 in well-differentiated and dedifferentiated liposarcomas whereas CDK4 belongs to a distinct inconsistent amplicon. *Int J Cancer* (2008) 122:2233–41. doi: 10.1002/ijc.23380

52. Louis-Brennetot C, Coindre JM, Ferreira C, Pérot G, Terrier P, Aurias A. The CDKN2A/CDKN2B/CDK4/CCND1 pathway is pivotal in well-differentiated and dedifferentiated liposarcoma oncogenesis: an analysis of 104 tumors. *Genes Chromosomes Cancer* (2011) 50:896–907. doi: 10.1002/gcc.20909

53. Bhalla AD, Landers SM, Singh AK, Landry JP, Yeagley MG, Myerson GSB, et al. Experimental models of undifferentiated pleomorphic sarcoma and malignant peripheral nerve sheath tumor. *Lab Invest* (2022) 102:658–66. doi: 10.1038/s41374-022-00734-6

54. Chaney KE, Perrino MR, Kershner LJ, Patel AV, Wu J, Choi K, et al. Loss in a model of neurofibroma demonstrates stepwise tumor progression to atypical neurofibroma and MPNST. *Cancer Res* (2020) 80:4720–30. doi: 10.1158/0008-5472.CAN-19-1429

55. Rhodes SD, He Y, Smith A, Jiang L, Lu Q, Mund J, et al. Cdkn2a (Arf) loss drives NF1-associated atypical neurofibroma and malignant transformation. *Hum Mol Genet* (2019) 28:2752–62. doi: 10.1093/hmg/ddz095

56. Clark J, Rocques PJ, Crew AJ, Gill S, Shipley J, Chan AM, et al. Identification of novel genes, SYT and SSX, involved in the t(X;18)(p11.2;q11.2) translocation found in human synovial sarcoma. *Nat Genet* (1994) 7:502–8. doi: 10.1038/ng0894-502

57. Ladanyi M, Antonescu CR, Leung DH, Woodruff JM, Kawai A, Healey JH, et al. Impact of SYT-SSX fusion type on the clinical behavior of synovial sarcoma: a multi-institutional retrospective study of 243 patients. *Cancer Res* (2002) 62:135–40.

58. Subramaniam MM, Noguera R, Piqueras M, Navarro S, López-Guerrero JA, Llombart-Bosch A. p16INK4A (CDKN2A) gene deletion is a frequent genetic event in synovial sarcomas. *Am J Clin Pathol* (2006) 126:866–74. doi: 10.1309/E2AAY2XXN431WL81

59. El Beaino M, Araujo DM, Lazar AJ, Lin PP. Synovial sarcoma: Advances in diagnosis and treatment identification of new biologic targets to improve multimodal therapy. *Ann Surg Oncol* (2017) 24:2145–54. doi: 10.1245/s10434-017-5855-x

60. Haldar M, Hancock JD, Coffin CM, Lessnick SL, Capecchi MR. A conditional mouse model of synovial sarcoma: insights into a myogenic origin. *Cancer Cell* (2007) 11:375–88. doi: 10.1016/j.ccr.2007.01.016

61. Chudasama P, Mughal SS, Sanders MA, Hübschmann D, Chung I, Deeg KI, et al. Integrative genomic and transcriptomic analysis of leiomyosarcoma. *Nat Commun* (2018) 9:144. doi: 10.1038/s41467-017-02602-0

62. Guo X, Jo VY, Mills AM, Zhu SX, Lee CH, Espinosa I, et al. Clinically relevant molecular subtypes in leiomyosarcoma. *Clin Cancer Res* (2015) 21:3501–11. doi: 10.1158/1078-0432.CCR-14-3141

63. Ognjanovic S, Olivier M, Bergemann TL, Hainaut P. Sarcomas in TP53 germline mutation carriers: a review of the IARC TP53 database. *Cancer* (2012) 118:1387–96. doi: 10.1002/cncr.26390

64. Bode-Lesniewska B, Zhao J, Speel EJ, Biraima AM, Turina M, Komminoth P, et al. Gains of 12q13-14 and overexpression of mdm2 are frequent findings in intimal sarcomas of the pulmonary artery. *Virchows Arch* (2001) 438:57–65. doi: 10.1007/s004280000313

65. Neuville A, Collin F, Bruneval P, Parrens M, Thivolet F, Gomez-Brouchet A, et al. Intimal sarcoma is the most frequent primary cardiac sarcoma: clinicopathologic and molecular retrospective analysis of 100 primary cardiac sarcomas. *Am J Surg Pathol* (2014) 38:461–9. doi: 10.1097/PAS.0000000000000184

66. Roszik J, Khan A, Conley AP, Livingston JA, Groisberg R, Ravi V, et al. Unique aberrations in intimal sarcoma identified by next-generation sequencing as potential therapy targets. *Cancers (Basel)* (2019) 11(9):1–8. doi: 10.3390/cancers11091283

67. Penel N, Taieb S, Ceugnart L, Dansin E, Hoguet D, Vanseymortier L, et al. Report of eight recent cases of locally advanced primary pulmonary artery sarcomas: failure of doxorubicin-based chemotherapy. *J Thorac Oncol* (2008) 3:907–11. doi: 10.1097/JTO.0b013e318180720d

68. Barr FG, Duan F, Smith LM, Gustafson D, Pitts M, Hammond S, et al. Genomic and clinical analyses of 2p24 and 12q13-q14 amplification in alveolar rhabdomyosarcoma: a report from the children's oncology group. *Genes Chromosomes Cancer* (2009) 48:661–72. doi: 10.1002/gcc.20673

69. Olanich ME, Sun W, Hewitt SM, Abdullaev Z, Pack SD, Barr FG. CDK4 amplification reduces sensitivity to CDK4/6 inhibition in fusion-positive rhabdomyosarcoma. *Clin Cancer Res* (2015) 21:4947–59. doi: 10.1158/1078-0432.CCR-14-2955

70. Mirabello L, Troisi RJ, Savage SA. Osteosarcoma incidence and survival rates from 1973 to 2004: data from the surveillance, epidemiology, and end results program. *Cancer* (2009) 115:1531–43. doi: 10.1002/cncr.24121

71. Chen X, Bahrami A, Pappo A, Easton J, Dalton J, Hedlund E, et al. Recurrent somatic structural variations contribute to tumorigenesis in pediatric osteosarcoma. *Cell Rep* (2014) 7:104–12. doi: 10.1016/j.celrep.2014.03.003

72. Fuchs B, Pritchard DJ. Etiology of osteosarcoma. *Clin Orthop Relat Res 40-52* (2002). doi: 10.1097/00003086-200204000-00007

73. Zhou Y, Shen JK, Yu Z, Hornicek FJ, Kan Q, Duan Z. Expression and therapeutic implications of cyclin-dependent kinase 4 (CDK4) in osteosarcoma. *Biochim Biophys Acta Mol Basis Dis* (2018) 1864:1573–82. doi: 10.1016/j.bbadis.2018.02.004

74. Asghar U, Witkiewicz AK, Turner NC, Knudsen ES. The history and future of targeting cyclin-dependent kinases in cancer therapy. *Nat Rev Drug Discovery* (2015) 14:130–46. doi: 10.1038/nrd4504

75. Luke JJ, D'Adamo DR, Dickson MA, Keohan ML, Carvajal RD, Maki RG, et al. The cyclin-dependent kinase inhibitor flavopiridol potentiates doxorubicin efficacy in advanced sarcomas: preclinical investigations and results of a phase I dose-escalation clinical trial. *Clin Cancer Res* (2012) 18:2638–47. doi: 10.1158/1078-0432.CCR-11-3203

76. Cicenas J, Kalyan K, Sorokinas A, Stankunas E, Levy J, Meskinyte I, et al. Roscovitine in cancer and other diseases. *Ann Transl Med* (2015) 3:135. doi: 10.3978/j.issn.2305-5839.2015.03.61

77. Whittaker SR, Mallinger A, Workman P, Clarke PA. Inhibitors of cyclin-dependent kinases as cancer therapeutics. *Pharmacol Ther* (2017) 173:83–105. doi: 10.1016/j.pharmthera.2017.02.008

78. Zhang M, Zhang L, Hei R, Li X, Cai H, Wu X, et al. CDK inhibitors in cancer therapy, an overview of recent development. *Am J Cancer Res* (2021) 11:1913–35.

79. Parry D, Guzi T, Shanahan F, Davis N, Prabhavalkar D, Wiswell D, et al. Dinaciclib (SCH 727965), a novel and potent cyclin-dependent kinase inhibitor. *Mol Cancer Ther* (2010) 9:2344–53. doi: 10.1158/1535-7163.MCT-10-0324

80. George MA, Qureshi S, Omene C, Toppmeyer DL, Ganesan S. Clinical and pharmacologic differences of CDK4/6 inhibitors in breast cancer. *Front Oncol* (2021) 11:693104. doi: 10.3389/fonc.2021.693104

81. Goel S, DeCristo MJ, Watt AC, BrinJones H, Sceneay J, Li BB, et al. CDK4/6 inhibition triggers anti-tumour immunity. *Nature* (2017) 548:471–5. doi: 10.1038/nature23465

82. Laphanuwat P, Jirawatnotai S. Immunomodulatory roles of cell cycle regulators. *Front Cell Dev Biol* (2019) 7:23. doi: 10.3389/fcell.2019.00023

83. Dickson MA, Schwartz GK, Keohan ML, D'Angelo SP, Gounder MM, Chi P, et al. Progression-free survival among patients with well-differentiated or dedifferentiated liposarcoma treated with CDK4 inhibitor palbociclib: A phase 2 clinical trial. *JAMA Oncol* (2016) 2:937–40. doi: 10.1001/jamaoncol.2016.0264

84. Dickson MA, Koff A, D'Angelo SP, Gounder MM, Keohan ML, Kelly CM, et al. Phase 2 study of the CDK4 inhibitor abemaciclib in dedifferentiated liposarcoma. *J Clin Oncol* (2019) 37:11004–4. doi: 10.1200/JCO.2019.37.15_suppl.11004

85. Takahashi S, Fujiwara Y, Nakano K, Shimizu T, Tomomatsu J, Koyama T, et al. Safety and pharmacokinetics of milademetan, a MDM2 inhibitor, in Japanese patients with solid tumors: A phase I study. *Cancer Sci* (2021) 112:2361–70. doi: 10.1111/cas.14875

86. Cornillie J, Wozniak A, Li H, Gebreyohannes YK, Wellens J, Hompes D, et al. Anti-tumor activity of the MDM2-TP53 inhibitor BI-907828 in dedifferentiated liposarcoma patient-derived xenograft models harboring MDM2 amplification. *Clin Transl Oncol* (2020) 22:546–54. doi: 10.1007/s12094-019-02158-z

87. Laroche-Clary A, Chaire V, Algeo MP, Derieppe MA, Loarer FL, Italiano A. Combined targeting of MDM2 and CDK4 is synergistic in dedifferentiated liposarcomas. *J Hematol Oncol* (2017) 10:123. doi: 10.1186/s13045-017-0482-3

88. Vilgelm AE, Saleh N, Shattuck-Brandt R, Riemenschneider K, Slesur L, Chen SC, et al. MDM2 antagonists overcome intrinsic resistance to CDK4/6 inhibition by inducing p21. *Sci Transl Med* (2019) 11(508):1–30. doi: 10.1126/scitranslmed.aav7171

89. Clark AS, Makhlin I, DeMichele A. Setting the pick: Can PI3K inhibitors circumvent CDK4/6 inhibitor resistance? *Clin Cancer Res* (2021) 27:371–3. doi: 10.1158/1078-0432.CCR-20-3624

90. Yuan Y, Lee JS, Yost SE, Frankel PH, Ruel C, Egelston CA, et al. Phase I/II trial of palbociclib, pembrolizumab and letrozole in patients with hormone receptor-positive metastatic breast cancer. *Eur J Cancer* (2021) 154:11–20. doi: 10.1016/j.ejca.2021.05.035

frontiers | Frontiers in Pharmacology

TYPE Original Research
PUBLISHED 03 February 2023
DOI 10.3389/fphar.2023.970457

OPEN ACCESS

EDITED BY
Andrea Cavazzoni,
University of Parma, Italy

REVIEWED BY
Xavier Bisteau,
Université libre de Bruxelles, Belgium
Kamal Eltayeb,
University of Parma, Italy

*CORRESPONDENCE
Claudia Arndt,
c.arnd@hzdr.de
Marc Schmitz,
marc.schmitz@tu-dresden.de

†These authors have contributed equally to this work and share first authorship

SPECIALTY SECTION
This article was submitted to Pharmacology of Anti-Cancer Drugs, a section of the journal Frontiers in Pharmacology

RECEIVED 16 June 2022
ACCEPTED 20 January 2023
PUBLISHED 03 February 2023

CITATION
Arndt C, Tunger A, Wehner R, Rothe R, Kourtellari E, Luttosch S, Hannemann K, Koristka S, Loureiro LR, Feldmann A, Tonn T, Link T, Kuhlmann JD, Wimberger P, Bachmann MP and Schmitz M (2023), Palbociclib impairs the proliferative capacity of activated T cells while retaining their cytotoxic efficacy. *Front. Pharmacol.* 14:970457. doi: 10.3389/fphar.2023.970457

Palbociclib impairs the proliferative capacity of activated T cells while retaining their cytotoxic efficacy

Claudia Arndt[1,2*†], Antje Tunger[3,4†], Rebekka Wehner[3,4,5], Rebecca Rothe[3,4], Eleni Kourtellari[4], Stephanie Luttosch[4], Katharina Hannemann[4], Stefanie Koristka[1], Liliana R. Loureiro[1], Anja Feldmann[1], Torsten Tonn[5,6,7], Theresa Link[3,5,8], Jan Dominik Kuhlmann[3,5,8], Pauline Wimberger[3,5,8], Michael Philipp Bachmann[1,3,5,9] and Marc Schmitz[3,4,5*]

[1]Department of Radioimmunology, Institute of Radiopharmaceutical Cancer Research, Helmholtz-Zentrum Dresden-Rossendorf, Dresden, Germany, [2]Mildred Scheel Early Career Center, Faculty of Medicine Carl Gustav Carus, TU Dresden, Dresden, Germany, [3]National Center for Tumor Diseases (NCT), University Hospital Carl Gustav Carus, TU Dresden, Dresden, Germany, [4]Institute of Immunology, Faculty of Medicine Carl Gustav Carus, TU Dresden, Dresden, Germany, [5]German Cancer Consortium (DKTK), Partner Site Dresden, German Cancer Research Center (DKFZ), Heidelberg, Germany, [6]German Red Cross Blood Donation Service North-East, Institute for Transfusion Medicine, Dresden, Germany, [7]Experimental Transfusion Medicine, Faculty of Medicine Carl Gustav Carus, TU Dresden, Dresden, Germany, [8]Department of Gynecology and Obstetrics, University Hospital Carl Gustav Carus, TU Dresden, Dresden, Germany, [9]Tumor Immunology, University Cancer Center (UCC), University Hospital Carl Gustav Carus, TU Dresden, Dresden, Germany

The cyclin-dependent kinase 4 and 6 (CDK4/6) inhibitor palbociclib is an emerging cancer therapeutic that just recently gained Food and Drug Administration approval for treatment of estrogen receptor (ER)-positive, human epidermal growth factor receptor (Her)2-negative breast cancer in combination with the ER degrader fulvestrant. However, CDK4/6 inhibitors are not cancer-specific and may affect also other proliferating cells. Given the importance of T cells in antitumor defense, we studied the influence of palbociclib/fulvestrant on human CD3+ T cells and novel emerging T cell-based cancer immunotherapies. Palbociclib considerably inhibited the proliferation of activated T cells by mediating G0/G1 cell cycle arrest. However, after stopping the drug supply this suppression was fully reversible. In light of combination approaches, we further investigated the effect of palbociclib/fulvestrant on T cell-based immunotherapies by using a CD3-PSCA bispecific antibody or universal chimeric antigen receptor (UniCAR) T cells. Thereby, we observed that palbociclib clearly impaired T cell expansion. This effect resulted in a lower total concentration of interferon-γ and tumor necrosis factor, while palbociclib did not inhibit the average cytokine release per cell. In addition, the cytotoxic potential of the redirected T cells was unaffected by palbociclib and fulvestrant. Overall, these novel findings may have implications for the design of treatment modalities combining CDK4/6 inhibition and T cell-based cancer immunotherapeutic strategies.

KEYWORDS

cancer immunotherapy, CDK4/6, palbociclib, fulvestrant, bispecific antibody, CAR T cell, adoptive T cell therapy

1 Introduction

Approximately 80% of breast cancers are hormone receptor-positive (HR+) and therefore represent the largest subtype of this malignancy. Endocrine therapies targeting the estrogen receptor (ER) using aromatase inhibitors, such as letrozole, preventing ER signaling (Finn et al., 2015; Finn et al., 2016b; Goetz et al., 2017), selective ER degraders, like fulvestrant (Turner et al., 2015; Sledge et al., 2017; Turner et al., 2018), or selective ER modulators as tamoxifen (Tripathy et al., 2018b) substantially reduced tumor recurrence and improved overall survival (OS) (Abe et al., 2005). However, a significant proportion of patients suffers from relapse following single-agent treatment (Abe et al., 2005; Baselga et al., 2012). To overcome resistance to endocrine therapy new treatment options were developed, such as cyclin-dependent kinase 4 and 6 (CDK4/6) inhibitors, which significantly improved clinical outcomes for these patients (Finn et al., 2015; Turner et al., 2018). CDK4/6 are fundamental drivers of the cell cycle by regulating initiation and progression through the G1 phase and are therefore also key players in various malignancies (Yu et al., 2006; Choi et al., 2012). Common dysregulations of the CDK4/6-retinoblastoma protein (Rb) axis, like copy-number variation or overexpression as well as loss of negative regulators of the pathway, can lead to cancer formation (Sherr et al., 2016). Accordingly, CDKs have long been attractive targets for pharmacologic inhibition in tumor therapy (Adams et al., 2015; Sherr et al., 2016).

The cytostatic potential of single-agent CDK4/6 inhibitors has been shown *in vitro*, causing downregulation of transcription factor E2F target genes, loss of proliferation markers and cell cycle arrest in G1 (Fry et al., 2004). In particular, HR+ breast cancer is susceptible to CDK4/6 inhibitor therapy (Finn et al., 2009; O'Leary et al., 2016). Given the fact that activation of the cyclin D-CDK4/6 complex depends on mitogenic stimuli, synergistic combinations of CDK4/6 inhibitors with signal transduction inhibitors have been developed. In particular, the three orally available CDK4/6 inhibitors palbociclib (PD-0332991; Ibrance; Pfizer), ribociclib (LEE011; Kisqali; Novartis) and abemaciclib (LY2835219; Verzenio; Lilly) received approval by the Food and Drug Administration (FDA) for treatment of patients with ER+, human epidermal growth factor receptor 2-negative (HER2-) advanced or metastatic breast cancer in combination with an aromatase inhibitor or fulvestrant (Finn et al., 2016a; Cristofanilli et al., 2016; Hortobagyi et al., 2016). Various clinical trials within the framework of the PALOMA, MONALEESA, and MONARCH study families form the basis for the FDA approvals, showing improved progression-free survival (PFS) and OS for treatment with CDK4/6 inhibitors and endocrine therapy in breast cancer patients (Finn et al., 2016b; Cristofanilli et al., 2016; Tripathy et al., 2018a; Turner et al., 2018; Im et al., 2019; Johnston et al., 2020; Slamon et al., 2020; Sledge et al., 2020). Beyond ER+ breast cancer, promising activity of CDK4/6 inhibitors in mantle cell lymphoma (MCL), liposarcoma, melanoma, non-small cell lung cancer (NSCLC), glioblastoma, neuroblastoma and malignant rhabdoid tumors has been shown (Leonard et al., 2012; Dickson et al., 2016; Patnaik et al., 2016; Geoerger et al., 2017). Further studies are currently underway, e.g. the evaluation of ribociclib for treatment of prostate cancer (Scheinberg et al., 2020).

However, resistance to therapy frequently occurs in treated patients (Finn et al., 2016a; Finn et al., 2016b; Cristofanilli et al., 2016; Hortobagyi et al., 2016). For this reason, new therapeutic strategies are required to overcome the resistance to CDK4/6 inhibition. The combination with other strategies, such as immunotherapeutic approaches, may represent an interesting treatment modality. There is increasing evidence that CDKs not only regulate cell cycle progression in tumor cells, but also development, differentiation and activation of immune cells (Wells and Morawski, 2014; Ameratunga et al., 2019; Laphanuwat and Jirawatnotai, 2019). T cells play a major role in antitumor immune defense. Based on their antitumoral properties, such as production of proinflammatory cytokines and cytotoxic activity, T cells emerged as a promising tool for cancer immunotherapy. An attractive approach is the genetic modification of autologous T cells with chimeric antigen receptors (CARs) targeting tumor-associated antigens (TAAs). By this, T cells can be redirected against tumor cells in a major histocompatibility complex (MHC)-independent manner (Sadelain et al., 2013). Currently, there are several clinical trials of CAR T cells targeting HER-2 (NCT01935843, NCT01022138), cMet (NCT03060356) or mesothelin (NCT02580747) in breast cancer patients. In this study, we used the switchable UniCAR system (Bachmann, 2019), that is also currently under clinical investigation in a phase I clinical trial (NCT04230265). As an adaptor CAR system, UniCAR T cells recognize a small epitope not present on the cell surface. Thus, they are *per se* inactive and have to be combined with a tumor-reactive target module (TM) to induce tumor lysis, thereby separating the signaling and tumor-targeting function of CARs (Bachmann, 2019; Arndt et al., 2020a). Here, we are utilizing a well-established prostate stem cell antigen (PSCA)-specific TM to redirect UniCAR T cells against prostate cancer cells (Arndt et al., 2014b; 2014a). Alternative strategies to redirect T cells towards tumor cells are bispecific antibodies (bsAbs) that simultaneously target CD3 and a TAA. Due to the bsAb-mediated cross-linkage, T cells can be efficiently engaged for tumor cell killing independent of their TCR-specificity and costimulatory signals (Wolf et al., 2005; Offner et al., 2006). In a phase II study (NCT04224272), the combination of the HER-2-targeting bsAb ZW25 and palbociclib plus fulvestrant for HER2+/HR+ advanced breast cancer is under investigation. Carcinoembryonic antigen (NCT01730612) and PSCA (NCT03927573) are further antigens for targeting breast cancer cells with bsAbs. Here, we used the CD3-PSCA bsAb, which triggers an efficient T cell-mediated killing of PSCA+ tumor cells (Feldmann et al., 2012; Arndt et al., 2014b).

Based on these findings, the aim of the present study was to examine the impact of palbociclib and fulvestrant alone or in combination on CD3+ T cells and novel emerging T cell-based cancer immunotherapies. In this context, we explored the impact of these two therapeutic agents on proliferation, cytokine production and cytotoxic potential of PSCA-specific UniCAR T cells (Feldmann et al., 2017) and T cells redirected *via* CD3-PSCA bsAb (Feldmann et al., 2012).

2 Materials and methods

2.1 Cell lines

All cell lines were maintained at 37°C in a humidified atmosphere with 5% CO_2. Recombinant antibody producing 3T3 cell lines were cultured in DMEM complete media (Feldmann et al., 2011). The prostate cancer cell lines PC3-PSCA/PSMA Luc+ and LNCaP-PSCA

Luc+ were generated and cultured as previously described (Feldmann et al., 2017).

2.2 Production and purification of recombinant antibody constructs

Construction and cloning of PSCA TM and CD3-PSCA bsAb have been published elsewhere (Feldmann et al., 2012; Arndt et al., 2014b). Recombinant antibodies were produced by 3T3 cell lines (Feldmann et al., 2012; Arndt et al., 2014b). Antibody purification from cell culture supernatants was performed *via* Ni-NTA affinity chromatography (Feldmann et al., 2011). After dialysis of elution fractions against 1x PBS, proteins were characterized *via* SDS-PAGE and immunoblotting as published previously (Feldmann et al., 2011; Feldmann et al., 2012; Arndt et al., 2018).

2.3 Immunomagnetic isolation of CD3+ T cells

The study was approved by the local institutional review board of the Faculty of Medicine of the TU Dresden (EK138042014). Peripheral blood mononuclear cells (PBMCs) were isolated from buffy coats of healthy donors *via* density gradient centrifugation. Untouched CD3+ T cells were isolated from freshly prepared PBMCs using immunomagnetic separation according to the manufacturer's instructions (Miltenyi Biotec GmbH, Bergisch Gladbach, Germany). The purity of the isolated cell population was > 90% as assessed by flow cytometric analysis. Isolated T cells were cultured in RPMI complete medium (Feldmann et al., 2011) supplemented with 50 U/ml interleukin (IL)-2 (Miltenyi Biotec GmbH).

2.4 Genetic modification of T cells

Generation of UniCAR T cells was carried out as described recently (Feldmann et al., 2020). Briefly, T cells were stimulated with T Cell TransAct™ (Miltenyi Biotec GmbH) and genetically modified *via* lentiviral transduction (Cartellieri et al., 2014) using a multiplicity of infection of 1–2. During transduction and expansion, T cells were maintained in TexMACS™ medium (Miltenyi Biotec GmbH) supplemented with human IL-2, human IL-7 and human IL-15 (all Miltenyi Biotec GmbH). Experiments were conducted with unsorted UniCAR T cells that were kept in RPMI complete medium (Feldmann et al., 2011) without additional cytokines for 24 h. Based on the co-translated EGFP marker protein expression, the proportion of UniCAR+ T cells was assessed *via* flow cytometry prior to each experiment.

2.5 Flow cytometric analysis

Analysis of surface molecules on CD3+ T cells was performed using the following monoclonal antibodies: APC-H7-conjugated anti-human CD3 (BD Biosciences, Heidelberg, Germany), anti-human CD4-VioBlue, anti-human CD3-FITC and anti-human CD8-APC (all Miltenyi Biotec GmbH). Immunofluorescence staining of cell surface molecules was performed using the relevant antibodies according to the provider's instructions. After the staining procedure, cells were washed and evaluated by BD LSRFortessa™ flow cytometer or MACSQuant Analyzer 10 (Miltenyi Biotec GmbH). Before measurement, 7-AAD (BD Biosciences), DAPI (Miltenyi Biotec GmbH) or propidium iodide solution (Thermo Fisher Scientific, Waltham, Massachusetts, USA) was added for live/dead discrimination.

2.6 T cell proliferation

In order to distinguish effector and target cells, CD3+ T cells and freshly prepared or thawed UniCAR T cells were stained with cell proliferation dye eFluor™ 670 according to the manufacturer's instructions (Thermo Fisher Scientific). Stained CD3+ T cells (2×10^5/well) were cultured in the presence of stimulating anti-CD3/CD28 beads (Thermo Fisher Scientific) as well as the presence or absence of palbociclib (1, 0.2 or 0.025 μM) and fulvestrant (0.1 or 0.025 μM) in different concentrations in round-bottomed 96-well plates. Palbociclib was added daily whereas fulvestrant was added only once to the corresponding wells, according to the clinical dosing schedule. Cells were harvested after 24, 48, 72, 96, 120, 144 or 168 h. After excluding doublets and distinguishing between live and dead cells, the percentage of eFluor670+-diminished T cells compared to the untreated control was analyzed and expressed as "% proliferation". Additionally, number of T cells were determined over time by gating on single, living eFluor670+ cells. Samples were analyzed after DAPI staining by utilizing a MACSQuant VYB flow cytometer (Miltenyi Biotec GmbH). For analysis of reversibility, palbociclib was only added at the first day and cells were harvested after 48 or 120 h and stained with anti-CD3 antibody. Percentage of eFluor™ 670 diminished CD3+ T cells was monitored by a BD LSRFortessa™ flow cytometer.

eFluor™ 670 stained unstimulated or UniCAR-modified T cells were incubated with tumor cells at an effector-to-target cell (E:T) ratio of 5:1 in the presence or absence of 30 nM CD3-PSCA bsAb or PSCA TM in a 96 h co-cultivation assay. Palbociclib (1, 0.2 or 0.025 μM) was added after 0, 24, 48 and 72 h. Fulvestrant (0.1 or 0.025 μM) was added just once at the beginning of the experiment (0 h). Effector cell numbers were determined by flow cytometry after 96 h as previously published (Arndt et al., 2020b). In brief, 20 μl of each sample was transferred to a 96-well round bottom plate and mixed with DAPI solution prior to measurement with the MACSQuant VYB analyzer (Miltenyi Biotec GmbH). Samples were first gated for T cells using SSC-A/FSC-A parameters. Subsequently, doublets were excluded by FSC-H/FSC-A gating and live/dead cells were distinguished by DAPI. Gating on eFluor670+ or eFluor670+ EGFP+ cells identified T cells or UniCAR T cells and allowed determination of T cell number.

2.7 EdU flow cytometry assay

To analyze DNA replication in proliferating cells the Click-iT® Plus EdU Flow Cytometry Assay Kit was utilized according to the manufacturer's instructions (Thermo Fisher Scientific). During DNA synthesis, the thymidine analog EdU (5-ethynyl-2′-deoxyuridine) was incorporated in the DNA and detected by flow cytometry after performing a copper catalyzed click reaction with the provided

Alexa Fluor 488 dye. In brief, CD3+ T cells of four healthy donors (2×10^5/well), being prepared as described in Section 2.3, were stimulated with human T-cell activator CD3/CD28 Dynabeads™ (Thermo Fisher Scientific) and cultured in the presence or absence of palbociclib at different concentrations (0.025, 0.2 or 1 μM) in round-bottomed 96-well plates. Unstimulated, untreated as well as stimulated and DMSO treated cells served as controls. Palbociclib was added daily during the experimental period of 4 days. 18 h prior to cell harvesting, cells were incubated with 10 μM EdU. The cells were harvested after 96 h and stained with an APC-coupled anti-CD3 antibody (BD Biosciences). Following surface antibody staining, cells were fixed and permeabilized using Click-iT® fixative and 1x Click-iT® saponin-based reagent, respectively, for 15 min each. Further, Click-iT® Plus reaction cocktail was added and the samples were incubated, protected from light, for another 30 min at room temperature. After staining and washing procedure, samples were incubated with DAPI (0.4 ng/μl) to stain the cells for DNA content. Finally, flow cytometric analysis was performed using MACSQuant Analyzer 10 (Miltenyi Biotec GmbH) with the appropriate laser and filter settings. FlowLogic™ software (version 8.6; Inivai Technologies, Mentone Victoria, Australia) was used for data evaluation.

2.8 Cytokine assay

To evaluate the interferon (IFN)-γ and tumor necrosis factor (TNF) secretion of activated T cells, 5×10^4 effector cells (unstimulated T cells or UniCAR T cells) and 1×10^4 tumor cells were incubated in the presence or absence of 30 nM of recombinant antibody (CD3-PSCA bsAb or PSCA TM) in round-bottomed 96-well plates. Palbociclib (1, 0.2 or 0.025 μM) was added after 0, 24, 48 and 72 h. Fulvestrant (0.1 or 0.025 μM) was added just once at the beginning of the experiment (0 h). After 96 h, cell-free supernatants were collected. IFN-γ and TNF were quantified by ELISA according to the manufacturer's instructions (BD Biosciences).

2.9 Luminescence-based killing assay

Luminescence-based killing assays were performed according to a previously published protocol (Mitwasi et al., 2017). Briefly, 5×10^4 effector cells (unstimulated T cells or UniCAR T cells) and 1×10^4 luciferase-expressing tumor cells were incubated with or without 30 nM of recombinant antibody (CD3-PSCA bsAb or PSCA TM). In addition, palbociclib (1, 0.2 or 0.025 μM) and/or fulvestrant (0.1 or 0.025 μM) were added to co-cultures. Alternatively, effector cells were first incubated with palbociclib (0.2 or 0.025 μM) and/or fulvestrant (0.1 or 0.025 μM) for 24 h. Thereafter, tumor cells and recombinant antibodies were added as described above. In addition, co-cultivation assays were repeatedly supplemented with palbociclib (1, 0.2 or 0.025 μM). Effector cells were prepared freshly or thawed 48 h prior to experiment. After 8 h of co-culture, 96-well white plates were centrifuged for 5 min at 360 × g. Subsequently, 100 μl supernatant was carefully removed and 50 μl ONE-Glo™ Luciferase reagent (Promega GmbH, Mannheim, Germany) added to each well. Following a 5 min incubation step, luminescence of each sample was measured using the Infinite® M200 pro microplate reader (Tecan Germany GmbH, Crailsheim, Germany). Specific tumor cell lysis was calculated as described elsewhere (Mitwasi et al., 2017).

2.10 Statistical analysis

Student's *t*-test was performed to evaluate the significance of the results. To compare samples to a control sample One-way ANOVA with posthoc Dunnett multiple comparison test was performed using GraphPad Prism 7 software (GraphPad Prism Inc., La Jolla, CA, United States). Values of $p \leq 0.05$ were considered as significant.

3 Results

3.1 Palbociclib reversibly inhibits proliferation of stimulated CD3+ T cells

The expansion, cytokine secretion and cytotoxic activity of T cells play an important role in antitumor immunity. Due to the fact, that T cells rapidly proliferate after antigen-specific activation, we explored the effect of the CDK4/6 inhibitor on T cell proliferation. To investigate whether palbociclib and/or fulvestrant alter this function, CD3+ T cells were maintained in the presence or absence of palbociclib or fulvestrant alone or in combination. T cells were stimulated to proliferate by anti-CD3/CD28 beads. Proliferation was measured every 24 h for 7 days by flow cytometry on the basis of eFluor™ 670 dilution over time. As depicted in Figure 1A, T cells displayed a strong proliferation upon stimulation in comparison to unstimulated control starting after 48 h. Palbociclib significantly impaired this ability of the CD3+ T cells in a concentration-dependent manner. Notably, 0.025–1 μM palbociclib clearly reduced the proliferative capacity of CD3+ T cells. The reduced proliferation, as measured by the dilution of the proliferation dye eFluor670™, is also reflected in a reduced number of T cells (Supplementary Figure S1). In contrast, fulvestrant did not influence this functional property of T cells (Figure 1A; Supplementary Figure S1).

We further investigated whether the inhibitory effect of palbociclib on T cell proliferation is reversible. Therefore, the CDK4/6 inhibitor was only added at the first day to stimulated CD3+ T cells instead of daily. Proliferation was analyzed after 48 h and 120 h. Although overall proliferation of stimulated T cells was less pronounced after 48 h, single-dosing of palbociclib alone or in combination with fulvestrant clearly impaired proliferation of CD3+ T cells (Figure 1B). However, after 120 h the inhibitory effect of palbociclib on T cell proliferation was almost abrogated (Figure 1C). These results indicate that the inhibitory effect of palbociclib on the proliferative capacity of T cells is reversible after stopping the drug application.

To study the underlying mechanisms of the palbociclib-mediated reduction in T cell proliferation, we performed an EdU assay with anti-CD3/CD28 bead-activated T cells treated with palbociclib (daily addition) for 96 h. We found a decreased percentage of T lymphocytes in S-phase of cell cycle when cells are exposed to 0.2 or 1 μM palbociclib (Figure 1D). In contrast, the percentage of T cells in G0/G1 phase increased under the same culture conditions. These findings indicate that the reduced proliferation of T cells is caused by a palbociclib-mediated G0/G1 cell cycle arrest.

3.2 Effect of palbociclib and fulvestrant on T cell-based immunotherapies

In view of potential combination therapies, we explored the influence of palbociclib and fulvestrant on two PSCA-specific T cell-based

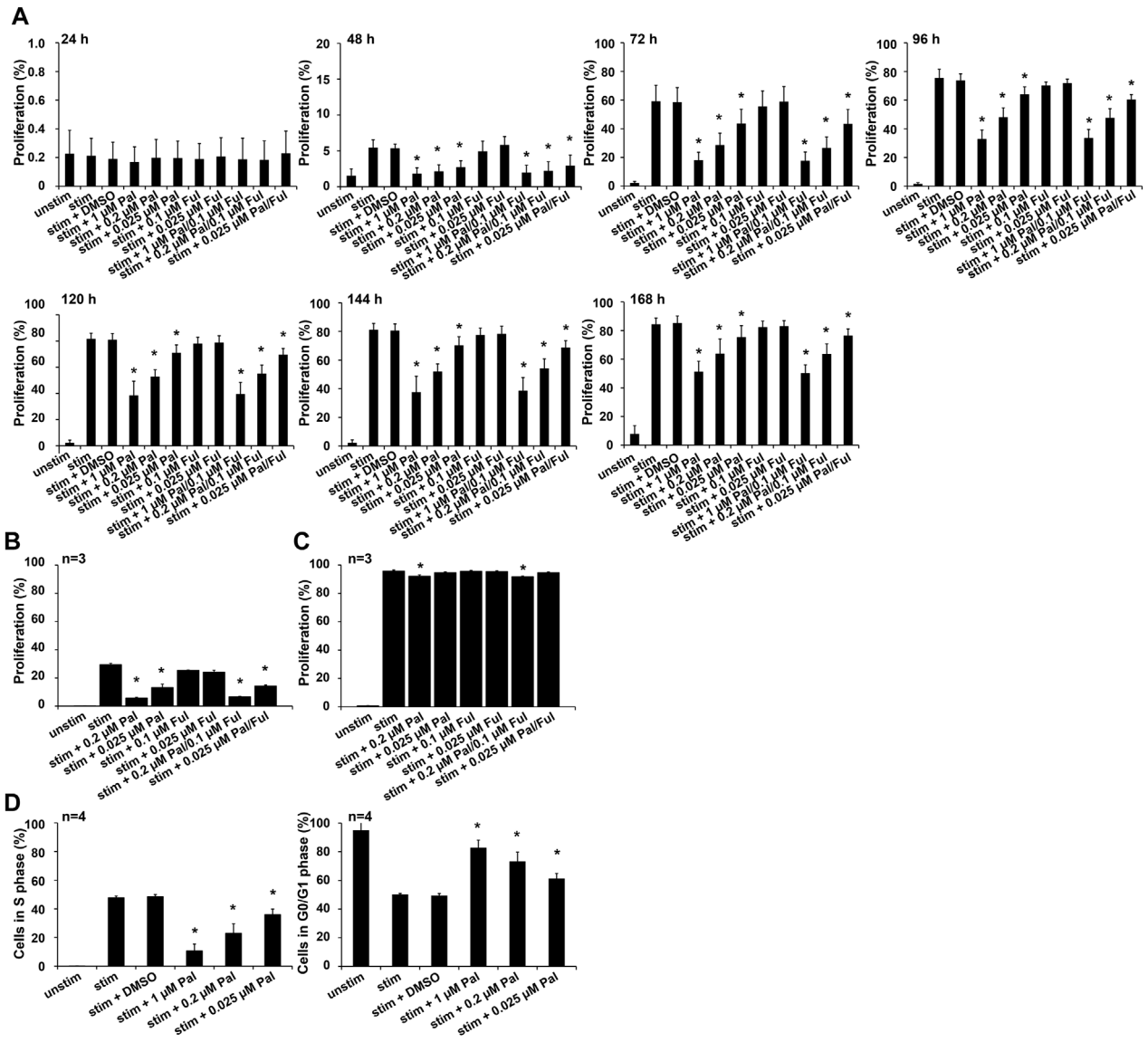

FIGURE 1
Influence of palbociclib and fulvestrant on T cell proliferation. **(A)** eFluor™ 670-stained T cells were stimulated by anti-CD3/CD28 beads and cultured in the presence or absence of palbociclib (daily addition), fulvestrant, or their combination at indicated concentrations for 24, 48, 72, 96, 120, 144, and 168 h. Cells were harvested and dilution of eFluor670™ dye was determined by flow cytometry. The results are depicted as the means ± SEM of four donors. (*$p \leq 0.05$ compared to control sample "stim + DMSO"). **(B,C)** eFluor™ 670-stained T cells were stimulated by anti-CD3/CD28 beads and cultured in the presence or absence of palbociclib (single administration), fulvestrant, or their combination for **(B)** 48 h and **(C)** 120 h. Cells were harvested and dilution of proliferation dye eFluor670™ was determined by flow cytometry. The results are depicted as the means ± SEM of three donors. (*$p \leq 0.05$ compared to control sample "stim"). **(D)** DNA replication in proliferating cells was analyzed by EdU flow cytometry assay. Therefore, T cells were stimulated by anti-CD3/CD28 beads and cultured in the presence of palbociclib (daily addition) at indicated concentrations for 96 h. 18 h prior to cell harvesting, cells were incubated with 10 µM EdU. Cells were harvested and percentage of EdU-positive cells was determined by flow cytometry. (*$p \leq 0.05$ compared to control sample "stim + DMSO").

immunotherapies. On the one hand, we selected the CD3-PSCA bsAb (Figure 2A) (Feldmann et al., 2012). As shown in previous studies, due to its dual specificity for CD3 and PSCA it can specifically cross-link T cells and PSCA-expressing tumor cells in a MHC- and TCR-independent manner that finally culminates in effective tumor cell elimination (Feldmann et al., 2012). On the other hand, we chose the switchable UniCAR T cell technology (Bachmann, 2019), which is composed of UniCAR-modified T cells and PSCA-specific TMs (Figure 2B) (Arndt et al., 2014a; Arndt et al., 2014b).

In order to assess the impact of palbociclib and fulvestrant on both T cell retargeting strategies, co-cultivation assays with two different prostate cancer cells lines were carried out. For this purpose, unstimulated T cells or UniCAR T cells in the presence or absence of the CD3-PSCA bsAb or the PSCA TM were used. Palbociclib and fulvestrant were added either alone or in combination at various concentrations.

3.2.1 Palbociclib markedly impairs the proliferative capacity of bsAb-engaged T cells and UniCAR T cells

For a sustained and efficient antitumor response mediated by T cell-based immunotherapies, proliferation and polyclonal expansion of effector T cell populations is required. Thus, first experiments

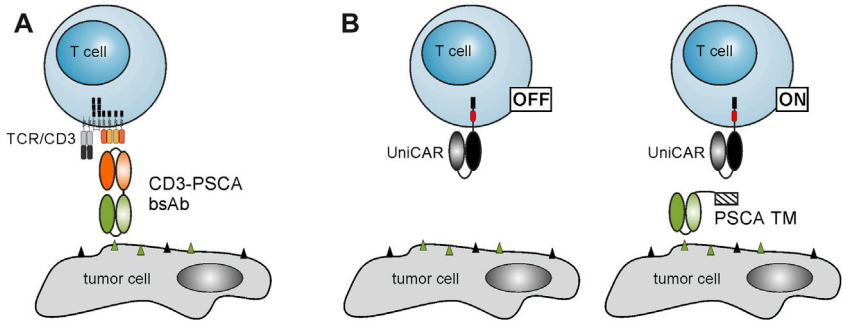

FIGURE 2
Schematic representation of T cell-based immunotherapies. **(A)** Due to its dual specificity for CD3 and PSCA, the CD3-PSCA bsAb is able to cross-link T cells and PSCA-expressing tumor cells. Subsequently, T cells are activated and kill the recognized target cell. **(B)** The UniCAR system is composed of UniCAR T cells and TAA-specific TMs. In the absence of TMs, UniCAR T cells are not activated. Upon addition of a PSCA-specific TM, UniCAR T cells can be cross-linked with PSCA-expressing tumor cells resulting in an efficient tumor cell lysis.

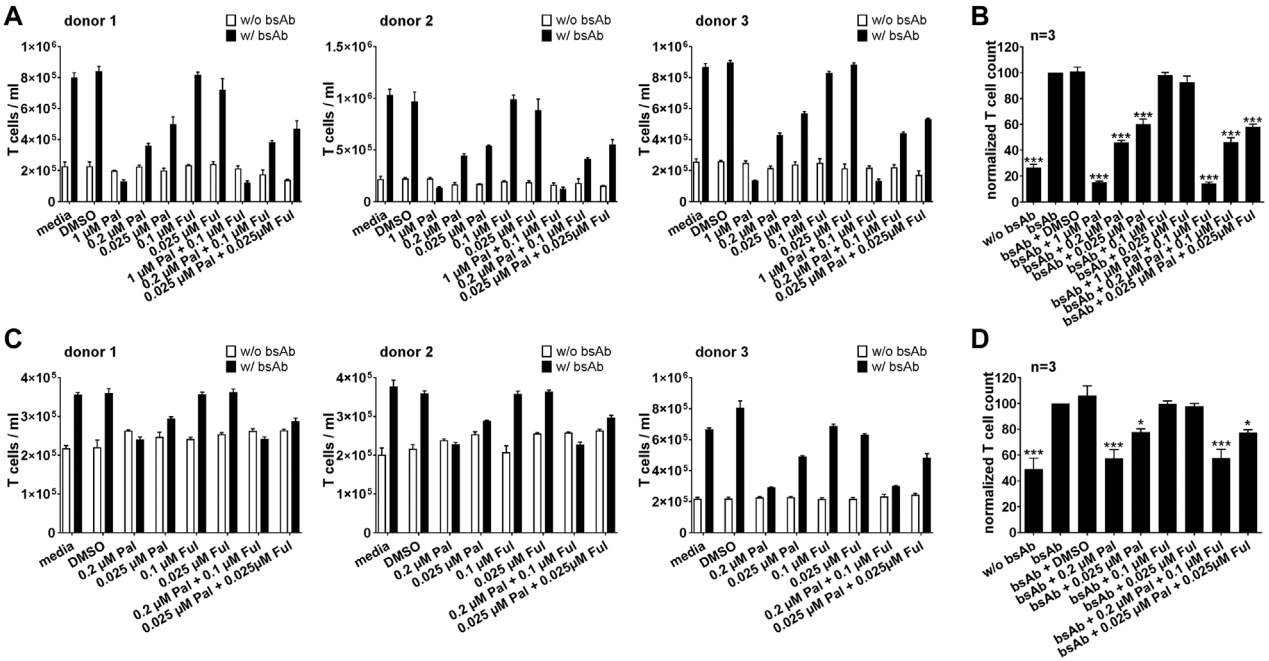

FIGURE 3
Effect of palbociclib and fulvestrant on bsAb-mediated T cell expansion. eFluor™ 670$^+$ T cells and **(A,B)** PC3-PSCA/PSMA Luc+ or **(C,D)** LNCaP-PSCA Luc+ cells were incubated with or without CD3-PSCA bsAb. Palbociclib and/or fulvestrant were added at indicated concentrations. After 96 h, numbers of eFluor™ 670$^+$ T cells were determined by flow cytometry using the MACSQuant® Analyzer. **(A,C)** Each diagram shows average T cell counts ± SEM of triplicates for one T cell donor. **(B,D)** Graphs summarize relative T cell counts ± SEM of three different T cell donors. T cell numbers in the presence of tumor cells and bsAb ("bsAb") were equalized to 100%. (*$p \leq 0.05$, ***$p \leq 0.001$ compared to control sample "bsAb"; One-way ANOVA with posthoc Dunnett multiple comparison test).

aimed to investigate the influence of palbociclib and fulvestrant on the proliferative capacity of specifically activated bsAb-engaged T cells and UniCAR T cells. As shown in Figure 3, upon cross-linkage with PC3-PSCA/PSMA Luc+ (Figures 3A, B) or LNCaP-PSCA Luc+ cells (Figures 3C, D) *via* the CD3-PSCA bsAb, T cell numbers increased up to 5-fold compared to the negative controls without bsAb after 96 h. However, in the presence of 0.2 or 1 µM palbociclib the proliferation and expansion of bsAb-redirected T cells was efficiently inhibited (Figure 3). Under these conditions, numbers of T cells did not or only slightly increase and were in some cases almost equal to T cell counts detected in samples without the CD3-PSCA bsAb. Similar results were obtained when palbociclib was applied in combination with 0.1 µM fulvestrant. Although suppressive effects of palbociclib on T cell proliferation were less profound at a lower concentration of 0.025 µM, T cell expansion was still significantly reduced compared to samples lacking the small-molecule inhibitor. In contrast, the selective ER degrader fulvestrant did not alter bsAb-mediated T cell expansion.

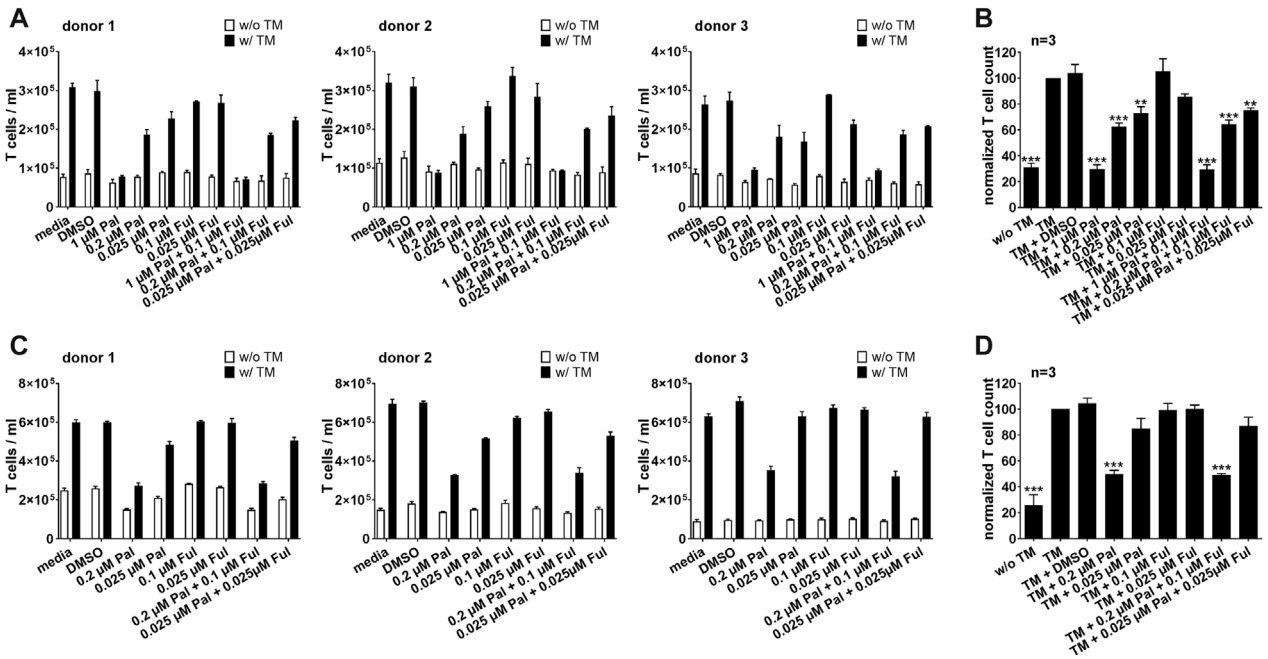

FIGURE 4
Effect of palbociclib and fulvestrant on TM-mediated UniCAR T cell expansion. eFluor™ 670$^+$ UniCAR T cells and **(A,B)** PC3-PSCA/PSMA Luc+ or **(C,D)** LNCaP-PSCA Luc+ cells were incubated with or without 30 nM of PSCA TM. Palbociclib and/or fulvestrant were added at indicated concentrations. After 96 h, numbers of eFluor™ 670+ UniCAR T cells were determined by flow cytometry using the MACSQuant® Analyzer. **(A,C)** Each diagram shows average T cell counts ± SEM of triplicates for one T cell donor. **(B,D)** Graphs summarize relative UniCAR T cell counts ± SEM of three different T cell donors. UniCAR T cell numbers in the presence of tumor cells and TM ("TM") were equalized to 100%. (***$p \leq 0.001$ compared to control sample "TM"; One-way ANOVA with posthoc Dunnett multiple comparison test).

These findings were not only limited to bsAb-redirected T cells, but could also be observed when palbociclib and fulvestrant were combined with the PSCA-specific UniCAR system. Expansion of redirected UniCAR T cells was significantly suppressed in the presence of 0.2 or 1 µM palbociclib alone or in combination with 0.1 µM fulvestrant (Figure 4). Fulvestrant alone exerted no inhibitory effects on the proliferative capacity of UniCAR T cells.

3.2.2 Impact of palbociclib on IFN-γ and TNF secretion by bsAb-engaged T cells and UniCAR T cells

As the proinflammatory cytokines IFN-γ and TNF can increase the therapeutic efficacy of T cell-based immunotherapies, we investigated the impact of palbociclib and fulvestrant on the secretion of IFN-γ and TNF by UniCAR T cells and bsAb-redirected T cells. Therefore, cytokine assays were performed with LNCaP-PSCA Luc+ or PC3-PSCA/PSMA Luc+ cells. Upon cross-linkage with PC3-PSCA/PSMA Luc+ (Figures 5A, B) or LNCaP-PSCA Luc+ cells (Figures 5C, D) *via* the CD3-PSCA bsAb, a higher IFN-γ concentration in the supernatants compared to the control was detected. Palbociclib used at a concentration of 0.2 or 1 µM significantly reduced the IFN-γ concentration in the supernatants of bsAb-redirected T cells. A lower palbociclib concentration (0.025 µM) exerted only minor or no inhibitory effects. Likewise, in the presence of 1 µM palbociclib, significantly lower levels of TNF were detected in the co-culture supernatants after 96 h (Supplementary Figures S2A, B). Fulvestrant alone did not affect the bsAb-mediated IFN-γ or TNF secretion by T cells.

Similar results were observed when palbociclib and fulvestrant were combined with the PSCA-specific UniCAR system (Figure 6; Supplementary Figures S2C, D). Cross-linkage of PSCA-specific UniCAR T cells with prostate cancer cells resulted in a higher IFN-γ and TNF concentration in the supernatants compared to the control. In the presence of palbociclib, the concentration of IFN-γ and TNF in the supernatants of redirected UniCAR T cells was reduced in a concentration-dependent manner. While in the presence of 0.2 or 1 µM palbociclib IFN-γ and TNF were significantly reduced, a lower palbociclib concentration only considerably altered TNF release. In contrast, fulvestrant had no inhibitory effect on this functional characteristic.

To explore whether the lower total concentrations of IFN-γ and TNF in the supernatants are associated with the palbociclib-mediated reduction of the T cell number, the amounts of IFN-γ and TNF detected in the supernatant after 96 h were calculated per T cell or UniCAR T cell. As summarized in Supplementary Figures S3, S4, in the presence of palbociclib average cytokine concentrations per cell did not significantly change or were even elevated compared to the settings without inhibitors, indicating that the lower concentrations of IFN-γ and TNF in the supernatants are associated with the palbociclib-induced decrease in T cell numbers.

3.2.3 Cytotoxic potential of bsAb-engaged T cells and UniCAR T cells is unaffected by palbociclib

For an effective combination therapy, it is important to ensure that palbociclib and fulvestrant do not impede antitumor cytotoxicity of T cell-based immunotherapies. Hence, the effect of palbociclib and

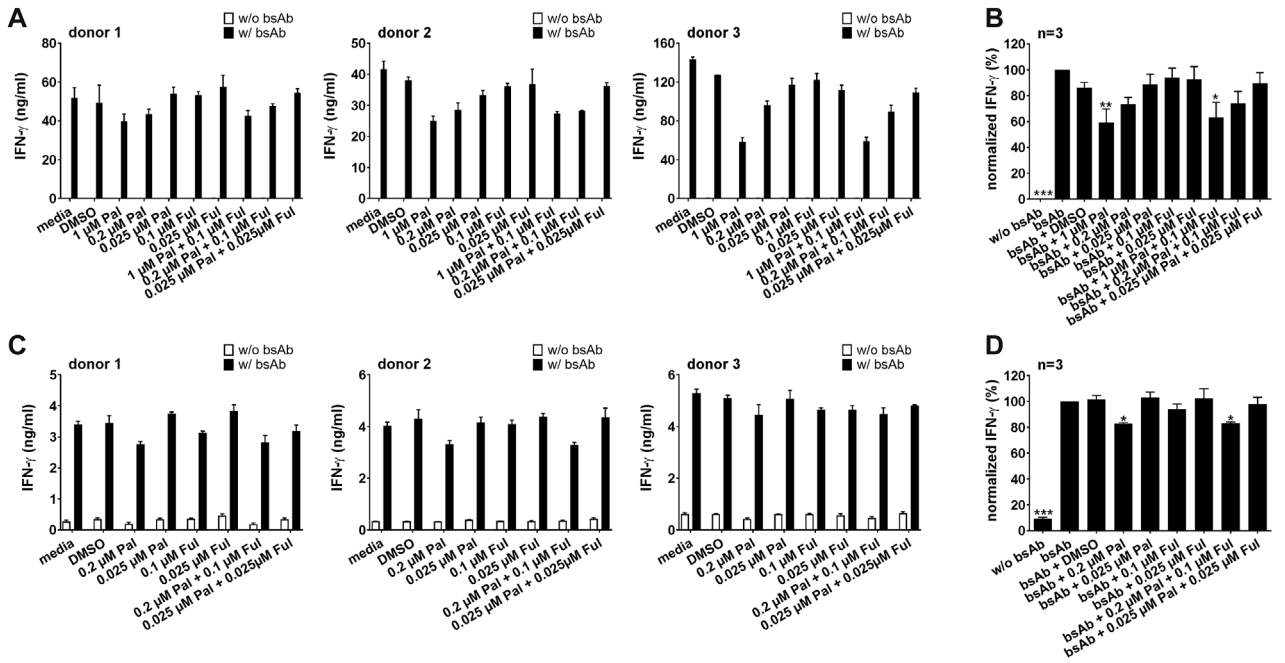

FIGURE 5
Effect of palbociclib and fulvestrant on IFN-γ release of bsAb-engaged T cells. T cells and **(A,B)** PC3-PSCA/PSMA Luc+ or **(C,D)** LNCaP-PSCA Luc+ cells were incubated with or without 30 nM of CD3-PSCA bsAb in the presence or absence of palbociclib and/or fulvestrant. After 96 h, IFN-γ concentrations in co-culture supernatants were analyzed by ELISA. **(A,C)** Each diagram shows average IFN-γ concentration ± SEM of triplicates for one T cell donor. **(B,D)** Graphs summarize relative IFN-γ release ± SEM of three different T cell donors. IFN-γ concentrations in the presence of T cells, tumor cells and bsAb ("bsAb") were equalized to 100%. (*$p \leq 0.05$, ***$p \leq 0.001$ compared to control sample "bsAb"; One-way ANOVA with posthoc Dunnett multiple comparison test).

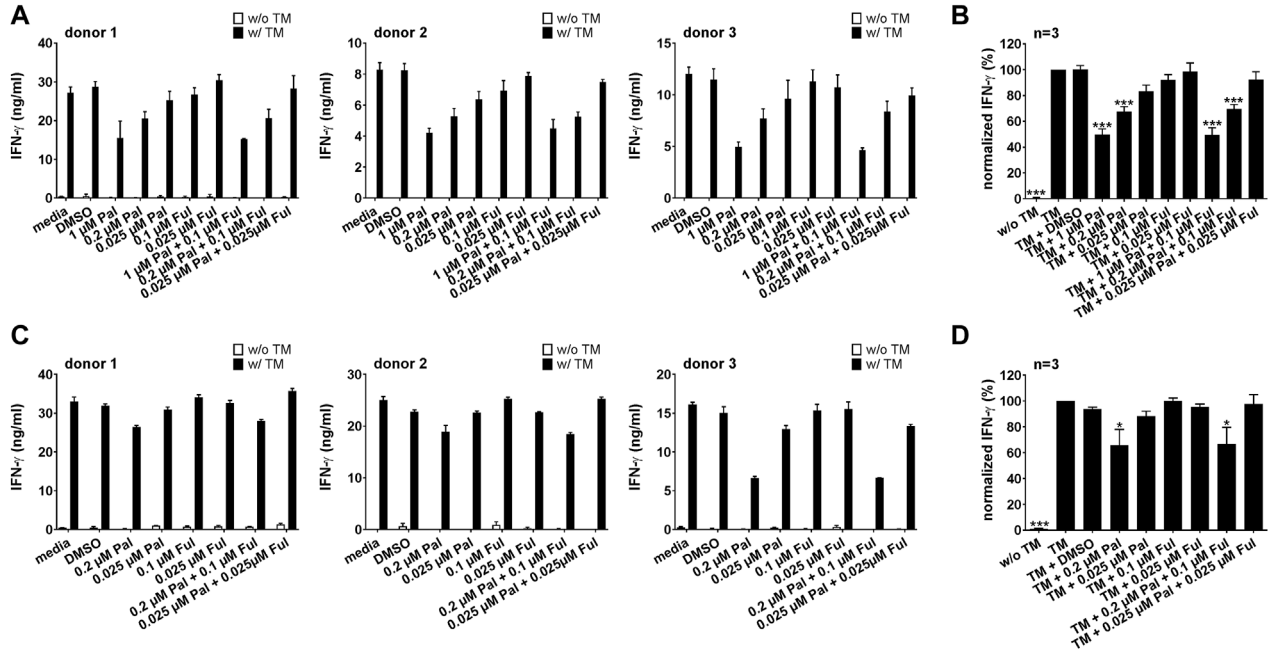

FIGURE 6
Effect of palbociclib and fulvestrant on IFN-γ release of TM-engaged UniCAR T cells. UniCAR T cells and **(A,B)** PC3-PSCA/PSMA Luc+ or **(C,D)** LNCaP-PSCA Luc+ cells were incubated with or without 30 nM of PSCA TM in the presence or absence of palbociclib and/or fulvestrant. After 96 h, IFN-γ concentrations in co-culture supernatants were analyzed by ELISA. **(A,C)** Each diagram shows average IFN-γ concentration ± SEM of triplicates for one T cell donor, respectively. **(B,D)** Graphs summarize relative IFN-γ release ± SEM of three different T cell donors. IFN-γ concentrations in the presence of UniCAR T cells, tumor cells and TM ("TM") were equalized to 100%. (*$p \leq 0.05$, **$p \leq 0.01$, ***$p \leq 0.001$ compared to control sample "TM"; One-way ANOVA with posthoc Dunnett multiple comparison test).

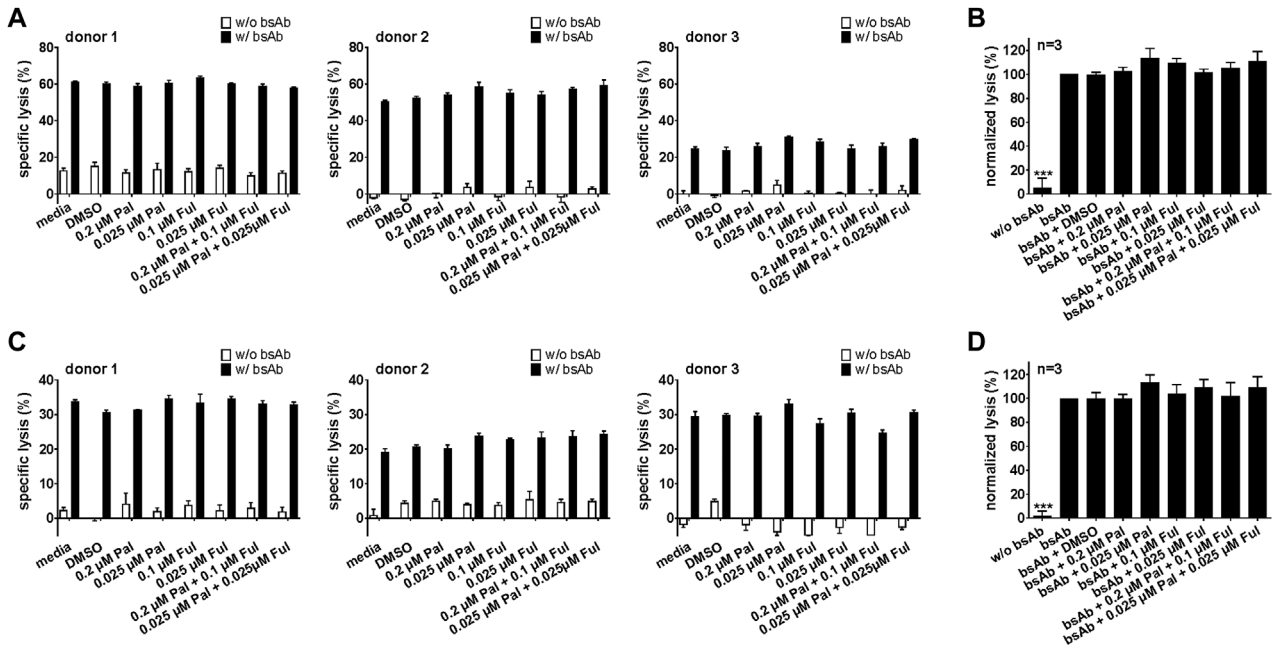

FIGURE 7
Effect of palbociclib and fulvestrant on bsAb-mediated tumor cell killing. T cells and **(A,B)** LNCaP-PSCA Luc+ or **(C,D)** PC3-PSCA/PSMA Luc+ cells were incubated with or without 30 nM of CD3-PSCA bsAb in the presence or absence of palbociclib and/or fulvestrant. After 8 h, tumor cell killing was calculated based on a luminescence-based killing assay. **(A,C)** Each diagram shows mean specific lysis ± SEM of triplicates for one T cell donor. **(B,D)** Graphs summarize relative tumor lysis ± SEM of three different T cell donors. Specific lysis in the presence of T cells and bsAb ("bsAb") were equalized to 100%. (***$p \leq 0.001$ compared to control sample "bsAb"; One-way ANOVA with posthoc Dunnett multiple comparison test).

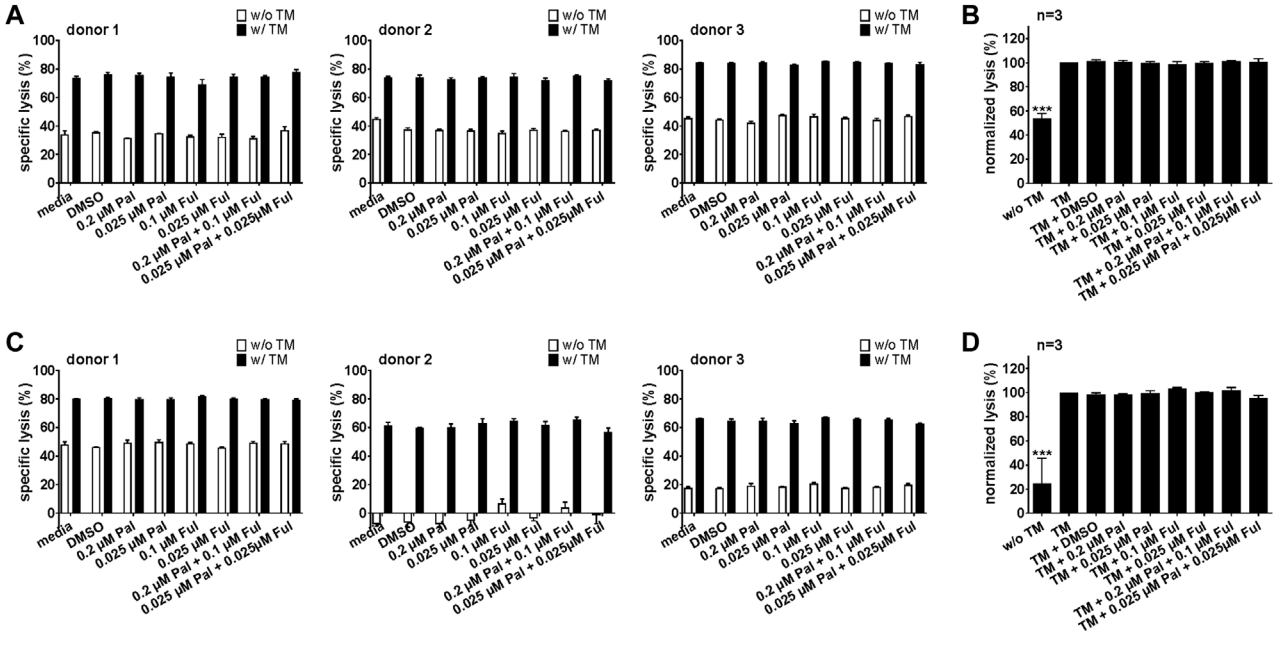

FIGURE 8
Effect of palbociclib and fulvestrant on UniCAR T cell-mediated tumor cell killing. UniCAR T cells and **(A,B)** LNCaP-PSCA Luc+ or **(C,D)** PC3-PSCA/PSMA Luc+ cells were incubated with or without 30 nM of PSCA TM in the presence or absence of palbociclib and/or fulvestrant. After 8 h, tumor cell killing was calculated based on a luminescence-based killing assay. **(A,C)** Each diagram shows mean specific lysis ± SEM of triplicates for one T cell donor. **(B,D)** Graphs summarize relative tumor lysis ± SEM of three different T cell donors. Specific lysis in the presence of UniCAR T cells and TM ("TM") were equalized to 100%. (***$p \leq 0.001$ compared to control sample "TM"; One-way ANOVA with posthoc Dunnett multiple comparison test).

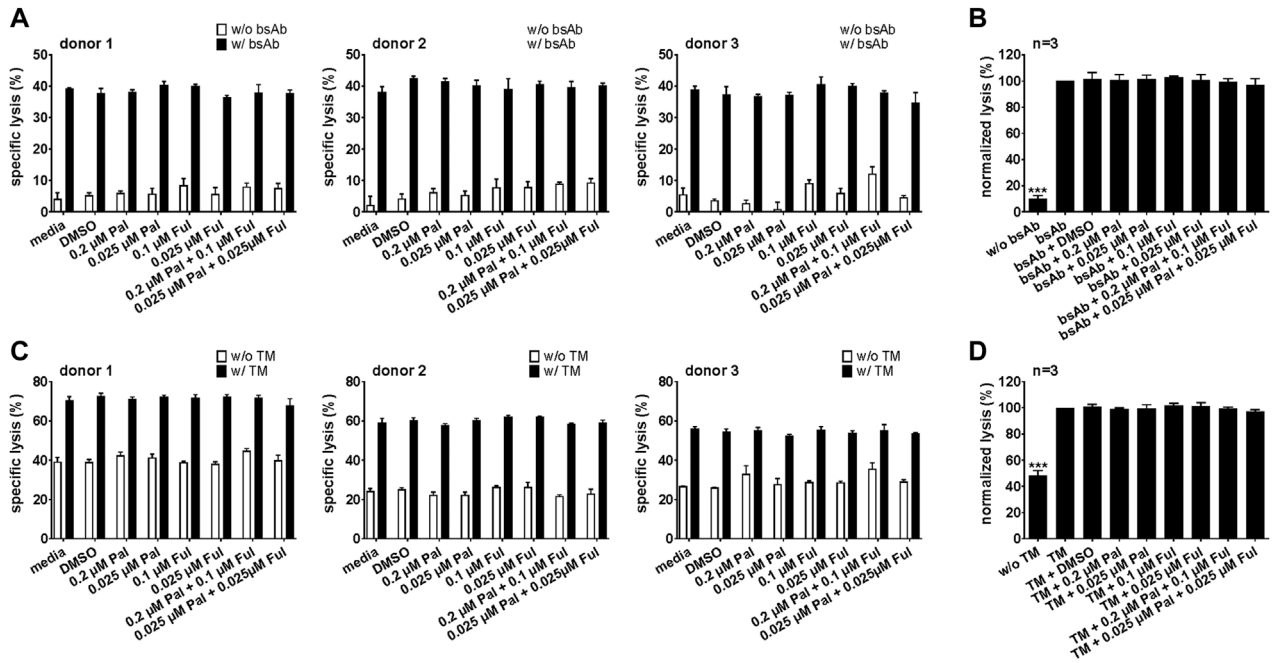

FIGURE 9
Cytotoxic capacity of palbociclib- and fulvestrant-pretreated bsAb-engaged T cells and UniCAR T cells. After pre-incubation of **(A,B)** T cells or **(C,D)** UniCAR T cells without or with palbociclib and/or fulvestrant for 24 h, luciferase-based killing assays were performed. Therefore, preincubated **(A,B)** T cells or **(C,D)** preincubated UniCAR T cells were cultured with PC3-PSCA/PSMA Luc+ cells in the presence or absence of 30 nM **(A,B)** CD3-PSCA bsAb or **(C,D)** PSCA TM. After 8 h, specific lysis was determined. **(A,C)** Each diagram shows mean specific lysis ± SEM of triplicates for one T cell donor. **(B,D)** Graphs summarize relative tumor lysis ± SEM of three different T cell donors. Specific lysis in the presence of **(B)** T cell and bsAb ("bsAb") or **(D)** UniCAR T cells and TM ("TM") were equalized to 100%. (***$p \leq 0.001$ compared to control sample "bsAb" or "TM"; One-way ANOVA with posthoc Dunnett multiple comparison test).

fulvestrant on bsAb- or UniCAR T cell-mediated tumor cell killing was investigated by performing luminescence-based killing assays with LNCaP-PSCA Luc+ or PC3-PSCA/PSMA Luc+ cells. As shown in Figure 7 and Supplementary Figures S5A, 5B, the CD3-PSCA bsAb was able to specifically engage T cells for killing of PSCA+ tumor cells already after 8 h. Interestingly, palbociclib and/or fulvestrant did not modulate this functional property of T cells.

Similar results were obtained for the PSCA-specific UniCAR system (Figure 8; Supplementary Figures S5C, D). Upon cross-linkage with prostate cancer cells *via* the PSCA TM, UniCAR T cells mediated efficient tumor cell lysis. Again, palbociclib and/or fulvestrant did not alter the cytotoxic activity of the UniCAR T cells.

In a next step, we also investigated whether pretreatment of T cells or UniCAR T cells with palbociclib and/or fulvestrant can influence their cytotoxic potential. For this purpose, T cells or UniCAR T cells were incubated with palbociclib and/or fulvestrant at 37°C. 24 h later, luminescence-based killing assays were performed in which drug-pretreated T cells or UniCAR T cells were co-cultured with PC3-PSCA/PSMA Luc+ cells and 30 nM CD3-PSCA bsAb or PSCA TM, respectively. Pre-incubation of T cells (Figures 9A,B) or UniCAR T cells (Figures 9C,D) with one or both drugs did neither influence tumor cell killing mediated by bsAb-redirected T cells nor by TM-engaged UniCAR T cells. These results provide evidence that palbociclib alone or in combination with fulvestrant retain the cytotoxic activity of bsAb-engaged T cells and UniCAR T cells.

4 Discussion

CDK4/6 inhibitors in combination with endocrine therapy received FDA approval for treatment of patients with ER+, HER2- advanced or metastatic breast cancer (Finn et al., 2016a; Cristofanilli et al., 2016; Hortobagyi et al., 2016). This kind of therapy has shown clinical efficacy by prolonging PFS and OS (Finn et al., 2016a; Cristofanilli et al., 2016; Hortobagyi et al., 2016; Im et al., 2019; Johnston et al., 2020; Slamon et al., 2020; Sledge et al., 2020). However, a proportion of patients experienced disease progression (Finn et al., 2016a; Finn et al., 2016b; Cristofanilli et al., 2016; Hortobagyi et al., 2016). Potential explanations for therapy resistance to CDK4/6 inhibition in these patients are intrinsic or acquired resistance, including deregulations of the immune pathway, such as activation of inhibitory immune checkpoint pathways and suppression of immune stimulatory pathways in palbociclib-resistant cells (Pandey et al., 2019; Pandey et al., 2021; Pancholi et al., 2020). Therefore, identification of novel therapeutic strategies for treatment of patients resistant to CDK4/6 inhibition is urgently needed. In the last few decades, immunotherapy has become an important treatment modality. Since functional T cells are a crucial component of the tumor microenvironment for efficient tumor eradication, they emerged as key players of diverse immunotherapeutic strategies, including inhibition of immune checkpoint molecules and adoptive cellular therapy. With regard to therapeutic combination strategies, first success was achieved combining palbociclib with immune checkpoint inhibitors (CPI) in an *ex vivo* organotypic tumor

spheroid culture system as well as in different mouse models (Deng et al., 2018; Zhang et al., 2018; Long et al., 2020). Furthermore, the comparison of patients with metastatic breast cancer treated with a combination of palbociclib, the CPI pembrolizumab and the aromatase inhibitor letrozole or with pembrolizumab and letrozole revealed that higher frequencies of blood-circulating effector memory T cells at baseline are potential predictive biomarkers of response to the combination of CDK4/6 inhibitors and CPI (Egelston et al., 2021). Additional attractive T cell-based strategies, such as bsAb (Wolf et al., 2005) and CAR T cell therapy (June et al., 2018; Arndt et al., 2020a), may also represent promising combinatorial partners for CDK4/6 inhibitors.

Emerging preclinical studies revealed diverse immunomodulatory effects of CDK4/6 inhibition, such as an enhanced immune infiltration into the tumor microenvironment, elevated antigen presentation and modulation of the cytokine milieu, supporting antitumor immune response (Ameratunga et al., 2019). Different murine models investigated the influence of CDK4/6 inhibition on tumor-infiltrating immune cells. In a breast cancer mouse model, a significant reduction of CD3+ tumor-infiltrating lymphocytes was observed under palbociclib treatment (Zhang et al., 2018). In contrast, Goel and colleagues reported significant increases of intratumoral CD3+ T cells in their transgenic mouse model of mammary carcinoma treated with abemaciclib or palbociclib (Goel et al., 2017). Another study also showed enhanced proportions of CD4+ and CD8+ T cells in lung tumors of genetically engineered mice after treatment with palbociclib or trilaciclib (Deng et al., 2018). However, this effect seems not to be based on increased proliferation, but on elevated homing of effector T cells to the tumor. These data are in line with observations by Schaer and colleagues, who demonstrated that abemaciclib increased the frequency of CD3+ T cell numbers within the tumor, but not the absolute numbers in a colon cancer mouse model (Schaer et al., 2018). By analyzing the functional status of the tumor-infiltrating T cells, Deng et al. (2018) observed an increased IFN-γ secretion by total splenocytes isolated from lung tumor-bearing mice, but not naïve mice, treated with trilaciclib *in vivo*. Moreover, Teo and colleagues have shown, that the CDK4/6 inhibitor ribociclib does not impair activation and cytotoxic potential of tumor-infiltrating CD8+ and CD4+ T cells in a triple-negative breast cancer mouse model (Teo et al., 2017).

Whereas all these findings rely on mouse models, little is known about the impact of palbociclib and fulvestrant on the functional properties of human immune cells. Heckler and colleagues investigated the impact of CDK4/6 inhibitors on activated CD8+ T cells of breast cancer patients and observed that CDK4/6 inhibition resulted in an increased frequency of memory CD8+ T cell precursors (Heckler et al., 2021). Based on the observation that higher frequencies of pre-existing effector memory T cells were detectable in the blood of responders to the combination of CDK4/6 inhibitors and CPI (Egelston et al., 2021), early treatment with CDK4/6 inhibitors to establish a memory CD8+ T cell pool followed by the CPI administration may represent a promising therapeutic strategy for cancer patients. Here, we examined the influence of palbociclib and fulvestrant on the proliferation and functional properties of bsAb-engaged T cells and UniCAR T cells in terms of a potential combinatorial approach of CDK4/6 inhibition and T cell-based immunotherapy. An important prerequisite for a durable and efficient antitumor T cell response is the proliferation and clonal expansion of the T cells. Therefore, we analyzed the impact of palbociclib and fulvestrant on the proliferative capacity of stimulated CD3+ T cells. We demonstrated that palbociclib clearly impairs the ability of T cells to proliferate upon anti-CD3/CD28 bead stimulation. This effect is based on a G0/G1 cell cycle arrest mediated by palbociclib. The palbociclib-mediated T cell inhibition was reversible after stopping the drug application. In contrast, fulvestrant did not influence this functional property. Furthermore, we analyzed the impact of palbociclib and fulvestrant on the proliferation of bsAb-engaged T cells and UniCAR T cells. Our studies were performed exemplarily with the CD3-PSCA bsAb (Feldmann et al., 2012) and the UniCAR technology using the PSCA TM (Arndt et al., 2014a; Arndt et al., 2014b; Bachmann, 2019). PSCA is a TAA upregulated in several major cancers, including prostate cancer, urinary bladder cancer, renal cell carcinoma, pancreatic cancer, ovarian mucinous tumor and NSCLC (Amara et al., 2001; Argani et al., 2001; Cao et al., 2005; Elsamman et al., 2006; Kawaguchi et al., 2010). Recently, PSCA expression in a subgroup of breast cancer patients was also reported (Link et al., 2017). Although T cell stimulation occurred *via* different methods, palbociclib but not fulvestrant prevented adequate proliferation and expansion of both bsAb-engaged T cells and redirected UniCAR T cells. Goel et al. also observed an inhibitory effect on the proliferation of CD4+ CD25- and CD8+ T cells derived from spleens and lymph nodes of wild-type mice after treatment with abemaciclib *in vitro*, concordant with our findings (Goel et al., 2017). Furthermore, *ex vivo* stimulation of splenocytes from lung tumor-bearing mice showed a reduced proliferation after anti-CD3/CD28 antibody stimulation and treatment with trilaciclib (Deng et al., 2018). In further experiments, we investigated the impact of palbociclib and/or fulvestrant on the cytokine production of T cells. The proinflammatory cytokine IFN-γ is an important player in the antitumoral immune response and may further enhance therapeutic effects of a T cell-based immunotherapy as it increases MHC class I expression and antigen presentation of tumor cells and further supports macrophages, cytotoxic T lymphocytes and natural killer cells in their antitumor response. TNF can also exhibit various antitumor effects, such as the induction of tumor cell apoptosis, and the recruitment and activation of tumor-reactive T cells. Palbociclib treatment of PSCA-specific UniCAR T cells and CD3-PSCA bsAb-engaged T cells co-cultured with prostate cancer cells resulted in lower total concentrations of IFN-γ and TNF in the supernatants. When investigating the underlying mechanism for this observation, we found that the lower concentrations of IFN-γ and TNF are linked to the palbociclib-mediated decrease in T cell numbers. For efficient tumor eradication, cytotoxic potential of T cells is a crucial parameter for immunotherapeutic strategies. For this reason, we further investigated the impact of palbociclib and fulvestrant on the UniCAR T cell- or bsAb-mediated cytotoxicity. The CD3-PSCA bsAb as well as the PSCA-specific UniCAR system have proven their capability to redirect T cells for efficient killing of PSCA+ tumor cells *in vitro* and in mouse models (Feldmann et al., 2012; Feldmann et al., 2017; Pishali Bejestani et al., 2017). We demonstrated under various conditions that neither palbociclib nor fulvestrant added either prior or during co-culture influence this functional property.

In summary, our data revealed that palbociclib reversibly impairs proliferation of activated CD3+ T cells and reduces expansion of UniCAR T cells and bsAb-engaged T cells. Furthermore, we observed

reduced amounts of IFN-γ and TNF in the supernatants of palbociclib-treated PSCA-specific UniCAR T cells and CD3-PSCA bsAb-engaged T cells co-cultured with prostate cancer cells, which is caused by the palbociclib-mediated decrease in T cell numbers. The cytotoxic potential of PSCA-specific UniCAR T cells and CD3-PSCA bsAb-engaged T cells was not affected by palbociclib. Fulvestrant did not show impact on any of these functional properties of stimulated CD3+ T cells, UniCAR T cells and bsAb-engaged T cells. These results provide evidence that the CDK4/6 inhibitor palbociclib has not only an impact on the cell cycle of tumor cells but also on T cells, which are crucial players in an antitumor immune response. Hence, palbociclib-mediated alterations of T cell functionality should be taken into consideration for future therapeutic recommendations and potential combinatorial approaches with T cell-based immunotherapy. Thus, a palbociclib-free time period may be required for an efficient T cell-based immunotherapy.

Data availability statement

The original contributions presented in the study are included in the article/Supplementary Material, further inquiries can be directed to the corresponding authors.

Ethics statement

The study was approved by the local institutional review board.

Author contributions

AT, CA, and MS contributed to conception and formal analysis. AT, CA, RR, EK, SL, KH, SK, and LL contributed to methodology and investigation. AT, CA, MB, and MS validated the study. AF, MB, and MS provided critical material and resources. AT, CA, and EK performed all experiments and curated data. AT and CA wrote the original draft of the manuscript. AF, RW, TT, TL, JK, PW, MB, and MS reviewed and edited the original draft of the manuscript. AT and CA visualized the data. MS supervised the project. AT, CA, and MS administered the project. All authors contributed to manuscript revision, read, and approved the submitted version.

Funding

This research was funded by the Federal Ministry of Education and Research (03ZU1111LA to AF and 03ZU1111LB to MB and MS).

Acknowledgments

CA is fellow of the Mildred Scheel Early Career Center Dresden P^2 funded by the German Cancer Aid (Deutsche Krebshilfe). We thank Kim Weiße, Luisa Zimmermann, Christine Gräfe and Cathleen Lippitsch for excellent technical assistance.

Conflict of interest

The authors declare that the research was conducted in the absence of any commercial or financial relationships that could be construed as a potential conflict of interest.

Publisher's note

All claims expressed in this article are solely those of the authors and do not necessarily represent those of their affiliated organizations, or those of the publisher, the editors and the reviewers. Any product that may be evaluated in this article, or claim that may be made by its manufacturer, is not guaranteed or endorsed by the publisher.

Supplementary material

The Supplementary Material for this article can be found online at: https://www.frontiersin.org/articles/10.3389/fphar.2023.970457/full#supplementary-material

References

Abe, O., Abe, R., Enomoto, K., Kikuchi, K., Koyama, H., Masuda, H., et al. (2005). Effects of chemotherapy and hormonal therapy for early breast cancer on recurrence and 15-year survival: An overview of the randomised trials. *Lancet* 365, 1687–1717. doi:10.1016/S0140-6736(05)66544-0

Adams, J. L., Smothers, J., Srinivasan, R., and Hoos, A. (2015). Big opportunities for small molecules in immuno-oncology. *Nat. Rev. Drug Discov.* 14, 603–622. doi:10.1038/nrd4596

Amara, N., Palapattu, G. S., Schrage, M., Gu, Z., Thomas, G. V., Dorey, F., et al. (2001). Prostate stem cell antigen is overexpressed in human transitional cell carcinoma. *Cancer Res.* 61, 4660–4665.

Ameratunga, M., Kipps, E., Okines, A. F. C., and Lopez, J. S. (2019). To cycle or fight—CDK4/6 inhibitors at the crossroads of anticancer immunity. *Clin. Cancer Res.* 25, 21–28. doi:10.1158/1078-0432.CCR-18-1999

Argani, P., Rosty, C., Reiter, R. E., Wilentz, R. E., Murugesan, S. R., Leach, S. D., et al. (2001). Discovery of new markers of cancer through serial analysis of gene expression: Prostate stem cell antigen is overexpressed in pancreatic adenocarcinoma. *Cancer Res.* 61, 4320–4324.

Arndt, C., Fasslrinner, F., Loureiro, L. R., Koristka, S., Feldmann, A., and Bachmann, M. (2020a). Adaptor car platforms—Next generation of T cell-based cancer immunotherapy. *Cancers (Basel)* 12, 1302. doi:10.3390/cancers12051302

Arndt, C., Feldmann, A., Koristka, S., Cartellieri, M., Dimmel, M., Ehninger, A., et al. (2014a). Simultaneous targeting of prostate stem cell antigen and prostate-specific membrane antigen improves the killing of prostate cancer cells using a novel modular T cell-retargeting system. *Prostate* 74, 1335–1346. doi:10.1002/pros.22850

Arndt, C., Feldmann, A., Töpfer, K., Koristka, S., Cartellieri, M., Temme, A., et al. (2014b). Redirection of CD4+ and CD8+ T lymphocytes via a novel antibody-based modular targeting system triggers efficient killing of PSCA+ prostate tumor cells. *Prostate* 74, 1347–1358. doi:10.1002/pros.22851

Arndt, C., Koristka, S., Feldmann, A., Bergmann, R., and Bachmann, M. (2018). Coomassie brilliant blue staining of polyacrylamide gels. *Methods Mol. Biol.* 1853, 27–30. doi:10.1007/978-1-4939-8745-0_4

Arndt, C., Loureiro, L. R., Feldmann, A., Jureczek, J., Bergmann, R., Máthé, D., et al. (2020b). UniCAR T cell immunotherapy enables efficient elimination of radioresistant cancer cells. *Oncoimmunology* 9, 1743036. doi:10.1080/2162402X.2020.1743036

Bachmann, M. (2019). The UniCAR system: A modular CAR T cell approach to improve the safety of CAR T cells. *Immunol. Lett.* 211, 13–22. doi:10.1016/j.imlet.2019.05.003

Baselga, J., Campone, M., Piccart, M., Burris, H. A., Rugo, H. S., Sahmoud, T., et al. (2012). Everolimus in postmenopausal hormone-receptor–positive advanced breast cancer. *N. Engl. J. Med.* 366, 520–529. doi:10.1056/NEJMoa1109653

Cao, D., Ji, H., and Ronnett, B. M. (2005). Expression of mesothelin, fascin, and prostate stem cell antigen in primary ovarian mucinous tumors and their utility in differentiating primary ovarian mucinous tumors from metastatic pancreatic mucinous carcinomas in the ovary. *Int. J. Gynecol. Pathol.* 24, 67–72. doi:10.1097/01.pgp.0000139648.17750.35

Cartellieri, M., Koristka, S., Arndt, C., Feldmann, A., Stamova, S., Von Bonin, M., et al. (2014). A novel *ex vivo* isolation and expansion procedure for chimeric antigen receptor engrafted human T cells. *PLoS One* 9, e93745. doi:10.1371/journal.pone.0093745

Choi, Y. J., Li, X., Hydbring, P., Sanda, T., Stefano, J., Christie, A. L., et al. (2012). The requirement for cyclin D function in tumor maintenance. *Cancer Cell* 22, 438–451. doi:10.1016/j.ccr.2012.09.015

Cristofanilli, M., Turner, N. C., Bondarenko, I., Ro, J., Im, S.-A., Masuda, N., et al. (2016). Fulvestrant plus palbociclib versus fulvestrant plus placebo for treatment of hormone-receptor-positive, HER2-negative metastatic breast cancer that progressed on previous endocrine therapy (PALOMA-3): Final analysis of the multicentre, double-blind, phase 3 randomised controlled trial. *Lancet. Oncol.* 17, 425–439. doi:10.1016/S1470-2045(15)00613-0

Deng, J., Wang, E. S., Jenkins, R. W., Li, S., Dries, R., Yates, K., et al. (2018). CDK4/6 inhibition augments antitumor immunity by enhancing T-cell activation. *Cancer Discov.* 8, 216–233. doi:10.1158/2159-8290.CD-17-0915

Dickson, M. A., Schwartz, G. K., Louise Keohan, M., D'Angelo, S. P., Gounder, M. M., Chi, P., et al. (2016). Progression-free survival among patients with well-differentiated or dedifferentiated liposarcoma treated with cdk4 inhibitor palbociclib a phase 2 clinical trial. *JAMA Oncol.* 2, 937–940. doi:10.1001/jamaoncol.2016.0264

Egelston, C., Guo, W., Yost, S., Lee, J. S., Rose, D., Avalos, C., et al. (2021). Pre-existing effector T-cell levels and augmented myeloid cell composition denote response to CDK4/6 inhibitor palbociclib and pembrolizumab in hormone receptor-positive metastatic breast cancer. *J. Immunother. cancer* 9, e002084. doi:10.1136/JITC-2020-002084

Elsamman, E. M., Fukumori, T., Tanimoto, S., Nakanishi, R., Takahashi, M., Toida, K., et al. (2006). The expression of prostate stem cell antigen in human clear cell renal cell carcinoma: A quantitative reverse transcriptase-polymerase chain reaction analysis. *BJU Int.* 98, 668–673. doi:10.1111/j.1464-410X.2006.06350.x

Feldmann, A., Arndt, C., Bergmann, R., Loff, S., Cartellieri, M., Bachmann, D., et al. (2017). Retargeting of T lymphocytes to PSCA- or PSMA positive prostate cancer cells using the novel modular chimeric antigen receptor platform technology "UniCAR. *Oncotarget* 8, 31368–31385. doi:10.18632/oncotarget.15572

Feldmann, A., Arndt, C., Töpfer, K., Stamova, S., Krone, F., Cartellieri, M., et al. (2012). Novel humanized and highly efficient bispecific antibodies mediate killing of prostate stem cell antigen-expressing tumor cells by CD8 + and CD4 + T cells. *J. Immunol.* 189, 3249–3259. doi:10.4049/jimmunol.1200341

Feldmann, A., Hoffmann, A., Bergmann, R., Koristka, S., Berndt, N., Arndt, C., et al. (2020). Versatile chimeric antigen receptor platform for controllable and combinatorial T cell therapy. *Oncoimmunology* 9, 1785608. doi:10.1080/2162402X.2020.1785608

Feldmann, A., Stamova, S., Bippes, C. C., Bartsch, H., Wehner, R., Schmitz, M., et al. (2011). Retargeting of T cells to prostate stem cell antigen expressing tumor cells: Comparison of different antibody formats. *Prostate* 71, 998–1011. doi:10.1002/pros.21315

Finn, R. S., Aleshin, A., and Slamon, D. J. (2016a). Targeting the cyclin-dependent kinases (CDK) 4/6 in estrogen receptor-positive breast cancers. *Breast Cancer Res.* 18, 17. doi:10.1186/s13058-015-0661-5

Finn, R. S., Crown, J. P., Lang, I., Boer, K., Bondarenko, I. M., Kulyk, S. O., et al. (2015). The cyclin-dependent kinase 4/6 inhibitor palbociclib in combination with letrozole versus letrozole alone as first-line treatment of oestrogen receptor-positive, HER2-negative, advanced breast cancer (PALOMA-1/TRIO-18): A randomised phase 2 study. *Lancet. Oncol.* 16, 25–35. doi:10.1016/S1470-2045(14)71159-3

Finn, R. S., Dering, J., Conklin, D., Kalous, O., Cohen, D. J., Desai, A. J., et al. (2009). PD 0332991, a selective cyclin D kinase 4/6 inhibitor, preferentially inhibits proliferation of luminal estrogen receptor-positive human breast cancer cell lines *in vitro*. *Breast Cancer Res.* 11, R77. doi:10.1186/bcr2419

Finn, R. S., Martin, M., Rugo, H. S., Jones, S., Im, S.-A., Gelmon, K., et al. (2016b). PALMO-2: Palbociclib and Letrozole in Advanced Breast Cancer (first line hormone positive disease). *N. Engl. J. Med.* 375, 1925–1936. doi:10.1056/NEJMoa1607303

Fry, D. W., Harvey, P. J., Keller, P. R., Elliott, W. L., Meade, M. A., Trachet, E., et al. (2004). Specific inhibition of cyclin-dependent kinase 4/6 by PD 0332991 and associated antitumor activity in human tumor xenografts. *Mol. Cancer Ther.* 3, 1427–1438. doi:10.1158/1535-7163.1427.3.11

Geoerger, B., Bourdeaut, F., DuBois, S. G., Fischer, M., Geller, J. I., Gottardo, N. G., et al. (2017). A phase I study of the CDK4/6 inhibitor ribociclib (LEE011) in pediatric patients with malignant rhabdoid tumors, neuroblastoma, and other solid tumors. *Clin. Cancer Res.* 23, 2433–2441. doi:10.1158/1078-0432.CCR-16-2898

Goel, S., Decristo, M. J., Watt, A. C., Brinjones, H., Sceneay, J., Li, B. B., et al. (2017). CDK4/6 inhibition triggers anti-tumour immunity. *Nature* 548, 471–475. doi:10.1038/nature23465

Goetz, M. P., Toi, M., Campone, M., Trédan, O., Bourayou, N., Sohn, J., et al. (2017). Monarch 3: Abemaciclib as initial therapy for advanced breast cancer. *J. Clin. Oncol.* 35, 3638–3646. doi:10.1200/JCO.2017.75.6155

Heckler, M., Ali, L. R., Clancy-Thompson, E., Qiang, L., Ventre, K. S., Lenehan, P., et al. (2021). Inhibition of CDK4/6 promotes CD8 T-cell memory formation. *Cancer Discov.* 11, 2564–2581. doi:10.1158/2159-8290.CD-20-1540

Hortobagyi, G. N., Stemmer, S. M., Burris, H. A., Yap, Y. S., Sonke, G. S., Paluch-Shimon, S., et al. (2016). Ribociclib as first-line therapy for HR-positive, advanced breast cancer. *N. Engl. J. Med.* 375, 1738–1748. doi:10.1056/NEJMoa1609709

Im, S.-A., Lu, Y.-S., Bardia, A., Harbeck, N., Colleoni, M., Franke, F., et al. (2019). Overall survival with ribociclib plus endocrine therapy in breast cancer. *N. Engl. J. Med.* 381, 307–316. doi:10.1056/nejmoa1903765

Johnston, S. R. D., Harbeck, N., Hegg, R., Toi, M., Martin, M., Shao, Z. M., et al. (2020). Abemaciclib combined with endocrine therapy for the adjuvant treatment of HR+, HER2–, node-positive, high-risk, early breast cancer (monarchE). *J. Clin. Oncol.* 38, 3987–3998. doi:10.1200/jco.20.02514

June, C. H., O'Connor, R. S., Kawalekar, O. U., Ghassemi, S., and Milone, M. C. (2018). CAR T cell immunotherapy for human cancer. *Science* 359, 1361–1365. doi:10.1126/science.aar6711

Kawaguchi, T., Sho, M., Tojo, T., Yamato, I., Nomi, T., Hotta, K., et al. (2010). Clinical significance of prostate stem cell antigen expression in non-small cell lung cancer. *Jpn. J. Clin. Oncol.* 40, 319–326. doi:10.1093/jjco/hyp181

Laphanuwat, P., and Jirawatnotai, S. (2019). Immunomodulatory roles of cell cycle regulators. *Front. Cell Dev. Biol.* 7, 23. doi:10.3389/fcell.2019.00023

Leonard, J. P., LaCasce, A. S., Smith, M. R., Noy, A., Chirieac, L. R., Rodig, S. J., et al. (2012). Selective CDK4/6 inhibition with tumor responses by PD0332991 in patients with mantle cell lymphoma. *Blood* 119, 4597–4607. doi:10.1182/blood-2011-10-388298

Link, T., Kuithan, F., Ehninger, A., Kuhlmann, J. D., Kramer, M., Werner, A., et al. (2017). Exploratory investigation of PSCA-protein expression in primary breast cancer patients reveals a link to HER2/neu overexpression. *Oncotarget* 8, 54592–54603. doi:10.18632/oncotarget.17523

Long, Q., Ma, A. H., Zhang, H., Cao, Z., Xia, R., Lin, T. Y., et al. (2020). Combination of cyclin-dependent kinase and immune checkpoint inhibitors for the treatment of bladder cancer. *Cancer Immunol. Immunother.* 69, 2305–2317. doi:10.1007/s00262-020-02609-5

Mitwasi, N., Feldmann, A., Bergmann, R., Berndt, N., Arndt, C., Koristka, S., et al. (2017). Development of novel target modules for retargeting of UniCAR T cells to GD2 positive tumor cells. *Oncotarget* 8, 108584–108603. doi:10.18632/oncotarget.21017

Offner, S., Hofmeister, R., Romaniuk, A., Kufer, P., and Baeuerle, P. A. (2006). Induction of regular cytolytic T cell synapses by bispecific single-chain antibody constructs on MHC class I-negative tumor cells. *Mol. Immunol.* 43, 763–771. doi:10.1016/j.molimm.2005.03.007

O'Leary, B., Finn, R. S., and Turner, N. C. (2016). Treating cancer with selective CDK4/6 inhibitors. *Nat. Rev. Clin. Oncol.* 13, 417–430. doi:10.1038/nrclinonc.2016.26

Pancholi, S., Ribas, R., Simigdala, N., Schuster, E., Nikitorowicz-Buniak, J., Ressa, A., et al. (2020). Tumour kinome re-wiring governs resistance to palbociclib in oestrogen receptor positive breast cancers, highlighting new therapeutic modalities. *Oncogene* 39, 4781–4797. doi:10.1038/s41388-020-1284-6

Pandey, K., An, H. J., Kim, S. K., Lee, S. A., Kim, S., Lim, S. M., et al. (2019). Molecular mechanisms of resistance to CDK4/6 inhibitors in breast cancer: A review. *Int. J. Cancer* 145, 1179–1188. doi:10.1002/ijc.32020

Pandey, K., Lee, E., Park, N., Hur, J., Cho, Y. B., Katuwal, N. B., et al. (2021). Deregulated immune pathway associated with palbociclib resistance in preclinical breast cancer models: Integrative genomics and transcriptomics. *Genes (Basel).* 12, 159. doi:10.3390/genes12020159

Patnaik, A., Rosen, L. S., Tolaney, S. M., Tolcher, A. W., Goldman, J. W., Gandhi, L., et al. (2016). Efficacy and safety of Abemaciclib, an inhibitor of CDK4 and CDK6, for patients with breast cancer, non–small cell lung cancer, and other solid tumors. *Cancer Discov.* 6, 740–753. doi:10.1158/2159-8290.CD-16-0095

Pishali Bejestani, E., Cartellieri, M., Bergmann, R., Ehninger, A., Loff, S., Kramer, M., et al. (2017). Characterization of a switchable chimeric antigen receptor platform in a pre-clinical solid tumor model. *Oncoimmunology* 6, e1342909. doi:10.1080/2162402X.2017.1342909

Sadelain, M., Brentjens, R., and Rivière, I. (2013). The basic principles of chimeric antigen receptor design. *Cancer Discov.* 3, 388–398. doi:10.1158/2159-8290.CD-12-0548

Schaer, D. A., Beckmann, R. P., Dempsey, J. A., Huber, L., Forest, A., Amaladas, N., et al. (2018). The CDK4/6 inhibitor abemaciclib induces a T cell inflamed tumor microenvironment and enhances the efficacy of PD-L1 checkpoint blockade. *Cell Rep.* 22, 2978–2994. doi:10.1016/j.celrep.2018.02.053

Scheinberg, T., Kench, J., Stockler, M., Mahon, K. L., Sebastian, L., Stricker, P., et al. (2020). Pharmacodynamics effects of CDK4/6 inhibitor LEE011 (ribociclib) in high-risk, localised prostate cancer: A study protocol for a randomised controlled phase II trial (leep study: LEE011 in high-risk, localised prostate cancer). *BMJ Open* 10, e033667. doi:10.1136/bmjopen-2019-033667

Sherr, C. J., Beach, D., and Shapiro, G. I. (2016). Targeting CDK4 and CDK6: From discovery to therapy. *Cancer Discov.* 6, 353–367. doi:10.1158/2159-8290.CD-15-0894

Slamon, D. J., Neven, P., Chia, S., Fasching, P. A., De Laurentiis, M., Im, S.-A., et al. (2020). Overall survival with ribociclib plus fulvestrant in advanced breast cancer. *N. Engl. J. Med.* 382, 514–524. doi:10.1056/nejmoa1911149

Sledge, G. W., Toi, M., Neven, P., Sohn, J., Inoue, K., Pivot, X., et al. (2017). Monarch 2: Abemaciclib in combination with fulvestrant in women with HR+/HER2-advanced breast cancer who had progressed while receiving endocrine therapy. *J. Clin. Oncol.* 35, 2875–2884. doi:10.1200/JCO.2017.73.7585

Sledge, G. W., Toi, M., Neven, P., Sohn, J., Inoue, K., Pivot, X., et al. (2020). The effect of abemaciclib plus fulvestrant on overall survival in hormone receptor-positive, ERBB2-negative breast cancer that progressed on endocrine therapy - MONARCH 2: A randomized clinical trial. *JAMA Oncol.* 6, 116–124. doi:10.1001/jamaoncol.2019.4782

Teo, Z. L., Versaci, S., Dushyanthen, S., Caramia, F., Savas, P., Mintoff, C. P., et al. (2017). Combined CDK4/6 and PI3Kα inhibition is synergistic and immunogenic in triple-negative breast cancer. *Cancer Res.* 77, 6340–6352. doi:10.1158/0008-5472.CAN-17-2210

Tripathy, D., Im, S. A., Colleoni, M., Franke, F., Bardia, A., Harbeck, N., et al. (2018a). Ribociclib plus endocrine therapy for premenopausal women with hormone-receptor-positive, advanced breast cancer (MONALEESA-7): A randomised phase 3 trial. *Lancet Oncol.* 19, 904–915. doi:10.1016/S1470-2045(18)30292-4

Tripathy, D., Sohn, J., Im, S.-A., Colleoni, M., Franke, F., Bardia, A., et al. (2018b). Abstract GS2-05: First-line ribociclib vs placebo with goserelin and tamoxifen or a non-steroidal aromatase inhibitor in premenopausal women with hormone receptor-positive, HER2-negative advanced breast cancer: Results from the randomized phase III MONALEESA-7 trial. *Cancer Res.* 78, GS2–05. GS2-05-GS2-05. doi:10.1158/1538-7445.sabcs17-gs2-05

Turner, N. C., Ro, J., André, F., Loi, S., Verma, S., Iwata, H., et al. (2015). Palbociclib in hormone-receptor-positive advanced breast cancer. *N. Engl. J. Med.* 373, 209–219. doi:10.1056/NEJMoa1505270

Turner, N. C., Slamon, D. J., Ro, J., Bondarenko, I., Im, S. A., Masuda, N., et al. (2018). Overall survival with palbociclib and fulvestrant in advanced breast cancer. *N. Engl. J. Med.* 379, 1926–1936. doi:10.1056/NEJMoa1810527

Wells, A. D., and Morawski, P. A. (2014). New roles for cyclin-dependent kinases in T cell biology: Linking cell division and differentiation. *Nat. Rev. Immunol.* 14, 261–270. doi:10.1038/nri3625

Wolf, E., Hofmeister, R., Kufer, P., Schlereth, B., and Baeuerle, P. A. (2005). BiTEs: Bispecific antibody constructs with unique anti-tumor activity. *Drug Discov. Today* 10, 1237–1244. doi:10.1016/S1359-6446(05)03554-3

Yu, Q., Sicinska, E., Geng, Y., Ahnström, M., Zagozdzon, A., Kong, Y., et al. (2006). Requirement for CDK4 kinase function in breast cancer. *Cancer Cell* 9, 23–32. doi:10.1016/j.ccr.2005.12.012

Zhang, J., Bu, X., Wang, H., Zhu, Y., Geng, Y., Nihira, N. T., et al. (2018). Cyclin D-CDK4 kinase destabilizes PD-L1 via cullin 3-SPOP to control cancer immune surveillance. *Nature* 553, 91–95. doi:10.1038/nature25015

Frontiers in Oncology

Advances knowledge of carcinogenesis and tumor progression for better treatment and management

The third most-cited oncology journal, which highlights research in carcinogenesis and tumor progression, bridging the gap between basic research and applications to imrpove diagnosis, therapeutics and management strategies.

Discover the latest Research Topics

See more →

Frontiers

Avenue du Tribunal-Fédéral 34
1005 Lausanne, Switzerland
frontiersin.org

Contact us

+41 (0)21 510 17 00
frontiersin.org/about/contact